Electromagnetic Properties of Strange Baryons

Elektromagnetische Eigenschappen van Vreemde Baryonen

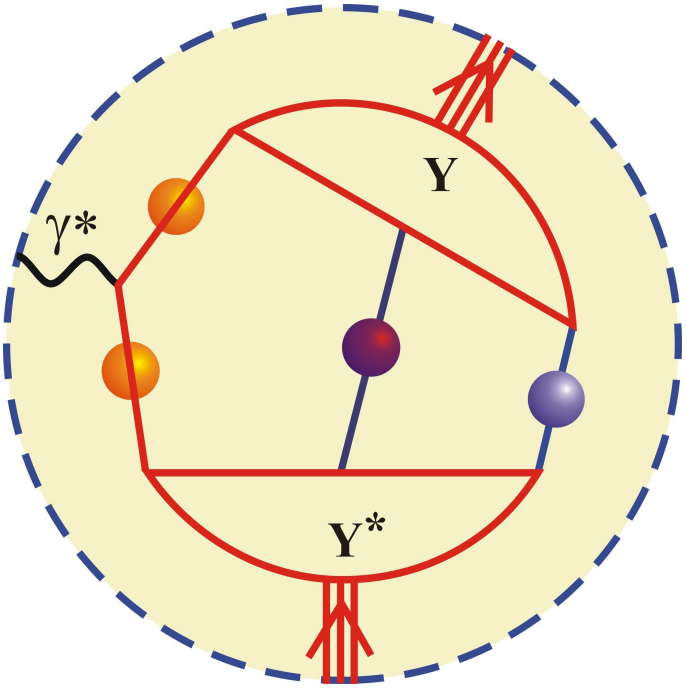

Tim Van Cauteren

Promotor: Prof. dr. Jan Ryckebusch

Proefschrift ingediend tot het behalen van de graad van
Doctor in de Wetenschappen: Natuurkunde

Universiteit Gent
Faculteit Wetenschappen
Vakgroep Subatomaire en Stralingsfysica
Academiejaar 2004-2005

UNIVERSITEIT GENT

Electromagnetic Properties of Strange Baryons

Elektromagnetische Eigenschappen van Vreemde Baryonen

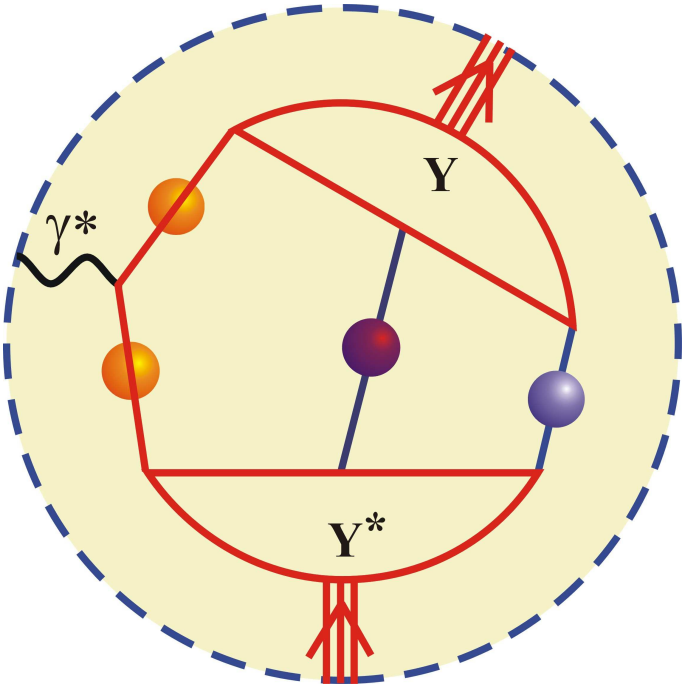

Tim Van Cauteren

Promotor: Prof. dr. Jan Ryckebusch

Proefschrift ingediend tot het behalen van de graad van
Doctor in de Wetenschappen: Natuurkunde

Universiteit Gent
Faculteit Wetenschappen
Vakgroep Subatomaire en Stralingsfysica
Academiejaar 2004-2005

UNIVERSITEIT GENT

I have imagined things
you could not even see.

I have dreamt of things
you could not even imagine.

I have seen things
you could not even dream of.

Anonymous

Canet ut Minerva

- He will sing like Minerva

Preface

It is *Standard Operating Procedure* (SOP) for the PhD. student to thank everyone who helped in the creation of his thesis. Yet, when I say "thank you", it's not because it's standard, it's because I mean it.
Thank you, Jan, for patiently helping and guiding me for almost five years. Thank you, Bernard, Herbert, Dirk, and all the other people from Bonn, for the help and the discussions leading to this thesis. Thank you, Pascal, on behalf of myself and Mr. Reeth Theo. Thank you, Stijn, for all interactions and continuous propagation. Thank you, Tamara and Annelies, for reading and correcting this manuscript, and for all the Twixen and Cokes you didn't bring me : it makes 5 kg of difference. Thank you, Wim, for the "strong" support. Thank you, Klaas, for backing me up when I needed it. Thank you Lode and Ruben, for the many years of simultaneous effort. Thank you, Christophe, Bart, and the many others of the institute for creating a unique atmosphere. And of course, thank you, Cris, for making me strong.
Thank you, Jan, Rik, Isabel en all the others whose name I still remember. Thank you, Hans, for 24 years. Thank you, fellow football players, for never letting me win.
Bedankt, vou, voor alle zorgen en steun door de jaren heen. Bedankt, Tine en Bernard, Tom en Els, voor de interesse en het geduld. Bedankt, Lisa en Rik, voor het spelen. Bedankt, mit, voor de enveloppen. Bedankt, mit Morena en nonkel Paul, voor de opvang in kwade dagen, en vooral voor al het eten. Zonder jullie en de rest van de familie lag er hier geen thesis.
At the end of the Preface, it is SOP to thank all the people one did not mention by name. I'd really like to write down all your names, but I'm afraid this would take too much time and too much paper. So please, forgive me and accept my gratitude.

Tim Van Cauteren,
maart 2005

Contents

Chapter 1

Introduction

Scales and Models

In the process of constructing a physical model for a certain phenomenon, two major questions have to be addressed. First, what are the relevant degrees of freedom ? And second, how do these degrees of freedom affect each other ?

The appropriate degrees of freedom depend largely on the distance and time scale at which phenomena occur. At extremely large distances and times, one talks about stars and planets. At a more down-to-earth scale, there are geological layers, drifting continental plates, volcanoes and earthquakes. At the smallest scales, particle physicists discuss the behaviour of fermions and bosons, of charged and neutral objects, of leptons and quarks.

The abundance of interesting phenomena in nature is caused by the interactions amongst the different degrees of freedom. Stars and planets form planetary systems through gravitation. Heath differences between the earth's core and mantle layers cause convection currents pushing the continental plates in certain directions. The friction between plates results in earthquakes and volcano eruptions. In the Standard Model, matter particles are fermions which interact through exchange of bosonic force carriers. Charged particles exchange photons. Quarks interact strongly through exchange of gluons, while leptons do not.

The examples listed above, are rather well understood in modern science. Yet, some processes occur at a scale which is on the boundary of validity for models with different degrees of freedom. For instance, a thin vibrating string with both

ends attached is very well described by the wave equation with Dirichlet boundary conditions. If the string gets thicker, the dynamics become involved and a description in terms of a density distribution and stress tensors is required. It is clear that the first model is more tractable, but that the latter model is applicable in a broader range of cases. However, in the limit of a zero-thickness string, the two models should give equal results. Then, it should be possible to relate the degrees of freedom of the first model, such as line density and tension, to the density distribution and stress tensor, as defined in the second model. The phenomenon of a real vibrating string can only be marked as understood if these relations are known.

In this work, we will take the $p(e, e'K)Y$ process as the system under investigation. In this reaction, an electron induces the creation of a kaon and a hyperon from a proton target. This process is situated in a domain of physics which is concerned with phenomena at distance scales of roughly 1 fm. One of the models to describe the process adopts *hadrons*, while the other uses *constituent quarks* as degrees of freedom.

Hadrons and Quarks

The term "hadron" was, rather contradictorily, coined in the late forties with the observation that the muon could not be responsible for binding the protons and neutrons inside a nucleus. The non-strongly-interacting behaviour of this particle made it clear that matter particles could be divided into two main classes, according to whether they interact strongly (hadrons) or not (leptons). At that time, one had not yet discovered lots of subatomic particles. The leptonic sector consisted of the electron, positron, electron (anti-)neutrino and muon. The proton and neutron were the sole known hadrons. The search for another hadron, which was predicted by Hideki Yukawa (Nobel Prize, 1949) as the carrier of the strong interaction between protons and neutrons, resulted in the discovery of the pion. However, this discovery sparked off the detection of a multitude of strongly interacting particles in the fifties. Since there seemed to be no end to the total amount of these particles, one spoke of a *hadron zoo*.

A first classification in the hadron zoo can be made according to the spin of the particles. Bosonic hadrons are called mesons, fermionic hadrons are baryons. Their masses span an energy range from 135 MeV to more than 10 GeV [1]. Other

quantum numbers such as *isospin* and *strangeness*, which are conserved in strong interactions, allow us to put more order in the zoo. In fact, possibly the largest breakthrough in hadronic physics was made when M. Gell-Mann (Nobel Prize, 1969) proposed his *Eightfold Way* to classify the lowest states in the baryon spectrum. This classification scheme made clear that the baryons and mesons with the lowest masses answer to an approximate symmetry called *flavour-*$SU(3)$, or $SU(3)_f$.

Just like Mendelejev's table hinted at an underlying structure for the atoms in terms of nuclei and electrons, the Eightfold Way suggested the existence of smaller particles whose properties were responsible for the ordering of hadrons into groups with similar characteristics. This idea resulted in the development of the *Quark Model*. In this model, baryons consist of three quarks and mesons of a quark/antiquark pair. The strong interaction between the quarks prevents them to appear as free particles, and assures that quarks cluster into hadrons.

Later, one realized that the constituents in hadrons and their interactions could be described with the aid of a quantum field theory, called *Quantum Chromodynamics* (QCD). In this theory, quarks and antiquarks interact strongly through the exchange of gluons. Hadrons are bound states of *valence* quarks, quark/antiquark pairs or *sea* quarks, and gluons. A quark as it was originally defined in the Quark Model, is identified with a valence quark, surrounded by a cloud of gluons and quark/antiquark pairs. As such, it is usually called a *constituent quark*, to distinguish it from the QCD-quarks.

Strange Reactions

The kaon and hyperon are so-called strange particles. From a hadronic point of view, this means that they have a non-zero strangeness quantum number. In the constituent-quark picture, kaon and hyperon contain at least one *strange* constituent quark or antiquark. A proton is a *nonstrange* particle, and the electroinduced creation of strangeness from a proton can only occur through a rearrangement of strange sea-quarks and -antiquarks, hidden inside the proton. The reaction can be written in terms of hadrons, yet it provides information about the quark content of the proton. Therefore, the $p(e,e'K)Y$ reaction is an ideal process to study the (phase) transition between hadronic and constituent-quark degrees of freedom.

A hadronic, or isobar, model for the $p(e,e'K)Y$ reaction was developed in

Refs. [2–6]. Here, the reaction dynamics were described within a Lagrangian formalism and with the aid of Feynman diagrams. At lowest order, the so-called tree level, each diagram contains one electromagnetic and one hadronic vertex, and an exchanged hadron. The intermediate hadron can be a ground-state baryon/meson, in which case the diagram is denoted as a *Born term*, or a baryon/meson resonance. These resonances are manifestations of the composite nature of hadrons. After all, every quantum-mechanical many-body system produces a spectrum of states, which is discrete when the particles are confined. Identifying the participating resonances in the $p(e, e'K)Y$ reaction gives us a handle to map out the nucleon spectrum and acquire knowledge about its inner structure.

In an isobar model, two classes of diagrams can be identified. *Background* terms produce a smooth energy dependence in the cross sections because the kinematical conditions are such that the exchanged particle is always far off its mass shell. *Resonant* terms can produce structure in the energy dependence of the cross sections when the conditions are such that the intermediate particle is on-shell and its propagator goes through a pole. In Refs. [2–6], it was shown that a proper description of the background is a primary condition for extracting reliable information about the resonant part, such as electromagnetic and hadronic coupling constants and form factors.

With the isobar model discussed above, the experimental $p(\gamma, K)Y$ data from the SAPHIR Collaboration at ELSA in Bonn, Germany [7, 8], could be very well reproduced, in three different versions for the background description. The identification in Ref. [9] of a nonstrange *missing resonance* with a mass around 1900 MeV and strong coupling to the $K\Lambda$ channel, was confirmed in all three background descriptions, but the quantum numbers of this resonance remain elusive [10]. Recently, improved data sets for the $p(e, e'K)Y$ and $p(\gamma, K)Y$ reactions were released by CLAS [11–13], SAPHIR [14, 15], and LEPS [16]. The large amount of new, high-quality data points will allow us to discriminate between the different background models and subsequently result in a better extraction of the properties of the participating resonances.

The coupling constants and form factors serve as fitting parameters for any isobar model. The first are the strength of the coupling of the exchanged, on-shell particle to the photon, or to the KY channel. The latter describe the dependence of

the vertex strength on the kinematics and the degree of off-shellness of the participating particles. The coupling constants and form factors can be compared with the string tension and line density of the vibrating-string problem mentioned earlier in this introduction. They characterize the system, and their values can be calculated from a deeper-lying model, just like the line density and string tension can be calculated from the density distribution and stress tensor. Predicting these quantities is a major challenge for any model concerned with the inner structure of hadrons.

The transition from isobar degrees of freedom to constituent-quark degrees of freedom is only fully characterized if an isobar model correctly predicts the cross section and polarization data, when using the coupling constants and form factors as computed in a constituent-quark model. In this work, we will focus on the calculation of electromagnetic form factors of strange baryons, which enter the isobar description of the $p(e, e'K)Y$ process at every photon-hyperon vertex. For this, we will use the Lorentz-covariant constituent quark model developed by the Bonn group, which is based on the *Bethe-Salpeter* approach for describing a system of interacting, relativistic particles.

The Bonn model starts out from the observation that the bound states of a system with a fixed number n of relativistic particles, produces poles in the $2n$-point Green's function. The residue at these poles provides us with the Bethe-Salpeter amplitude, which describes a bound state of a relativistic many-body system. The self-consistent Bethe-Salpeter equation for the $2n$-point Green's function can be related to an equation for the Bethe-Salpeter amplitude, at kinematics near the poles. Solving this equation yields the Bethe-Salpeter amplitudes, paving the way for the computation of matrix elements of *e.g.* the current operator. Since electromagnetic form factors are, in general, linear combinations of reduced current matrix elements, the Bonn model offers the possibility of computing the form factors of hadrons, respecting Lorentz covariance.

Outline

In this work, constituent-quark-model predictions for electromagnetic form factors of strange baryons and a gauge-invariant manner to incorporate them in the isobar models, will be presented. In Chap. 2, the Bonn model will be discussed in detail. The constituent-quark degrees of freedom and the effective instantaneous

interactions lead to the Bethe-Salpeter equation for the Bethe-Salpeter amplitude. This equation is solved in lowest order, and the resulting amplitudes will be used to compute current and hadronic matrix elements. The connection between the current matrix elements and on-shell electromagnetic form factors will also be outlined.

In Chap. 3, the isobar model for $p(e, e'K)Y$ reactions will be discussed. The gauge-invariant introduction of hadronic form factors in the tree-level isobar model vertex will be dealt with. The introduction of electromagnetic form factors in a gauge-invariant manner will also be presented. Finally, the expressions for the observables of the $p(e, e'K)Y$ process in terms of hadronic tensors will be given.

The results of the numerical calculations for the electromagnetic form factors of hyperons will be given in Chap. 4. The computed electric and magnetic form factors of the ground-state hyperons will be discussed, and compared with the experimental data and with predictions from other models. The helicity amplitudes of the lowest lying hyperon resonances will also be presented. Hereby, special attention will be paid to their asymptotic behaviour at high squared four-momenta. The numerical accuracy of the predictions will be investigated with two representative examples.

The conclusions of this work are presented in Chap. 5, where also an outlook is given. Appendix A sketches the quark-quark effective interactions in the Bonn model. The potential responsible for confinement and the residual interaction are discussed. The first one is a linear function of the interquark distance, multiplied with an appropriate Dirac structure. The latter is the two-particle interaction, discovered by Gerard 't Hooft [17], which is induced by instanton effects. In Appendix B, the effective interactions between the hadron fields used in the isobar model are given in the Lagrangian formalism. The interaction Lagrangians lead to tree-level amplitudes, which are also presented. The Lagrangians and amplitudes as discussed in Appendix B are an extension of the ones given in Ref. [6]. In particular, contributions stemming from the longitudinal coupling of the virtual photon to the particles, are explicitly included.

Chapter 2

The Bonn Constituent Quark Model

This chapter highlights the model we have used to compute electromagnetic and strong properties of baryon resonances. It starts from the idea that hadrons are composed of point-like constituent quarks (Sect. 2.1). It shows in detail how the physical concept of interacting constituent quarks results in the creation of bound states, using techniques from relativistic many-body theory (Sect. 2.2). Furthermore, the *Bethe-Salpeter amplitudes* for the bound states in terms of constituent-quark degrees of freedom, can be employed in the computation of $\mathcal{S}$-matrix elements. The current matrix element is, almost traditionally, the first $\mathcal{S}$-matrix element to be investigated (Sect. 2.3), since the well-known electromagnetic interaction is the best probe for lesser-known strongly interacting systems. This leads to the concept of electromagnetic form factors and helicity amplitudes, which describe the charge and magnetization density distributions inside the baryon (Sect. 2.4). Also other $\mathcal{S}$-matrix elements can be computed within the Bonn constituent quark model. The hadronic decay of baryon resonances to a meson-baryon final state is qualitatively explained within constituent quark models by the creation of a constituent quark/antiquark pair from the vacuum, and a subsequent rearrangement of the constituent quarks. A quantitative description of this process (Sect. 2.5) is one of the many different possibilities of the Bonn constituent quark model.

2.1 Constituent Quarks

The story of the development of a theory for the strong interaction is a long one, and is still being written. A great leap forward was made in the beginning of the sixties, when Murray Gell-Mann [18, 19] and Yuval Ne'eman [20] suggested a classification scheme for the *Hadron Zoo*, work for which M. Gell-Mann received the Nobel Prize in 1969. This classification scheme, which still stands today, is based on the representations of the $SU(3)$ group. The difficulty in arriving at $SU(3)$ as the governing symmetry group lies in the apparent non-realisation of its fundamental representations in nature. The existence of objects belonging to a fundamental representation, however, had been proposed earlier by George Zweig [21, 22], but remained a question of debate for years in a row.

Biology is broader than classifying the species, chemistry is wider than naming the molecules, and likewise, physics is more than grouping the different particles. Merely establishing order in the Hadron Zoo is not sufficient to predict *e.g.* the outcome of scattering experiments. The main merit of the classification scheme is, that it provides insight into how the underlying theory yields bound states. Thus, after the introduction of $SU(3)$ as the protagonistic symmetry, the search for a theory for strong interactions based on $SU(3)$ continued. The proof that non-Abelian Yang-Mills gauge theories are renormalizable, given by G. 't Hooft and M. Veltman in the beginning of the seventies (Nobel Prize, 1999), paved the way for a gauge theory for strong interactions based on $SU(3)$-color symmetry : *Quantum Chromodynamics* or QCD.

QCD is a theory with a *running coupling constant*, which is small for high momentum transfer Q^2, but large for small Q^2. This has direct implications for the corresponding techniques for solving the field equations. At high Q^2, perturbative calculus is in order; for low Q^2, on the other hand, one has to resort to models for strongly interacting systems for which the governing equations lack a fundamental justification in terms of the QCD equations, but do embody some of the QCD characteristics. In recent years, however, computer power has expanded to the level at which it is possible to calculate static properties of strongly-bound states using equations which are derived directly from QCD. These equations are perturbative in the sense that one introduces a lattice spacing parameter to make space-time discrete, which one can make smaller in a consistent way. This technique,

called *lattice-QCD*, still introduces approximations (*e.g.* quenching) at this moment, but quantitative results have already been obtained for the masses of the lightest hadrons (Refs. [23–26]) and it is expected that more results for hadron masses and moments will follow in the near future.

The classification scheme of M. Gell-Mann shows up in QCD by identifying the three lightest flavours of matter fields (quarks) with the three states of the fundamental representation of the $SU(3)$-flavor symmetry. The apparent non-realisation already mentioned, is attributed to a phenomenon called *confinement*, which states that quarks are always clustered into hadrons. Confinement is believed, but not proved, to be inherent to the QCD field equations. This highly non-perturbative property is widely accepted as playing an important role in determining the low-lying bound states of the theory (ground states and lowest excited states), and is usually the first aspect to be incorporated into any model of hadronic interactions. For higher-excited states, many other phenomena have been predicted (*e.g.* the restoration of chiral symmetry [27] and the existence of exotic hadrons as the recently discovered pentaquark [28–31]). The extraction of the properties for these higher-lying states from experiments is cumbersome and requires a thorough analysis of background and interference processes. As a consequence, the resulting experimental quantities (resonance masses, partial decay widths, etc. ...) are rather poor, and models are mainly assessed by measure of agreement with the experimentally better-known properties of ground and low-lying excited states.

To date, many existing models for hadrons use the concept of *constituent quarks* (CQ's) in identifying the suitable degrees of freedom. Usually, one connects these effective with QCD degrees of freedom by noting that CQ's are conglomerates of quarks, antiquarks and gluons, such that the quantum numbers of the composed hadron depend only on those of the conglomerate. Thereby, one presumes that the quark and gluon degrees of freedom can be efficiently described by means of constituent quarks in the energy domain where the full QCD equations cannot be solved perturbatively. This procedure results in equations that are easier to handle than those obtained within the framework of nonperturbative QCD, but still carry all the complications connected with the (relativistic) treatment of a two- and three-body problem. The major justification for CQ models is their effectiveness in describing hadron spectra, symmetry properties and electromagnetic form factors.

We will use a CQ model to predict these latter quantities.

2.2 The Bethe-Salpeter Equation for Bound States

2.2.1 Green's Functions and Bethe-Salpeter Amplitudes

The Bethe-Salpeter (BS) formalism outlined in this thesis, is based on the discussion of Le Yaouanc *et al.* [32]. It was described in great detail and applied for mesons and baryons by the Bonn group in Refs. [33–35]. The basic idea of the formalism is to connect n-point Green's functions to the BS amplitudes, describing the bound states of a relativistic many-body system. Through an ingenious application of the time-ordering operator, the Green's function can be written as a sum over terms, of which some contain products of normal and adjoint BS amplitudes of one of the particles involved. The latter terms also have denominators which produce poles at those values of the kinematic variables where the particles are on shell. Knowledge of the Green's function in the vicinity of these poles yields the BS amplitudes of the particles. It then boils down to finding an equation for the Green's function which can be solved consistently to a certain order in the coupling constants of the interactions. In the course of this work, zeroth- and first-order approximations will be adopted. This will be indicated explicitly only when it is deemed necessary.

In the Bonn CQ model, the basic quantity describing a baryon is the three-quark BS amplitude :

$$\chi_{\overline{P},a_1,a_2,a_3}(x_1,x_2,x_3) \;\equiv\; \langle 0|T\big(\Psi_{a_1}(x_1)\Psi_{a_2}(x_2)\Psi_{a_3}(x_3)\big)|\overline{P}\rangle \;, \tag{2.1}$$

where T is the time-ordering operator acting on the Heisenberg quark-field operators Ψ_{a_i}, and $\overline{P}$ is the total four-momentum of the baryon with $\overline{P}_\mu\overline{P}^\mu = M^2$. (We use the standard convention $a\cdot b = a_\mu b^\mu = a_0 b^0 - \mathbf{a}\cdot\mathbf{b}$ to denote the Minkowski scalar product of two fourvectors.) The a_i denote the quantum numbers in Dirac, flavor and color space. In order not to overload the notation, these quantum numbers are frequently dropped. The Fourier transform of the above quantity is defined by :

$$\begin{aligned}\chi_{\overline{P}}(x_1,x_2,x_3) &= e^{-i\overline{P}\cdot X}\chi_{\overline{P}}(\xi,\eta)\\ &\equiv e^{-i\overline{P}\cdot X}\int\frac{\mathrm{d}^4p_\xi}{(2\pi)^4}\frac{\mathrm{d}^4p_\eta}{(2\pi)^4}e^{-ip_\xi\cdot\xi}e^{-ip_\eta\cdot\eta}\chi_{\overline{P}}(p_\xi,p_\eta)\;.\end{aligned} \tag{2.2}$$

Here, we have used the symmetry requirement of translational invariance of the BS amplitude in configurational space. This results in a BS amplitude depending on the total four-momentum $\overline{P}$ only parametrically, as is clear in the notation. The standard definition of the Jacobi coordinates and momenta is adopted :

$$\left\{ \begin{array}{rcl} X &=& \frac{1}{3}(x_1+x_2+x_3)\ , \\ \xi &=& x_1-x_2\ , \\ \eta &=& \frac{1}{2}(x_1+x_2-2x_3)\ , \end{array} \right. \tag{2.3a}$$

and

$$\left\{ \begin{array}{rcl} P &=& p_1+p_2+p_3\ , \\ p_\xi &=& \frac{1}{2}(p_1-p_2)\ , \\ p_\eta &=& \frac{1}{3}(p_1+p_2-2p_3)\ . \end{array} \right. \tag{2.3b}$$

Remark that in Eq. (2.3a), we have not introduced any dependence on the energies of the CQ's. The generalized coordinates (X,ξ,η) are therefore not canonically conjugated to the generalized Jacobi momenta (P,p_ξ,p_η) of Eq. (2.3b), but can always be used to write down the dependence of certain quantities on the (canonical) quark coordinates (x_1,x_2,x_3) in a more elegant way. If one wants to work at all times with canonically conjugated coordinates and momenta, one should use expressions such as $\Omega X=\omega_1 x_1+\omega_2 x_2+\omega_3 x_3$, where Ω stands for the total energy and ω_i for the energy of quark i.

The BS amplitude $\chi_{\overline{P}} \equiv \chi_{\overline{P}}(x_1,x_2,x_3)$ is the solution to the BS equation [36] which is derived from the BS equation for the six-point Green's function :

$$\begin{aligned} G^{(6)}_{a_1,a_2,a_3;a_1',a_2',a_3'}\left(x_1,x_2,x_3;x_1',x_2',x_3'\right) \ &= \\ -\ \langle\, \mathbf{0}\,|\,\mathbf{T}\left\{\Psi_{a_1}(x_1)\Psi_{a_2}(x_2)\Psi_{a_3}(x_3)\bar{\Psi}_{a_1'}(x_1')\bar{\Psi}_{a_2'}(x_2')\bar{\Psi}_{a_3'}(x_3')\right\}|\,\mathbf{0}\,\rangle\ , \end{aligned} \tag{2.4}$$

where the operators and states are taken in the *Heisenberg picture*. We are only interested in that part of the six-point Green's function with the relevant time-ordering, *i.e.* the terms which describe three incoming and three outgoing quarks. Moreover, we want to find the bound states of three quarks and therefore introduce a complete set into Eq. (2.4). We will denote this part of $G^{(6)}$ as $\widetilde{G}^{(6)}$:

$$\begin{aligned} \widetilde{G}^{(6)}\left(x_1,x_2,x_3;x_1',x_2',x_3'\right) \ &= \ -\int \frac{\mathrm{d}^3P}{(2\pi)^3\,2\omega_{\overline{P}}}\,\Theta\left(X^0-X'^0\right) \\ &\times\ \langle\,\mathbf{0}\,|\,\mathbf{T}\big\{\Psi(x_1)\Psi(x_2)\Psi(x_3)\big\}\,|\,\overline{P}\,\rangle\,\langle\,\overline{P}\,|\,\mathbf{T}\big\{\bar{\Psi}(x_1')\bar{\Psi}(x_2')\bar{\Psi}(x_3')\big\}\,|\,\mathbf{0}\,\rangle\ , \end{aligned} \tag{2.5}$$

with $\omega_{\overline{P}} = \sqrt{M^2 + |\mathbf{P}|^2}$ the energy of the on-shell bound state. The Θ function ensures that the variables of the outgoing quarks have *later* time-components than those of the incoming quarks (actually the argument of the Θ function in Eq. (2.5) is exactly $(X^0 - X'^0)$ only at the three-quark bound-state poles as is explained in Appendix A of Ref. [37]). It can be written as an integral over a complex function :

$$\Theta(x) = \frac{i}{2\pi} \int \mathrm{d}q^0 \frac{e^{-iq^0 x}}{q^0 + i\epsilon} , \qquad \epsilon > 0 . \tag{2.6}$$

The matrix elements in Eq. (2.5) between bound states and the vacuum can be identified as the BS amplitude and its adjoint :

$$\begin{aligned} \widetilde{G}^{(6)}\left(x_1, x_2, x_3; x_1', x_2', x_3'\right) = -i \int \frac{\mathrm{d}^3 P}{(2\pi)^3 \, 2\omega_{\overline{P}}} \frac{\mathrm{d}q^0}{(2\pi)} \frac{e^{-iq^0\left(X^0 - X'^0\right)}}{q^0 + i\epsilon} \\ \times \chi_{\overline{P}}\left(x_1, x_2, x_3\right) \overline{\chi}_{\overline{P}}\left(x_1', x_2', x_3'\right) . \end{aligned} \tag{2.7}$$

The Fourier transform of quantities which are translationally invariant and which describe the propagation of an object consisting of three particles is defined as :

$$\begin{aligned} A\left(P, p_\xi, p_\eta; P', p_\xi', p_\eta'\right) &= (2\pi)^4 \, \delta^{(4)}\left(P - P'\right) A_P\left(p_\xi, p_\eta; p_\xi', p_\eta'\right) \\ &= \int \mathrm{d}^4 X \mathrm{d}^4 \xi \mathrm{d}^4 \eta \mathrm{d}^4 X' \mathrm{d}^4 \xi' \mathrm{d}^4 \eta' e^{iP\cdot X + ip_\xi \cdot \xi + ip_\eta \cdot \eta} \\ &\quad \times A\left(X - X'; \xi, \eta; \xi', \eta'\right) e^{-iP'\cdot X' - ip_\xi' \cdot \xi' - ip_\eta' \cdot \eta'} . \end{aligned} \tag{2.8}$$

Applying this definition to Eq. (2.7), we get :

$$\widetilde{G}_P^{(6)}\left(p_\xi, p_\eta; p_\xi', p_\eta'\right) = \frac{-i}{2\omega_{\overline{P}}} \frac{\chi_{\overline{P}}\left(p_\xi, p_\eta\right) \overline{\chi}_{\overline{P}}\left(p_\xi', p_\eta'\right)}{P^0 - \omega_{\overline{P}} + i\epsilon} . \tag{2.9}$$

One can easily see that for on-shell momenta ($P^0 = \omega_{\overline{P}}$), the six-point Green's function reaches a pole, and that its residue is proportional to the product of the normal and the adjoint BS amplitude of the on-shell particle. Knowledge of the Green's function near this pole yields the BS amplitude and the mass of the bound state. It should be stressed that if we move further away from the pole, we do not have a physical interpretation of the Green's function in terms of BS amplitudes.

The equation for the six-point Green's function is derived in Ref. [34]. Thereby, a non-perturbative technique for summing an infinite number of Feynman diagrams is employed, which in lowest order reduces to the *ladder* approximation. The result

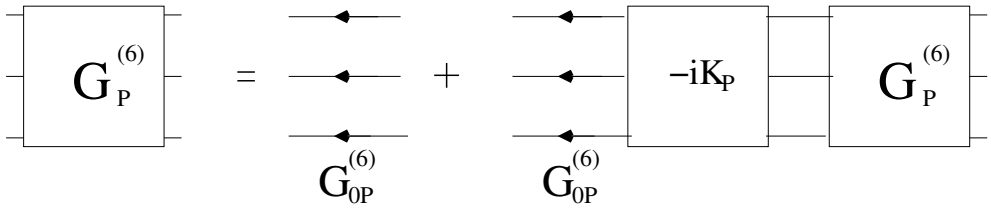

Figure 2.1 *Diagrammatic representation of the BSE for the six-point Green's function. Arrows denote CQ propagators. Connected objects, as in the second term on the RHS, entail integration and summation over dummy variables and quantum numbers.*

is the Bethe-Salpeter Equation (BSE) for $G^{(6)}$, which is an integral equation with integral kernels that are intimately connected to the quark-quark interactions. The shorthand version of this equation and the (equivalent) adjoint equation is [34] :

$$G_P^{(6)} = G_{0P}^{(6)} - i\, G_{0P}^{(6)}\, K_P\, G_P^{(6)} \,, \tag{2.10a}$$

$$G_P^{(6)} = G_{0P}^{(6)} - i\, G_P^{(6)}\, K_P\, G_{0P}^{(6)} \,. \tag{2.10b}$$

For notational simplicity, we have left out all variables and quantum numbers as well as the integrals and summations over dummy variables (Einstein convention). Eqs. (2.10) can be more easily interpreted diagrammatically. To illustrate this, we show Eq. (2.10a) in Fig. 2.1.

In Eqs. (2.10) $G_{0P}^{(6)}$ is the unperturbed three-quark propagator, and K_P is the integral kernel. The quantity $G_{0P}^{(6)}$ is the direct product (denoted with the symbol $\otimes$) of the dressed propagators of the three quarks. In momentum space, it reads :

$$\begin{aligned} G_{0P}^{(6)}(p_\xi, p_\eta; p'_\xi, p'_\eta) \;=\; & S_F^1\left(\frac{1}{3}P + p_\xi + \frac{1}{2}p_\eta\right) \otimes S_F^2\left(\frac{1}{3}P - p_\xi + \frac{1}{2}p_\eta\right) \\ & \otimes\; S_F^3\left(\frac{1}{3}P - p_\eta\right) (2\pi)^4\, \delta^{(4)}\left(p_\xi - p'_\xi\right) (2\pi)^4\, \delta^{(4)}\left(p_\eta - p'_\eta\right) \,. \end{aligned} \tag{2.11}$$

The dressed propagators S_F^i (with $i = 1, 2, 3$) are approximated by the propagators of free constituent quarks. Thereby, we adopt the form

$$S_F^i(p_i) = \frac{i}{\not{p}_i - m_i + i\epsilon} \,, \tag{2.12}$$

where m_i is the effective mass of the i'th constituent quark.

As was mentioned before, the integral kernel K_P is closely connected to the quark-quark interactions in the baryon. The exact form of these interactions is

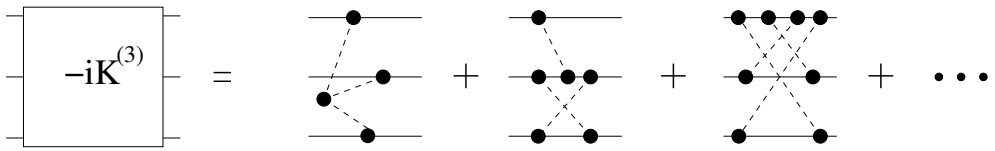

Figure 2.2 *The three-particle irreducible kernel $K^{(3)}$ is the sum over all three-particle irreducible diagrams of which some are depicted here.*

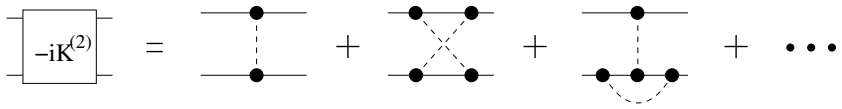

Figure 2.3 *Same as in Fig. 2.2, but for the two-particle irreducible kernel $K^{(2)}$.*

model-specific, and is not derived directly from QCD. The approximate nature of the solutions to the BSE finds its origin in the choice of the model for the interaction kernels and the order at which one cuts the infinite sum of diagrams. This is nothing new, since all CQ models face the problem of finding proper forms for the effective interactions between the CQ's.

The interaction kernels used in our model are described in Refs. [34] and [38], and are discussed briefly in Appendix A. There are two kinds of contributions to K_P. Feynman diagrams for three quarks which cannot be made unconnected by cutting three (internal) quark lines are called three-particle irreducible (Fig. 2.2). Diagrams which remain connected after cutting two (internal) quark lines are called two-particle irreducible (Fig. 2.3). Since we do not include quark loops in our model, K_P can always be written as the sum of two- and three-quark irreducible kernels.

We now have an equation for the six-point Green's function (2.10), which can be expressed near its poles in terms of the BS amplitudes $\chi_{\overline{P}} \equiv \chi_{\overline{P}}(p_\xi, p_\eta)$ and their adjoints (2.9). It is now possible to derive an equation for the BS amplitudes (as was done in Ref. [36]). In momentum space, the BSE for the amplitudes can be schematically written as

$$\chi_{\overline{P}} \;=\; -i\, G_{0\overline{P}}^{(6)} \left(K_{\overline{P}}^{(3)} + \bar{K}_{\overline{P}}^{(2)} \right) \chi_{\overline{P}} \;, \tag{2.13}$$

which is valid for on-shell momenta $\overline{P}$ only. Its diagrammatical analogue is shown

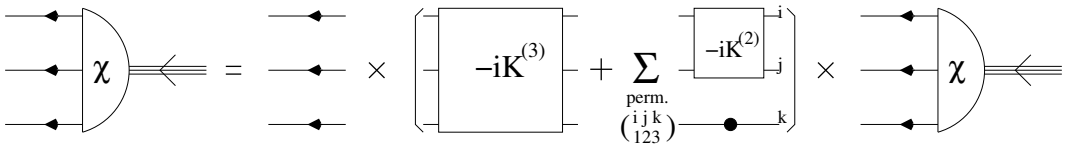

Figure 2.4 *The BS equation in a schematic form. Arrows represent quark propagators, a filled dot denotes an inverse propagator.*

in Fig. 2.4. The quantity denoted by $K^{(3)}_{\overline{P}}$ is the three-particle irreducible interaction kernel for on-shell momenta $\overline{P}$. Further, $\overline{K}^{(2)}_{\overline{P}}$ is a sum of two-particle irreducible interaction kernels, each multiplied by the inverse propagator of the spectator quark as can be seen in Fig. 2.4 and the expression :

$$\begin{aligned}\overline{K}^{(2)}_{\overline{P}}\left(p_\xi,p_\eta;p'_\xi,p'_\eta\right) \;=\; & K^{(2)}_{\left(\frac{2}{3}\overline{P}+p_\eta\right)}\left(p_\xi,p'_\xi\right)\otimes\left[S_F^3\left(\frac{1}{3}\overline{P}-p_\eta\right)\right]^{-1} \\ & \times\;(2\pi)^4\,\delta^{(4)}\left(p_\eta-p'_\eta\right) \qquad + \textit{cycl. perm. in quarks (123)}\;. \end{aligned} \tag{2.14}$$

Here, one should note that $\frac{2}{3}\overline{P}+p_\eta = p_1+p_2$, that $\frac{1}{3}\overline{P}-p_\eta = p_3$, and that the argument of the δ-function can be read as $\frac{1}{3}\left(p_1+p_2-2p_3\right)-\frac{1}{3}\left(p'_1+p'_2-2p'_3\right)$, which makes it easier to perform the cyclic permutation in the quarks.

Combining Eqs. (2.9) and (2.10) not only yields the BSE for the amplitudes, but also provides us with the normalization condition [34]

$$-i\,\overline{\chi}_{\overline{P}}\left[P^\mu\,\frac{\partial}{\partial P^\mu}\left(G_{0P}^{(6)^{-1}}+iK_P\right)\right]_{P=\overline{P}}\chi_{\overline{P}} \;=\; 2M^2\;. \tag{2.15}$$

The BSE's for the Green's function and the BS amplitudes, and the normalization condition (2.15) are Lorentz covariant. The tranformation properties of the quantities involved are well-known, so that if we can find a solution for *e.g.* the BS amplitude in one Lorentz frame, we can find it in any other. We will use the relativistic covariance of the model extensively to calculate a particle's BS amplitude or related quantities in its center-of-mass frame and then boost it to the desired frame in order to evaluate matrix elements.

In any CQ model, there exists some freedom with respect to the plausible types of interactions between the constituent quarks. We will use the instantaneous approximation. In the center-of-mass frame, the instantaneous approximation implies

that the interaction kernels $K^{(3)}_{\overline{P}}$ and $K^{(2)}_{p_i+p_j}$ are independent of the energy components of the Jacobi-momenta :

$$K^{(3)}_{\overline{P}}\left(p_\xi, p_\eta; p'_\xi, p'_\eta\right)\Big|_{P=(M,\mathbf{0})} = V^{(3)}\left(\mathbf{p}_\xi, \mathbf{p}_\eta; \mathbf{p}'_\xi, \mathbf{p}'_\eta\right) \ , \tag{2.16a}$$

$$K^{(2)}_{(\frac{2}{3}P+p_\eta)}\left(p_\xi, p'_\xi\right)\Big|_{P=(M,\mathbf{0})} = V^{(2)}\left(\mathbf{p}_\xi, \mathbf{p}'_\xi\right) \ . \tag{2.16b}$$

We should mention here that whenever a quantity is to be evaluated in the rest frame of the baryon, we will indicate this by the index M, to make it clear that in this case $\overline{P} = (M, \mathbf{0})$.

In contrast to what might be expected at first sight, the instantaneous approximation does not violate the Lorentz covariance of the theory. This is made explicit by writing the inter-quark potentials as depending only on the components of the variables perpendicular ($\perp$) to the total four-momentum of the particle :

$$p^\mu_\parallel = \frac{p\cdot P}{P^2}P^\mu \ , \tag{2.17a}$$

$$p^\mu_\perp = p^\mu - \frac{p\cdot P}{P^2}P^\mu \ . \tag{2.17b}$$

When boosting the particle to an arbitrary four-momentum, the interactions will remain dependent on the perpendicular components only.

The potentials used in our calculations are those of model $\mathcal{A}$ of Ref. [38], since these gave the best results for the baryon spectrum. The three-particle interaction is given by a *confinement* potential $V^{(3)}_{\text{conf}}$ which rises linearly with the sum of the distances between the three CQ's [37]

$$\begin{aligned} V^{(3)}_{\text{conf}}\left(\mathbf{x}_1, \mathbf{x}_2, \mathbf{x}_3\right) &= a\frac{3}{4}\left(\mathbb{1}\otimes\mathbb{1}\otimes\mathbb{1} + \gamma^0\otimes\gamma^0\otimes\mathbb{1} + \gamma^0\otimes\mathbb{1}\otimes\gamma^0 + \mathbb{1}\otimes\gamma^0\otimes\gamma^0\right) \\ &+ b\sum_{i<j}|\mathbf{x}_i - \mathbf{x}_j|\frac{1}{2}\Big(-\mathbb{1}\otimes\mathbb{1}\otimes\mathbb{1} + \gamma^0\otimes\gamma^0\otimes\mathbb{1} + \gamma^0\otimes\mathbb{1}\otimes\gamma^0 + \mathbb{1}\otimes\gamma^0\otimes\gamma^0\Big) \ . \end{aligned} \tag{2.18}$$

The two-particle residual interaction is that part of the *'t Hooft Instanton Induced Interaction* $V^{(2)}_{\text{III}}$ which acts between pairs of quarks having antisymmetric spin, flavor and color wave functions :

$$V^{(2)}_{\text{III}}\left(x_1, x_2; x'_1, x'_2\right) = V^{(2)}_{\text{'t Hooft}}\left(\mathbf{x}_1 - \mathbf{x}_2\right)\delta^{(1)}(x^0_1 - x^0_2)\delta^{(4)}(x_1 - x'_1)\delta^{(4)}(x_2 - x'_2) \ , \tag{2.19}$$

with the 't Hooft two-body potential given by :

$$V^{(2)}_{\text{'t Hooft}}\left(\mathbf{x}_1-\mathbf{x}_2\right) = -4\, v_{reg}\left(\mathbf{x}_1-\mathbf{x}_2\right)\left(\mathbb{1}\otimes\mathbb{1}+\gamma^5\otimes\gamma^5\right) \times\ \mathcal{P}^{\mathcal{D}}_{S_{12}=0}\ \otimes\ \left(g_{nn}\mathcal{P}^{\mathcal{F}}_{\mathcal{A}}(nn)+g_{ns}\mathcal{P}^{\mathcal{F}}_{\mathcal{A}}(ns)\right)\ \otimes\ \mathcal{P}^{\mathcal{C}}_{\bar{3}}\ . \quad (2.20)$$

Here, $v_{reg}\left(\mathbf{x}_1-\mathbf{x}_2\right)$ is a Gaussian regulating function, and the $\mathcal{P}$'s are projectors working in colour ($\mathcal{C}$), flavour ($\mathcal{F}$) and Dirac ($\mathcal{D}$) space. The interaction potentials are discussed in more detail in Appendix A.

2.2.2 Reduction to the Salpeter Equation

The problem of solving Eq. (2.13) can be simplified by exploiting the instantaneous property of the interaction kernels because the integration over the energy components of the Jacobi momenta can be performed analytically. This gives rise to a new object Φ_M, the Salpeter amplitude, which can be directly obtained from the full BS amplitude :

$$\Phi_M\left(\mathbf{p}_\xi,\mathbf{p}_\eta\right) \;=\; \int\frac{\mathrm{d}p^0_\xi}{(2\pi)}\frac{\mathrm{d}p^0_\eta}{(2\pi)}\chi_M\left((p^0_\xi,\mathbf{p}_\xi),(p^0_\eta,\mathbf{p}_\eta)\right)\ . \quad (2.21)$$

The integration over the energy components is easily performed in case there are no genuine two-particle irreducible interactions in Eq. (2.13), *e.g.* for the ground-state decuplet baryons which have symmetric spin wave functions. For other baryons, where the 't Hooft instanton induced interaction $V^{(2)}_{\text{III}}$ is non-vanishing, the inverse quark propagator in the two-particle kernel, Eq. (2.14), will introduce an extra dependence on the energy components of the Jacobi momenta in the right-hand side of Eq. (2.13). This makes it impossible to do the integration analytically and a slightly different approach is needed, as is explained in Ref. [34] and in the Appendix of Ref. [35]. There, it is pointed out that for reconstructing the Bethe-Salpeter amplitude (2.1), it suffices to compute the projection of the Salpeter amplitude (2.21) onto the purely positive-energy and negative-energy states. This can be accomplished in the standard manner by introducing the energy-projection operators :

$$\Lambda^{\pm}_i\left(\mathbf{p}_i\right) \;=\; \frac{\omega_i\left(\mathbf{p}_i\right)\mathbb{1}\pm H_i\left(\mathbf{p}_i\right)}{2\omega_i\left(\mathbf{p}_i\right)}\ , \quad (2.22)$$

where $\omega_i(\mathbf{p}_i)=\sqrt{m_i^2+|\mathbf{p}_i|^2}$ denotes the energy and

$$H_i(\mathbf{p}_i) \;=\; \gamma^0\left(\gamma\cdot\mathbf{p}_i+m_i\right) \quad (2.23)$$

is the free Hamiltonian of the i'th CQ. With the above definitions, we can project the Salpeter amplitude to its purely positive- and purely negative-energy components :

$$\Phi_M^\Lambda(\mathbf{p}_\xi,\mathbf{p}_\eta) = \left[\Lambda^{+++}(\mathbf{p}_\xi,\mathbf{p}_\eta)+\Lambda^{---}(\mathbf{p}_\xi,\mathbf{p}_\eta)\right] \times \int \frac{\mathrm{d}p_\xi^0}{(2\pi)}\frac{\mathrm{d}p_\eta^0}{(2\pi)}\chi_M\left((p_\xi^0,\mathbf{p}_\xi),(p_\eta^0,\mathbf{p}_\eta)\right) , \quad (2.24)$$

where $\Lambda^{+++}(\mathbf{p}_\xi,\mathbf{p}_\eta)=\Lambda_1^+(\mathbf{p}_1)\otimes\Lambda_2^+(\mathbf{p}_2)\otimes\Lambda_3^+(\mathbf{p}_3)$ and $\Lambda^{---}(\mathbf{p}_\xi,\mathbf{p}_\eta)=\Lambda_1^-(\mathbf{p}_1)\otimes\Lambda_2^-(\mathbf{p}_2)\otimes\Lambda_3^-(\mathbf{p}_3)$. After a tedious calculation [37], one obtains an equation for the projected Salpeter amplitude, which is given by :

$$\begin{aligned}\Phi_M^\Lambda(\mathbf{p}_\xi,\mathbf{p}_\eta) &= \left[\frac{\Lambda^{+++}(\mathbf{p}_\xi,\mathbf{p}_\eta)}{M-\Omega(\mathbf{p}_\xi,\mathbf{p}_\eta)+i\varepsilon}+\frac{\Lambda^{---}(\mathbf{p}_\xi,\mathbf{p}_\eta)}{M+\Omega(\mathbf{p}_\xi,\mathbf{p}_\eta)-i\varepsilon}\right]\gamma^0\otimes\gamma^0\otimes\gamma^0 \\ &\quad\times\int\frac{\mathrm{d}^3p'_\xi}{(2\pi)^3}\frac{\mathrm{d}^3p'_\eta}{(2\pi)^3}\,V^{(3)}(\mathbf{p}_\xi,\mathbf{p}_\eta;\mathbf{p}'_\xi,\mathbf{p}'_\eta)\,\Phi_M^\Lambda(\mathbf{p}'_\xi,\mathbf{p}'_\eta) \\ &+ \left[\frac{\Lambda^{+++}(\mathbf{p}_\xi,\mathbf{p}_\eta)}{M-\Omega(\mathbf{p}_\xi,\mathbf{p}_\eta)+i\varepsilon}-\frac{\Lambda^{---}(\mathbf{p}_\xi,\mathbf{p}_\eta)}{M+\Omega(\mathbf{p}_\xi,\mathbf{p}_\eta)-i\varepsilon}\right] \\ &\quad\times\int\frac{\mathrm{d}^3p'_\xi}{(2\pi)^3}\left[\left[\gamma^0\otimes\gamma^0\,V^{(2)}(\mathbf{p}_\xi,\mathbf{p}'_\xi)\right]\otimes\mathbb{1}\right]\Phi_M^\Lambda(\mathbf{p}'_\xi,\mathbf{p}_\eta) \\ &+ \textit{cycl. perm. in quarks (123)} , \end{aligned} \quad (2.25)$$

where $\Omega(\mathbf{p}_\xi,\mathbf{p}_\eta)$ is the sum of the energies of the three CQ's in the center-of-mass frame :

$$\Omega = \sum_{i=1}^3\omega_i = \sum_{i=1}^3\sqrt{|\mathbf{p}_i|^2+m_i^2}\,. \quad (2.26)$$

In principle, one would need the full Salpeter amplitude to reconstruct the BS amplitude, but it turns out that the terms with the smallest denominators are exactly those with projector structures $\Lambda^{+++}(\mathbf{p}_\xi,\mathbf{p}_\eta)$ and $\Lambda^{---}(\mathbf{p}_\xi,\mathbf{p}_\eta)$. The denominators of the terms with other projector structures are large enough to be safely neglected [37].

Once the Salpeter equation (2.25) has been solved, the vertex function Γ_M^Λ can be constructed :

$$\Gamma_M^\Lambda(\mathbf{p}_\xi,\mathbf{p}_\eta) = -i\int\frac{\mathrm{d}^3p'_\xi}{(2\pi)^3}\frac{\mathrm{d}^3p'_\eta}{(2\pi)^3} \times\left[V_\Lambda^{(3)}(\mathbf{p}_\xi,\mathbf{p}_\eta;\mathbf{p}'_\xi,\mathbf{p}'_\eta)+V_M^{eff^{(1)}}(\mathbf{p}_\xi,\mathbf{p}_\eta;\mathbf{p}'_\xi,\mathbf{p}'_\eta)\right]\Phi_M^{\Lambda,(1)}(\mathbf{p}'_\xi,\mathbf{p}'_\eta)\,. \quad (2.27)$$

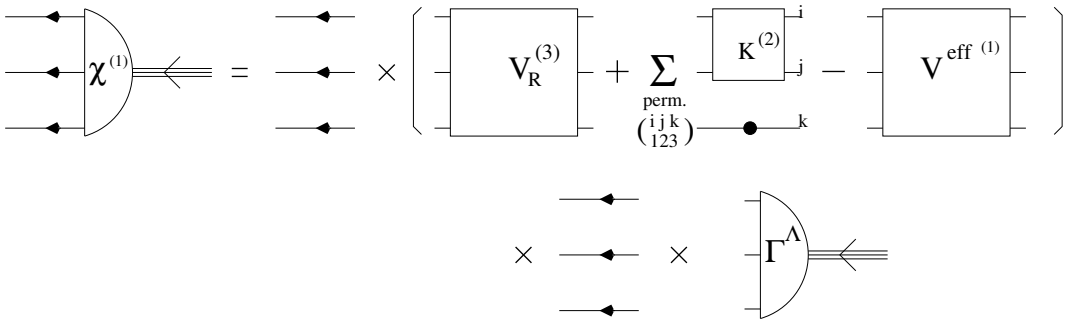

Figure 2.5 *The reconstruction of the BS amplitude from the vertex function according to Eq. (2.28).*

This vertex function describes at first order (superscript $^{(1)}$ in the right-hand side of Eq. (2.27)) how the three CQ's couple to form a baryon. It can be related to the BS amplitude through :

$$\chi_{\overline{P}} \approx \chi^{(1)}_{\overline{P}} = \left[G_{0\overline{P}} \left(V^{(3)}_R + \bar{K}^{(2)}_{\overline{P}} - V^{eff(1)}_{\overline{P}} \right) G_{0\overline{P}} \right] \Gamma^{\Lambda}_{\overline{P}} \,, \tag{2.28}$$

of which a diagram is shown in Fig. 2.5.

In Eqs. (2.27) and (2.28), we have defined

$$V^{(3)}_{\Lambda} = \left(\gamma^0 \otimes \gamma^0 \otimes \gamma^0\right) \left(\Lambda^{+++} + \Lambda^{---}\right) \left(\gamma^0 \otimes \gamma^0 \otimes \gamma^0\right) V^{(3)} \left(\Lambda^{+++} + \Lambda^{---}\right) \,, \tag{2.29}$$

which is that part of the three-body potential which couples only to purely positive-energy and negative-energy components of the amplitudes. $V^{(3)}_R = V^{(3)} - V^{(3)}_{\Lambda}$ is the remaining part which couples to the mixed-energy components only. $V^{eff(1)}_{\overline{P}}$ is a first-order approximation of an effective potential with three-body structure which parameterizes the two-body interaction [34, 35]. Further, $\bar{K}^{(2)}_{\overline{P}}$ is defined in Eqs. (2.14) and (2.16b).

2.3 Current Matrix Elements

When describing processes for which one or more incoming particles are transformed into one or more outgoing particles through the operation of a certain interaction, the dynamics are contained in the matrix elements of the interaction operator for those particular incoming and outgoing states. These matrix elements are

the overlaps of the initial state which the interaction operator has acted upon, with the the final state. The computation of matrix elements is an indispensable step in computing observables starting from a theoretical framework.

In CQ model discussed here, it is possible to calculate the matrix elements of any operator which can be written down in terms of quark-field creation and annihilation operators. In this section, we will focus on the *Current Matrix Elements* (CME's) for one incoming and one outgoing baryon or baryon resonance. The current operator we use in this work, describes electromagnetic (EM) transitions. The incoming and outgoing states entering the calculation, are bound states of three constituent quarks, described by the BS amplitudes discussed in Sect. 2.2. In this section, we will derive how exactly the CME's are related to the BS amplitudes. We will then derive the lowest-order expression for the CME's in terms of the lowest-order approximations to the BS amplitudes and the most simple expression for the photon coupling to a three-quark bound state.

Once the BS amplitudes and the accompanying vertex functions have been determined, the electromagnetic CME's can be computed through the following definition of the current operator $j^\mu(x)$

$$\langle\, \bar{P} \,|\, j^\mu(x) \,|\, \bar{P}' \,\rangle \;=\; \langle\, \bar{P} \,|\, \bar{\Psi}(x)\, \hat{q}\, \gamma^\mu\, \Psi(x) \,|\, \bar{P}' \,\rangle \;, \tag{2.30}$$

where Ψ and $\hat{q}$ are the CQ field in the Heisenberg picture and the charge operator respectively. The current operator $j^\mu(x)$ depends on only one space-time point x, since we assume that the photon couples to a point-like CQ. The above matrix element can be expressed in terms of the objects defined in Secs. 2.2.1 and 2.2.2. To this end, we consider the seven-point Green's function for three incoming and three outgoing quarks and the current operator :

$$\begin{aligned} &G^\mu_{a_1,a_2,a_3;a;a'_1,a'_2,a'_3}\left(x_1,x_2,x_3;x;x'_1,x'_2,x'_3\right) \;= \\ &\quad -\,\langle\, \mathbf{0} \,|\, \mathbf{T}\left\{ \Psi_{a_1}(x_1)\, \Psi_{a_2}(x_2)\, \Psi_{a_3}(x_3)\; j^\mu_a(x)\; \bar{\Psi}_{a'_1}(x'_1)\, \bar{\Psi}_{a'_2}(x'_2)\, \bar{\Psi}_{a'_3}(x'_3) \right\} \,|\, \mathbf{0} \,\rangle \;. \end{aligned} \tag{2.31}$$

It speaks for itself that the Green's function should be invariant under translations (Poincaré invariance). We can make explicit use of this fact by rewriting the Green's function in the frame where the photon coupling occurs at the origin. Omitting the

a_i quantum numbers for notational purposes, we get :

$$\begin{aligned}
&G^\mu\left(x_1,x_2,x_3;\,x\,;x_1',x_2',x_3'\right) \;=\\
&G^\mu\left(x_1-x,x_2-x,x_3-x;\,0\,;x_1'-x,x_2'-x,x_3'-x\right) \;=\\
&G^\mu\left(X-x,\xi,\eta;\,0\,;X'-x,\xi',\eta'\right) \;=\\
&-\left\langle\,\mathbf{0}\,\middle|\,\mathbf{T}\left\{\Psi(x_1{-}x)\,\Psi(x_2{-}x)\,\Psi(x_3{-}x)\,j^\mu(0)\,\overline{\Psi}(x_1'{-}x)\,\overline{\Psi}(x_2'{-}x)\,\overline{\Psi}(x_3'{-}x)\right\}\,\middle|\,\mathbf{0}\,\right\rangle .
\end{aligned} \tag{2.32}$$

In this expression for the Green's function, the use of the time-operator $\mathbf{T}$ indicates that this is actually a sum over all possible time-orderings. However, one can restrict oneself to those terms that contain three quark-creation operators with earlier times than the current operator, which on its turn has an earlier time than the three outgoing quark-annihilation operators. This constraint ensures that we are looking at a three-quark bound state which couples to a photon, resulting in a (new) three-quark bound state, and not at *e.g.* a $q\overline{q}$ bound state which couples to a photon and decays to a $qq\overline{qq}$ bound state. The condition for the time variables of the operators in Eq. (2.32) is therefore :

$$\max\left(x_1'^0-x^0,x_2'^0-x^0,x_3'^0-x^0\right)<0<\min\left(x_1^0-x^0,x_2^0-x^0,x_3^0-x^0\right)\,. \tag{2.33}$$

As was the case in Eq. (2.5), this condition on the time-ordering will introduce Θ-functions for the time variables in expression (2.32) in order to filter out the right terms in the seven-point Green's function. Introducing two complete sets of bound states, one can see that the CME between two three-quark bound states manifests itself in the equation :

$$\begin{aligned}
&G^\mu\left(X-x,\xi,\eta;0;X'-x,\xi',\eta'\right) \;=\; -\int\frac{\mathrm{d}^3P_a}{(2\pi)^3\,2\omega_a}\frac{\mathrm{d}^3P_b'}{(2\pi)^3\,2\omega_b'}\\
&\left\langle\,\mathbf{0}\,\middle|\,\mathbf{T}\left\{\Psi(x_1-x)\,\Psi(x_2-x)\,\Psi(x_3-x)\right\}\,\middle|\,\overline{P}_a\,\right\rangle\,\left\langle\,\overline{P}_a\,\middle|\,j^\mu(0)\,\middle|\,\overline{P}_b'\,\right\rangle\\
&\left\langle\,\overline{P}_b'\,\middle|\,\mathbf{T}\left\{\overline{\Psi}(x_1'-x)\,\overline{\Psi}(x_2'-x)\,\overline{\Psi}(x_3'-x)\right\}\,\middle|\,\mathbf{0}\,\right\rangle\,\Theta\left(X^0-x^0\right)\,\Theta\left(x^0-X'^0\right)\\
&\qquad\qquad +\text{ other time-orderings} +\text{ non-bound states}\,.
\end{aligned} \tag{2.34}$$

Using the definitions (2.1) and (2.2) for the BS amplitudes, but this time referenced to the event of the photocoupling, and expression (2.6) for the Θ-functions,

we obtain the following expression :

$$\widetilde{G}^{\mu}\left(X-x,\xi,\eta;\,0\,;X'-x,\xi',\eta'\right) \;=\; \frac{1}{(2\pi)^8}\int \frac{\mathrm{d}^3P_a}{2\omega_a}\,\frac{\mathrm{d}^3P_b'}{2\omega_b'}\,\mathrm{d}q_a\,\mathrm{d}q_b\,\frac{e^{-iq_a(X^0-x^0)}}{q_a+i\epsilon}$$
$$\frac{e^{-iq_b(x^0-X'^0)}}{q_b+i\epsilon}\,e^{-i\overline{P}_a\cdot(X-x)}\,e^{i\overline{P}_b'\cdot(X'-x)}\,\chi_{\overline{P}_a}(\xi,\eta)\,\langle\,\overline{P}_a\,|\,j_a^{\mu}(0)|\,\overline{P}_b'\,\rangle\,\overline{\chi}_{\overline{P}_b'}\left(\xi',\eta'\right)\,. \tag{2.35}$$

Again, we have used a *tilde* on the Green's function to denote that we have dropped the terms with unappropriate time-ordering or which have contributions of non-$3q$ bound states. We can simplify the notation by introducing new, off-shell four-momenta :

$$P_a^* \;=\; (\omega_a+q_a,\mathbf{P}_a)\;, \tag{2.36a}$$
$$P_b'^* \;=\; \left(\omega_b'+q_b,\mathbf{P}_b'\right)\;. \tag{2.36b}$$

Introducing these definitions in Eq. (2.35), we see that $\widetilde{G}^{\mu}$ shows an analogous pole structure as $\widetilde{G}^{(6)}$ in Sect. 2.2.1. However, $\widetilde{G}^{\mu}$ displays *two* distinct poles :

$$\widetilde{G}^{\mu}\left(X-x,\xi,\eta;\,0\,;X'-x,\xi',\eta'\right) \;=\; \frac{1}{(2\pi)^8}\int \frac{\mathrm{d}^4P_a^*}{2\omega_a}\,\frac{\mathrm{d}^4P_b'^*}{2\omega_b'}$$
$$\times\;\frac{e^{-iP_a^*\cdot X}\chi_{\overline{P}_a^*}(\xi,\eta)}{P_a^{*0}-\omega_a+i\epsilon}\,e^{iP_a^*\cdot x}\,\langle\,\overline{P}_a^*\,|\,j^{\mu}(0)\,|\,\overline{P}_b'^*\,\rangle\,e^{-iP_b'^*\cdot x}\,\frac{\overline{\chi}_{\overline{P}_b'^*}(\xi',\eta')\,e^{iP_b'^*\cdot X'}}{P_b'^{*0}-\omega_b'+i\epsilon}\;, \tag{2.37}$$

where we have used that $\overline{P}_a=\overline{P}_a^*$ and $\overline{P}_b'=\overline{P}_b'^*$, since on-shell momenta depend on the threevector only.

The Fourier transform of Eq. (2.37) is now easily obtained. Integration over (ξ,η) and (ξ',η') results in BS amplitudes in momentum space, while the integrations over X, x and X' result in three δ-functions. Two of these δ-functions can be used in the integration over the general four-momenta P_a^* and $P_b'^*$, and the third takes care of total four-momentum conservation, which is the momentum-space equivalent of translational invariance. As a result, we find :

$$(2\pi)^4\,\delta^{(4)}\left(P-P'-q\right)\widetilde{G}^{\mu}_{P;q;P'}\left(p_\xi,p_\eta;p_\xi',p_\eta'\right) \;=$$
$$\frac{(2\pi)^4\,\delta^{(4)}\left(P-P'-q\right)}{4\omega_{\overline{P}}\omega_{\overline{P}'}}\,\frac{\chi_{\overline{P}}\left(p_\xi,p_\eta\right)}{P^0-\omega_{\overline{P}}+i\epsilon}\,\langle\,\overline{P}\,|\,j^{\mu}(0)\,|\,\overline{P}'\,\rangle\,\frac{\overline{\chi}_{\overline{P}'}\left(p_\xi',p_\eta'\right)}{P'^0-\omega_{\overline{P}'}+i\epsilon}\;. \tag{2.38}$$

The equation for the seven-point Green's function describing a photon coupling to a three-quark system is depicted in Fig. 2.6. It is the Feynman-diagram representation of an equation which explicitly reads :

$$\begin{aligned}
&G^{\mu}\left(x_1,x_2,x_3;\,x\,;x_1',x_2',x_3'\right) \;=\\
&G^{\mu}\left(x_1-x,x_2-x,x_3-x;\,0\,;x_1'-x,x_2'-x,x_3'-x\right) \;=\\
&\int \mathrm{d}^4x_1''\mathrm{d}^4x_2''\mathrm{d}^4x_3''\mathrm{d}^4x_1'''\mathrm{d}^4x_2'''\mathrm{d}^4x_3'''\; G^{(6)}\left(x_1-x,x_2-x,x_3-x;x_1'',x_2'',x_3''\right)\\
&\times\; K^{\mu}\left(x_1'',x_2'',x_3'';\,0\,;x_1''',x_2''',x_3'''\right)\; G^{(6)}\left(x_1''',x_2''',x_3''';x_1'-x,x_2'-x,x_3'-x\right)\;.
\end{aligned} \tag{2.39}$$

where the six-point Green's function from Eq. (2.4) is used. The seven-point kernel function K^{μ} is that part of G^{μ} which describes the actual photon coupling, and is not concerned with the propagation of three bound CQ's.

The introduction of complete sets of bound states, and of Θ-functions for the relevant time-ordering in Eq. (2.39), results in an expression for $\widetilde{G}^{\mu}$ in terms of the BS amplitudes of the baryons involved and the seven-point kernel function K^{μ} :

$$\begin{aligned}
&\widetilde{G}^{\mu}\left(x_1-x,x_2-x,x_3-x;\,0\,;x_1'-x,x_2'-x,x_3'-x\right) \;=\\
&\frac{-1}{(2\pi)^8}\int \frac{\mathrm{d}^4X''\mathrm{d}^4\xi''\mathrm{d}^4\eta''\mathrm{d}^4X'''\mathrm{d}^4\xi'''\mathrm{d}^4\eta'''\mathrm{d}^4P_a^*\mathrm{d}^4P_b'^*}{4\omega_a\omega_b'\left(P_a^{*0}-\omega_a+i\epsilon\right)\left(P_b'^{*0}-\omega_b'+i\epsilon\right)}\\
&\times\; \chi_{\overline{P}_a^*}\left(\xi,\eta\right)e^{-iP_a^*\cdot(X-X'')}\,\overline{\chi}_{\overline{P}_a^*}\left(\xi'',\eta''\right)\; e^{i(P_a^*-P_b'^*)\cdot x}\\
&\times\; K^{\mu}\left(X'',\xi'',\eta'';\,0\,;X''',\xi''',\eta'''\right)\;\chi_{\overline{P}_b'^*}\left(\xi''',\eta'''\right)e^{-iP_b'^*\cdot(X'''-X')}\,\overline{\chi}_{\overline{P}_b'^*}\left(\xi',\eta'\right)\;.
\end{aligned} \tag{2.40}$$

Here, we have used the definitions (2.36) for the off-shell four-momenta.

It is now rather straightforward to rewrite the BSE (2.40) in momentum space. The integration over the double- and triple-primed configurational coordinates will turn into an integration over double- and triple-primed relative momenta. The integration over the relative coordinates ξ, η, ξ' and η' will give rise to BS amplitudes in momentum space, while the integration over X, x and X' will result in three δ-functions. The final integration over the four-momenta P_a^* and $P_b'^*$ is then easily performed using two of these δ-functions. The remaining one takes care of four-

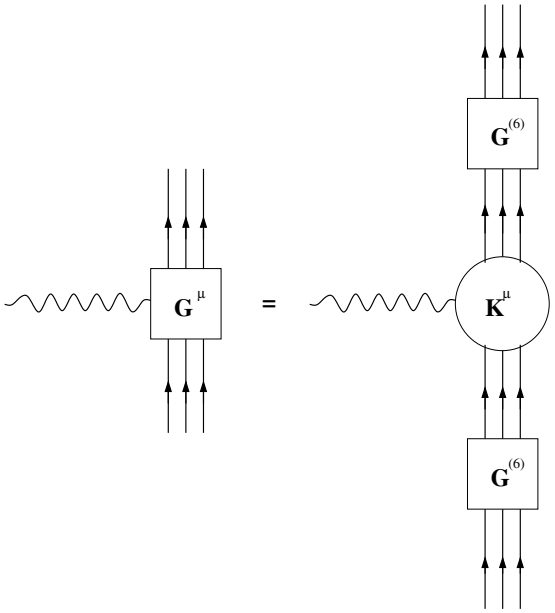

Figure 2.6 *The BSE for the Green's function describing the coupling of a photon to a baryon or baryon resonance according to Eq. (2.39).*

momentum conservation. So we finally come to :

$$
\begin{aligned}
&(2\pi)^4\,\delta^{(4)}\left(P-P'-q\right)\widetilde{G}^{\mu}_{P;q;P'}\left(p_\xi,p_\eta;p'_\xi,p'_\eta\right) \;=\\
&-\;\frac{(2\pi)^4\,\delta^{(4)}\left(P-P'-q\right)}{4\omega_{\overline{P}}\omega_{\overline{P}'}}\,\frac{\chi_{\overline{P}}\left(p_\xi,p_\eta\right)}{\left(P^0-\omega_{\overline{P}}+i\epsilon\right)}\\
&\times\int\frac{\mathrm{d}^4p''_\xi}{(2\pi)^4}\frac{\mathrm{d}^4p''_\eta}{(2\pi)^4}\frac{\mathrm{d}^4p'''_\xi}{(2\pi)^4}\frac{\mathrm{d}^4p'''_\eta}{(2\pi)^4}\overline{\chi}_{\overline{P}}\left(p''_\xi,p''_\eta\right)K^{\mu}_{P;P'}\left(p''_\xi,p''_\eta;p'''_\xi,p'''_\eta\right)\chi_{\overline{P}'}\left(p'''_\xi,p'''_\eta\right)\\
&\qquad\qquad\times\;\frac{\overline{\chi}_{\overline{P}'}\left(p'_\xi,p'_\eta\right)}{\left(P'^0-\omega_{\overline{P}'}+i\epsilon\right)}\;. \qquad (2.41)
\end{aligned}
$$

Through comparing Eq. (2.38) with Eq. (2.41), we obtain the following expression for the CME :

$$
\begin{aligned}
\langle\,\overline{P}\,|\,j^{\mu}(0)\,|\,\overline{P}'\,\rangle \;=\; -\int\frac{\mathrm{d}^4p_\xi}{(2\pi)^4}\frac{\mathrm{d}^4p_\eta}{(2\pi)^4}\frac{\mathrm{d}^4p'_\xi}{(2\pi)^4}\frac{\mathrm{d}^4p'_\eta}{(2\pi)^4}\,\overline{\chi}_{\overline{P}}\left(p_\xi,p_\eta\right)\\
\times\;K^{\mu}_{P;q;P'}\left(p_\xi,p_\eta;p'_\xi,p'_\eta\right)\,\chi_{\overline{P}'}\left(p'_\xi,p'_\eta\right)\;. \qquad (2.42)
\end{aligned}
$$

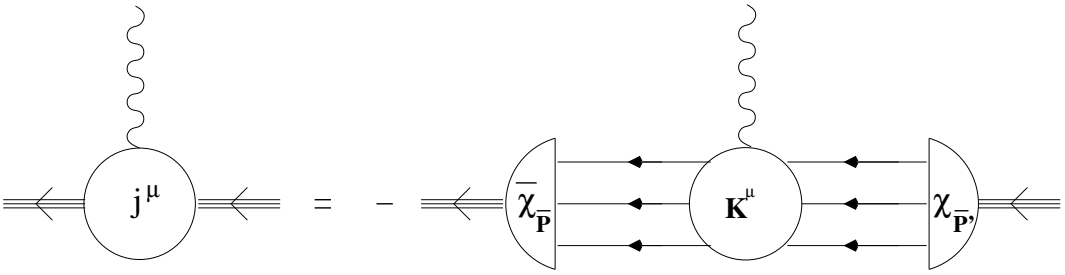

Figure 2.7 *Diagrammatic representation of Eq (2.42) for the CME.*

This equation is most easily interpreted with the aid of Feynman diagrams, as shown in Fig. 2.7.

Up to now, we have not introduced any approximation concerning the order of the interactions in Eqs. (2.18) and (2.19). However, in acquiring the BS amplitudes within the framework of Sect. 2.2, we had to restrict ourselves to the lowest order for the three-particle and two-particle irreducible kernels in order to make the equations analytically tractable and numerically computable. It is therefore obvious to make a lowest-order approximation for the kernel K^μ as well, in order to have a consistent calculation. The kernel K^μ in Eq. (2.42) should thus be formulated in terms of one-quark propagators and interaction kernels up to lowest order. Using Wick's theorem, we can then write down all connected terms without any interactions contributing to the seven-point Green's function. We find 18 terms, which can be subdivided into three groups, the terms of one group being interconnected by a permutation operator on the CQ's. Since the BS amplitudes are antisymmetric in the CQ's by construction, and the kernel is eventually to be evaluated between two BS amplitudes, only three terms will have to be taken into account for the kernel, each of which describes the coupling to one of the CQ's (Fig. 2.8).

We can get an analytical expression for K^μ up to zeroth order by inserting the

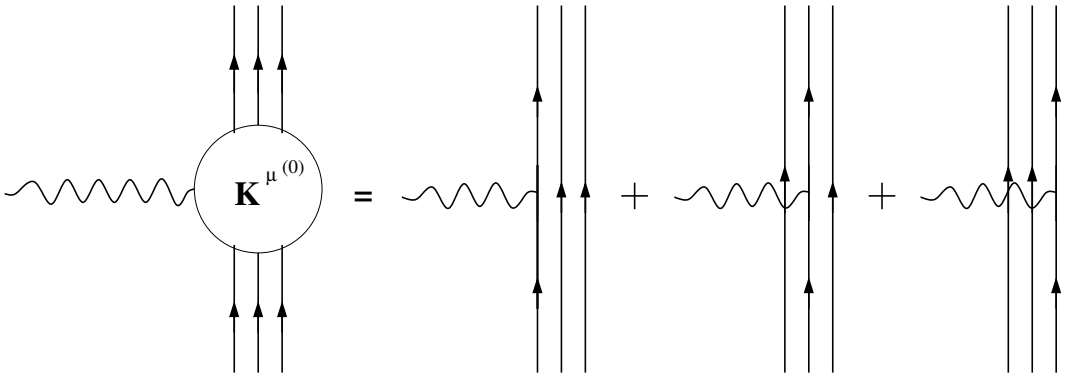

Figure 2.8 *The interaction kernel for the electromagnetic coupling up to lowest order consists of three terms describing the coupling to the three CQ's.*

three terms from Fig. 2.8 into Eq. (2.39) :

$$\begin{aligned}
&K^{\mu(0)}\left(x_1'',x_2'',x_3'';x;x_1''',x_2''',x_3'''\right) \;= \\
&S_F^{1\,-1}\left(x_1''-x_1'''\right)\otimes S_F^{2\,-1}\left(x_2''-x_2'''\right)\otimes\left[\delta^{(4)}\left(x_3''-x\right)\hat{q}\gamma^{\mu}\,\delta^{(4)}\left(x-x_3'''\right)\right] \\
&+\; S_F^{1\,-1}\left(x_1''-x_1'''\right)\otimes\left[\delta^{(4)}\left(x_2''-x\right)\hat{q}\gamma^{\mu}\,\delta^{(4)}\left(x-x_2'''\right)\right]\otimes S_F^{3\,-1}\left(x_3''-x_3'''\right) \\
&+\left[\delta^{(4)}\left(x_1''-x\right)\hat{q}\gamma^{\mu}\,\delta^{(4)}\left(x-x_1'''\right)\right]\otimes S_F^{2\,-1}\left(x_2''-x_2'''\right)\otimes S_F^{3\,-1}\left(x_3''-x_3'''\right)\;,
\end{aligned} \tag{2.43}$$

which can be transformed to momentum space :

$$\begin{aligned}
&(2\pi)^4\,\delta^{(4)}\left(P''-P'''-q\right)K^{\mu(0)}_{P'';q;P'''}\left(p_\xi'',p_\eta'';p_\xi''',p_\eta'''\right) \;= \\
&(2\pi)^4\,\delta^{(4)}\left(P''-P'''-q\right)\;S_F^{1\,-1}\left(\frac{P''}{3}+p_\xi''+\frac{p_\eta''}{2}\right)\otimes S_F^{2\,-1}\left(\frac{P''}{3}-p_\xi''+\frac{p_\eta''}{2}\right) \\
&\qquad\otimes\left[(2\pi)^8\,\delta^{(4)}\left(p_\xi'''-p_\xi''\right)\delta^{(4)}\left(p_\eta'''-p_\eta''-\frac{2}{3}q\right)\hat{q}\gamma^{\mu}\right]\;+\;\textit{cycl. perm.}\;.
\end{aligned} \tag{2.44}$$

The lowest-order expression for the kernel from Eq. (2.44) can now be used to evaluate Eq. (2.42). Making use of the cyclic permutation symmetry, we find the lowest-order expression for the CME in terms of the BS amplitudes of incoming

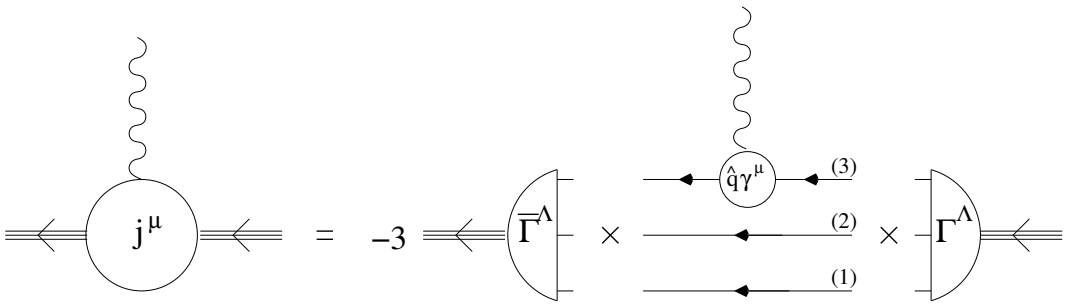

Figure 2.9 *Feynman diagram showing the coupling of the photon to the third CQ as in Eq. (2.46). The other two CQ's are spectators.*

and outgoing three-quark bound states :

$$\langle\, \overline{P}\,|\, j^{\mu}(0)\,|\, \overline{P}'\,\rangle \;\simeq\; (-3)\int \frac{\mathrm{d}^4p_\xi}{(2\pi)^4}\frac{\mathrm{d}^4p_\eta}{(2\pi)^4}\;\overline{\chi}^{(1)}_{\overline{P}}\,(p_\xi,p_\eta)$$
$$\times\left[S_F^{1\,-1}\left(\frac{P}{3}+p_\xi+\frac{p_\eta}{2}\right)\otimes S_F^{2\,-1}\left(\frac{P}{3}-p_\xi+\frac{p_\eta}{2}\right)\otimes\hat{q}\gamma^{\mu}\right]\;\chi^{(1)}_{\overline{P}'}\left(p_\xi,p_\eta+\frac{2}{3}q\right)\,, \tag{2.45}$$

where we have used the superscript (1) to denote that we are using the first order approximation to the BS amplitudes from Eq. (2.28). This latter equation relates the first-order BS amplitudes to the first-order vertex functions, which are computed in practice. Instead of explicitly calculating the BS amplitudes with Eq. (2.28) and inserting them into Eq. (2.45) for the CME's, it would be easier to find an expression for the CME's in terms of the vertex functions themselves. We thus insert the vertex functions $\Gamma^{\Lambda}_{\overline{P}}$ from Eqs. (2.28) and (2.27) into our approximate formula for the CME and take the lowest-order terms. We finally get [35, 39] :

$$<\overline{P}|j^{\mu}(0)|M>\simeq\;(-3)\int\frac{d^4p_\xi}{(2\pi)^4}\frac{d^4p_\eta}{(2\pi)^4}\;\overline{\Gamma}^{\Lambda}_{\overline{P}}\,(p_\xi,p_\eta)$$
$$\times\;S_F^1\left(\frac{M}{3}+p_\xi+\frac{p_\eta}{2}\right)\otimes S_F^2\left(\frac{M}{3}-p_\xi+\frac{p_\eta}{2}\right)$$
$$\otimes\left[S_F^3\left(\frac{M}{3}-p_\eta+q\right)\hat{q}\gamma^{\mu}\,S_F^3\left(\frac{M}{3}-p_\eta\right)\right]\Gamma^{\Lambda}_{M}\left(p_\xi,p_\eta+\frac{2}{3}q\right)\,, \tag{2.46}$$

where q is the (incoming) photon four-momentum, and $\hat{q}$ is the charge operator working on the third CQ only. Further, $\overline{\Gamma}^{\Lambda}_{\overline{P}}$ is the adjoint vertex function, calculated

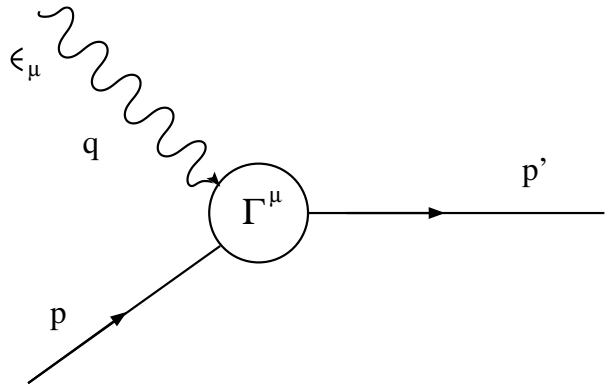

Figure 2.10 *A photon with four-momentum q and polarization ϵ_μ couples to an incoming fermion (baryon) with four-momentum p, resulting in an outgoing fermion with four-momentum p'. In the Bonn model, we can compute the on-shell form factors and helicity amplitudes, in which case both the incoming and outgoing fermion are placed on the mass shell.*

in the c.o.m. frame according to

$$\overline{\Gamma}^{\Lambda}_{M} = -\left(\Gamma^{\Lambda}_{M}\right)^{\dagger} \gamma^0 \otimes \gamma^0 \otimes \gamma^0 \,. \tag{2.47}$$

Under a Lorentz boost, this vertex function transforms as [39]

$$\Gamma_{\overline{P}}\left(p_\xi, p_\eta\right) \;=\; S^1_\Lambda \otimes S^2_\Lambda \otimes S^3_\Lambda \; \Gamma_{\Lambda^{-1}\overline{P}}\Big(\Lambda^{-1}\left(p_\xi\right), \Lambda^{-1}\left(p_\eta\right)\Big) \,, \tag{2.48}$$

with Λ the boost matrix and S^i_Λ the corresponding boost operator acting on the i'th quark (which is not to be confused with the propagator of the i'th quark S^i_F). Eq. (2.46) is a consistent lowest-order approximation of the CME. We refer the reader to Refs. [39] and [35] for more details, and to Fig. 2.9 for a schematic representation of Eq. (2.46). The integration over the energy variables can be performed analytically. In the remaining integral over $\mathbf{p}_\xi$ and $\mathbf{p}_\eta$, the azimuthal dependence can be reduced to $(\phi_\xi - \phi_\eta)$, leaving one with five-dimensional integrals, which are computed numerically.

2.4 Electromagnetic Form Factors

2.4.1 General Electromagnetic Vertex

The coupling of a photon to an extended particle such as a baryon as illustrated in Fig. 2.10, can be parameterized in different ways, which should all be equivalent in

principle. Since the photon is a (massless) vector particle with quantum numbers $J^\pi = 1^-$, the coupling can be expressed in the form of a fourvector. This fourvector will be a linear combination of the fourvectors inherent to the system and the coefficients are functions of the scalar quantities of the system. These functions are the electromagnetic (EM) form factors of the vertex. In Sect. 2.4.2, we will focus on the case where the incoming and outgoing particles are identical with spin and parity $J^\pi = 1/2^+$. In the following sections, we will treat the different cases where the particles are not identical. In Sect. 2.4.2, Sect. 2.4.3 and Sect. 2.4.4, we will treat the transition between a $J^\pi = 1/2^+$ ground-state particle and a $J^\pi = 1/2^+$, a $J^\pi = 1/2^-$ and a $J \geq 3/2$ resonance respectively.

The number of form factors required to model an EM vertex is not always clear from the start. Many models that incorporate an EM coupling to an extended particle use an expression like :

$$\Gamma^\mu \;=\; F_1^B(Q^2)\,\gamma^\mu \;+\; F_2^B(Q^2)\,\frac{i\sigma^{\mu\nu}q_\nu}{2M_p}\;, \tag{2.49}$$

with M_p the proton mass, $Q^2 = -q^2 = -(p' - p)^2$ the squared four-momentum of the photon, and $\sigma^{\mu\nu} \equiv \frac{i}{2}\,[\gamma^\mu, \gamma^\nu]$. This is, however, not the most general expression for an EM vertex. It is only valid for the specific case that the incoming and outgoing particles are identical and both on-shell ($p'^2 = p^2 = m^2$). The only conditions on the structure of the vertex operator are that it must be Lorentz-covariant (a Lorentz fourvector) and that :

$$\epsilon_\mu(q)\Gamma^\mu(p', p)\;, \tag{2.50}$$

is hermitean and invariant to charge-conjugation, parity and time-reversal operations. Here, ϵ_μ is the photon polarization vector.

2.4.2 Spin $1/2^+ \rightarrow 1/2^+$ Transitions

The fourvectors in the system under consideration are p^μ, p'^μ, q^μ and ϵ^μ. Since fermions are involved, one should also consider the fourvector of Dirac matrices γ^μ. The EM current operator describing a photon coupling to a system of particles can always be written as in Eq. (2.50), *i.e.* as the contraction of the polarization fourvector of the photon ϵ_μ contracted with a fourvector Γ^μ which is independent of the polarization. This implies that in the case of the reaction shown in Fig. 2.10,

the vertex Γ^μ must be a linear combination of p^μ, p'^μ, q^μ and γ^μ. Of these fourvectors, p^μ, p'^μ and q^μ are linearly dependent because of four-momentum conservation. One can thus work with p^μ, p'^μ and γ^μ only. Alternatively, we can make the following, more symmetric, choice for the independent fourvectors : $q^\mu = p'^\mu - p^\mu$ is the four-momentum of the incoming photon, $P^\mu = (p'^\mu + p^\mu)/2$ is the averaged four-momentum of the incoming (p^μ) and outgoing (p'^μ) baryon, and γ^μ is the Dirac-matrix fourvector.

The three independent four-momenta q^μ, P^μ and γ^μ can be multiplied by operators in Dirac space, which are scalars in configuration space. The only independent scalar operators in the problem can be chosen as : $\mathbb{1}$, $\not{q}$, $\not{P}$, $\not{q}\not{P}$, and γ_5, $\not{q}\gamma_5$, $\not{P}\gamma_5$, $\not{q}\not{P}\gamma_5$. The reduction of any higher-order scalar operator to a linear combination of these eight basis operators can be easily performed using the anticommutation rules for the Dirac matrices $\{\gamma^\mu, \gamma^\nu\} = g^{\mu\nu}$ and $\{\gamma^\mu, \gamma_5\} = 0$, and noting that $\not{q}\not{q} = q^2$, $\not{P}\not{P} = P^2$, and $\gamma^\mu\gamma_\mu = 4\ \mathbb{1}$. Since in this section, we will discuss only on-shell form factors and helicity amplitudes, we can furthermore reduce the number of scalar operators with the aid of the Dirac equation (*e.g.* $(\not{P} - \not{q}/2)u(\mathbf{p}) = \not{p}u(\mathbf{p}) = mu(\mathbf{p})$). Thus, the only scalar operators which remain are $\mathbb{1}$ and γ_5. The combinations of the three independent four-momenta with γ_5 are needed for the situations of *abnormal-parity* transitions, such as $1/2^- \to 1/2^+$ and $3/2^+ \to 1/2^+$, and can be discarded in this section. For *normal-parity* transitions, such as $1/2^+ \to 1/2^+$, the vertex describing the coupling of a photon to an incoming particle with spin-parity $J^\pi = 1/2^+$ and an outgoing particle with spin-parity $J'^{\pi'} = 1/2^+$ particle has three independent terms. We adopt the following expression :

$$\overline{u}(\mathbf{p}')\,\Gamma^\mu\left(\overline{p}', \overline{p}\right)\ u(\mathbf{p}) \ = e\,\overline{u}(\mathbf{p}')\left[f_1\gamma^\mu + f_2\frac{i\sigma^{\mu\nu}q_\nu}{2M_p} + f_3 q^\mu\right] u(\mathbf{p})\ , \tag{2.51}$$

where e is the positron charge. In the above expression, the form factors f_i of the vertex are functions of the squared four-momentum of the photon. It should be clear that with another *basis set* of fourvectors, *e.g.* the set $(\gamma^\mu, P^\mu, q^\mu)$ instead of the set $(\gamma^\mu, \frac{i\sigma^{\mu\nu}q_\nu}{2M_p}, q^\mu)$, we would get other form factors which would depend linearly on the f_i's of Eq. (2.51).

The condition for gauge invariance is, in case the ingoing and outgoing particles are on-shell :

$$\overline{u}(\mathbf{p}')\ q_\mu\Gamma^\mu\left(\overline{p}', \overline{p}\right)\ u(\mathbf{p}) \ = \ 0\ . \tag{2.52}$$

This condition relates f_3 to f_1 :

$$q^2\ f_3\left(q^2\right)\ =\ -(m'-m)\ f_1\left(q^2\right)\ , \tag{2.53}$$

where m and m' are the masses of incoming and outgoing fermion respectively.

Elastic Processes

In the case of an elastic scattering process, incoming and outgoing fermion are the same, and thus have the same mass. Eq. (2.53) becomes :

$$q^2\ f_3\left(q^2\right)\ =\ 0\ . \tag{2.54}$$

Since this should be so for both real and virtual photons, we see that f_3 vanishes, and the EM vertex adopts the following form :

$$\overline{u}(\mathbf{p}')\ \Gamma^{\mu}\left(\overline{p}',\overline{p}\right)\ u(\mathbf{p})\ =\ \overline{u}(\mathbf{p}')\ \left[f_1\gamma^{\mu}+f_2\frac{i\sigma^{\mu\nu}q_{\nu}}{2M_p}\right]\ u(\mathbf{p})\ . \tag{2.55}$$

This EM vertex resembles the common form of Eq. (2.49), provided one identifies the Dirac and Pauli form factors with the on-shell ones :

$$F_1^B(Q^2)\ =\ f_1(q^2)\ , \tag{2.56a}$$
$$F_2^B(Q^2)\ =\ f_2(q^2)\ , \tag{2.56b}$$

where we have introduced the scalar quantity $Q^2=-q^2$, which is normally used in processes involving spacelike photons (with $q^2\leq 0$). Note also that in Eqs. (2.56), and in the following, we are using the sub- and superscript "B" to emphasize that we are discussing general spin $J=1/2$ baryons and not only nucleons.

The vertex of Eq. (2.49) or Eq. (2.55), is used in the description of elastic electron-proton scattering in the one-photon-exchange approximation. The values of the form factors at $Q^2\to 0$ correspond to an unphysical situation. Due to four-momentum conservation, a real photon cannot be absorbed by a particle which remains on-shell. The value for the form factors at the real-photon point should therefore be derived in a physical limit. One can argue that for $Q^2\to 0$, one probes the particle as a whole and its EM properties are integrated over the complete spacetime. This can be interpreted as if one increasingly looks at the particle as a point object. So the physical limit of $Q^2\to 0$ boils down to considering the probed particle as

point-like. Point particles have constant form factors. This is most easily understood in the non-relativistic limit by interpreting the form factors as Fourier transforms of the charge and magnetization density distribution [40]. The value of the form factors for point particles is *normalized* to the charge and anomalous magnetic moment. This argument allows us to put the values of $F_1(Q^2 \to 0)$ and $F_2(Q^2 \to 0)$ to the charge e_N in units of e and the anomalous magnetic moment κ in units of the nuclear magneton $\mu_N = \frac{e\hbar}{2M_p}$ respectively. The limits of the elastic, on-shell form factors are a consequence of the normalization of the coupling constants, and not of gauge invariance as in the half or total off-shell case (Sect. 3.3.2).

The quantities which are typically computed within the context of constituent quark models, are the current matrix elements discussed in Sect. 2.3. They can be related to the elastic form factors by putting forward the following identity :

$$\begin{aligned} \langle B, \overline{p}', \lambda' |\, j^\mu(0)\, | B, \overline{p}, \lambda \rangle &= \langle B, \overline{p}', \lambda' |\, e\, \overline{\Psi}_B\, \Gamma_B^\mu\, \Psi_B\, | B, \overline{p}, \lambda \rangle \\ &= e\, \overline{u}_{\lambda'}(\overline{p}') \left[\gamma^\mu F_1^B(Q^2) + \frac{i\sigma^{\mu\nu} q_\nu}{2M_p} F_2^B(Q^2) \right] u_\lambda(\overline{p}) \,, \end{aligned} \tag{2.57}$$

where $\lambda^{(')}$ denotes the baryon helicity, $\overline{p}^{(')}$ the baryon on-shell four-momentum and $u_\lambda(\overline{p})$ a Dirac spinor, normalized according to

$$\overline{u}_{\lambda'}(\overline{p})\, u_\lambda(\overline{p}) = 2m\, \delta_{\lambda\lambda'} \,. \tag{2.58}$$

The Ψ_B and $\overline{\Psi}_B$ in Eq. (2.58) are the baryon annihilation and creation operators. They also turn up in the interaction Lagrangian $\mathcal{L}_{\gamma BB} = -e\, \overline{\Psi}_B\, \Gamma_B^\mu\, \Psi_B\, A_\mu$ describing the coupling of the baryon EM current j^μ to the Maxwell field A_μ. This type of interaction Lagrangians will be extensively used in the isobar model discussed in Chapter 3 and in Appendix B.

The Sachs form factors are defined in the standard fashion

$$G_E^B(Q^2) = F_1^B(Q^2) - \frac{Q^2}{4M_p m} F_2^B(Q^2) \,; \tag{2.59a}$$

$$G_M^B(Q^2) = F_1^B(Q^2) + \frac{m}{M_p} F_2^B(Q^2) \,. \tag{2.59b}$$

The equations connecting the Sachs form factors to the current matrix elements

in the rest frame of the incoming baryon read :

$$G_E^B(Q^2) = \frac{\langle B, \overline{p}', \frac{1}{2}|\, j^0(0)\, |B, \overline{m}, \frac{1}{2}\rangle}{\sqrt{4m^2+Q^2}}\ ; \tag{2.60a}$$

$$G_M^B(Q^2) = \frac{\langle B, \overline{p}', \frac{1}{2}|\, j^1(0) + i\, j^2(0)\, |B, \overline{m}, -\frac{1}{2}\rangle}{2\sqrt{Q^2}}\ . \tag{2.60b}$$

Measurements of the magnetic moments for the octet baryons represent a direct test of the calculations which will be presented here. These values should be compared to the values of the magnetic Sachs form factors at $Q^2 = 0$. From the slope of the form factors at $Q^2 = 0$, the electric and magnetic mean square radii of the baryons can be deduced from :

$$\langle r^2 \rangle = -6 \frac{1}{G(0)} \frac{dG(Q^2)}{dQ^2}\bigg|_{Q^2=0}\ , \tag{2.61}$$

if the form factor does not go to zero for $Q^2 \to 0$, and :

$$\langle r^2 \rangle = -6 \frac{dG(Q^2)}{dQ^2}\bigg|_{Q^2=0}\ , \tag{2.62}$$

if the form factor vanishes at $Q^2 = 0$. The experimental information on the radii of baryons is rather limited. The electric and magnetic mean square radii of the proton and the neutron have been obtained with reasonable accuracy (see *e.g.* [1, 41]), but for other (ground-state) baryons, the information is scarce. Two recent measurements at CERN [42] and Fermilab [43] provided the first values for the electric mean square radius of the Σ^- hyperon. To our knowledge, the Σ^- is the only hyperon for which such information is presently available.

Transition Processes

If one looks at the electromagnetic transition of *e.g.* a nucleon resonance to the nucleon ground state, the particle changes identity. If the resonance has the same spin and parity as the ground state, namely $J^\pi = 1/2^+$, we can describe this process with the vertex of Eq. (2.51). Gauge invariance then gives us the condition of Eq. (2.53), relating two of the three form factors. The difference with the elastic process is that $m' \neq m$. The f_3 form factor does not necessarily vanish, but on can

eliminate it :

$$f_3(q^2) \;=\; -\frac{m'-m}{q^2} f_1(q^2)\;. \tag{2.63}$$

The on-shell EM vertex obeying gauge invariance can then be written as :

$$\overline{u}(\mathbf{p}')\,\Gamma^\mu\left(\overline{p}',\overline{p}\right)\;u(\mathbf{p}) \;=\; \overline{u}(\mathbf{p}')\;\left[f_1\left(\gamma^\mu - \frac{m'-m}{q^2}q^\mu\right) + f_2\frac{i\sigma^{\mu\nu}q_\nu}{2M_p}\right]\;u(\mathbf{p})\;. \tag{2.64}$$

It is clear that the situation $q^2 = 0$ requires special care in order to avoid divergences. Then, the left-hand side of (2.53) is zero, resulting in :

$$f_1\left(q^2\to 0\right) \;=\; 0\;. \tag{2.65}$$

At first sight, this means that only the contribution from the f_2 term survives at the real-photon point. An example of such a process is the EM decay of an on-shell baryon resonance to the ground state. Measuring this reaction allows us to determine the only free parameter in the vertex, $f_2(0)$, which is identified with the anomalous transition magnetic moment κ_{B^*B}. Regretfully, this is not the full story. The fact that f_1 vanishes, does not mean that there is no contribution from it ! If f_1 approaches zero proportionally with q^2, there is still a contribution to the vertex which is proportional to $(m'-m)q^\mu$ (the proportionality constant can be identified with a mean-square radius, *cfr.* Eq. (2.62)). This term is usually neglected for real photons, where the gauge is mostly chosen to satisfy $\epsilon_\mu q^\mu = 0$. Since the vertex Γ^μ has to be contracted with the photon polarization, these *longitudinal* terms decouple from the amplitude.

Tree-level isobar models for electromagnetically induced meson production from a baryon B, hereafter denoted as $B\left(\gamma^{(\prime)},M\right)B'$, require a parameterization for the EM transitions between hadrons. For a $J^* = 1/2$ baryon resonance, the parameterization of the most general transition $\gamma^* + B^* \longrightarrow B$ is usually given by :

$$\Gamma^\mu\left(\overline{p},\overline{p}^*\right) \;=\; F_1^{B^*B}(Q^2)\left(\gamma^\mu - \frac{m-m^*}{q^2}q^\mu\right) \;+\; \frac{F_2^{B^*B}(Q^2)\kappa_{B^*B}}{2M_p}i\sigma^{\mu\nu}q_\nu\;, \tag{2.66}$$

where $\overline{p}^*$ ($\overline{p}$) is the on-shell four-momentum of the incoming baryon resonance (outgoing ground-state baryon), m^* and m are the masses of the baryon resonance and the ground state respectively, and $F_1^{B^*B}(Q^2)$ and $F_2^{B^*B}(Q^2)$ are the two transition

form factors, which are related to the form factors introduced earlier through (see Eq. (2.64)) :

$$F_1^{B^*B}(Q^2) = f_1(q^2)\,, \tag{2.67a}$$
$$\kappa_{B^*B} F_2^{B^*B}(Q^2) = f_2(q^2)\,. \tag{2.67b}$$

Note that the transition magnetic moment κ_{B^*B} (expressed in units of the nuclear magneton μ_N) was separated from the Pauli transition form factor, which is then normalized to $F_2^{B^*B}(Q^2=0)=1$.

For the sake of conciseness of the notations, the following quantities are introduced :

$$\mathcal{M}^{+}_{\lambda,\lambda^*} = \langle\, B,\overline{p},\lambda \mid j^1(0) + i\, j^2(0) \mid B^*,\overline{p}^*,\lambda^* \,\rangle\,, \tag{2.68a}$$
$$\mathcal{M}^{-}_{\lambda,\lambda^*} = \langle\, B,\overline{p},\lambda \mid j^1(0) - i\, j^2(0) \mid B^*,\overline{p}^*,\lambda^* \,\rangle\,, \tag{2.68b}$$
$$\mathcal{M}^{0}_{\lambda,\lambda^*} = \langle\, B,\overline{p},\lambda \mid j^0(0) \mid B^*,\overline{p}^*,\lambda^* \,\rangle\,. \tag{2.68c}$$

It is clear that not all CME's are independent, given the rotation, charge conjugation, parity and time-reversal symmetries. For $B^*(J^* \geq 3/2) \to B(J=1/2)$ transitions, there are three independent CME's. For $B^*(J^*=1/2) \to B(J=1/2)$ transitions, studied in this section, there are only two.

In the rest frame of the incoming baryon $B^*(J^*=1/2)$, the following relations between the transition form factors and the CME's hold :

$$eF_1^{B^*B}(Q^2) = \frac{Q^2}{Q^+\sqrt{Q^-}}\left[\frac{m+m^*}{|\mathbf{p}|}\mathcal{M}^0_{\frac{1}{2},\frac{1}{2}} - \frac{1}{2}\mathcal{M}^+_{\frac{1}{2},-\frac{1}{2}}\right]\,; \tag{2.69a}$$
$$\frac{e\kappa_{B^*B}F_2^{B^*B}(Q^2)}{2M_p} = \frac{-1}{Q^+\sqrt{Q^-}}\left[\frac{Q^2}{|\mathbf{p}|}\mathcal{M}^0_{\frac{1}{2},\frac{1}{2}} + \frac{m+m^*}{2}\mathcal{M}^+_{\frac{1}{2},-\frac{1}{2}}\right]\,, \tag{2.69b}$$

with $|\mathbf{p}|$ the magnitude of the three-momentum of the outgoing baryon, and $Q^\pm = Q^2 + (m^* \pm m)^2$. With these definitions for the transition form factors, $F_1^{B^*B}(0)$ gives the *transition* charge, which has to be equal to zero, due to the constraint of Eq. (2.65). Since in the right hand side of Eq. (2.69a), we see an explicit factor of Q^2, and all other factors are finite, this condition is always fulfilled. Further, κ_{B^*B} is the transition magnetic moment, since $F_2^{B^*B}(0)=1$ by convention, as was discussed previously.

2.4.3 Spin $1/2^- \rightarrow 1/2^+$ Transitions

The expression for a general EM vertex describing the transition of a spin $\frac{1}{2}^-$ resonance to a spin $\frac{1}{2}^+$ ground state can be derived following the same guidelines as outlined in the previous section. Also in this case, we can work with the fourvectors $q^\mu = p'^\mu - p^\mu$, $\frac{i\sigma^{\mu\nu}q_\nu}{2M_p}$ and the Dirac matrices γ^μ. The difference lies in the scalar operator with which we have to multiply these fourvectors. Since we are discussing an *abnormal-parity* transition, we have to include a γ_5 factor in the vertex. In case the incoming baryon $B^*(J^{*\pi^*} = 1/2^-)$ transforms through the EM interaction into the ground-state baryon $B(J^\pi = 1/2^+)$, we can propose the following vertex :

$$\overline{u}_B(\mathbf{p}')\,\Gamma^\mu\left(\overline{p}',\overline{p}\right)\;u_{B^*}(\mathbf{p}) \;= e\,\overline{u}_B(\mathbf{p}')\left[f_1\gamma^\mu + f_2\frac{i\sigma^{\mu\nu}q_\nu}{2M_p} + f_3 q^\mu\right]\gamma_5\,u_{B^*}(\mathbf{p})\;. \quad (2.70)$$

This vertex has to fulfill the condition of Eq. (2.52) in order to be gauge invariant. Keeping in mind that $\{\gamma^\mu,\gamma_5\} = 0$, we obtain the following relation between the f_1 and f_3 form factor :

$$q^2\;f_3\left(q^2\right) \;=\; -(m_{B^*} + m_B)\;f_1\left(q^2\right)\;, \quad (2.71)$$

which allows us to eliminate f_3 in terms of f_1 in Eq. (2.70). However, we should be careful in letting $f_1 \rightarrow 0$ for $q^2 \rightarrow 0$, in order to avoid any poles. A contribution proportional to $(m_{B^*} + m_B)q^\mu$ could still arise if the behaviour of f_1 is proportional to q^2. We obtain :

$$\begin{aligned}\overline{u}_B(\mathbf{p}')\,\Gamma^\mu\left(\overline{p}',\overline{p}\right)\;u_{B^*}(\mathbf{p}) \;=& \\ \overline{u}_B(\mathbf{p}')\;&\left[f_1\left(\gamma^\mu - \frac{m_{B^*}+m_B}{q^2}q^\mu\right) + f_2\frac{i\sigma^{\mu\nu}q_\nu}{2M_p}\right]\;\gamma_5\,u_{B^*}(\mathbf{p})\;. \quad (2.72)\end{aligned}$$

It is now possible to express the two form factors f_1 and f_2 as linear combinations of the CME's of Eq. (2.68) with coefficients which depend only on the kinematics. We get the following expressions in the rest frame of the incoming resonance $B^*(J^{*\pi^*} = 1/2^-)$:

$$eF_1^{B^*B}(Q^2) \;=\; \frac{Q^2}{Q^-\sqrt{Q^+}}\left[\frac{m_{B^*}-m_B}{|\mathbf{p}|}\mathcal{M}^0_{\frac{1}{2},\frac{1}{2}} + \frac{1}{2}\mathcal{M}^+_{\frac{1}{2},-\frac{1}{2}}\right]\;; \quad (2.73a)$$

$$\frac{e\kappa_{B^*B}F_2^{B^*B}(Q^2)}{2M_p} \;=\; \frac{1}{Q^-\sqrt{Q^+}}\left[\frac{Q^2}{|\mathbf{p}|}\mathcal{M}^0_{\frac{1}{2},\frac{1}{2}} - \frac{m_{B^*}-m_B}{2}\mathcal{M}^+_{\frac{1}{2},-\frac{1}{2}}\right]\;, \quad (2.73b)$$

Here, we have again introduced the more standard form factors

$$F_1^{B^*B}(Q^2) = f_1(q^2)\ , \tag{2.74a}$$

$$\kappa_{B^*B} F_2^{B^*B}(Q^2) = f_2(q^2)\ , \tag{2.74b}$$

with the usual definition of $Q^2 = -q^2$ and the transition magnetic moment $\kappa_{B^*B} = f_2(0)$. Remark that the condition that $F_1(Q^2 \to 0) \to 0$ is automatically fulfilled due to the appearance of the factor Q^2 in the right-hand side of Eq. (2.73a).

An alternative way of representing the EM properties of spin $J = 1/2$ resonances are the helicity amplitudes, which are proportional to the CME's of Eq. (2.68). We will discuss helicity amplitudes in the next section for higher-spin baryon resonances. The discussion in that section is directly applicable to spin $J = 1/2$ resonances, provided that one notes that in this case, there are only two non-zero helicity amplitudes.

2.4.4 Helicity Amplitudes of Spin $J \geq 3/2$ Resonances

The literature on EM decays of baryon resonances for $J \geq 3/2$ is vast [44, 45]. For $J \geq 3/2$, the concept of form factors as coefficients to EM-vertex structures is involved. In general, the EM properties are parameterized in terms of *helicity amplitudes (HA's)*. These quantities can be directly written in terms of the CME's of the constituent quark model.

For spin $J \geq 3/2$, there are three independent CME's and therefore three HA's. One can see this in two different ways. One could make the same derivation as in Sect. 2.4.1, where it is argued that, apart from the fourvector of Dirac matrices γ^μ, there are three independent fourvectors in the system that one can use in the expression for the vertex : ϵ^μ, q^μ, and $P^\mu = (p'^\mu + p^\mu)/2$. In the case of spin $J \geq 3/2$ resonances, the particles need extra Lorentz-indices to describe the polarization. The maximum number of linearly independent fourvectors in $(3+1)$-dimensional spacetime is, however, limited to four. For normal-parity transitions (*e.g.* $3/2^- \to 1/2^+$ and $5/2^+ \to 1/2^+$), one has to multiply the fourvectors by the scalar operator $\mathbb{1}$, while for abnormal-parity transitions (*e.g.* $3/2^+ \to 1/2^+$ and $5/2^- \to 1/2^+$), one has to multiply each fourvector with the γ_5 operator. We are thus left with four form factors. Keeping in mind that gauge invariance will eliminate one of the form factors in terms of the others, we are left with a gauge invariant vertex

for on-shell spin $J \geq 3/2$ baryons with three vertex structures, each of which can be multiplied by a form factor which is a function of the squared four-momentum of the photon. These three form factors are related to the three aforementioned independent CME's.

Another way of deriving the number of independent CME's and HA's for on-shell particles, is by noting that the electromagnetic current is a fourvector. The spatial components of this fourvector transform under rotations as a threevector. This implies that the matrix elements of the spatial components of the EM current between different states which belong to the same representation of the rotation group are related by Clebsch-Gordan coefficients, and that we only need the three reduced matrix elements to calculate all CME's. Together with the reduced matrix element of the time component of the EM current, which belongs to a one-dimensional (scalar) representation of the rotation group, we have four reduced matrix elements which describe all CME's. Current conservation, or gauge invariance, will eliminate one of these four, leaving us with three independent quantities to describe the on-shell EM vertex. The three form factors are then nothing more than linear combinations of these three remaining independent reduced matrix elements, with kinematic coefficients (see *e.g.* Refs. [46, 47]).

The definitions of the HA's vary, depending on the choices made with respect to normalization factors. Using the conventions of Ref. [35], we get for the EM transitions between two baryons :

$$A_{1/2}\,(B^* \to B) \;=\; \sqrt{\frac{\pi\alpha}{2m(m^{*2}-m^2)}}\,\mathcal{M}^{+}_{\frac{1}{2},-\frac{1}{2}}\;, \tag{2.75a}$$

$$A_{3/2}\,(B^* \to B) \;=\; \sqrt{\frac{\pi\alpha}{2m(m^{*2}-m^2)}}\,\mathcal{M}^{+}_{-\frac{1}{2},-\frac{3}{2}}\;, \tag{2.75b}$$

$$C_{1/2}\,(B^* \to B) \;=\; \sqrt{\frac{\pi\alpha}{2m(m^{*2}-m^2)}}\,\mathcal{M}^{0}_{\frac{1}{2},\frac{1}{2}}\;, \tag{2.75c}$$

where it is understood that $A_{3/2}$ is zero when both incoming and outgoing baryon have spin $J^* = J = 1/2$ (as such, there are only two independent CME's for $B^*(J^* = 1/2) \to B(J = 1/2)$ EM transitions). With these normalizations, the EM decay width of an excited state B^* with mass m^* to a ground state baryon B with mass m and spin $J = 1/2$, is given by :

$$\Gamma_\gamma \;=\; \frac{|\mathbf{q}|^2}{4\pi^2\alpha}\,\frac{2m}{(2J^*+1)\,m^*}\,\left[|A_{1/2}|^2 + |A_{3/2}|^2\right]\;. \tag{2.76}$$

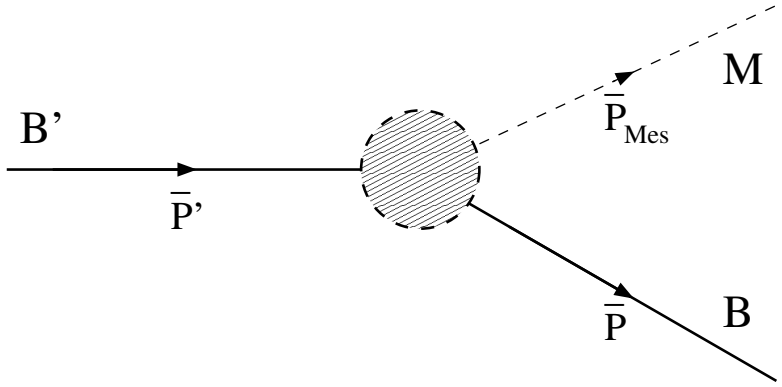

Figure 2.11 *A baryon resonance B' with four-momentum $\overline{P}'$ decays into a baryon or baryon resonance B with four-momentum $\overline{P}$ and a meson M with four-momentum $\overline{P}_{Mes}$. All three particles are on the mass shell. What exactly goes on in the shaded area is unknown and must be parameterized in all existing models for strong decays.*

Here, $\mathbf{q} = \frac{m^{*2}-m^2}{2m^*}$ is the three-momentum of the photon in the rest frame of the initial baryon resonance, and $\alpha = \frac{e^2}{4\pi} \simeq \frac{1}{137}$ is the EM fine-structure constant. This definition of the EM decay width differs from the one given by the *Particle Data Group (PDG)* [1] by a factor of $e^2 = 4\pi\alpha$. In the PDG tables, only the experimentally known EM decay widths and photo-amplitudes $A_i\left(Q^2 \to 0\right)$ are presented. We will present our results for the EM properties of hyperon resonances in terms of HA's directly in Sect. 4.2.

2.5 Strong Decays

This section aims at giving a derivation of the formulas needed to calculate strong decay matrix elements in the framework of the relativistic CQ model. With this, we want to illustrate the possibility of the Bonn CQ model of providing us with all the information necassary to describe processes such as meson electroproduction.

The process we will examine, is depicted in Fig. 2.11. It shows the decay of a baryon resonance B' to another baryon or baryon resonance B and a meson M. The four-momenta of the three particles, $\overline{P}'$, $\overline{P}$ and $\overline{P}_{Mes}$, are all on the mass shell, hence the *barred* notation.

The exact dynamics governing the strong decay, represented by the shaded area in Fig. 2.11, are described by the QCD equations in the non-perturbative region. Be-

cause of their intrinsic non-linearity in this region, they are not much of practical use. Therefore, one has to resort to (semi-)phenomenological models based on effective interactions which take into account certain aspects of the strong interaction such as confinement, chiral symmetry, $SU(3)$-flavour symmetry and Lorentz covariance.

Although one uses similar type of modelling for the generation of the hadron spectra, it appears that every model presented in the literature needs extra ingredients for the description of strong decays. This is a consequence of the extra degrees of freedom entering the strong-decay reactions compared to the generation of hadron spectra. Firstly, there is extra kinematical freedom because of the extra particle created in the process. An extra four-momentum is introduced in the process and a proper description of the boost-effects inherent to particle-production processes is required. Secondly, for practical reasons, one needs to choose the effective description of the strong-decay reaction dynamics. In quantum mechanics, this involves choosing the operator for the strong decay which has to be "sandwiched" between the state for the incoming baryon resonance and the one for the outgoing baryon-meson system. The multitude of choices is reflected by the vast amount of publications in the field of constituent quark models for strong decays of baryon resonances (*e.g.* the elementary meson emission model [48, 49], the $^3P_0$ quark pair creation model [50], the flux-tube breaking model [51–53], ...). For an extensive discussion, we refer the reader to *e.g.* the review of Capstick and Roberts [54] or the book of Le Yaouanc *et al.* [32]. Also in the field of isobar models and *Quantum Hadrodynamics* (QHD), there is ambiguity in the choice for the baryon-baryon-meson coupling. Here, one is concerned with the questions of off-shell effects and strong form factors [55], soft vs. hard form factors [3], pseudoscalar vs. vector coupling [56], *etc*.

In the following sections, we will discuss how to compute strong decay matrix elements in the framework developed in this chapter. In the Bonn CQ model, the extra kinematical degree of freedom (fourvector $\overline{P}_{Mes}$ of the meson) and its (boost) effects are taken into account from the onset, because of the Lorentz covariance of the model. The choice for the transition operator reflects both the model assumptions for the quark-quark interactions, and the approximations made for dealing with the strong-decay kernel. In practice, one has to restrict the numerical calcu-

lations to the lowest order, which results in calculating the overlap of the hadrons' BS amplitudes. This approximation does not introduce any new dynamics into the problem (the operator is the unity operator), which offers the advantage of making the calculations parameter-free.

Sect. 2.5.1 deals with the link between the elements of the $\mathcal{S}$-matrix for $B' \to B+M$ reactions and the eight-point Green's function. A discussion of the BSE for this Green's function will be presented in Sect. 2.5.2. This will result in an expression for the $\mathcal{S}$-matrix element in terms of the BS amplitudes of the two baryons and the meson which are involved in the reaction, and a strong-decay kernel. This kernel will be approximated to zeroth order in Sect. 2.5.3, where we will also derive the expression for the $\mathcal{S}$-matrix element in terms of the vertex functions for the participating hadrons.

2.5.1 Linking the Strong Decay Matrix Element to a Green's Function

We need to establish the relation between the strong-decay matrix element (or $\mathcal{S}$-matrix element) :

$$\mathcal{S}_{\overline{P}' \to \overline{P}\overline{P}_{Mes}} \;=\; \langle\, \overline{P}\,,\, \overline{P}_{Mes} \mid \mathcal{S} \mid \overline{P}^{\,\prime} \,\rangle \tag{2.77}$$

and the eight-point Green's function in coordinate space :

$$\begin{aligned} &G^{(8)}_{a_1,a_2,a_3,b,b';a_1',a_2',a_3'}\left(x_1,x_2,x_3,y,y';x_1',x_2',x_3'\right) \;= \\ &\langle\, \mathbf{0} \mid \mathbf{T}\left\{\Psi_{a_1}(x_1)\,\Psi_{a_2}(x_2)\,\Psi_{a_3}(x_3)\,\Psi_b(y)\,\overline{\Psi}_{b'}(y')\right. \\ &\qquad\qquad \left. \times\;\overline{\Psi}_{a_1'}(x_1')\,\overline{\Psi}_{a_2'}(x_2')\,\overline{\Psi}_{a_3'}(x_3')\right\} \mid \mathbf{0}\,\rangle\;. \end{aligned} \tag{2.78}$$

Here, the state $|\,\mathbf{0}\,\rangle$ should be interpreted as the true physical vacuum state (*i.e.* the vacuum state of the full Hamiltonian) and the operators $\Psi_{a_i}(x_i)$ and $\overline{\Psi}_{a_i'}(x_i')$ are Heisenberg destruction and creation operators. This means that all the strong dynamics is contained in the operators and that the interactions responsible for binding the quarks in hadrons also govern the strong decay. The number of participating quarks and antiquarks, however, is fixed. As usual, the a_i and b_i denote the quantum numbers in Dirac, flavor and color space, and will be left out for notational ease.

The time-ordering operator $\mathbf{T}$ plays a key role in the subsequent derivations. Studying the strong decay of a baryon into a baryon and a meson, only that part of

the eight-point Green's function with the appropriate time-ordering is required :

$$\begin{aligned} & G^{(8)}\left(x_1,x_2,x_3,y,y';x_1',x_2',x_3'\right) \;= \\ & \langle\,\mathbf{0}\mid \mathbf{T}\left\{\Psi(x_1)\,\Psi(x_2)\,\Psi(x_3)\,\Psi(y)\,\overline{\Psi}(y')\right\}\mathbf{T}\left\{\overline{\Psi}(x_1')\,\overline{\Psi}(x_2')\,\overline{\Psi}(x_3')\right\}\mid\mathbf{0}\,\rangle \\ & \qquad\qquad \Theta\left(x_1^0,x_2^0,x_3^0,y^0,y'^0;x_1'^0,x_2'^0,x_3'^0\right) \;+\; \text{other time-orderings}\;. \end{aligned} \tag{2.79}$$

where the Θ-function merely states that all the time-components of the outgoing particles should be *later* than all the time-components of the incoming ones :

$$\min\left(x_1^0,x_2^0,x_3^0,y^0,y'^0\right) \;>\; \max\left(x_1'^0,x_2'^0,x_3'^0\right)\;. \tag{2.80}$$

The other time-orderings in Eq. (2.79) contain contributing terms from *e.g.* meson-meson scattering, four-quark propagation, tetraquarks, *etc.*

We can now introduce a complete set of Heisenberg $3q$ and $q\overline{q}$ bound states (with masses M, M' and M_{Mes}) between the time-ordered groups of operators. To this purpose, we use the momentum representation of these states :

$$\begin{aligned} & G^{(8)}\left(x_1,x_2,x_3,y,y';x_1',x_2',x_3'\right) \;=\; \int \frac{\mathrm{d}^3P_H}{(2\pi)^3\,2\omega_{\overline{P}}}\,\frac{\mathrm{d}^3P_{Mes,H}}{(2\pi)^3\,2\omega_{Mes}}\,\frac{\mathrm{d}^3P_H'}{(2\pi)^3\,2\omega_{\overline{P}'}} \\ & \times\,\langle\,\mathbf{0}\mid\mathbf{T}\left\{\Psi(x_1)\,\Psi(x_2)\,\Psi(x_3)\right\}\mathbf{T}\left\{\Psi(y)\,\overline{\Psi}(y')\right\}\,\Theta\left(x_1^0,x_2^0,x_3^0;y^0,y'^0\right) \\ & +\mathbf{T}\left\{\Psi(y)\,\overline{\Psi}(y')\right\}\,\mathbf{T}\left\{\Psi(x_1)\,\Psi(x_2)\,\Psi(x_3)\right\}\Theta\left(y^0,y'^0;x_1^0,x_2^0,x_3^0\right)\mid\overline{P}_H\,,\overline{P}_{Mes,H}\,\rangle \\ & \times\,\langle\,\overline{P}_H\,,\overline{P}_{Mes,H}\mid\overline{P}_H'\,\rangle \\ & \times\,\langle\,\overline{P}_H'\mid\mathbf{T}\left\{\overline{\Psi}(x_1')\,\overline{\Psi}(x_2')\,\overline{\Psi}(x_3')\right\}\mid\mathbf{0}\,\rangle\;\;\Theta\left(x_1^0,x_2^0,x_3^0,y^0,y'^0;x_1'^0,x_2'^0,x_3'^0\right) \\ & \qquad\qquad +\;\text{other time-orderings}\;+\;\text{other intermediate states}\;, \end{aligned} \tag{2.81}$$

where we have used the normalization $\langle\,\overline{P}\,|\,\overline{P}'\,\rangle \;=\; (2\pi)^3\;2\omega_{\overline{P}}\,\delta^{(3)}\left(\mathbf{P}-\mathbf{P}'\right)$ with $\omega_{\overline{P}}^2 = m^2+|\mathbf{P}|^2$. The terms originating from non- or differently-bound states such as unbound three-quark propagation or a pentaquark ($qqqq\overline{q}$) state, are taken into account by the phrase *other intermediate states*, but are not important for the following discussion. We have also explicitly written the subscript H for the bound states, to underline that these are states in the Heisenberg picture. This means that they are eigenstates of the *full* Hamiltonian. The matrix element $\langle\,\overline{P}_H\,,\overline{P}_{Mes,H}\;\mid\;\overline{P}_H'\,\rangle$ can now be rewritten in terms of eigenstates of the *free* Hamiltonian :

$$\begin{aligned} \langle\,\overline{P}_H\,,\overline{P}_{Mes,H}\mid\overline{P}_H'\,\rangle \;&=\; \langle\,\overline{P}\,,\overline{P}_{Mes}\mid\widehat{U}\,(+\infty,-\infty)\;\mid\overline{P}'\,\rangle \\ &=\; \langle\,\overline{P}\,,\overline{P}_{Mes}\mid\mathcal{S}\mid\overline{P}'\,\rangle\;=\;\mathcal{S}_{\overline{P}'\to\overline{P}\,\overline{P}_{Mes}}\;. \end{aligned} \tag{2.82}$$

We now assume that the interaction takes place at a certain time t_0. We can remark that the times $x_1'^0$, $x_2'^0$ and $x_3'^0$ should then be close to one another and all $\lesssim t_0$, while the times x_1^0, x_2^0 and x_3^0 should be close to one another and $\gtrsim t_0$, and likewise for y^0 and y'^0. Since we furthermore assume that the outgoing baryon and meson do not interact with each other, we can rewrite Eq. (2.81) as :

$$\begin{aligned}\widetilde{G}^{(8)}\left(x_1,x_2,x_3,y,y',x_1',x_2',x_3'\right) \;=\; & \int \frac{\mathrm{d}^3P_H}{(2\pi)^3\,2\omega_{\overline{P}}}\,\frac{\mathrm{d}^3P_{Mes,H}}{(2\pi)^3\,2\omega_{Mes}}\,\frac{\mathrm{d}^3P'_H}{(2\pi)^3\,2\omega_{\overline{P}'}} \\ \times\; \langle\,\mathbf{0}\mid \mathbf{T}\left\{\Psi(x_1)\,\Psi(x_2)\,\Psi(x_3)\right\}\mid \overline{P}_H\,\rangle\,\langle\,\mathbf{0}\mid \mathbf{T}\left\{\Psi(y)\,\overline{\Psi}(y')\right\}\mid \overline{P}_{Mes,H}\,\rangle \\ \times\; \mathcal{S}_{\overline{P}'\to\overline{P}\overline{P}_{Mes}}\;\times\;\langle\,\overline{P}'_H\mid \mathbf{T}\left\{\overline{\Psi}(x_1')\,\overline{\Psi}(x_2')\,\overline{\Psi}(x_3')\right\}\mid \mathbf{0}\,\rangle \\ \times\;\Theta(X^0-t_0)\;\Theta(X^0_{Mes}-t_0)\;\Theta(t_0-X'^0)\;, \end{aligned} \tag{2.83}$$

where the *tilde* on the Green's function denotes that we have left out the terms with other time-ordering and the ones resulting from non- or differently-bound states. The X^0's are the time components of the absolute Jacobi coordinates of the bound states (in contrast with the relative Jacobi coordinates ξ and η, recall Eq. (2.3a)). Furthermore, the coordinates with subscript 'Mes' denote the meson Jacobi coordinates, which are defined in a similar way as the baryon Jacobi coordinates :

$$\left\{\begin{array}{rcl} X_{Mes} &=& \frac{1}{2}(x_q+x_{\overline{q}})\;, \\ \xi_{Mes} &=& x_q-x_{\overline{q}}\;, \end{array}\right. \tag{2.84a}$$

and

$$\left\{\begin{array}{rcl} P_{Mes} &=& p_q+p_{\overline{q}}\;, \\ p_{Mes} &=& \frac{1}{2}(p_q-p_{\overline{q}})\;. \end{array}\right. \tag{2.84b}$$

Here, the indices q and $\overline{q}$ refer to the quark and the antiquark in the meson respectively. It should be noted that the arguments of the Θ-functions in Eq. (2.83) are a little more complicated than is written here. However, when performing the Fourier transform (see later in this section), those parts of the arguments that depend on relative coordinates will only introduce a phase factor which can be absorbed in the definition of the Bethe-Salpeter amplitude, and which becomes 1 for on-shell momenta. The vital conditions are :

$$X'^0 \;<\; t_0\;; \tag{2.85a}$$

$$X^0\,,\,X^0_{Mes} \;>\; t_0\;. \tag{2.85b}$$

We will use $t_0 = 0$, because it simplifies the formulas without touching the essentials of the derivation.

In Eq. (2.83), the required strong-decay matrix element from Eq. (2.77) emerges. In order to bring it in a more tractable form, Eq. (2.83) needs to be expressed in momentum space. Therefore, we define the (adjoint) Bethe-Salpeter (BS) amplitudes for the baryons as in Eqs. (2.1) and (2.2), and analogously for the meson :

$$\langle\, \overline{P}'_H \mid \mathbf{T} \left\{ \overline{\Psi}(x'_1)\, \overline{\Psi}(x'_2)\, \overline{\Psi}(x'_3) \right\} \mid \mathbf{0} \,\rangle \;=\; \overline{\chi}_{\overline{P}'} \left(\xi', \eta'\right)\, e^{i\overline{P}'\cdot X'} \;; \tag{2.86a}$$

$$\langle\, \mathbf{0} \mid \mathbf{T} \left\{ \Psi(x_1)\, \Psi(x_2)\, \Psi(x_3) \right\} \mid \overline{P}_H \,\rangle \;=\; \chi_{\overline{P}} \left(\xi, \eta\right)\, e^{-i\overline{P}\cdot X} \;; \tag{2.86b}$$

$$\langle\, \mathbf{0} \mid \mathbf{T} \left\{ \Psi(y)\, \overline{\Psi}(y') \right\} \mid \overline{P}_{Mes,H} \,\rangle \;=\; \chi_{\overline{P}_{Mes}} \left(\xi_{Mes}\right)\, e^{-i\overline{P}_{Mes}\cdot X_{Mes}} \;, \tag{2.86c}$$

where use has been made of the translational invariance of BS amplitudes by writing the dependence on the X coordinate as a pure phase factor. The dependence of the BS amplitudes on the four-momenta $\overline{P}'$, $\overline{P}$ and $\overline{P}_{Mes}$ is merely parametric and these four-momenta are presumed to be on the mass shell.

We can now perform a Fourier transformation on $\widetilde{G}^{(8)}$ from Eq. (2.83), going from configurational coordinates (X, ξ, η) to momentum coordinates (P, p_ξ, p_η). The Fourier transforms of the BS amplitudes are :

$$\overline{\chi}_{\overline{P}'} \left(p'_\xi, p'_\eta\right) \;=\; \int \mathrm{d}^4\xi' \mathrm{d}^4\eta'\; \overline{\chi}_{\overline{P}'} \left(\xi', \eta'\right)\, e^{-ip'_\xi\cdot\xi'}\, e^{-ip'_\eta\cdot\eta'} \;; \tag{2.87a}$$

$$\chi_{\overline{P}} \left(p_\xi, p_\eta\right) \;=\; \int \mathrm{d}^4\xi \mathrm{d}^4\eta\; \chi_{\overline{P}} \left(\xi, \eta\right)\, e^{ip_\xi\cdot\xi}\, e^{ip_\eta\cdot\eta} \;; \tag{2.87b}$$

$$\chi_{\overline{P}_{Mes}} \left(p_{Mes}\right) \;=\; \int \mathrm{d}^4\xi_{Mes}\; \chi_{\overline{P}_{Mes}} \left(\xi_{Mes}\right)\, e^{ip_{Mes}\cdot\xi_{Mes}} \;. \tag{2.87c}$$

The total four-momentum in the definitions for Green's functions and BS amplitudes gives rise to a phase factor only, and can therefore be considered as a parameter. Performing a Fourier transformation on a phase factor results in a δ-function, and we can thus consistently alter the definition for Fourier transforms of quantities describing the evolution of a particle from one (primed) set of coordinates to another (unprimed) set when the total four-momentum remains constant :

$$\begin{aligned} (2\pi)^4\, \delta^{(4)} \left(P - P'\right)\, A_P \left(p_\xi, p_\eta; p'_\xi, p'_\eta\right) \;=\; & \int \mathrm{d}^4X\, \mathrm{d}^4\xi\, \mathrm{d}^4\eta\, \mathrm{d}^4X'\, \mathrm{d}^4\xi'\, \mathrm{d}^4\eta' \\ \times\; A \left((X - X'); \xi, \eta; \xi', \eta'\right)\, & e^{iP\cdot X} e^{ip_\xi\cdot\xi} e^{ip_\eta\cdot\eta} e^{-iP'\cdot X'} e^{-ip'_\xi\cdot\xi'} e^{-ip'_\eta\cdot\eta'} \;. \end{aligned} \tag{2.88}$$

The δ-function on the left-hand side ensures four-momentum conservation. It should be clear that for quantities concerning a meson, the integration over η-coordinates can be dropped.

With the ingredients given above, we can now calculate the Fourier transform of the term $\widetilde{G}^{(8)}$ from Eq. (2.83) :

$$
\begin{aligned}
&(2\pi)^4\,\delta^{(4)}\left(P+P_{Mes}-P'\right)\,\widetilde{G}^{(8)}_{P,P_{Mes};P'}\left(p_\xi,p_\eta,p_{Mes};p'_\xi,p'_\eta\right)\;=\\
&\frac{1}{(2\pi)^9}\int\frac{\mathrm{d}^3P'_a}{2\omega_a}\,\frac{\mathrm{d}^3P_b}{2\omega_b}\,\frac{\mathrm{d}^3P_{Mes,c}}{2\omega_c}\int\mathrm{d}^4X\;\mathrm{d}^4X_{Mes}\;\mathrm{d}^4X'\\
&\times\;e^{i\left(P-\overline{P}_b\right)\cdot X}\;e^{i\left(P_{Mes}-\overline{P}_{Mes,c}\right)\cdot X_{Mes}}\;\chi_{\overline{P}_b}\left(p_\xi,p_\eta\right)\;\chi_{\overline{P}_{Mes,c}}\left(p_{Mes}\right)\\
&\quad\times\;\mathcal{S}_{\overline{P}'_a\to\overline{P}_b\overline{P}_{Mes,c}}\;\overline{\chi}_{\overline{P}'_a}\left(p'_\xi,p'_\eta\right)\;e^{i\left(\overline{P}'_a-P'\right)\cdot X'}\;\Theta\left(X^0\right)\;\Theta\left(X^0_{Mes}\right)\;\Theta\left(-X'^0\right)\;,
\end{aligned}
\tag{2.89}
$$

where the integration over the relative coordinates (ξ, η) has resulted in BS amplitudes depending on relative momenta (p_ξ, p_η). The *unbarred* four-momenta are not necessarily on-shell. The integration over the spatial components of the X-coordinates will result in δ-functions for the three-momenta. The integration over the time components of the X coordinates is made more difficult by the presence of the Θ-functions. We can rewrite these functions with the aid of their momentum representation (2.6). This results in the following expression for $\widetilde{G}^8$ in momentum space :

$$
\begin{aligned}
&(2\pi)^4\,\delta^{(4)}\left(P+P_{Mes}-P'\right)\,\widetilde{G}^{(8)}_{P,P_{Mes};P'}\left(p_\xi,p_\eta,p_{Mes};p'_\xi,p'_\eta\right)\;=\\
&\int\mathrm{d}X^0\;\mathrm{d}X^0_{Mes}\;\mathrm{d}X'^0\;\frac{\mathrm{d}q_a}{2\pi}\;\frac{\mathrm{d}q_b}{2\pi}\;\frac{\mathrm{d}q_c}{2\pi}\;\frac{-i}{8\,\omega_{\overline{P}}\,\omega_{Mes}\,\omega_{\overline{P}'}}\\
&\times\;e^{i\left(P^0-\omega_{\overline{P}}-q_b\right)X^0}\;e^{i\left(P^0_{Mes}-\omega_{Mes}-q_c\right)X^0_{Mes}}\;e^{i\left(-P'^0+\omega_{\overline{P}'}+q_a\right)X'^0}\\
&\qquad\times\;\frac{\chi_{\overline{P}}\left(p_\xi,p_\eta\right)}{q_b+i\epsilon}\;\frac{\chi_{\overline{P}_{Mes}}\left(p_{Mes}\right)}{q_c+i\epsilon}\;\mathcal{S}_{\overline{P}'\to\overline{P}\overline{P}_{Mes}}\;\frac{\overline{\chi}_{\overline{P}'}\left(p'_\xi,p'_\eta\right)}{q_a+i\epsilon}\;.
\end{aligned}
\tag{2.90}
$$

The integral in the right-hand side of Eq. (2.90) can be easily calculated by performing the integration over the X^0 variables first, resulting in δ-functions for the q

variables. The integration over these q variables is then straightforward. We find :

$$(2\pi)^4\,\delta^{(4)}\left(P+P_{Mes}-P'\right)\,\widetilde{G}^{(8)}_{P,P_{Mes};P'}\left(p_\xi,p_\eta,p_{Mes};p'_\xi,p'_\eta\right) \;=\; \frac{-i}{8\,\omega_{\overline{P}}\,\omega_{Mes}\,\omega_{\overline{P}'}}$$
$$\times\;\frac{\chi_{\overline{P}}\left(p_\xi,p_\eta\right)}{P^0-\omega_{\overline{P}}+i\epsilon}\;\frac{\chi_{\overline{P}_{Mes}}\left(p_{Mes}\right)}{P^0_{Mes}-\omega_{Mes}+i\epsilon}\;\mathcal{S}_{\overline{P}'\to\overline{P}\overline{P}_{Mes}}\;\frac{\overline{\chi}_{\overline{P}'}\left(p'_\xi,p'_\eta\right)}{P'^0-\omega_{\overline{P}'}+i\epsilon}\,. \quad (2.91)$$

This is the equation connecting the $\mathcal{S}$-matrix element to the term in the eight-point Green's function in momentum space which has poles for on-shell four-momenta.

2.5.2 Calculating the Green's Function from the Bethe-Salpeter Equation

In the previous Sect. 2.5.1, we have shown that the hadronic matrix element (HME) are related to the poles of the eight-point Green's function. Knowledge of this Green's function in the vicinity of the poles therefore leads to the HME. In this section we will start from the equation, governing the process of three incoming, and five outgoing (interacting) quarks. We will show how we can link the HME directly to the interaction kernels appearing in this BS equation.

The BSE for the eight-point Green's function with three incoming quarks and five outgoing quarks ($4q+\overline{q}$) implies the introduction of the full $3q$- and $5q$-propagators, and an irreducible kernel [39]. The Feynman diagram of the BSE is shown in Fig. 2.5.2, and the mathematical formulation is given by :

$$G^{(8)}\left(x_1,x_2,x_3,y_1,y'_1;x'_1,x'_2,x'_3\right) \;=\; \int \mathrm{d}^4x''_1\,\mathrm{d}^4x''_2\,\mathrm{d}^4x''_3\,\mathrm{d}^4y_2\,\mathrm{d}^4y'_2$$
$$\times\int \mathrm{d}^4x'''_1\,\mathrm{d}^4x'''_2\,\mathrm{d}^4x'''_3\,G^{(10)}\left(x_1,x_2,x_3,y_1,y'_1;y_2,y'_2,x'''_1,x'''_2,x'''_3\right)$$
$$\times\;K\left(x'''_1,x'''_2,x'''_3,y_2,y'_2;x''_1,x''_2,x''_3\right)\,G^{(6)}\left(x''_1,x''_2,x''_3;x'_1,x'_2,x'_3\right)\;, \quad (2.92)$$

where the summation over common indices for the Dirac, flavor and color quantum numbers is left out. Further, we have introduced the ten-point and six-point Green's functions. These represent $(4q+\overline{q})$- and $3q$-propagators respectively.

In deriving Eq. (2.83), we assumed that the baryon and meson decay products do not interact. This is represented by the rightmost diagram in Fig 2.5.2, where the ten-point Green's function is separated into the product of a six-point and a

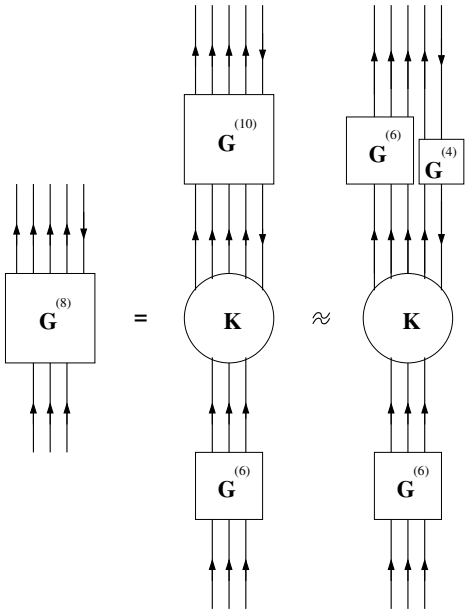

Figure 2.12 *Diagrammatic representation of the BS equation for the eight-point Green's function with three incoming quarks and five outgoing quarks ($4q + \overline{q}$).*

four-point Green's function :

$$G^{(10)}\left(x_1, x_2, x_3, y_1, y_1'; y_2, y_2', x_1''', x_2''', x_3'''\right) = G^{(6)}\left(x_1, x_2, x_3; x_1''', x_2''', x_3'''\right) \otimes G^{(4)}\left(y_1, y_1'; y_2, y_2'\right) \ . \quad (2.93)$$

As in Sect. 2.5.1, one can introduce complete sets of $3q$ and $q\overline{q}$ bound states and look for terms with the proper time-ordering. The calculation of the Fourier transform of Eq. (2.92) is rather lengthy, but using the techniques of Sect. 2.5.1 one arrives at :

$$\begin{aligned}\widetilde{G}^{(8)}_{P,P_{Mes};P'}\left(p_\xi, p_\eta, p_{Mes}; p_\xi', p_\eta'\right) &= \frac{-i}{8\,\omega_{\overline{P}}\,\omega_{Mes}\,\omega_{\overline{P}'}} \frac{\chi_{\overline{P}}\left(p_\xi, p_\eta\right)}{P^0 - \omega_{\overline{P}} + i\epsilon} \\ \times \frac{\chi_{\overline{P}_{Mes}}\left(p_{Mes}\right)}{P^0_{Mes} - \omega_{Mes} + i\epsilon} \times &\int \frac{\mathrm{d}^4 p_\xi'''}{(2\pi)^4} \frac{\mathrm{d}^4 p_\eta'''}{(2\pi)^4} \frac{\mathrm{d}^4 p'_{Mes}}{(2\pi)^4} \frac{\mathrm{d}^4 p_\xi''}{(2\pi)^4} \frac{\mathrm{d}^4 p_\eta''}{(2\pi)^4} \\ \overline{\chi}_{\overline{P}}\left(p_\xi''', p_\eta'''\right)\, \overline{\chi}_{\overline{P}_{Mes}}\left(p'_{Mes}\right)\, &K_{P,P_{Mes};P'}\left(p_\xi''', p_\eta''', p'_{Mes}; p_\xi'', p_\eta''\right)\, \chi_{\overline{P}'}\left(p_\xi'', p_\eta''\right) \\ &\times \frac{\overline{\chi}_{\overline{P}'}\left(p_\xi', p_\eta'\right)}{P'^0 - \omega_{\overline{P}'} + i\epsilon} \ . \quad (2.94)\end{aligned}$$

2.5.3 The Strong-decay Matrix Element

It is now easy to compare Eqs. (2.91) and (2.94). We can identify the HME with the integral :

$$\begin{aligned}\mathcal{S}_{\overline{P}'\to\overline{P}\overline{P}_{Mes}} &= (2\pi)^4\,\delta^{(4)}\left(P+P_{Mes}-P'\right)\\ \times\int\frac{\mathrm{d}^4p'''_\xi}{(2\pi)^4}\,\frac{\mathrm{d}^4p'''_\eta}{(2\pi)^4}\,&\frac{\mathrm{d}^4p'_{Mes}}{(2\pi)^4}\,\frac{\mathrm{d}^4p''_\xi}{(2\pi)^4}\,\frac{\mathrm{d}^4p''_\eta}{(2\pi)^4}\;\overline{\chi}_{\overline{P}}\left(p'''_\xi,p'''_\eta\right)\;\overline{\chi}_{\overline{P}_{Mes}}\left(p'_{Mes}\right)\\ &\times\;K_{P,P_{Mes};P'}\left(p'''_\xi,p'''_\eta,p'_{Mes};p''_\xi,p''_\eta\right)\;\chi_{\overline{P}'}\left(p''_\xi,p''_\eta\right)\;,\end{aligned}\tag{2.95}$$

where the kernel K remains unspecified at this point. In order to find an expression for this kernel, we remark that the eight-point Green's function $G^{(8)}$ describes the diagram of Fig. 2.13. In zeroth order, the incoming quark lines are connected with the outgoing ones without being subject to any interaction. There are 4! possible ways of doing this. Six of them lead to *unconnected* diagrams, meaning that the line of the sole antiquark (y') is connected to the quark line of the meson-quark (y). The other 18 diagrams are easy to draw using Wick's theorem. However, since the BS amplitudes of the baryons in Eq. (2.95) are antisymmetric in their configurational coordinates (x_1,x_2,x_3) and (x'_1,x'_2,x'_3), only an antisymmetric combination of the 18 connected terms will contribute. Eventually, this procedure leads to an expression for $G^{(8)}$ with three terms :

$$\begin{aligned}G^{(8)}\;&\left(x_1,x_2,x_3,y_1,y'_1;x'_1,x'_2,x'_3\right)\;=\\ &\quad S_F^1\left(x_1-x'_1\right)\otimes S_F^2\left(x_2-x'_2\right)\otimes S_F^3\left(x_3-y'_1\right)\otimes S_F^3\left(y_1-x'_3\right)\\ &+S_F^1\left(x_1-x'_1\right)\otimes S_F^2\left(x_2-y'_1\right)\otimes S_F^2\left(y_1-x'_2\right)\otimes S_F^3\left(x_3-x'_3\right)\\ &+S_F^1\left(x_1-y'_1\right)\otimes S_F^1\left(y_1-x'_1\right)\otimes S_F^2\left(x_2-x'_2\right)\otimes S_F^3\left(x_3-x'_3\right)\\ &+\text{higher-order terms}\,.\end{aligned}\tag{2.96}$$

The three terms in this equation clearly show the coupling of the meson to the three quarks of the incoming baryon.

In zeroth order, the ten-point Green's function and the six-point Green's function in Eq. (2.92) are merely products of quark propagators describing non-interacting

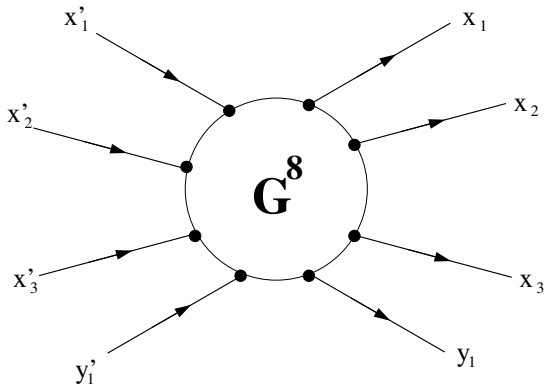

Figure 2.13 *The eight-point Green's function describes how four incoming quark lines are connected to four outgoing quark lines. One of the incoming quark lines (y_1') is an outgoing antiquark in our approach.*

quarks. Eq. (2.92) can be approximated by :

$$
\begin{aligned}
&G^{(8)}_{a_1,a_2,a_3;b_1,b_1';a_1',a_2',a_3'}\left(x_1,x_2,x_3;y_1,y_1';x_1',x_2',x_3'\right) \;= \\
&\sum_{(a_1''',a_2''',a_3''')}\;\sum_{(b_2,b_2')}\;\sum_{(a_1'',a_2'',a_3'')}\int \mathrm{d}^4x_1''\;\mathrm{d}^4x_2''\;\mathrm{d}^4x_3''\;\mathrm{d}^4y_2\;\mathrm{d}^4y_2'\;\mathrm{d}^4x_1'''\;\mathrm{d}^4x_2'''\;\mathrm{d}^4x_3''' \\
&\times\; S_{Fa_1,a_1'''}\left(x_1-x_1'''\right)\; S_{Fa_2,a_2'''}\left(x_2-x_2'''\right)\; S_{Fa_3,a_3'''}\left(x_3-x_3'''\right) \\
&\times\; S_{Fb_1,b_2}\left(y_1-y_2\right)\; S_{Fb_2',b_1'}\left(y_2'-y_1'\right) \\
&\times\; K_{a_1''',a_2''',a_3''';b_2,b_2';a_1'',a_2'',a_3''}\left(x_1''',x_2''',x_3''';y_2,y_2';x_1'',x_2'',x_3''\right) \\
&\qquad\times\; S_{Fa_1'',a_1'}\left(x_1''-x_1'\right)\; S_{Fa_2'',a_2'}\left(x_2''-x_2'\right)\; S_{Fa_3'',a_3'}\left(x_3''-x_3'\right)\;. \qquad (2.97)
\end{aligned}
$$

Here, we have explicitly written the indices of the Green's function and the CQ propagators, since it is instructive to see how the kernel K connects the different incoming with the outgoing quark lines. Comparing Eqs. (2.96) and (2.97), one can write the zeroth order expression for the kernel K

$$
\begin{aligned}
&K_{a_1''',a_2''',a_3''';b_2,b_2';a_1'',a_2'',a_3''}\left(x_1''',x_2''',x_3''';y_2,y_2';x_1'',x_2'',x_3''\right) \;= \\
&S^{-1}_{Fa_1''',a_1''}\left(x_1'''-x_1''\right) S^{-1}_{Fa_2''',a_2''}\left(x_2'''-x_2''\right) S^{-1}_{Fa_3''',b_2'}\left(x_3'''-y_2'\right) S^{-1}_{Fb_2,a_3''}\left(y_2-x_3''\right) \\
&+\; S^{-1}_{Fa_1''',a_1''}\left(x_1'''-x_1''\right) S^{-1}_{Fa_2''',b_2'}\left(x_2'''-y_2'\right) S^{-1}_{Fb_2,a_2''}\left(y_2-x_2''\right) S^{-1}_{Fa_3''',a_3''}\left(x_3'''-x_3''\right) \\
&+ S^{-1}_{Fa_1''',b_2'}\left(x_1'''-y_2'\right) S^{-1}_{Fb_2,a_1''}\left(y_2-x_1''\right) S^{-1}_{Fa_2''',a_2''}\left(x_2'''-x_2''\right) S^{-1}_{Fa_3''',a_3''}\left(x_3'''-x_3''\right)\;, \qquad (2.98)
\end{aligned}
$$

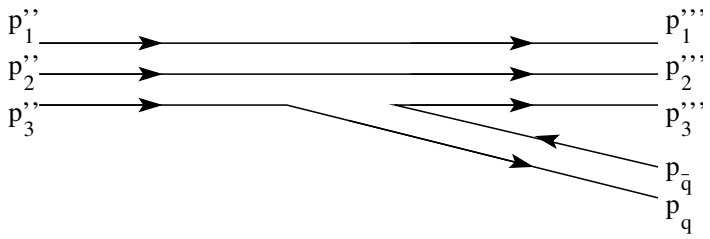

Figure 2.14 *Diagrammatic representation of the first term of Eq. (2.99).*

where the structure of Eq. (2.96) with respect to the coupling to the three quarks emerges. Since all calculations are more easily performed in momentum space, we can use the Fourier transform of the kernel at zeroth order :

$$
\begin{aligned}
&K^0_{P,P_{Mes};P'}\left(p'''_\xi, p'''_\eta, p'_{Mes}; p''_\xi, p''_\eta\right) \;= \\
&\quad (2\pi)^{12}\;\delta^{(4)}\left(p'''_3 + p_{\overline{q}}\right)\;\delta^{(4)}\left(p'''_1 - p''_1\right)\;\delta^{(4)}\left(p'''_2 - p''_2\right) \\
&\qquad\qquad \times\; {S_F}^{-1}\left(p'''_1\right)\;{S_F}^{-1}\left(p'''_2\right)\;{S_F}^{-1}\left(p'''_3\right)\;{S_F}^{-1}\left(p''_3\right) \\
&+\;(2\pi)^{12}\;\delta^{(4)}\left(p'''_2 + p_{\overline{q}}\right)\;\delta^{(4)}\left(p'''_1 - p''_1\right)\;\delta^{(4)}\left(p'''_3 - p''_3\right) \\
&\qquad\qquad \times\; {S_F}^{-1}\left(p'''_1\right)\;{S_F}^{-1}\left(p'''_2\right)\;{S_F}^{-1}\left(p''_2\right)\;{S_F}^{-1}\left(p'''_3\right) \\
&+\;(2\pi)^{12}\;\delta^{(4)}\left(p'''_1 + p_{\overline{q}}\right)\;\delta^{(4)}\left(p'''_2 - p''_2\right)\;\delta^{(4)}\left(p'''_3 - p''_3\right) \\
&\qquad\qquad \times\; {S_F}^{-1}\left(p'''_1\right)\;{S_F}^{-1}\left(p''_1\right)\;{S_F}^{-1}\left(p'''_2\right)\;{S_F}^{-1}\left(p'''_3\right)\;. \qquad (2.99)
\end{aligned}
$$

This time, we again have left out the Dirac, flavour and colour indices, and we have separated the overall δ-function according to the definition (2.89) for the Fourier transform of translationally invariant quantities. The other δ-functions merely state which incoming quark line is connected to which outgoing quark line (see Fig. 2.14 for a diagram of the first term). The p'''_i, p''_j and $p_{\overline{q}}$ denote the four-momenta of the i'th outgoing quark, the j'th incoming quark and the (outgoing) antiquark respectively (*cfr.* Eqs. (2.3b) and (2.84b)).

Using the zeroth order expression of the kernel from Eq. (2.99), and the antisymmetry of the baryon BS amplitudes to calculate the HME, the following expression

emerges :

$$\begin{aligned}
\mathcal{S}_{\overline{P}'\to\overline{P}\overline{P}_{Mes}} &= 3.\,(2\pi)^4\,\delta^{(4)}\left(\overline{P}+\overline{P}_{Mes}-\overline{P}'\right)\int\frac{\mathrm{d}^4p_\xi}{(2\pi)^4}\frac{\mathrm{d}^4p_\eta}{(2\pi)^4}\\
&\times\ \overline{\Gamma}^{\Lambda,(0)}_{\overline{P};a_1',a_2',a_3'}\left(p_\xi,\frac{2}{3}\overline{P}_{Mes}+p_\eta\right)\ S_{Fa_1',a_1}\left(\frac{\overline{P}'}{3}+p_\xi+\frac{p_\eta}{2}\right)\\
&\times\ S_{Fa_2',a_2}\left(\frac{\overline{P}'}{3}-p_\xi+\frac{p_\eta}{2}\right)\ S_{Fa_3',b_1'}\left(\frac{\overline{P}'}{3}-\overline{P}_{Mes}-p_\eta\right)\\
&\quad\times\ \overline{\Gamma}^{\Lambda,(0)}_{\overline{P}_{Mes};b_1',b_1}\left(\frac{\overline{P}'}{3}-\frac{\overline{P}_{Mes}}{2}-p_\eta\right)S_{Fb_1,a_3}\left(\frac{\overline{P}'}{3}-p_\eta\right)\Gamma^{\Lambda,(0)}_{\overline{P}';a_1,a_2,a_3}\left(p_\xi,p_\eta\right)\ .
\end{aligned}\tag{2.100}$$

The procedure of evaluating this integral is identical as for the electromagnetic case. The vertex functions Γ, defined in Eqs. (2.27) and (2.28), are expanded in a (truncated) basis, and the integral reduces to a linear combination of integrals over the basis states.

Chapter 3

Isobar Model for $p(\gamma^*, K)Y$ Reactions

The electromagnetic production of mesons from the proton or nucleus comprises a large part of the world-wide theoretical and experimental efforts made by the hadronic physics community. Witness to this are the abundance of conferences covering this specific and heavily-correlated subjects (BARYONS, MENU, NSTAR, ...). A number of dedicated electron accelerator and synchroton radiation facilities, for example those located in Newport News (JLab), Mainz (MAMI), Grenoble (GRAAL), Aioi (SPring-8), Middleton (MIT-Bates), Bonn (ELSA), *etc*, have been specifically designed with the eye on studying hadronic matter with the aid of the electromagnetic probe. Accordingly, it is not surprising that the literature on meson photo- and electroproduction is extensive, and that many models for reactions with one or more mesons in the final state have been developed throughout the years.

This chapter focuses on the electroproduction of kaons from the proton, denoted as $p(e, e'K)Y$, where Y is the outgoing (ground-state) hyperon. This process is also commonly referred to as $p(\gamma^*, K)Y$, when the one-photon-exchange approximation seems justified. Data for kaon electroproduction reactions with $Y = \Lambda, \Sigma^0$ were recently released in Ref. [13]. In the forthcoming sections, a flexible isobar model will be discussed which addresses the different aspects inherent to the electromagnetic production of kaons from the nucleon. More specifically, a rather general discussion about the degrees of freedom and the effective interactions will be presented in Sect. 3.1. A more detailed discussion of the model characteristics

will be given in Sect. 3.2. The inclusion of electromagnetic form factors in a gauge-invariant manner is the topic of Sect. 3.3. Finally, in Sect. 3.4, the expressions for the virtual-photon differential cross sections and polarization observables are presented. The reader is also referred to Appendix B, where the Lagrangian formalism is developed which will allow us to handle the dynamics and compute the reaction amplitude.

3.1 Hadrons and Photons

At the start of the construction of a model for $p(\gamma^*, K)Y$, it is essential to address the two fundamental questions already raised in the introduction. What are the relevant degrees of freedom in the process, and how do they interact with one another ? Answering these questions is the topic of this section.

3.1.1 Confined in a Small Space

In Chap. 2, the relevant degrees of freedom were constituent quarks and photons, which interacted through instantaneous forces and the electromagnetic interaction. In this picture, the $p(\gamma^{(*)}, K)Y$ process is a manifestation of strange constituent quark/antiquark pair creation from the vacuum, induced by a photon. The created strange CQ pair is rearranged, together with the CQ's already present in the proton. The result is a final state of CQ's confined into two small clusters, the kaon and the hyperon.

One can now look at the same process from a larger distance. Then, it gets difficult to distinguish the separate CQ's. Only the clusters in the initial and final state become clearly observable. The $p(\gamma^{(*)}, K)Y$ reaction is a manifestation of electromagnetic and hadronic interactions, and the process can be described without the notion of constituent quarks.

The distance scale at which this transition between the relevant degrees of freedom occurs, is typically of the order of 1 fm. For reactions covering energies, ranging from the pion mass (140 MeV, 1.4 fm) to about 400 MeV (or 0.5 fm), one expects that a description in terms of the lightest mesons (pions) and baryons (nucleon, delta) is adequate. Representative processes in this region are (virtual) Compton scattering $p(\gamma^{(*)}, \gamma)p$ and pion production $p(\gamma^{(*)}, \pi)N$. It is also expected that

when moving to higher energies, of about 2.0 GeV (or 0.1 fm), one may enter a region where sub-nucleonic degrees of freedom come into play. This is the region of baryon and meson resonances, which arise in a natural manner from the constituent-quark picture. Therefore, the production of heavier mesons (such as the kaon) from the proton is a typical reaction, bridging the world of constituent quarks with the one of hadrons.

The model presented in this chapter, adopts hadronic degrees of freedom to describe the $p(\gamma^{(*)}, K)Y$ reaction. This means that the effective fields are the baryonic and mesonic ground states *and* resonances. In other words, the resonances are treated on the same footing as the ground states.

3.1.2 Interaction Lagrangians and Effective Field Theory

The interactions between the hadron fields are usually written in terms of interaction Lagrangian densities (also called interaction Lagrangians or vertex Lagrangians). This formulation allows to satisfy the requirement of Lorentz invariance. The fundamental interactions of the Standard Model can be formulated in a similar fashion, and our model will therefore have many things in common with fundamental theories, including the property of gauge invariance. In fact, one sometimes speaks of *Quantum Hadrodynamics* (QHD) when discussing relativistic quantum field theories with hadron fields.

It should be noted, however, that there are obvious differences between *fundamental* and *effective* quantum field theories. The most obvious one is the finite extension of some, or all, of the particles involved, which seriously affects the way the particles interact. These finite extensions are modelled through the inclusion of form factors. If the interaction Lagrangian describes the coupling of a hadron to the photon field, one talks about *electromagnetic* form factors. In the case of a vertex Lagrangian describing the coupling of hadron fields to each other, one has to include *strong* or *hadronic* form factors. The introduction of form factors has a serious impact on the properties of a model. For example, it is a well-known phenomenon that the insertion of strong form factors breaks the gauge invariance of isobar models for meson photo- and electroproduction [57].

Another difference between fundamental and effective field theories is the *ad hoc* appearance of a *cutoff mass* in the latter, which sets a limit in the energy scale for

its validity. While fundamental theories seem to define their own limits, effective field theories require external input to determine the energy boundaries for their predictive power. The values for the cutoff masses are closely connected to the degrees of freedom, and are therefore necessarily model dependent. In our model, cutoff masses will show up within the expressions for the form factors.

A last difference is the introduction of decay widths in the propagators for the different hadron fields. In fundamental theories, the decay width of a particle is dynamically generated, and there is no need to include it explicitly. Tree-level models do not account for rescattering of the hadrons into different channels (*e.g.* the two-step process of the $\gamma p \to \pi N \to KY$ type). So-called *coupled-channel models*, do take into account different decay channels simultaneously. Given the large amount of known hadrons, it is a bold enterprise to account for all possible decay channels, and even the coupled-channel models have to include decay widths (albeit smaller ones) in the propagators of the hadron fields.

3.1.3 Photo- and Electroproduction

Quantum Electrodynamics (QED) is an indispensable tool in modelling photo- and electroproduction processes. It describes the basic interaction of charged objects with real photons, and the EM interaction of charged particles with each other through the exchange of virtual photons. In Fig. 3.1, we display the reaction kinematics for electroproduction of a kaon from the proton. The left part shows the lepton-scattering plane. The right part is the hadronic plane, where a virtual photon hits the proton to create a kaon and a hyperon. For photoproduction, only the latter plane is of any relevance.

Kinematical Degrees of Freedom

An important difference between photo- and electroproduction is the additional kinematical degree of freedom contained in the latter. In electroproduction, two variables are needed to describe the kinematics of the QED part of the process, *e.g.* the incoming electron energy (E_i) and the angle between incoming and outgoing electron in the lab frame (θ_e). This is reflected in the virtual-photon variables ω and $|\mathbf{q}|$ fixing the photon four-momentum $q^\mu = (\omega, \mathbf{q})$. Only the magnitude of the photon three-momentum is an independent variable, since one can always rotate

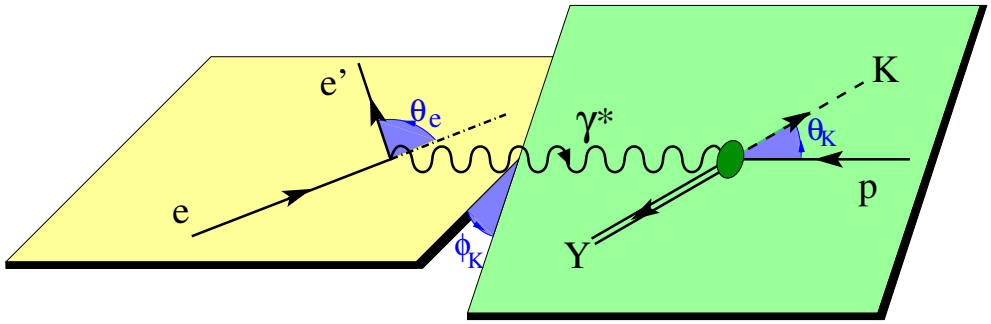

Figure 3.1 *The $p(e, e'K)Y$ process is split up into two parts, the leptonic part on the left (yellow plane), and the hadronic part $p(\gamma^*, K)Y$ on the right (green plane). For photoproduction, only the hadronic part is of relevance.*

the system in such a way, that $\mathbf{q}$ is directed along the positive z-axis, leading to $q^\mu = (\omega, 0, 0, |\mathbf{q}|)$. For the electroproduction case, where the electron is scattered from a target, the exchanged photon has a space-like four-momentum $q^2 \equiv -Q^2 < 0$ (time-like momenta occur in *e.g.* electron-positron annihilation).

The fact that the squared four-momentum of the exchanged photon is strictly negative, has yet another consequence. The inverse of the squared four-momentum transfer $-\frac{1}{q^2} = \frac{1}{Q^2}$ is a measure of how far the photon propagates in spacetime. As such, real photons ($Q^2 = 0$) propagate along the whole of spacetime, *i.e.* they probe the particles' EM properties integrated over all of spacetime, or equivalently, they see a particle as if it were pointlike. Virtual photons, on the other hand, probe a finite part of spacetime. They offer the ability to look inside the probed particles and gather information about their charge and magnetization density distributions. This information is parameterized by the EM form factors. In fact, in the non-relativistic limit, one can relate the EM form factors of a particle to the Fourier transforms of the charge and magnetization density.

Polarization Degrees of Freedom

A second major difference between $p(\gamma, K)Y$ and $p(\gamma^*, K)Y$ processes is the number of polarization degrees of freedom. A real photon as a free and massless spin-1 particle, has two polarization degrees of freedom. A virtual photon is not free, and has three polarization degrees of freedom. This extra polarization degree of free-

dom is required to transfer the polarizations of the incoming and outgoing electron to the hadronic scattering plane (right part of Fig. 3.1). Both the incoming and outgoing electron have two possible helicity states, so there are four different (double-)polarized cross sections : $\sigma_{\uparrow\uparrow}$, $\sigma_{\uparrow\downarrow}$, $\sigma_{\downarrow\uparrow}$, and $\sigma_{\downarrow\downarrow}$. A virtual photon, however, has three polarization states $\lambda = 0, \pm 1$, and three corresponding cross sections σ_λ. This apparent reduction of the number of polarized processes is resolved by the inversion symmetry of the reactions we are looking at. Parity invariance guarantees that $\sigma_{\uparrow\uparrow} = \sigma_{\downarrow\downarrow}$ and $\sigma_{\uparrow\downarrow} = \sigma_{\downarrow\uparrow}$, but it imposes only one constraint on the virtual-photon cross sections : $\sigma_{\lambda=+1} = \sigma_{\lambda=-1}$.

It is clear that in the limit of $Q^2 \to 0$, one of the virtual-photon polarizations ($\lambda = 0$) should decouple from physical processes. This can be illustrated with a small calculation. Using the conventions of Ref. [6], the longitudinal basis vector $\epsilon^\mu_{\lambda=0} = (|\mathbf{q}|, 0, 0, \omega)/\sqrt{Q^2}$ coupling to the hadronic current J_μ, results in the amplitude $\mathcal{M}_{\lambda=0} = (|\mathbf{q}|J^0 - \omega J^3)/\sqrt{Q^2}$. Gauge invariance assures that $q^\mu J_\mu = \omega J^0 - |\mathbf{q}|J^3 = 0$. If one is working in a frame where $|\mathbf{q}| \neq 0$, J^3 can be eliminated from the expression for the amplitude (in the case $|\mathbf{q}| = 0$, one can eliminate J^0 with the same result). Thus, we obtain $\mathcal{M}_{\lambda=0} = \frac{\sqrt{Q^2}}{|\mathbf{q}|} J^0$, which obviously vanishes when $Q^2 \to 0$.

3.2 The Tree-Level Isobar Model

3.2.1 Tree-Level versus Coupled-Channel

In Fig. 3.2, all types of diagrams included in our $p(\gamma^*, K)Y$ model are shown. In the lowest-order approximation to the $p(\gamma^*, K)Y$ process, all diagrams contain two vertices and one intermediate particle. This is commonly called the tree-level approximation, because it has no internal loops (just like a tree, where the branches stick out in the air and the roots stick out in the ground without folding back towards the stem of the tree).

A major problem when using the concept of Feynman diagrams in isobar models, is that they are meant to describe reaction amplitudes order by order in the coupling constants (perturbation series). However, the process one faces here involves the strong interaction in an energy region where the effective coupling constants are of order ~ 1 (non-perturbative effective field theory). This observation

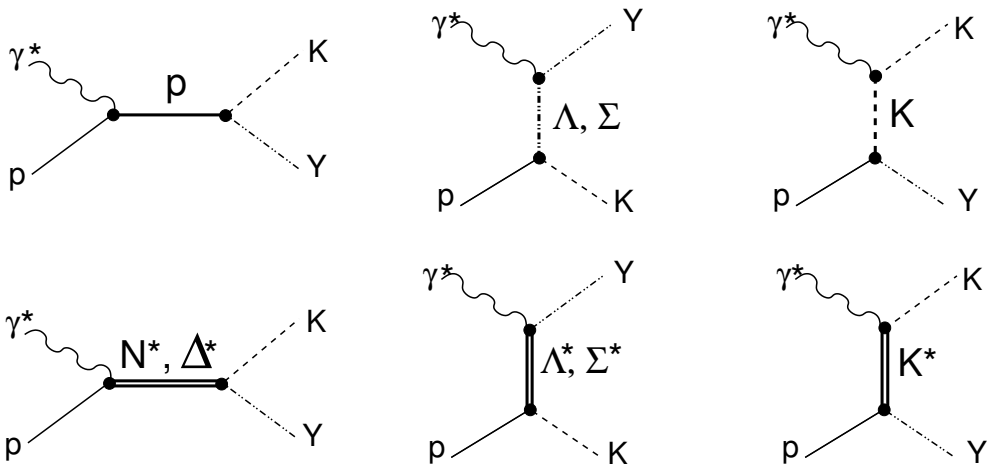

Figure 3.2 *Tree-level diagrams for the $p(\gamma^*, K)Y$ process. The upper row are the Born terms. The lower row corresponds to the exchange of nucleon ($T = 1/2$) and Δ ($T = 3/2$) resonances in the s-channel, Λ and Σ resonances in the u-channel, and kaon resonances in the t-channel.*

leads to the idea that rescattering effects are important in the description of meson production and scattering from the nucleon. A coupled-channel (CC) approach, where all rescattering channels are taken into account, is expected to provide more reliable quantitative results than a tree-level approach. There are, however, good arguments to further develop a model at tree level :

- The coupled-channel calculations reported in Ref. [58] show that CC effects, originating mainly from the $\gamma^* \to \pi N \to KY$ multi-step process, can be as large as 20% for the $\gamma p \to K^+\Lambda$ cross section. This implies that the tree-level diagrams dominate the production process.

- CC models usually have a large number of parameters which need to be fitted to very large data sets. This includes the search for a global minimum of a χ^2-function in a highly dimensional parameter space. In Refs. [10, 59], we pointed out that optimizing about 20 parameters to the kaon-photoproduction data is already far from trivial in a tree-level model. In fact, there appear to be many different sets of parameters describing the data equally well.

- In order to guarantee the unitarity of the $\mathcal{S}$-matrix, CC models usually place the intermediate (rescattered) particles on the mass shell (K-matrix approx-

imation). This introduces off-shell ambiguities whose impact is unknown. Tree-level models have no off-shell ambiguities in the propagators of the exchanged particles.

- CC models need tree level diagrams such as those in Fig. 3.2 as input for one single rescattering. A good knowledge of the process at tree level is therefore indispensable.
- In order to respect unitary constraints, CC models need to include all possible rescattering channels. This is a gigantic task, since channels such as $\pi\pi N$ are difficult to model [60]. Unitarity is not the major concern of tree-level models.
- Structures in the data can arise from resonances in a single vertex or can be a rescattering effect. It is not always obvious to find out which of the two possibilities is at the origin of the structure. This is illustrated in Fig. 3.3. Tree-level models can parameterize meson-baryon intermediate states as a single resonance. CC models need to distinguish between genuine resonances and resonances which are generated dynamically through meson-baryon interactions. Otherwise, these meson-baryons states are double-counted.

3.2.2 Gauge Invariance

There are many textbooks dealing with the subject of QED, each of which touches upon the topic of *gauge invariance*, or a related one such as *charge conservation* or *minimal substitution*. Yet, most of them assume an exemplary system, populated with point-like charged leptons and photons, and then proceed with giving some examples of how charged extended objects might couple to the photon field. As yet, a consistent treatment is not available for the simple reason that we do not even know in full how the photon field couples to the proton. A forceful reminder of this was the confirmation of the discrepancy between the G_E/G_M form-factor ratios obtained from two different techniques : the Rosenbluth-separation [61] and the polarization-transfer method [62, 63]. It has recently been suggested that two-photon exchange mechanisms may be at the origin of this discrepancy [64].

In this section, we will discuss the coupling of a real or virtual photon to a strongly interacting system, and how the property of gauge invariance can be realized in an isobar model for meson photoproduction on the nucleon. First, the effects

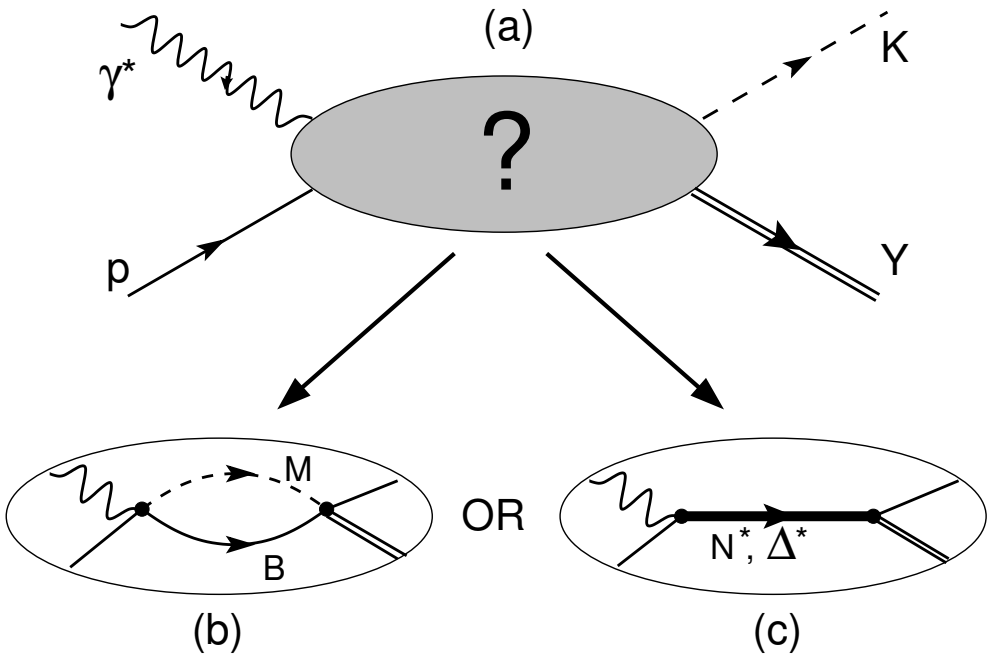

Figure 3.3 *Schematic representation of the two most likely physical mechanisms which can be at the origin of structures observed in the energy dependence of cross sections and polarization observables for the $p(\gamma^*, K)Y$ processes (a) ? A structure can follow from meson-baryon rescattering effects (b), or from resonance contributions (c). Rescattering effects can be described by the inclusion of an (effective) resonance, in which case CC models face the problem of double counting.*

of including strong form factors are presented. Then, the method outlined in many QED-textbooks to impose gauge invariance at amplitude level will be sketched and its shortcomings when applied to effective field theories will be discussed.

Hadronic Form Factors Break Gauge Invariance

In a typical isobar model, the gauge-invariance breaking terms arise from the inclusion of hadronic form factors for the Born terms which have an electric coupling. For example, in the $p(\gamma^{(*)}, K)\Lambda$ process, the s-channel proton and t-channel kaon (K^+) terms violate gauge invariance. To sketch the problem, let us look at the am-

plitudes arising from the electric terms in the $p(\gamma^{(*)}, K)\Lambda$ reaction [6] :

$$\epsilon_\mu \mathcal{M}^\mu_{s-electric} = \epsilon_\mu e g_{K^+\Lambda p} \overline{u}_\Lambda \gamma_5 \frac{(\not{p} + \not{q}) + m_p}{s - m_p^2} \gamma^\mu u_p \ , \tag{3.1a}$$

$$\epsilon_\mu \mathcal{M}^\mu_{t} = \epsilon_\mu e g_{K^+\Lambda p} \overline{u}_\Lambda \frac{2p^\mu_K - q^\mu}{t - m_K^2} \gamma_5 u_p \ . \tag{3.1b}$$

Here, we have introduced the four-momenta of proton (p^μ), kaon (p^μ_K) and photon (q^μ), the polarization vector of the photon (ϵ_μ), and the spinors of the incoming proton (u_p) and outgoing Λ-hyperon ($\overline{u}_\Lambda$). We have also used the Mandelstam variables, which are in this case defined as :

$$s = (p+q)^2 \ , \quad t = (p_K - q)^2 \ , \quad u = (p_\Lambda - q)^2 \ . \tag{3.2}$$

Gauge invariance is ensured if the total amplitude obeys the Lorentz condition $q_\mu \mathcal{M}^\mu = 0$. Using the anticommutation relations for the γ-matrices and the Dirac equation for the spinors, it is straightforward to show that the sum of the electric amplitudes in Eqs. (3.1a) and (3.1b) fulfills the condition $q_\mu(\mathcal{M}^\mu_{s-electric} + \mathcal{M}^\mu_t = 0$. When inserting hadronic form factors which are different for the s- and the t-channel, gauge invariance is violated. At first, it may appear strange that the inclusion of form factors at the hadronic vertex breaks gauge invariance, which is a property of the electromagnetic interaction. However, instead of interpreting the hadronic form factor as a modification to the strong vertex, one could absorb it into the propagator of the off-shell intermediate particle. Then, we see that it can also change the properties of the EM vertex. While quantum physics normally states that the probe influences the system, here, one can put forward that the system changes the probe.

Many recipes are available for restoring gauge invariance for the Born contributions. The most widely used procedure is the introduction of a contact term which cancels out all gauge invariant terms and results in a modification of the electric terms with the same form factor $\hat{F}$ [57]. For the $p(\gamma^{(*)}, K)\Lambda$ process, we obtain :

$$\epsilon_\mu \mathcal{M}^\mu_{contact} = \epsilon_\mu e g_{K^+\Lambda p} \overline{u}_\Lambda \gamma_5 \left[\frac{2p^\mu + \not{q}\gamma^\mu}{s - m_p^2} \left(\hat{F} - F_s \right) + \frac{2p^\mu_K}{t - m_K^2} \left(\hat{F} - F_t \right) \right] u_p \ . \tag{3.3}$$

Here, F_s and F_t are the hadronic form factors for the s- and the t-channel respectively. The form factor $\hat{F}$ should go to 1 in the soft-photon limit ($q \to 0$). A functional form has been proposed by Davidson and Workman in Ref. [65], which frees

the contact term from the poles at $s = m_p^2$ and $t = m_K^2$ by putting $\hat{F}_{s=m_p^2} = F_s$ and $\hat{F}_{t=m_K^2} = F_t$ respectively. In our isobar model, we put forward the form :

$$F_x(\Lambda) = \frac{\Lambda^4}{\Lambda^4 + (x - m_x^2)^2} \qquad (x = s, t, u) \ , \tag{3.4}$$

for the hadronic form factor in the x-channel. This kind of form factor smoothens the off-shell and high-energy (short range) effects hard or gently, depending on the value of the cutoff mass Λ. With this functional form, we can apply the prescription of Ref. [65] to obtain :

$$\hat{F} = \hat{F}_{DW} \equiv F_s(\Lambda) + F_t(\Lambda) - F_s(\Lambda)F_t(\Lambda) \ . \tag{3.5}$$

This above procedure for restoring gauge invariance after the inclusion of strong form factors, can only be applied to the Born terms (top row of Fig. 3.2). For the resonance contributions, a different approach is adopted. There, we impose the various contributions to be gauge invariant one-by-one. This allows for a systematic investigation of the role of the different resonances in the reaction mechanism in a way which always respects gauge invariance.

The inclusion of strong form factors is necessary in the description of both photo- and electroproduction of kaons from the proton. The inclusion of electromagnetic form factors in a gauge-invariant way will be discussed in Sect. 3.3. There, a consistent treatment will be given for all terms in isobar models in which an electromagnetic vertex appears.

Ward-Takahashi Identities

The most powerful tool for discussing gauge invariance at amplitude level, is the set of Ward-Takahashi (WT) identities, which are presented in many textbooks (*e.g.* in Ref. [66]). When the amplitudes of a model fulfill the WT identities, gauge invariance is automatically respected. In an isobar model, the WT identities can be used to impose gauge invariance on the Born terms when introducing strong and electromagnetic form factors. This is not possible for the extended Born terms and the resonance terms, because in those diagrams, the particle changes identity after coupling to the photon. This is another difference between fundamental theories like QED and QCD, and a typical isobar model. For the fundamental theories, one has

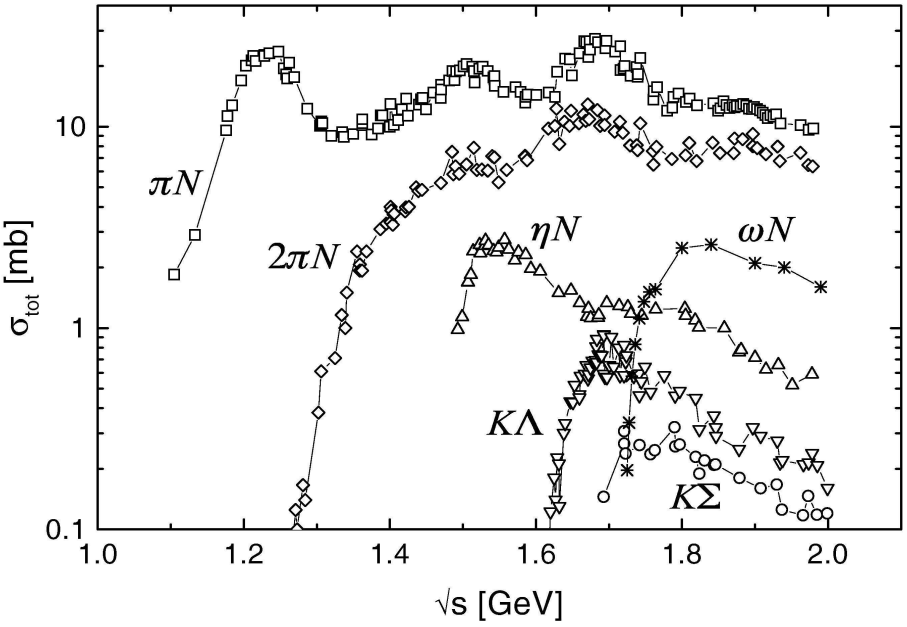

Figure 3.4 *Total $\pi N \to X$ cross sections, where X stands for the different channels as described in the figure. The figure is from Ref. [67], the data are taken from Ref. [68]. The curves are meant to guide the eye.*

matter particles that keep their identity after the interactions (although some quantum numbers can change), and the WT identities can be employed on all diagrams. In isobar models, the resonance and extended Born terms involve the transformation of a ground-state hadron to a different particle, which makes the WT identities of little use for these diagrams. As mentioned before, one forces these terms to be separately gauge invariant.

3.2.3 Background Diagrams

Fig. 3.4 from Ref. [67] illustrates the relative size of the meson-baryon channels which can be produced by πN collisions in the intermediate energy region. It is clear that the strangeness-production channels $K\Lambda$ and $K\Sigma$ constitute but a small fraction of the total strength in the final channels. The relatively small cross sections induce complications in the isobar description of kaon-production processes

which did not turn up in the non-strangeness-production channels. Finding an appropriate description of the background is by far the toughest problem. The background part of the computed cross sections is that part corresponding to Feynman diagrams which are free of poles in the kinematical region of the $p(\gamma^{(*)}, K)Y$ process. In fact, the background consists of all diagrams shown in Fig. 3.2, except the ones containing nucleon or delta resonances with masses larger than (or just below) the threshold for the KY channel (the resonant part originates from these s-channel resonances). The specific contributions to the background are the Born terms. These are constituted of an off-shell proton in the s-channel, kaon exchange in the t-channel, and hyperon exchange in the u-channel of the $p(\gamma^{(*)}, K)Y$ process (upper row of diagrams in Fig. 3.2). Furthermore, for the $K\Lambda$ channel, the $K^*(892)$ vector resonance and the $K_1(1270)$ axial-vector resonance are taken into account. For the $K\Sigma$ channels, only the $K^*(892)$ is included. The *background problem* in $p(\gamma^{(*)}, K)Y$ processes has been discussed elaborately in Refs. [2–6].

The importance of the background problem is clearly illustrated in Fig. 3.5. Here, the total cross sections originating from only the Born terms are displayed for the three isospin channels, when the couplings of the proton to the KY channels are derived from the well-known πNN-coupling through $SU(3)_f$-symmetry [69, 70] :

$$-4.5 \leq \quad g_{K^+\Lambda p}/\sqrt{4\pi} \quad \leq -3.0\ , \tag{3.6a}$$

$$0.9 \leq \quad g_{K^+\Sigma^0 p}/\sqrt{4\pi} \quad \leq 1.3\ . \tag{3.6b}$$

Here, the coupling constants g_{KYp} are allowed to differ up to 20% from their $SU(3)_f$ predictions, since this symmetry is only approximate. While the contributions stemming from the Born terms to the background in πN scattering and π-photoproduction are small to moderate, the cross sections computed with only the Born terms, overshoot the data by an order of magnitude.

In the following, three different schemes (models A, B and C) are presented which succeed in reducing the strength stemming from the Born terms. This strength is characterized by the product of the proton-kaon-hyperon coupling and a strong form factor :

$$G_{KYp} \;=\; g_{KYp} \;\cdot\; F_x(\Lambda)\ . \tag{3.7}$$

Here, $F_x(\Lambda)$ was defined previously in Eq. (3.4). It is clear that the schemes should

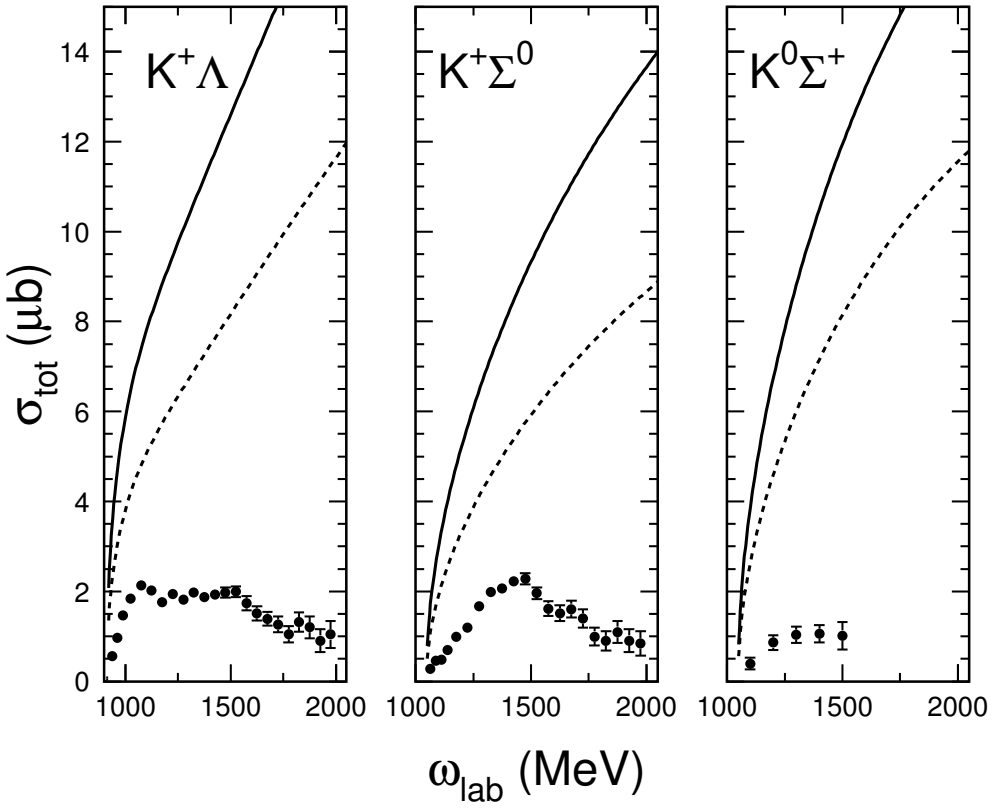

Figure 3.5 *The cross sections originating from only the Born terms are shown as a function of the photon lab energy for the three $\gamma p \to KY$ channels. The solid line results from using the $SU(3)_f$ predictions for the strong coupling constants, the dashed line is for values which are 20% smaller due to limited $SU(3)_f$-symmetry breaking (*cfr. *Eqs. (3.6)). The data are from Refs. [7, 8].*

either try to diminish G_{KYp} directly, or include new terms which interfere destructively with the Born terms.

Model A

In model A, the strong coupling constants are kept within the boundaries of Eqs. (3.6) for limited $SU(3)_f$-breaking. With such values of the coupling constants, the reduction of the background strength to an acceptable level requires the introduction of *soft* hadronic form factors. It is obvious that the quantity G_{KYp} from Eq. (3.7) diminishes for smaller values for the cutoff mass Λ in the definition for the strong

form factor. In practice, the cutoff masses is allowed to be as small as 0.4 GeV, which is smaller than the kaon mass. It is clear that for such small values, the form factors play a key role in the dynamics of the reaction under consideration already near threshold.

Model B

In this model, the background strength is reduced through the inclusion of new terms which interfere destructively with the Born terms. The new terms arise from contributions of hyperon resonances in the u-channel (lower right diagram of Fig. 3.2). This allows for a fair description of the kaon-production data with values for the strong coupling constants g_{KYp} within the boundaries of Eqs. (3.6), and with reasonably high cutoff mass for the strong form factors ($\Lambda \gtrsim 1.5$ GeV).

The experimental data for electromagnetic and strong decays of hyperon resonances is rather scarce. Therefore, the exact choice for the hyperon resonances to be included in the background description, is biased by the predictions of constituent quark models for electromagnetic and hadronic coupling constants. The thorough study of the EM properties of hyperon resonances within the Bonn constituent quark model done in this work, provides one partly with the necessary information.

Model C

The cutoff mass used in the strong form factors of the Born terms is kept moderately high (~ 1.1 GeV) in model C. No hyperon resonances in the u-channel are considered. The background strength is reduced by softening the imposed constraints of Eqs. (3.6) on the strong coupling constants. A proper fit of the data can only be reached with values for $g_{K^+\Lambda p}$ and $g_{K^+\Sigma^0 p}$ which are about 25% of the $SU(3)_f$ predictions.

3.3 Electromagnetic Form Factors

The topic of electromagnetic (EM) form factors was already covered in Sect. 2.4. There, we have taken the point of view of the constituent-quark modeller, and discussed how the current matrix elements, computed in the Bonn model, can be re-

lated to the on-shell form factors and helicity amplitudes of the baryons and baryon resonances. Here, we use the looking glasses of an "isobar" modeller. Then, including EM form factors is more involved than merely plugging in the values computed in Chap. 4 with the Bonn constituent quark model. The complications arise from the interplay between off-shell effects and gauge-breaking (or, -restoring) mechanisms. Off-shell effects are present in any tree-level isobar model, since the intermediate particles are virtual and therefore off their mass shell. Only for s-channel resonance exchange, the intermediate particle can be on-shell for some particular kinematics.

In this section, a method for dealing with the off-shell effects in electromagnetic vertices will be outlined. This vertex has to fulfill the conditions for gauge invariance. This condition will be affected by the degree of off-shellness of the particles and the inclusion of strong form factors, which by itself is also an off-shell effect. In Sect. 3.3.1, arguments for constraining the form of the EM vertex on very general grounds will be presented. In Sect. 3.3.2, the WT identities will be used to impose gauge invariance on the Born terms, and in Sects. 3.3.3 and 3.3.4, it will be outlined how EM transition form factors can be introduced in a gauge-invariant manner. It will be made clear what happens to the form factors when one or more of the particles involved are put on the mass shell.

3.3.1 General Electromagnetic Vertex

We consider the process shown in Fig. 3.6, whereby both fermions are not necessarily on the mass shell. Yet, the EM vertex (including the external photon line) can still be written as in Eq. (2.50) :

$$\epsilon_\mu(q)\Gamma^\mu\left(p',p\right) \ . \tag{3.8}$$

This contraction of photon polarization vector and vertex operator should be hermitean, as well as a Lorentz scalar.

The form of Γ^μ is determined by the fourvectors in the system. Let us consider the EM transition of a spin $J=3/2$ to another spin $J'=3/2$ particle. The relevant fourvectors are then (*cfr.* Fig. 3.6) : ϵ^μ, q^μ, p^μ, V^μ, p'^μ, and V'^μ. There are more than four fourvectors, which means that some of them can be written as a linear combination of the others. It is therefore sufficient to build the vertex $\epsilon_\mu\Gamma^\mu$ with only four fourvectors and the Dirac matrices.

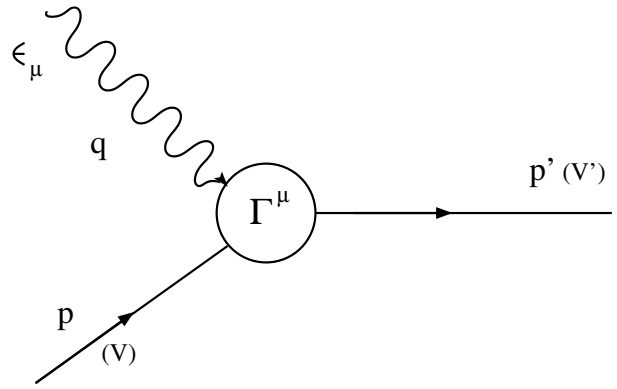

Figure 3.6 *A photon with four-momentum q and polarization fourvector ϵ_μ couples to an incoming fermion (baryon) with four-momentum p, resulting in an outgoing fermion with four-momentum p'. For $J \geq 3/2$ fermions, one or more extra fourvectors are needed to describe their polarization (V and V'). The fermions can either be both off shell, both on shell, or one can be off shell and the other on shell.*

Let us take the following choice of fourvectors : ϵ^μ, $q^\mu = p'^\mu - p^\mu$, $P^\mu = (p'^\mu + p^\mu)/2$ and V^μ. Furthermore, the fourvector ϵ^μ must occur linearly in any vertex term so that it can be separated, as in Eq. (3.8). The vertex Γ^μ is therefore a linear combination of the fourvectors q^μ, P^μ, V^μ and γ^μ, but the coefficients can still be operators in Dirac space. Since the latter can be written as 4×4 matrices, there can be at most 16 linearly independent Dirac-space operators, which can be written in terms of : $(\mathbb{1}, \not{q}, \not{P}, \not{V}, \not{q}\not{P}, \not{q}\not{V}, \not{P}\not{V}, \not{q}\not{P}\not{V}) \times (\mathbb{1}, \gamma^5)$. The $J = 3/2 \rightarrow J' = 3/2$ EM transition can thus be expressed in terms of 64 structures, which read :

$$\epsilon_\mu \cdot (q^\mu, P^\mu, V^\mu, \gamma^\mu) \times (\mathbb{1}, \not{q}, \not{P}, \not{V}, \not{q}\not{P}, \not{q}\not{V}, \not{P}\not{V}, \not{q}\not{P}\not{V}) \times (\mathbb{1}, \gamma^5) \, . \tag{3.9}$$

This is clearly the maximum number of independent terms, since the momentum space has 4 basis vectors and Dirac operators can be expressed in a 4×4 basis. Each of the above terms can enter the vertex, multiplied by a function of the scalar quantities in the system (such as q^2, $q \cdot P$, $q \cdot V$, ...). These 64 functions are the EM form factors of the vertex.

In the following sections, we will restrict ourselves to EM transitions from a spin $J = 1/2$ to a spin $J' = 1/2$ particle. Since no extra fourvectors V are needed to describe the polarizations of the particles, one only has three independent fourvectors in the system, *e.g* ϵ^μ, $q^\mu = p'^\mu - p^\mu$, $P^\mu = (p'^\mu + p^\mu)/2$, plus the fourvector

of Dirac matrices γ^μ. Again, the photon polarization fourvector ϵ^μ should appear exactly once in every term of the vertex, and so we must write Γ^μ from Eq. (3.8) in terms of the fourvectors q^μ, P^μ and γ^μ.

The three independent four-momenta p^μ, p'^μ and γ^μ can be multiplied by operators in Dirac-space which are scalars in configuration space. Thus the only independent scalar operators in the problem read : $(\mathbb{1}, \not{q}, \not{P}, \not{q}\not{P}) \times (\mathbb{1}, \gamma^5)$. The reduction of any higher-order scalar operator to a linear combination of these four basis operators can be easily performed using the anticommutation rules for the Dirac-matrices $\{\gamma^\mu, \gamma^\nu\} = 2g^{\mu\nu}\mathbb{1}$ and noting that $\not{q}\not{q} = q^2$, $\not{P}\not{P} = P^2$, and $\gamma^\mu\gamma_\mu = 4\,\mathbb{1}$.

Any product of four-momenta and Dirac-matrices which can contribute to the vertex Γ^μ can thus be written as a linear combination of 24 *basis vertex structures* :

1. q^μ	5. P^μ	9. γ^μ	13. $q^\mu\gamma^5$	17. $P^\mu\gamma^5$	21. $\gamma^\mu\gamma^5$
2. $q^\mu\not{q}$	6. $P^\mu\not{q}$	10. $\gamma^\mu\not{q}$	14. $q^\mu\not{q}\gamma^5$	18. $P^\mu\not{q}\gamma^5$	22. $\gamma^\mu\not{q}\gamma^5$
3. $q^\mu\not{P}$	7. $P^\mu\not{P}$	11. $\gamma^\mu\not{P}$	15. $q^\mu\not{P}\gamma^5$	19. $P^\mu\not{P}\gamma^5$	23. $\gamma^\mu\not{P}\gamma^5$
4. $q^\mu\not{q}\not{P}$	8. $P^\mu\not{q}\not{P}$	12. $\gamma^\mu\not{q}\not{P}$	16. $q^\mu\not{q}\not{P}\gamma^5$	20. $P^\mu\not{q}\not{P}\gamma^5$	24. $\gamma^\mu\not{q}\not{P}\gamma^5$.

(3.10)

One can write this set of basis vertex structures in a more concise way as $(q^\mu, P^\mu, \gamma^\mu)\times (\mathbb{1}, \not{q}, \not{P}, \not{q}\not{P}) \times (\mathbb{1}, \gamma^5)$.

QED imposes the condition that the EM vertex of Eq. (3.8) should be a scalar and not a pseudoscalar because of the parity invariance of the EM interaction. However, QED is a fundamental theory dealing with point particles, which do not change parity during the interaction. We are working with extended particles, baryons, which can change identity by means of the EM interaction (*e.g* a nucleon resonance can change into the nucleon ground-state after emitting a photon). The parity of the incoming baryon is not necessarily equal to the one of the outgoing baryon. We have already coined the expressions *normal-parity* and *abnormal-parity* transitions in Sects. 2.4.2 and 2.4.3. A normal-parity transition occurs when the difference in spin of ingoing and outgoing baryon is an integer l, and the parity is changed by a factor $(-1)^l$. An abnormal-parity transition then corresponds to the case where the parity is changed by a factor $(-1)^{l+1}$. This has its effects on the form of the vertex. If the transition has normal parity, *e.g.* $J'^{\pi'} = 1/2^+ \to J^\pi = 1/2^+$, the terms with γ^5 have to vanish in order to conserve parity of the complete amplitude, so their coefficients

(EM form factors) will vanish. In the case of an abnormal-parity transition, on the other hand, only the terms with a γ^5 survive, and form factors corresponding to other terms vanish. This observation allows us to divide the discussion into two parts. Normal-parity transitions will be discussed in Sect. 3.3.2 for elastic vertices (*i.e.* incoming and outgoing particle are identical) and in Sect. 3.3.3 for transitions between two spin $J'^{\pi'} = J^{\pi} = 1/2^+$ baryons. In Sect. 3.3.4, the abnormal-parity vertex for $J'^{\pi'} = 1/2^- \rightarrow J^{\pi} = 1/2^+$ transitions will be discussed.

3.3.2 Elastic Electromagnetic Vertex

The twelve vertex structures from Eq. (3.10) which do not depend on γ^5, are not the ones usually adopted in the description of the EM vertex. As one wishes a functional form for Γ^μ which resembles the on-shell form of Eq. (2.49), the following most general form for the off-shell case appears adequate as a starting point [71] :

$$\begin{aligned}
\Gamma^\mu\left(p',p\right) &= \not{p}' \left(f_1^{11}\gamma^\mu + f_2^{11}\frac{i\sigma^{\mu\nu}q_\nu}{2M_p} + f_3^{11}q^\mu \right) \not{p} \\
&+ \not{p}' \left(f_1^{10}\gamma^\mu + f_2^{10}\frac{i\sigma^{\mu\nu}q_\nu}{2M_p} + f_3^{10}q^\mu \right) \mathbb{1} \\
&+ \mathbb{1} \left(f_1^{01}\gamma^\mu + f_2^{01}\frac{i\sigma^{\mu\nu}q_\nu}{2M_p} + f_3^{01}q^\mu \right) \not{p} \\
&+ \mathbb{1} \left(f_1^{00}\gamma^\mu + f_2^{00}\frac{i\sigma^{\mu\nu}q_\nu}{2M_p} + f_3^{00}q^\mu \right) \mathbb{1} \,. \qquad (3.11)
\end{aligned}$$

Obviously, we now use another set of basis vertex structures : $(\not{p}', \mathbb{1}) \times \left(\gamma^\mu, \frac{i\sigma^{\mu\nu}q_\nu}{2M_p}, q^\mu\right) \times (\not{p}, \mathbb{1})$. Using the anticommutation relations for the Dirac-matrices, the proof of the equivalence of the two basis sets is straightforward, but too lengthy to be shown here in detail. The form factors $f_i^{\lambda'\lambda}$ are functions of the three independent scalars in the problem : p'^2, p^2 and q^2. Applying the time-reversal and parity-changing operators on the system, which involves interchanging the incoming and outgoing particles, and the invariance of the operator (2.50) under the same discrete transformations for a normal-parity transition, puts the following conditions on the form factors :

$$f_{1,2}^{\lambda',\lambda}(p'^2,p^2,q^2) = f_{1,2}^{\lambda,\lambda'}(p^2,p'^2,q^2) \,, \qquad (3.12a)$$

$$f_3^{\lambda',\lambda}(p'^2,p^2,q^2) = -\, f_3^{\lambda,\lambda'}(p^2,p'^2,q^2) \,, \qquad (3.12b)$$

where $\lambda, \lambda' \in \{1, 0\}$.

The expression of Eq. (3.11) is the most general expression for an interaction vertex involving particles with $J^\pi = 1^-$, coupling to $J'^{\pi'} = J^\pi = 1/2^+$ particles. For identical incoming and outgoing baryons, one can impose gauge invariance at the level of the vertex by constraining it to fulfill the *Ward-Takahashi (WT) identities*. These general identities are usually derived using Feynman diagrams and relate the EM vertex to the propagators :

$$-i\, e\, q_\mu \Gamma^\mu \left(p', p\right) = \; e\, e_N \; \left[S^{-1}(p') - S^{-1}(p)\right] \; , \tag{3.13}$$

where $S^{-1}(p) = (-i)\,(\not{p} - m + i\epsilon)$ denotes the inverse of the propagator of the particle with four-momentum p and mass m, while e_N is the particle charge in units of the positron charge e. Substituting the vertex from Eq. (3.11) into the above WT identity, one obtains :

$$\begin{aligned} -\,i\,e\; \left(f_1^{11}\not{p}'\not{q}\not{p} + f_3^{11}q^2\not{p}'\not{p} + f_1^{10}\not{p}'\not{q} + f_3^{10}q^2\not{p}' + f_1^{01}\not{q}\not{p} + f_3^{01}q^2\not{p} + f_1^{00}\not{q} + f_3^{00}q^2\right) \\ = \; -i\; e\; e_N \; \left(\not{p}' - \not{p}\right) \; . \end{aligned} \tag{3.14}$$

The terms containing $\frac{i\sigma^{\mu\nu}q_\nu}{2M_p}$ do not contribute to the emerging constraint, because $\sigma^{\mu\nu} = -\sigma^{\nu\mu}$. The above condition can be reorganized in such a way that only terms in the scalar operators $(\mathbb{1}, \not{q}, \not{P}, \not{q}\not{P})$ survive :

$$\begin{aligned} &\mathbb{1}\left[\left(p^2 - \frac{q^2}{2}\right) q^2 f_3^{11} + \left(p'^2 - p^2 + \frac{q^2}{2}\right) f_1^{10} - \frac{q^2}{2} f_1^{01} + q^2 f_3^{00}\right] \\ &+ \not{q}\left[-\frac{p'^2 + p^2}{2} f_1^{11} + \frac{q^2}{2} f_3^{10} - \frac{q^2}{2} f_3^{01} + f_1^{00} - e_N\right] \\ &\quad + \not{P}\left[\left(p'^2 - p^2\right) f_1^{11} + q^2 f_3^{10} + q^2 f_3^{01}\right] \; + \; \not{q}\not{P}\left[q^2 f_3^{11} - f_1^{10} + f_1^{01}\right] = 0 \end{aligned} \tag{3.15}$$

The coefficients corresponding with the scalar operators $\mathbb{1}$, $\not{q}$, $\not{P}$ and $\not{q}\not{P}$ should vanish. This results in constraints on the off-shell form factors $f_i^{\lambda'\lambda}\left(p'^2, p^2, q^2\right)$:

$$q^2\; f_3^{11} \;=\; f_1^{10} - f_1^{01} \; , \tag{3.16a}$$

$$q^2\; f_3^{10} \;=\; p^2 f_1^{11} - f_1^{00} + e_N \; , \tag{3.16b}$$

$$q^2\; f_3^{01} \;=\; -p'^2 f_1^{11} + f_1^{00} - e_N \; , \tag{3.16c}$$

$$q^2\; f_3^{00} \;=\; -p'^2 f_1^{10} + p^2 f_1^{01} \; . \tag{3.16d}$$

Remark that there are no constraints on the f_2 form factors.

The four constraints of Eq. (3.16) diminish the number of independent form factors in the vertex of Eq. (3.11). As a matter of fact, the $f_3^{\lambda',\lambda}$ form factors can be completely eliminated. The most general vertex which automatically implies gauge invariance can then be written as :

$$\begin{aligned}
\Gamma^{\mu}\left(p',p\right) &= \not{p}'\left[f_1^{11}\left(\gamma^{\mu}-\frac{\not{q}q^{\mu}}{q^2}\right)+f_2^{11}\frac{i\sigma^{\mu\nu}q_{\nu}}{2M_p}\right]\not{p} \\
&+ \not{p}'\left[f_1^{10}\left(\gamma^{\mu}-\frac{\not{q}q^{\mu}}{q^2}\right)+f_2^{10}\frac{i\sigma^{\mu\nu}q_{\nu}}{2M_p}\right]\mathbb{1} \\
&+ \mathbb{1}\left[f_1^{01}\left(\gamma^{\mu}-\frac{\not{q}q^{\mu}}{q^2}\right)+f_2^{01}\frac{i\sigma^{\mu\nu}q_{\nu}}{2M_p}\right]\not{p} \\
&+ \mathbb{1}\left[f_1^{00}\left(\gamma^{\mu}-\frac{\not{q}q^{\mu}}{q^2}\right)+f_2^{00}\frac{i\sigma^{\mu\nu}q_{\nu}}{2M_p}\right]\mathbb{1} \\
&+ e_N\,\frac{q^{\mu}}{q^2}\not{q}\,. \qquad (3.17)
\end{aligned}$$

It can be easily confirmed that this vertex operator satisfies the WT identity (3.13).

For $q^2 = 0$, the vertex function of Eq. (3.17) displays divergencies. However, for $q^2 \to 0$, the following relations can be directly extracted from the conditions of Eq. (3.16) :

$$f_1^{11}\left(p'^2,p^2,q^2\to 0\right) = 0\,, \qquad (3.18a)$$

$$f_1^{10}\left(p'^2,p^2,q^2\to 0\right) = f_1^{01}\left(p'^2,p^2,q^2\to 0\right) = 0\,, \qquad (3.18b)$$

$$f_1^{00}\left(p'^2,p^2,q^2\to 0\right) = e_N\,. \qquad (3.18c)$$

The f_1^{11}, f_1^{10} or f_1^{01} form factors can go to zero, proportionally with q^2. In this case, the real-photon vertex acquires longitudinal parts proportional to $\not{p}'\not{q}q^{\mu}\not{p}$, $\not{p}'\not{q}q^{\mu}$, and $\not{q}q^{\mu}\not{p}$ respectively.

We can now consistently simplify the expression for the EM vertex (3.11) in the case one (Sect. 3.3.2) or two particles (Sect. 3.3.2) are on the mass shell.

Half Off-shell Vertex

For the situation with one particle on-shell, the vertex (3.11) and the WT identities (3.13) take on a simpler form. Let us assume that the outgoing Dirac particle is

on the mass shell ($\overline{u}(\mathbf{p}')(\not{p}' - m) = 0$). The vertex then takes the form :

$$\overline{u}(\mathbf{p}')\,\Gamma^{\mu}\left(\overline{p}', p\right) = \overline{u}(\mathbf{p}')\left[\left(f'^{1}_{1}\gamma^{\mu} + f'^{1}_{2}\frac{i\sigma^{\mu\nu}q_{\nu}}{2M_p} + f'^{1}_{3}q^{\mu}\right)\not{p} + \left(f'^{0}_{1}\gamma^{\mu} + f'^{0}_{2}\frac{i\sigma^{\mu\nu}q_{\nu}}{2M_p} + f'^{0}_{3}q^{\mu}\right)\mathbb{1}\right] . \tag{3.19}$$

The six half off-shell form factors in this expression are related to the twelve off-shell form factors from Eq. (3.11) :

$$f'^{1}_{i}\left(p^2, q^2\right) = m f^{11}_{i}\left(m^2, p^2, q^2\right) + f^{01}_{i}\left(m^2, p^2, q^2\right) , \tag{3.20a}$$

$$f'^{0}_{i}\left(p^2, q^2\right) = m f^{10}_{i}\left(m^2, p^2, q^2\right) + f^{00}_{i}\left(m^2, p^2, q^2\right) . \tag{3.20b}$$

The WT identity (3.13) simplifies since the operation of the inverse propagator on an on-shell spinor gives zero :

$$-ie\overline{u}(\mathbf{p}')q_{\mu}\Gamma^{\mu}\left(\overline{p}', p\right) = -iee_N\overline{u}(\mathbf{p}')\left(-\not{p} + m\right) . \tag{3.21}$$

Applying the WT identity (3.21) to the vertex (3.19) produces two constraints for the form factors :

$$q^2 f'^{1}_{3} = -m f'^{1}_{1} + f'^{0}_{1} - e_N , \tag{3.22a}$$

$$q^2 f'^{0}_{3} = p^2 f'^{1}_{1} - m f'^{0}_{1} + m e_N . \tag{3.22b}$$

The expressions are consistent with the WT constraints of Eq. (3.16) and the definitions (3.20) of the half off-shell form factors. Introducing these constraints in the half off-shell EM vertex (3.19) yields a gauge-invariant EM vertex when the outgoing particle is on-shell :

$$\overline{u}(\mathbf{p}')\Gamma^{\mu}\left(\overline{p}', p\right) = \overline{u}(\mathbf{p}')\left[f'^{1}_{1}\left(\gamma^{\mu} - \frac{\not{q}q^{\mu}}{q^2}\right)\not{p} + f'^{1}_{2}\frac{i\sigma^{\mu\nu}q_{\nu}}{2M_p}\not{p} + f'^{0}_{1}\left(\gamma^{\mu} - \frac{\not{q}q^{\mu}}{q^2}\right) + f'^{0}_{2}\frac{i\sigma^{\mu\nu}q_{\nu}}{2M_p} - e_N\frac{q^{\mu}}{q^2}\left(\not{p} - m\right)\right] . \tag{3.23}$$

Here, $\not{q}$ can be replaced with $m - \not{p}$. As for the off-shell vertex (3.17), one should look at what happens in the real photon point. Putting the left-hand sides of Eqs. (3.22) to zero and putting p' on the mass shell ($p'^2 = m^2$), one arrives at :

$$f'^{1}_{1}\left(p^2, q^2 \to 0\right) = 0 , \tag{3.24a}$$

$$f'^{0}_{1}\left(p^2, q^2 \to 0\right) = e_N . \tag{3.24b}$$

When imposing the constraints (3.24) in the EM vertex (3.23) for real photons, the divergent terms (with a factor q^{-2}) cancel. If the f_1 form factors behave like q^2 for $q^2 \to 0$, terms proportional to $\not{q} q^\mu$ also survive :

$$\overline{u}(\mathbf{p}')\Gamma^\mu\left(\overline{p}', p\right) = \overline{u}(\mathbf{p}')\left[-\not{q} q^\mu(a'\not{p} + b') + \frac{i\sigma^{\mu\nu}q_\nu}{2M_p}\left(f'^1_2\not{p} + f'^0_2\right) + e_N\gamma^\mu\right], \quad (3.25)$$

where a' and b' are the coefficients of q^2 in the McLaurin series expansion of the f'^1_1 and f'^0_1 form factors respectively. They can still be a function of the square of the off-shell particle four-momentum p^2. In Eq. (3.25), one already notices the resemblance between this vertex and the commonly used vertex (2.49).

The half off-shell EM vertex is important in tree-level isobar models. The WT identity (3.21) eliminates two of the six form factors in Eq. (3.19). Therefore, tree-level models require four form factors in the EM vertex of the s- and u-channel Born terms.

To finish, two remarks are in order. First, the presented situation with an on-shell outgoing and an off-shell incoming particle occurs for example in the u-channel of tree-level models for meson electroproduction. It is clear that one can derive similar expressions for the s-channel, where the opposite situation occurs. Second, the Bonn model described in Chap. 2, does not allow one to compute half off-shell form factors. Indeed, the BS approach is based on the behaviour of the Green's function near the poles, and the BS amplitudes are only defined for on-shell particles. Therefore, the sole calculable EM form factors are the on-shell ones. This peculiar case will be the topic of the following section.

On-shell Vertex

The subject of elastic on-shell EM form factors was already covered in Sect. 2.4.2. However, it is quite instructive to see how the half off-shell vertex of Eq. (3.23) reduces to the on-shell one of Eq. (2.51), which was the starting point for the derivation of the relations between the on-shell EM form factors and the current matrix elements in Sect. 2.4.

When the incoming and outgoing baryon are on the mass shell, they can both be represented by a Dirac spinor ($\overline{u}(\mathbf{p}')(\not{p}' - m) = 0$ and $(\not{p} - m)u(\mathbf{p}) = 0$). Eq. (3.19)

then reduces to Eq. (2.51) :

$$\overline{u}(\mathbf{p}')\,\Gamma^{\mu}\left(\overline{p}',\overline{p}\right)\,u(\mathbf{p}) = e\,\overline{u}(\mathbf{p}')\left[f_1\gamma^{\mu}+f_2\frac{i\sigma^{\mu\nu}q_{\nu}}{2M_p}+f_3q^{\mu}\right]u(\mathbf{p})\,, \tag{2.51}$$

where the three on-shell form factors can be related to the off-shell and half off-shell form factors by :

$$\begin{aligned} f_i\left(q^2\right) &= m\,f'^{1}_{i}\left(m^2,q^2\right)+f'^{0}_{i}\left(m^2,q^2\right)\,, && \text{(3.26a)}\\ &= m^2\,f_i^{11}\left(m^2,m^2,q^2\right)+m\,f_i^{10}\left(m^2,m^2,q^2\right)\\ &\quad +m\,f_i^{01}\left(m^2,m^2,q^2\right)+f_i^{00}\left(m^2,m^2,q^2\right)\,, && \text{(3.26b)}\\ &= m\,f_i^{1}\left(m^2,q^2\right)+f_i^{0}\left(m^2,q^2\right)\,. && \text{(3.26c)} \end{aligned}$$

In the last line, we have introduced the unprimed half off-shell form factors for an on-shell incoming particle. They play the same role as the $f'^{1,0}_{i}$ in the opposite situation with an off-shell incoming and on-shell outgoing particle.

The WT identity for this peculiar situation reduces to :

$$\overline{u}(\mathbf{p}')\,q_{\mu}\Gamma^{\mu}\left(\overline{p}',\overline{p}\right)\,u(\mathbf{p}) = 0\,. \tag{2.52}$$

This condition eliminates the f_3 form factor :

$$q^2\,f_3\left(q^2\right) = 0\,. \tag{2.54}$$

The resulting EM vertex was already thoroughly discussed in Sect. 2.4.2.

3.3.3 Normal-Parity Transition Electromagnetic Vertex

In this section, the EM vertex for the situation $J'^{\pi'}=J^{\pi}=1/2^{\pm}$ and non-identical particles $m'\neq m$ will be discussed. One can start from the general expression for a $J'^{\pi'}=1/2^{\pm}\rightarrow J^{\pi}=1/2^{\pm}$ EM vertex of Eq. (3.11). Again, the (transition) form factors have to fulfill the conditions of Eq. (3.12).

The major difference between the elastic and the transition EM vertex stems from gauge-invariance conditions. The WT identities are of little use for transition EM vertices. One of the conditions for the WT identities to apply, is that the gauge boson does not change the identity of the particle, something which is clearly not satisfied for hadrodynamic models. It is a major and unsolved problem to impose gauge invariance in such models. It can be seen as one of the shortcomings of the

isobar model - and of any effective field theory in general - that the original meaning of gauge invariance is lost. After all, gauge invariance is the local conservation of charge, and when discussing extended objects, the charge is effectively spread over a finite part of spacetime. The whole idea of introducing form factors hinges on the approximation of writing the EM interaction with an extended object as if it were a point coupling (local interaction) with the strength depending on spacetime variables.

The common approximation adopted in isobar models is to apply the condition of Eq. 2.52, which is strictly speaking only valid for on-shell incoming and outgoing particles, also to off-shell particles :

$$q_\mu \, \Gamma^\mu \left(p', p\right) \; = \; 0 \; . \tag{3.27}$$

After all, only the total amplitude has to be gauge invariant and here we assume that all parts of the amplitude have to be gauge invariant separately.

Using the gauge-invariance condition of Eq. (3.27) to constrain the EM vertex of Eq. (3.11), one obtains the following conditions for the form factors :

$$q^2 \; f_3^{11} \;\; = \;\; f_1^{10} - f_1^{01} \; , \tag{3.28a}$$

$$q^2 \; f_3^{10} \;\; = \;\; p^2 f_1^{11} - f_1^{00} \; , \tag{3.28b}$$

$$q^2 \; f_3^{01} \;\; = \;\; -p'^2 f_1^{11} + f_1^{00} \; , \tag{3.28c}$$

$$q^2 \; f_3^{00} \;\; = \;\; -p'^2 f_1^{10} + p^2 f_1^{01} \; . \tag{3.28d}$$

The resulting EM vertex does not contain any f_3 form factors :

$$\begin{aligned}
\Gamma^\mu \left(p', p\right) \;\; = \;\; & \not{p}' \left[f_1^{11} \left(\gamma^\mu - \frac{\not{q} q^\mu}{q^2} \right) + f_2^{11} \frac{i \sigma^{\mu\nu} q_\nu}{2 M_p} \right] \not{p} \\
+ \;\; & \not{p}' \left[f_1^{10} \left(\gamma^\mu - \frac{\not{q} q^\mu}{q^2} \right) + f_2^{10} \frac{i \sigma^{\mu\nu} q_\nu}{2 M_p} \right] \mathbb{1} \\
+ \;\; & \mathbb{1} \left[f_1^{01} \left(\gamma^\mu - \frac{\not{q} q^\mu}{q^2} \right) + f_2^{01} \frac{i \sigma^{\mu\nu} q_\nu}{2 M_p} \right] \not{p} \\
+ \;\; & \mathbb{1} \left[f_1^{00} \left(\gamma^\mu - \frac{\not{q} q^\mu}{q^2} \right) + f_2^{00} \frac{i \sigma^{\mu\nu} q_\nu}{2 M_p} \right] \mathbb{1} \; .
\end{aligned} \tag{3.29}$$

As in the elastic case, the vertex (3.29) displays divergencies for real photons ($q^2 = 0$). Then, the left-hand sides of the constraints in Eq. (3.28) vanish, which results in :

$$f_1^{\lambda', \lambda} \left(p'^2, p^2, q^2 \to 0\right) \;\; = \;\; 0 \; . \tag{3.30}$$

Thus, there are no more γ^μ terms in the real photon case. However, if the f_1 form factors vary $\sim q^2$ close to the real photon limit, longitudinal terms proportional to $\not{q}q^\mu$ survive. All information about the EM transition is then contained in the coefficients of these terms and in the f_2 form factors of Eq. (3.29).

In the following subsections, we will discuss briefly what happens if we put one particle (Sect. 3.3.3) or both particles (Sect. 3.3.3) on the mass shell.

Half Off-shell Vertex

In this section, the outgoing Dirac particle is on-shell ($\overline{u}(\mathbf{p}')(\not{p}' - m') = 0$). This simplifies the EM vertex of Eq. (3.29) to :

$$\begin{aligned}\overline{u}(\mathbf{p}')\Gamma^\mu\left(\overline{p}', p\right) \;=\; \overline{u}(\mathbf{p}')\Bigg[f'^1_1\left(\gamma^\mu - \frac{\not{q}q^\mu}{q^2}\right)\not{p} + f'^1_2\frac{i\sigma^{\mu\nu}q_\nu}{2M_p}\not{p} \\ + f'^0_1\left(\gamma^\mu - \frac{\not{q}q^\mu}{q^2}\right) + f'^0_2\frac{i\sigma^{\mu\nu}q_\nu}{2M_p}\Bigg] ,\end{aligned} \tag{3.31}$$

where we can evaluate $\not{q}$ as $m' - \not{p}$. The half off-shell form factors are defined as :

$$f'^1_i\left(p^2, q^2\right) \;=\; m' f^{11}_i\left(m'^2, p^2, q^2\right) + f^{01}_i\left(m'^2, p^2, q^2\right) , \tag{3.32a}$$

$$f'^0_i\left(p^2, q^2\right) \;=\; m' f^{10}_i\left(m'^2, p^2, q^2\right) + f^{00}_i\left(m'^2, p^2, q^2\right) . \tag{3.32b}$$

The condition for these form factors in the real-photon limit is :

$$f'^1_1\left(p^2, q^2 \to 0\right) \;=\; f'^0_1\left(p^2, q^2 \to 0\right) \;=\; 0 . \tag{3.33}$$

and the corresponding EM vertex reads :

$$\overline{u}(\mathbf{p}')\Gamma^\mu\left(\overline{p}', p\right) = \overline{u}(\mathbf{p}')\left[-\not{q}q^\mu(a'\not{p} + b') + \frac{i\sigma^{\mu\nu}q_\nu}{2M_p}\left(f'^1_2\not{p} + f'^0_2\right)\right] . \tag{3.34}$$

Here, a' or b' are non-zero only if the f'^1_1 or f'^0_1 behaves as q^2 for vanishing squared momentum transfer.

On-shell Vertex

For on-shell incoming *and* outgoing Dirac particles, the EM vertex is further simplified to :

$$\overline{u}(\mathbf{p}')\,\Gamma^\mu\left(\overline{p}', \overline{p}\right)\,u(\mathbf{p}) \;=\; \overline{u}(\mathbf{p}')\left[f_1\left(\gamma^\mu - \frac{m' - m}{q^2}q^\mu\right) + f_2\frac{i\sigma^{\mu\nu}q_\nu}{2M_p}\right]\,u(\mathbf{p}) , \tag{2.64}$$

which was already derived in Sect. 2.4.2 from the same principles.

The on-shell form factors are defined as :

$$\begin{aligned} f_i\left(q^2\right) &= m\, f'^1_i\left(m^2, q^2\right) + f'^0_i\left(m^2, q^2\right) \ , && \text{(3.35a)} \\ &= m' m\, f_i^{11}\left(m'^2, m^2, q^2\right) + m'\, f_i^{10}\left(m'^2, m^2, q^2\right) \\ &\quad + m\, f_i^{01}\left(m'^2, m^2, q^2\right) + f_i^{00}\left(m'^2, m^2, q^2\right) \ , && \text{(3.35b)} \\ &= m'\, f_i^1\left(m'^2, q^2\right) + f_i^0\left(m'^2, q^2\right) \ . && \text{(3.35c)} \end{aligned}$$

In the last line, the half off-shell form factors for the case when the incoming particle is on its mass shell, are used.

In order to avoid divergencies in Eq. (2.64) for $q^2 \to 0$, the f_1 form factors should vanish :

$$f_1\left(q^2 \to 0\right) \ \to \ 0 \ . \qquad \text{(2.65)}$$

If f_1 is proportional to q^2 in the real-photon limit, the EM vertex has a longitudinal term, proportional to $(m' - m)q^\mu$, and a transverse term, proportional to $i\sigma^{\mu\nu}q_\nu$.

3.3.4 Abnormal-Parity Transition Electromagnetic Vertex

The EM transition of a particle with spin and parity $J^\pi = 1/2^-$ to a particle with spin and parity $J'^{\pi'} = 1/2^+$ involves an abnormal-parity vertex. This means that on has to use terms with an additional γ^5 (*cfr.* terms 13 to 24 of Eq. (3.10)), leading to the following expression :

$$\begin{aligned} \Gamma^\mu\left(p', p\right) &= \not{p}' \left[f_1^{11}\gamma^\mu + f_2^{11}\frac{i\sigma^{\mu\nu}q_\nu}{2M_p} + f_3^{11}q^\mu \right] \gamma^5 \not{p} \\ &+ \not{p}' \left[f_1^{10}\gamma^\mu + f_2^{10}\frac{i\sigma^{\mu\nu}q_\nu}{2M_p} + f_3^{10}q^\mu \right] \gamma^5 \mathbb{1} \\ &+ \mathbb{1} \left[f_1^{01}\gamma^\mu + f_2^{01}\frac{i\sigma^{\mu\nu}q_\nu}{2M_p} + f_3^{01}q^\mu \right] \gamma^5 \not{p} \\ &+ \mathbb{1} \left[f_1^{00}\gamma^\mu + f_2^{00}\frac{i\sigma^{\mu\nu}q_\nu}{2M_p} + f_3^{00}q^\mu \right] \gamma^5 \mathbb{1} \ . \end{aligned} \qquad \text{(3.36)}$$

One can write this set of Dirac structures as $(\not{p}', \mathbb{1}) \times (\gamma^\mu, \frac{i\sigma^{\mu\nu}q_\nu}{2M_p}, q^\mu) \times \gamma^5 \times (\not{p}, \mathbb{1})$.

Gauge invariance is imposed through the same restriction as for a $J^\pi = 1/2^+ \to J'^{\pi'} = 1/2^+$ transition :

$$q_\mu \Gamma^\mu\left(p', p\right) = 0 \ . \qquad \text{(3.37)}$$

This results in four constraints on the form factors, which are slightly different from the ones of Eq. (3.16) :

$$q^2 f_3^{11} = -f_1^{10} - f_1^{01} , \tag{3.38a}$$
$$q^2 f_3^{10} = -p^2 f_1^{11} - f_1^{00} , \tag{3.38b}$$
$$q^2 f_3^{01} = -p'^2 f_1^{11} - f_1^{00} , \tag{3.38c}$$
$$q^2 f_3^{00} = -p'^2 f_1^{10} - p^2 f_1^{01} . \tag{3.38d}$$

Implementing these gauge-invariance constraints on the general vertex of Eq. (3.36) results in :

$$\begin{aligned}\Gamma^\mu\left(p',p\right) &= \not{p}'\left[f_1^{11}\left(\gamma^\mu - \frac{\not{q}q^\mu}{q^2}\right) + f_2^{11}\frac{i\sigma^{\mu\nu}q_\nu}{2M_p}\right]\gamma^5\not{p} \\ &+ \not{p}'\left[f_1^{10}\left(\gamma^\mu - \frac{\not{q}q^\mu}{q^2}\right) + f_2^{10}\frac{i\sigma^{\mu\nu}q_\nu}{2M_p}\right]\gamma^5\mathbb{1} \\ &+ \mathbb{1}\left[f_1^{01}\left(\gamma^\mu - \frac{\not{q}q^\mu}{q^2}\right) + f_2^{01}\frac{i\sigma^{\mu\nu}q_\nu}{2M_p}\right]\gamma^5\not{p} \\ &+ \mathbb{1}\left[f_1^{00}\left(\gamma^\mu - \frac{\not{q}q^\mu}{q^2}\right) + f_2^{00}\frac{i\sigma^{\mu\nu}q_\nu}{2M_p}\right]\gamma^5\mathbb{1} .\end{aligned} \tag{3.39}$$

As was the case for natural-parity transitions (Sect. 3.3.3), the singularities in the real photon point are avoided through :

$$f_1^{\lambda'\lambda}\left(p'^2, p^2, q^2 \to 0\right) \to 0 . \tag{3.40}$$

If the f_1 form factors behave like q^2 in the real photon limit, the longitudinal terms of the type $(\not{p}', \mathbb{1}) \times \not{q}q^\mu\gamma^5 \times (\not{p}, \mathbb{1})$ survive.

Half Off-shell Vertex

One can now put the outgoing Dirac-particle with spin and parity $J'^{\pi'} = 1/2^+$ and four-momentum p' on its mass shell ($\overline{u}(\mathbf{p}')(\not{p}' - m') = 0$). The resulting vertex is :

$$\begin{aligned}\overline{u}(\mathbf{p}')\Gamma^\mu\left(\overline{p}',p\right) = \overline{u}(\mathbf{p}')\Big[&f'^1_1\left(\gamma^\mu - \frac{\not{q}q^\mu}{q^2}\right)\gamma^5\not{p} + f'^1_2\frac{i\sigma^{\mu\nu}q_\nu}{2M_p}\gamma^5\not{p} \\ &+ f'^0_1\left(\gamma^\mu - \frac{\not{q}q^\mu}{q^2}\right)\gamma^5 + f'^0_2\frac{i\sigma^{\mu\nu}q_\nu}{2M_p}\gamma^5\Big] ,\end{aligned} \tag{3.41}$$

with the same definitions of the half off-shell form factors as in Eq. (3.32a), and where $\not{q}$ is evaluated as $m' - \not{p}$.

For real photons, the f_1 form factors should vanish, resulting in an EM vertex depending only on f_2 terms and possible longitudinal terms :

$$\overline{u}(\mathbf{p}')\Gamma^{\mu}\left(\overline{p}', p\right) = \overline{u}(\mathbf{p}')\left[-\not{q}q^{\mu}\gamma^5(a'\not{p} + b') + \frac{i\sigma^{\mu\nu}q_{\nu}}{2M_p}\gamma^5\left(f'^1_2\not{p} + f'^0_2\right)\right] . \quad (3.42)$$

Again, $a'(p^2)$ and $b'(p^2)$ are the coefficients of the term in q^2 in the McLaurin series expansion of the f'^1_1 and f'^0_1 form factors respectively.

On-shell Vertex

If the incoming particle is also on-shell ($(\not{p} - m)u(\mathbf{p}) = 0$), the EM coupling becomes :

$$\overline{u}(\mathbf{p}')\,\Gamma^{\mu}\left(\overline{p}', \overline{p}\right)\,u(\mathbf{p}) = \overline{u}(\mathbf{p}')\left[f_1\left(\gamma^{\mu} - \frac{m' + m}{q^2}q^{\mu}\right) + f_2\frac{i\sigma^{\mu\nu}q_{\nu}}{2M_p}\right]\gamma^5\,u(\mathbf{p}) . \quad (3.43)$$

This expression differs from the vertex for normal-parity transitions of Eq. 2.64 by the positive sign between the masses, and the γ^5 factor in front of the spinor of the incoming particle. The on-shell form factors can be written in terms of the half off-shell and off-shell ones as in Eq. (3.35). Vertex (3.43) is the same as the one in Eq. (2.72), except for the subscripts B and B^*.

For real photons, the singularities are avoided if the f_1 form factor vanishes :

$$f_1\left(q^2 \to 0\right) = 0 . \quad (2.65)$$

Then, one is left with only the f_2 term and a longitudinal term proportional to $(m' + m)q^{\mu}$ if f_1 behaves as q^2 in the real-photon limit.

3.4 Observables

In Fig. 3.1, the kinematical variables occuring the KY electroproduction reaction :

$$p(p) + e(k_1) \to e'(k_2) + K(p_K) + Y(p_Y) , \quad (3.44)$$

are displayed. The four-momenta are defined as [6] :

$$\begin{array}{lllllllll} k_1^{\mu} & = & (\varepsilon_1, \mathbf{k}_1) , & k_2^{\mu} & = & (\varepsilon_2, \mathbf{k}_2) , & q^{\mu} & = & (\omega, \mathbf{q}) , \\ p^{\mu} & = & (E_p, -\mathbf{q}^*) , & p_K^{\mu} & = & (E_K, \mathbf{p}_K) , & p_Y^{\mu} & = & (E_Y, -\mathbf{p}_K) , \end{array} \quad (3.45)$$

where $q^\mu = k_1^\mu - k_2^\mu$ refers to the four-momentum of the virtual photon in the lab frame. When probing a hadronic system with electrons, it is common to describe the electron kinematics in the lab frame, and the hadron kinematics in the (γ^*, p) center-of-momentum frame. The angle between the incoming and outgoing electron in the lab frame is θ_e (see Fig. 3.1). The angle between the lepton-scattering plane and the hadronic plane is ϕ_K. The angle between the incoming virtual photon and outgoing kaon in the c.o.m. frame of the hadronic system is θ_K. The virtual photon transfers all the kinematical and polarization degrees of freedom of the lepton-scattering plane to the hadronic plane. Its four-momentum in the lab frame is given in Eq. (3.45) by $(\omega, \mathbf{q})$, while in the hadronic c.o.m. frame, it is denoted by $(\omega^*, \mathbf{q}^*)$. The two sets of coordinates are connected by a Lorentz boost along the photon three-momentum :

$$\mathbf{q}^* = \mathbf{q}\left(\frac{M_p}{W}\right) , \tag{3.46a}$$

$$\begin{aligned} \omega^* &= W - (\omega + M_p)\frac{M_p}{W} , \\ &= \frac{s - M_p^2 - Q^2}{2W} . \end{aligned} \tag{3.46b}$$

Herein, $W \equiv \sqrt{s}$ is the total c.m. energy and $Q^2 = -\,q_\mu q^\mu$.

The electroproduction differential cross section can be written as :

$$\frac{\mathrm{d}^5\sigma}{\mathrm{d}\varepsilon_2\,\mathrm{d}^2\Omega_2\,\mathrm{d}^2\Omega_K} = \frac{1}{32(2\pi)^5}\frac{1}{M_p}\frac{|\mathbf{p}_K|}{W}\frac{\varepsilon_2}{\varepsilon_1}\overline{\sum_{\lambda_i}}|\mathcal{M}_{\lambda_i}|^2 , \tag{3.47}$$

where subscript λ_i in $\mathcal{M}$ denotes that it depends on the polarizations and spins of the different particles (electrons, nucleon and hyperon). In the one-photon-exchange approximation, one can separate the transverse and longitudinal parts of the cross section. For unpolarized electrons, we have :

$$\begin{aligned} \frac{\mathrm{d}^5\sigma}{\mathrm{d}\varepsilon_2\,\mathrm{d}^2\Omega_2\,\mathrm{d}^2\Omega_K^*} = \Gamma\Big[&\frac{\mathrm{d}\sigma_T}{\mathrm{d}^2\Omega_K} + \varepsilon\frac{\mathrm{d}\sigma_L}{\mathrm{d}^2\Omega_K} + \varepsilon\frac{\mathrm{d}\sigma_{TT}}{\mathrm{d}^2\Omega_K}\cos(2\phi_K) \\ &+ \sqrt{\varepsilon(1+\varepsilon)}\frac{\mathrm{d}\sigma_{TL}}{\mathrm{d}^2\Omega_K}\cos(\phi_K)\Big] , \end{aligned} \tag{3.48}$$

where the virtual photon flux factor is given by :

$$\Gamma = \frac{\alpha}{2\pi}\frac{\varepsilon_2}{\varepsilon_1}\frac{K_H}{Q^2}\frac{1}{1-\varepsilon} , \tag{3.49}$$

with $K_H = \omega - Q^2/(2M_p)$ the equivalent real-photon lab energy. Further, ε is the degree of transverse polarization of the virtual photon :

$$\varepsilon = \left[1 + \frac{2|\mathbf{q}|^2}{Q^2} \tan^2\left(\frac{\theta_e}{2}\right)\right]^{-1} . \tag{3.50}$$

This formalism allows one to write the structure functions as functions of kinematical variables from the hadronic plane only, *e.g.* $(\omega^*, |\mathbf{q}^*|, \theta_K)$ or (s, t, Q^2). The virtual-photon cross sections are expressed as functions of hadronic tensors :

$$\frac{\mathrm{d}\sigma_T}{\mathrm{d}^2\Omega_K} = \chi \frac{1}{(4\pi)^2} \left(\mathcal{H}_{1,1} + \mathcal{H}_{-1,-1}\right) , \tag{3.51a}$$

$$\frac{\mathrm{d}\sigma_L}{\mathrm{d}^2\Omega_K} = 2\chi \frac{1}{(4\pi)^2} \mathcal{H}_{0,0} , \tag{3.51b}$$

$$\frac{\mathrm{d}\sigma_{TT}}{\mathrm{d}^2\Omega_K} = -\chi \frac{1}{(4\pi)^2} \left(\mathcal{H}_{1,-1} + \mathcal{H}_{-1,1}\right) , \tag{3.51c}$$

$$\frac{\mathrm{d}\sigma_{TL}}{\mathrm{d}^2\Omega_K} = -\chi \frac{1}{(4\pi)^2} \left(\mathcal{H}_{0,1} + \mathcal{H}_{1,0} - \mathcal{H}_{-1,0} - \mathcal{H}_{0,-1}\right) , \tag{3.51d}$$

where χ is a purely kinematic factor :

$$\chi \equiv \frac{1}{16} \frac{1}{W^2} \frac{|\mathbf{p}_K|}{K_H} \frac{W}{M_p} . \tag{3.52}$$

These hadronic tensors $\mathcal{H}_{\lambda,\lambda'}$ are squared amplitudes, which can be expressed in terms of traces :

$$\begin{aligned} \mathcal{H}_{\lambda,\lambda'} &= \sum_{\lambda_i,\lambda_f} \mathcal{M}_{\lambda}^{\lambda_i,\lambda_f} \left(\mathcal{M}_{\lambda'}^{\lambda_i,\lambda_f}\right)^{\dagger} , \\ &= \sum_{\lambda_i,\lambda_f} \left(\overline{u}_Y^{\lambda_f}(p_Y) \mathcal{T}^{\mu} \epsilon_{\mu}^{\lambda} u_p^{\lambda_i}(p)\right) \left(\overline{u}_p^{\lambda_i}(p) \overline{\mathcal{T}}^{\nu} \epsilon_{\nu}^{\lambda'*} u_Y^{\lambda_f}(p_Y)\right) , \\ &= Tr\left[(\not{p}_Y + m_Y) \mathcal{T}^{\mu} \epsilon_{\mu}^{\lambda} (\not{p} + M_p) \overline{\mathcal{T}}^{\nu} \epsilon_{\nu}^{\lambda'*}\right] . \end{aligned} \tag{3.53}$$

Here, $\lambda^{(')}$ denotes the polarization of the virtual photon. We will work in the Lorentz gauge ($epsilon_{\mu} q^{\mu} = 0$) and in the frame in which the virtual photon's three-momentum is directed along the positive z-axis. The three basis vectors for the photon polarization can thus be chosen to be :

$$\epsilon^{\lambda=0} = \frac{1}{\sqrt{Q^2}} \left(|\mathbf{q}^*|, 0, 0, \omega^*\right) , \tag{3.54a}$$

$$\epsilon^{\lambda=\pm1} = \mp \frac{1}{\sqrt{2}} \left(0, 1, \pm i, 0\right) . \tag{3.54b}$$

The $\mathcal{T}^\mu$ are the amputated amplitudes for the diagrams in Fig. 3.2, from which also the photon polarization vector is explicitly separated. They are a combination of the EM vertex Γ^μ from the previous sections, the propagator of the intermediate particle and the strong vertex. In Appendix B, we will present the expressions for these amplitudes in more detail.

We will also give the expressions for the cross sections in the case of a polarized incoming or outgoing electron. The differential cross section acquires extra terms depending on the helicity h of the incoming electron. Note that parity invariance allows us not having to discuss the case when both incoming and outgoing electron are polarized (*cfr.* Sect. 3.1.3). One obtains for the cross section :

$$\frac{\mathrm{d}^5\sigma}{\mathrm{d}\varepsilon_2\,\mathrm{d}^2\Omega_2\,\mathrm{d}^2\Omega_K} = \left.\frac{\mathrm{d}^5\sigma}{\mathrm{d}\varepsilon_2\,\mathrm{d}^2\Omega_2\,\mathrm{d}^2\Omega_K}\right|_{\text{unpol}} + h\,\Gamma\left[\sqrt{1-\varepsilon^2}\,\frac{\mathrm{d}\sigma_{TT'}}{\mathrm{d}^2\Omega_K} + \sqrt{\varepsilon(\varepsilon-1)}\,\frac{\mathrm{d}\sigma_{TL'}}{\mathrm{d}^2\Omega_K}\,\sin(\phi_K)\right] . \quad (3.55)$$

The two new cross sections are now defined in terms of hadronic tensors as :

$$\frac{\mathrm{d}\sigma_{TT'}}{\mathrm{d}^2\Omega_K} = \chi\frac{1}{(4\pi)^2}\left(\mathcal{H}_{1,1} - \mathcal{H}_{-1,-1}\right) , \quad (3.56a)$$

$$\frac{\mathrm{d}\sigma_{TL'}}{\mathrm{d}^2\Omega_K} = -\chi\frac{i}{(4\pi)^2}\left(\mathcal{H}_{1,0} - \mathcal{H}_{0,1} - \mathcal{H}_{-1,0} + \mathcal{H}_{0,-1}\right) . \quad (3.56b)$$

For more details, we refer the reader to the works of S. Janssen [6] and of G. Knöchlein *et al.* [72].

Chapter 4

Electromagnetic Properties of Strange Hadrons

The work presented in this chapter is part of an attempt to develop a consistent description of kaon production processes of the type $p(\gamma, K^+)Y$ and $p(e, e'K^+)Y$ [2–5]. New data for these processes have recently been released by the CLAS Collaboration at Jefferson Laboratory [11], by the LEPS Collaboration at SPring-8 [16], and by the SAPHIR Collaboration at ELSA in Bonn [14, 15]. Also the GRAAL Collaboration at Grenoble [73] will provide sizeable amounts of polarization data for kaon photoproduction in the very near future. The abundant amount of new data calls for an appropriate theoretical treatment covering the complete data base. Such a theoretical model appears indispensable for a proper interpretation of the experimental results. One of the major sources of theoretical uncertainties when modeling $p(\gamma^{(*)}, K)Y$ reactions is the strength of the electromagnetic couplings involved. This holds especially true for kaon electroproduction, where the EM coupling depends on Q^2, the squared four-momentum transfered by the virtual photon. The Q^2 dependence of the EM form factors is largely unknown for the "strange" baryons [5], because they are not directly accessible experimentally. For this, one would need a hyperon beam with sufficient intensity. This is practically impossible at present since *e.g.* the Λ hyperon decays in $\tau = (2.632 \pm 0.020) \times 10^{-10}$s, corresponding with a traveling distance of $c\tau = 7.89$cm.

The center column of Fig. 3.2 in Chap. 3 contains the u-channel contributions to the kaon electroproduction process : the virtual photon couples to the hyperon

with a strength of which the magnitude depends on the form factors of the strange baryon. These form factors are input to isobar models. However, one does not have sufficient data to constrain the EM form factors of hyperons. This means that one would introduce a large degree of uncertainty when guessing the functional form of the form factors. In this Chapter, we will try to resolve this problem, by presenting results for the hyperon elastic and transition form factors as they are computed within the framework of the Bonn CQ model. The hyperon form factors are calculated in a parameter-free manner, and are compared with the (scarce) data. In this way we test the predictive power of the Bonn CQ model.

The Bonn CQ model can also provide us with the EM form factors of other hadrons. Previous work has been reported for mesons and for nonstrange baryons. For the pseudoscalar- and vector-meson elastic and transition form factors [33], an excellent description of the data was reached both in the time-like [74–77] and space-like [78–85] region. For the pion, the outcome of the calculations was reasonable, considering the high values for the CQ masses in the model. For the nonstrange baryons [35], the results for the form factors and helicity amplitudes are reasonable to excellent. Data for the EM couplings of the nonstrange baryons can be found in Refs. [41, 62, 63, 86–99] for the nucleon, in Refs. [100–103] for the Δ resonance, and in Refs. [104–114] for the lowest-lying nucleon and Δ resonances. The rather good agreement of the abovementioned calculations with experimental data, justifies the extension of the Bonn CQ model to the hyperon sector.

There have already been many attempts to predict (or, *postdict*,) the EM properties of hyperons and hyperon resonances. For the ground-state hyperons (Λ, Σ, Ξ), a previous investigations of the on-shell form factors used a chiral quark/soliton model [115]. Very recently, these calculations have been extended by A. Silva [116]. Predictions based on chiral perturbation theory, for magnetic moments, charge and magnetic mean-square radii, and EM form factors up to $Q^2 = 0.3$ (GeV/c)^2, have been published by Kubis *et al.* [117, 118]. Both models provide results for the octet and decuplet baryons, but not for their resonances.

For the resonances, a number of theoretical studies for the photo- and helicity amplitudes have been performed since the beginning of the eighties. These include studies of the EM decay width and helicity amplitudes of the lowest-lying hyperon resonances ($S_{01}(1405)$ and $D_{03}(1520)$) to the octet ($\Lambda(1116)$ and $\Sigma(1192)$)

and decuplet ($\Sigma^*(1385)$) ground states in Refs. [119, 120]. Here, a nonrelativistic CQ model and a bag model were used. A more elaborate treatment within the framework of the chiral bag model was presented in the early nineties by Umino and Myhrer in Refs. [121–123]. More recent approaches adopt lattice-QCD [124], heavy-baryon chiral perturbation theory [125], the bound-state soliton model [126, 127], the Skyrme model [128, 129], and the chiral constituent quark model [130, 131]. Most of these model calculations are restricted to the first and second hyperon resonance region (decuplet hyperons, $S_{01}(1405)$, and $D_{03}(1520)$). Note that the data on EM couplings are restricted to these states. Results for the other resonances cannot be directly constrained against data and should be interpreted as predictions or extrapolations.

Since only static EM properties of the hyperons and hyperon resonances have been measured (magnetic moments and charge radii), most of the previous studies ignored the Q^2-dependence of the helicity amplitudes. In addition, the validity of some models at intermediate and high momentum transfers is rather questionable. For $Q^2 \simeq m^2 \simeq m^{*2}$, the velocities of the moving particles in the lab frame is already $v^2/c^2 \simeq 5/9$. This hints at sizeable boost effects and at the necessity of a Lorentz-covariant model. Also the validity of models based on chiral perturbation theory is restricted to momenta transfers smaller than a certain parameter which is typically of the order of the mass of the nucleon. In the following sections, we will present the form factors and helicity amplitudes of the ground-state and excited hyperons for $0 \leq Q^2 \leq 6$ GeV^2.

In Sect. 4.1 the focus is on the electric and magnetic form factors of strange baryons, as well as the electromagnetic form factors of the $\Sigma^0 \to \Lambda$ transition. Whenever possible we will compare our predictions with experimental data and other calculations. The work contained in Sect. 4.1 has been published in Ref. [132]. Sect. 4.2 contains the logical continuation and extension of the results presented in Sect. 4.1. There, we discuss the predictions for the EM decay of higher-lying and higher-spin Λ and Σ resonances to the Λ and Σ ground state. Finally, in Sect. 4.4, we will discuss the accuracy and stability of our numerical calculations.

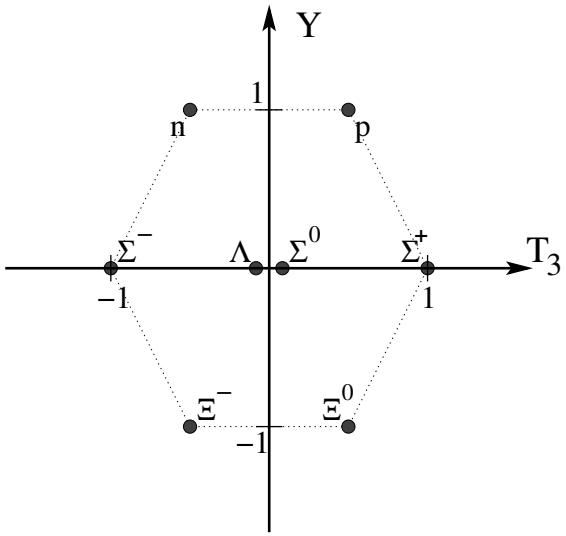

Figure 4.1 *The baryon octet in the plane spanned by the hypercharge Y and the third component of the isospin T_3. In this Chapter, we focus on the strange baryons, with hypercharge $Y \leq 0$.*

4.1 Ground-state Hyperons

In this section, results for the computed electric and magnetic form factors of the strange particles belonging to the baryon octet (see Fig. 4.1) will be presented. We will discuss the elastic and the $\Sigma^0 \to \Lambda$ transition form factors. Comparisons with other calculations will be made. In Ref. [115], Kim *et al.* present calculations for the elastic form factors of the ground-state octet baryons up to $Q^2 = 1.0$ GeV^2 within the framework of the chiral quark/soliton model (CQSM). This model adopts the view of pions as Goldstone bosons due to the spontaneous chiral symmetry breaking. The CQSM was extended by A. Silva (see Ref. [116]), who recomputed the elastic form factors of the octet baryons. Kubis *et al.* have computed electric and magnetic form factors of the hyperons for $Q^2 < 0.2$ GeV^2 in the framework of heavy-baryon chiral perturbation theory (HB) in Ref. [117] and later extended their model to fourth order [118] to recalculate the electric form factors of the baryon octet and the $\Sigma^0 \to \Lambda$ transition form factor $F_1^{B^*B}(Q^2)$ for $Q^2 < 0.3$ GeV^2. In the same article, relativistic baryon chiral perturbation employing infrared regulators (IR) is used and shown to have predictive value. Since these investigations

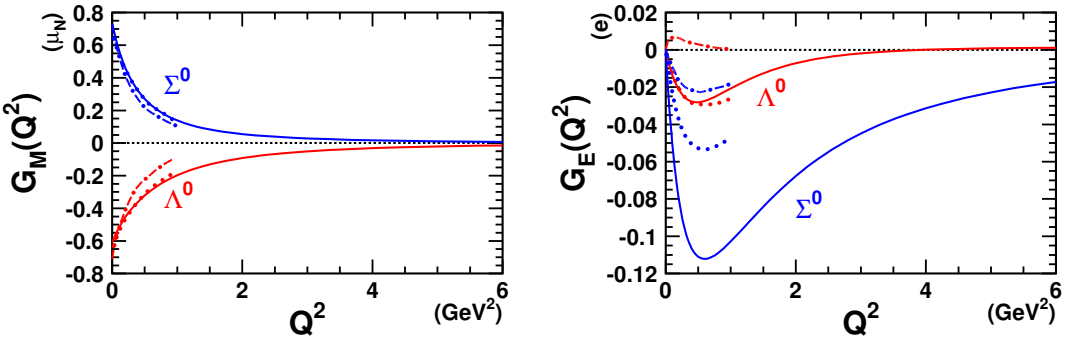

Figure 4.2 *Calculated magnetic (left) and electric (right) form factors of the Λ and Σ^0 hyperon (solid lines). The dot-dashed (dotted) curves are the predictions from Ref. [115] ([116]).*

are confined to small values for Q^2, we can only compare our results for the magnetic moments (Table 4.1) and the mean square radii (Table 4.2) with the HB and IR results. We will also confront our predictions with those presented in Ref. [133], where results are shown of CQ calculations based on a Goldstone-Boson Exchange (GBE) quark-quark interaction [27, 134] and a one-gluon exchange (OGE) interaction [135, 136].

In Fig. 4.2, our results for the neutral baryons with strangeness quantum number $S = -1$ are displayed. The computed Q^2 dependence of the magnetic form factors of the neutral hyperons nicely follows that of a dipole,

$$G(Q^2) = \frac{G(0)}{\left(1 + \frac{Q^2}{\Lambda^2}\right)^2} \,, \tag{4.1}$$

with cutoff masses $\Lambda_M = 0.88$ GeV and 1.14 GeV for the Σ^0- and the Λ-hyperon respectively (Table 4.2). For comparison, the proton has a cutoff mass $\Lambda_M^{exp} = 0.84$ GeV, and for point particles the cutoff goes to infinity, so that the Λ hyperon seems be more pointlike than the Σ^0 hyperon and the proton. Their values in $Q^2 = 0$ are the magnetic moments $\mu_{\Sigma^0} = 0.73$ and $\mu_\Lambda = -0.61$ in units of the nuclear magneton μ_N, which are very realistic (Table 4.1). The electric form factors in the right panel of Fig. 4.2 have the opposite sign in comparison with the neutron electric form factor. This can be attributed to the presence of the heavier s-quark in the hyperons, which has a higher probability of residing near the center of mass of the hyperon, making the electric density negative at small r, whereas it is positive

Table 4.1 Magnetic moments of strange baryons in units of μ_N. The $SU(6)$ predictions are given in the fourth column. Predictions from the chiral quark/soliton model are presented in the fifth column. The notation *GBE/OGE* (*HB,IR*) refers to the two different models discussed in Ref. [133] ([118]). In Ref. [118], only the transition magnetic moment for $\Sigma^0 \to \Lambda$ is a real prediction. Experimental values are taken from Ref. [1], except for $\mu_{\Sigma^0} = (\mu_{\Sigma^+} + \mu_{\Sigma^-})/2$, for which isospin invariance is used. For the $\Sigma^0 \to \Lambda$ transition, the absolute value is given.

Baryon	μ_Y^{exp}	μ_Y^{calc}	$\mu_Y^{SU(6)}$	$\mu_Y^{[115]/[116]}$	$\mu_{Y\,(GBE/OGE)}^{[133]}$	$\mu_{Y\,(HB/IR)}^{[118]}$
$\Lambda^0(1116)$	-0.613 ± 0.004	-0.61	exp.	$-0.77/-0.652$	$-0.59/-0.59$	exp.
$\Sigma^+(1189)$	2.458 ± 0.010	2.47	2.67	2.42/2.306	2.34/2.20	exp.
$\Sigma^0(1189)$	0.649	0.73	0.79	0.75/0.675	0.70/0.66	exp.
$\Sigma^-(1189)$	-1.160 ± 0.025	-0.99	-1.09	$-0.92/-957$	$-0.94/-0.89$	exp.
$\lvert\Sigma^0 \to \Lambda\rvert$	1.61 ± 0.08	1.41	1.63	1.51/—	—	1.46/1.61
$\Xi^0(1315)$	-1.250 ± 0.014	-1.33	-1.43	$-1.64/-1.404$	$-1.27/-1.27$	exp.
$\Xi^-(1315)$	-0.6507 ± 0.0025	-0.57	-0.49	$-0.68/-0.605$	$-0.67/-0.57$	exp.

for the neutron [40]. The predicted negative values for G_E for the Σ^0 and Λ, are in contradiction with the results from Refs. [115] and [118]. Kim *et al.* predict a positive G_E for the Λ and Kubis *et al.* predict a negative mean square radius for the Σ^0 hyperon (Table 4.3). It should also be noted that for neutral hyperons, our results for the electric form factors are about a factor of five larger in magnitude than those of Ref. [115]. The recent CQSM calculations of Ref. [116], however, are in rather good agreement with ours (dotted curves in Fig. 4.2). For the Σ^0, the electric form factor is about a factor of two smaller, but for the Λ, the agreement is astonishingly good. The fact that these two rather different models give comparable results for such small quantities as the electric form factors of neutral baryons, is evidence for the need to include the common aspects of the models, such as (homogenous) Lorentz covariance and the importance of instanton-induced effects !

The obtained predictions for the Σ^+ and Σ^- are shown in Fig. 4.3. Again, the results for the magnetic moments $\mu_{\Sigma^+} = 2.47\,\mu_N$ and $\mu_{\Sigma^-} = -0.99\,\mu_N$ are in excellent agreement with experiment (Table 4.1). Whilst the magnetic form factor of the Σ^+ resembles a dipole with cutoff $\Lambda_M = 0.79$ GeV, the one for the Σ^- drops relatively fast and even changes sign at $Q^2 \approx 1.6$ GeV, remaining small at high Q^2. A similar qualitative behavior is observed for the electric form factor of the Σ^+, changing

Table 4.2 Magnetic mean square radii of strange baryons in units of fm^2. All magnetic form factors resemble dipoles, except for the Σ^-, and our fitted value for the cutoff mass is given. The notation *HB/IR* refers to the two models presented in Ref. [118].

Baryon	$< r_M^2 >^{calc}$	$< r_M^2 >^{[115]/[116]}$	$< r_M^2 >^{[118]}_{(HB/IR)}$	Λ_M (GeV)
$\Lambda^0(1116)$	0.40	0.70/0.457	0.30/0.48	1.14
$\Sigma^+(1189)$	0.69	0.71/0.619	0.74/0.80	0.79
$\Sigma^0(1189)$	0.60	0.70/0.550	0.20/0.45	0.88
$\Sigma^-(1189)$	0.81	0.74/0.718	1.33/1.20	—
$\Sigma^0 \to \Lambda$	1.96	— / —	0.60/0.72	0.82
$\Xi^0(1315)$	0.47	0.75/0.535	0.44/0.61	0.94
$\Xi^-(1315)$	0.38	0.51/0.318	0.44/0.50	1.03

Table 4.3 Electric mean square radii of strange baryons in units of fm^2. The same conventions as in Tables 4.1 and 4.2 are adopted.

Baryon	$< r_E^2 >^{exp}$	$< r_E^2 >^{calc}$	$< r_E^2 >^{[115]/[116]}$	$< r_E^2 >^{[118]}_{(HB/IR)}$	$< r_E^2 >^{[133]}_{(GBE/OGE)}$	Λ_E (GeV)
$\Lambda^0(1116)$	—	0.038	$-0.04/0.039$	0.00/0.11	—	—
$\Sigma^+(1189)$	—	0.79	0.79/0.811	0.72/0.60	—	—
$\Sigma^0(1189)$	—	0.150	0.02/0.075	$-0.08/-0.03$	—	—
$\Sigma^-(1189)$	$0.60^{[43]}/0.91^{[42]}$	0.49	0.75/0.662	0.88/0.67	0.49/0.44	0.93
$\Sigma^0 \to \Lambda$	—	-0.120	— / —	$-0.09/0.03$	—	—
$\Xi^0(1315)$	—	0.140	$-0.06/0.102$	0.08/0.13	—	—
$\Xi^-(1315)$	—	0.47	0.72/0.546	0.75/0.49	—	0.93

sign at $Q^2 \approx 1.1$ GeV^2. For $Q^2 > 2.6$ GeV^2, the form factors of Σ^+ and Σ^- become practically indistinguishable. Since the two charged Σ's only have the s-quark in common, it seems that longitudinal photons with high virtuality preferentially couple to this quark, resulting in a negative electric form factor. In configuration space, this can be translated in the observation that the s-quark resides near the center of mass of the charged Σ hyperons, just as for the Λ and Σ^0. Inspecting Fig. 4.3, it is clear that our predictions for the magnetic form factors agree remarkably well with those of the CQSM at low values of Q^2 [115, 116].

To our knowledge, for the electric mean square radius of the Σ^- hyperon, the

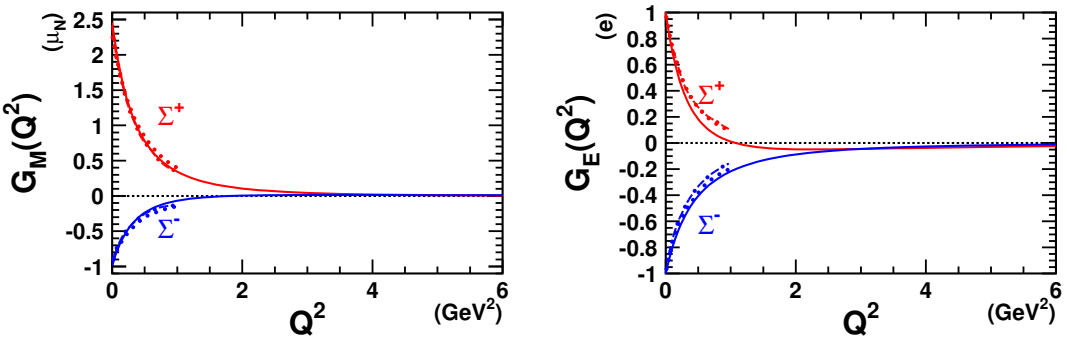

Figure 4.3 *Calculated magnetic and electric form factors of the Σ^+ and Σ^- hyperons. The dot-dashed (dotted) curves are the predictions from Ref. [115] ([116]).*

following experimental values are presently available :

$$< r_E^2 >_{\Sigma^-} = 0.60 \pm 0.08 \text{ (stat.)} \ \pm 0.08 \text{ (syst.) fm}^2 \tag{4.2}$$

from Ref [43], and :

$$< r_E^2 >_{\Sigma^-} = 0.91 \pm 0.32 \text{ (stat.)} \ \pm 0.40 \text{ (syst.) fm}^2 \tag{4.3}$$

from Ref [42]. Our prediction $< r_E^2 >_{\Sigma^-} = 0.49$ fm^2 (Table 4.3) is compatible with both of these values.

The experimental information regarding the Ξ doublet is scarce. To complete the description of ground-state hyperons, we have calculated its elastic form factors. The form factors of the Ξ^0 are displayed in Fig. 4.4. The $G_E(Q^2)$ changes sign about $Q^2 = 3.0$ GeV^2 and $G_M(Q^2)$ can be nicely fitted with a dipole with $\Lambda_M = 0.94$ GeV and magnetic moment $\mu_{\Xi^0} = -1.33\ \mu_N$. Again, this value for μ_{Ξ^0} is in good agreement with the experimentally determined value (Table 4.1). The Ξ^- exhibits dipole-like behavior in both $G_E(Q^2)$ and $G_M(Q^2)$ (Fig. 4.5) with cutoffs $\Lambda_E = 0.93$ GeV and $\Lambda_M = 1.03$ GeV, respectively. Our prediction for the magnetic moment, $\mu_{\Xi^-} = -0.57\ \mu_N$, is close to the experimental value $-0.6507 \pm 0.0025\ \mu_N$ [1].

As is the case for the Λ hyperon, the CQSM calculations of Ref. [115] predict a different sign and a smaller magnitude for the Ξ^0 electric form factor, but the newer calculations of Ref. [116] agree very well with ours (Fig. 4.4). The results of both models for the magnetic form factor of the Ξ^0 and for both form factors of

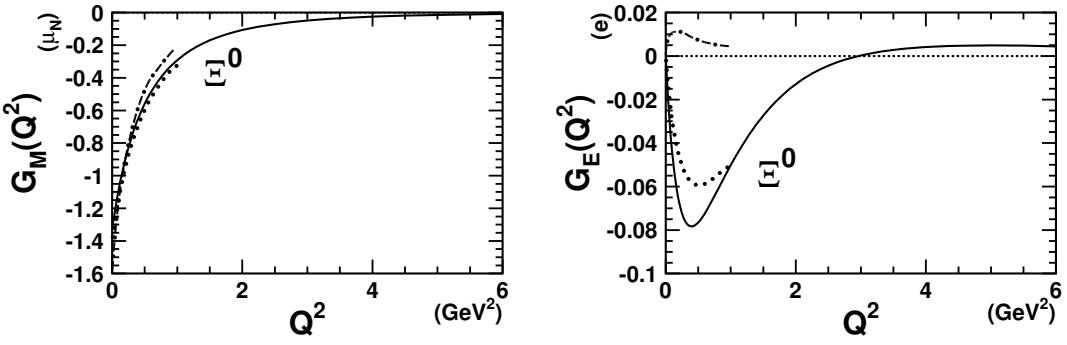

Figure 4.4 *Calculated magnetic and electric form factors of the Ξ^0 hyperon. The dot-dashed (dotted) curves are the predictions from Ref. [115] ([116]).*

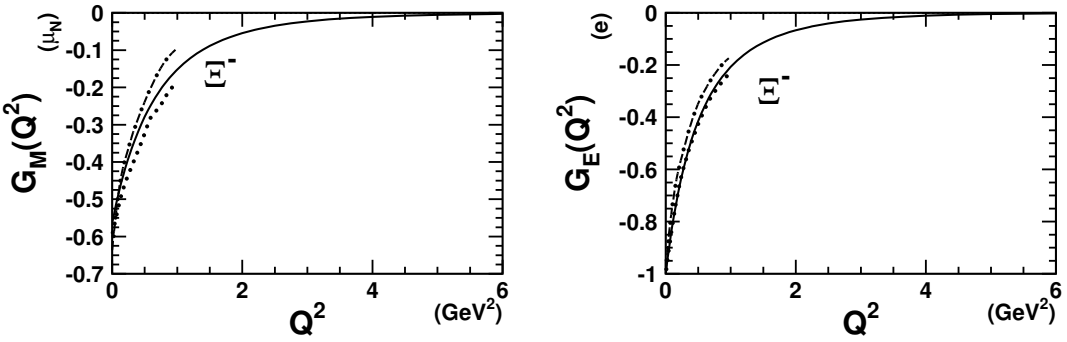

Figure 4.5 *Calculated magnetic and electric form factor of the Ξ^- hyperon. The dot-dashed (dotted) curves are the predictions from Ref. [115] ([116]).*

the Ξ^- (Fig. 4.5) are in good agreement. Also the predictions for magnetic moments and mean-square radii from Refs. [117, 118] compare favourably (see Tables 4.1, 4.2, and 4.3).

The last point of our discussion concerns the form factors related to the $\gamma^* + \Sigma^0 \to \Lambda$ transition. We show the two transition form factors $F_1^{\Sigma\Lambda}(Q^2)$ and $F_2^{\Sigma\Lambda}(Q^2)$ in Fig. 4.6, calculated with Eqs. (2.69). The link with experiment is the transition magnetic moment $|\mu_{\Sigma\Lambda}| = 1.61 \pm 0.08\ \mu_N$ from [1]. Our prediction of $|\mu_{\Sigma\Lambda}| = 1.41\ \mu_N$ is somewhat smaller.

In this section, the electromagnetic form factors for the ground-state hyperons have been presented. Comparison with experimentally determined values is possible for the magnetic moments and the electric mean square radius of the Σ^- hy-

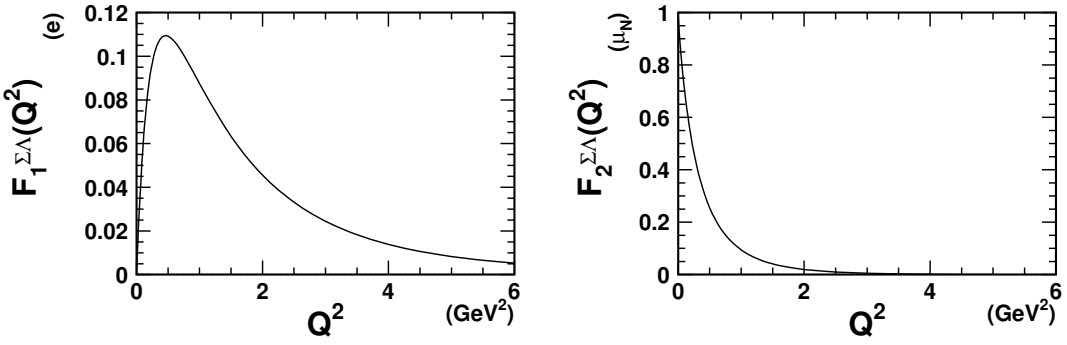

Figure 4.6 *The Q^2 dependence of the $\gamma^* + \Sigma^0 \to \Lambda$ transition form factors.*

peron. A nice agreement between our predictions and the data is observed. As illustrated in Figs. 4.2 and 4.4, the different hadron models tend to predict negative electric form factors for the neutral hyperons (Λ, Σ^0, and Ξ^0) at small Q^2, in contrast with the neutron electric form factor. From this it becomes obvious that the (measured) G_E^n neutron form factor cannot be considered as a realistic approximation for the G_E^Λ, $G_E^{\Sigma^0}$ and $G_E^{\Xi^0}$.

4.2 Hyperon Resonances

In this section, results are presented for the helicity amplitudes (HA's) of hyperon resonances decaying to the Λ or Σ ground-state hyperons. The HA's are defined in Eqs. (2.75). We will organize our results according to the quantum numbers of the resonances and the ground-state hyperon to which they decay. Most of the computed low-lying states can be identified with experimentally known resonances [138] by comparing the calculated with the experimental mass spectrum. This is illustrated in Fig. 4.7. Only for the higher-lying $F_{05}(2110)$ and $D_{03}(2325)$, there is no direct correspondence with a single computed state.

We will use the nomenclature adopted by the *Particle Data Group* (PDG) [1] to identify a state (*e.g.* $D_{03}(1520)$ for the lowest-lying Λ resonance with $J^\pi = 3/2^-$). In those situations where there is no clear identification possible, the excited state with given quantum numbers will be labeled with a number. The lowest-lying *resonance* gets number '1', the second resonance '2', ... Occasionally, the ground state will be identified with a '0'. (Note that what we call a ground state, is a member of the

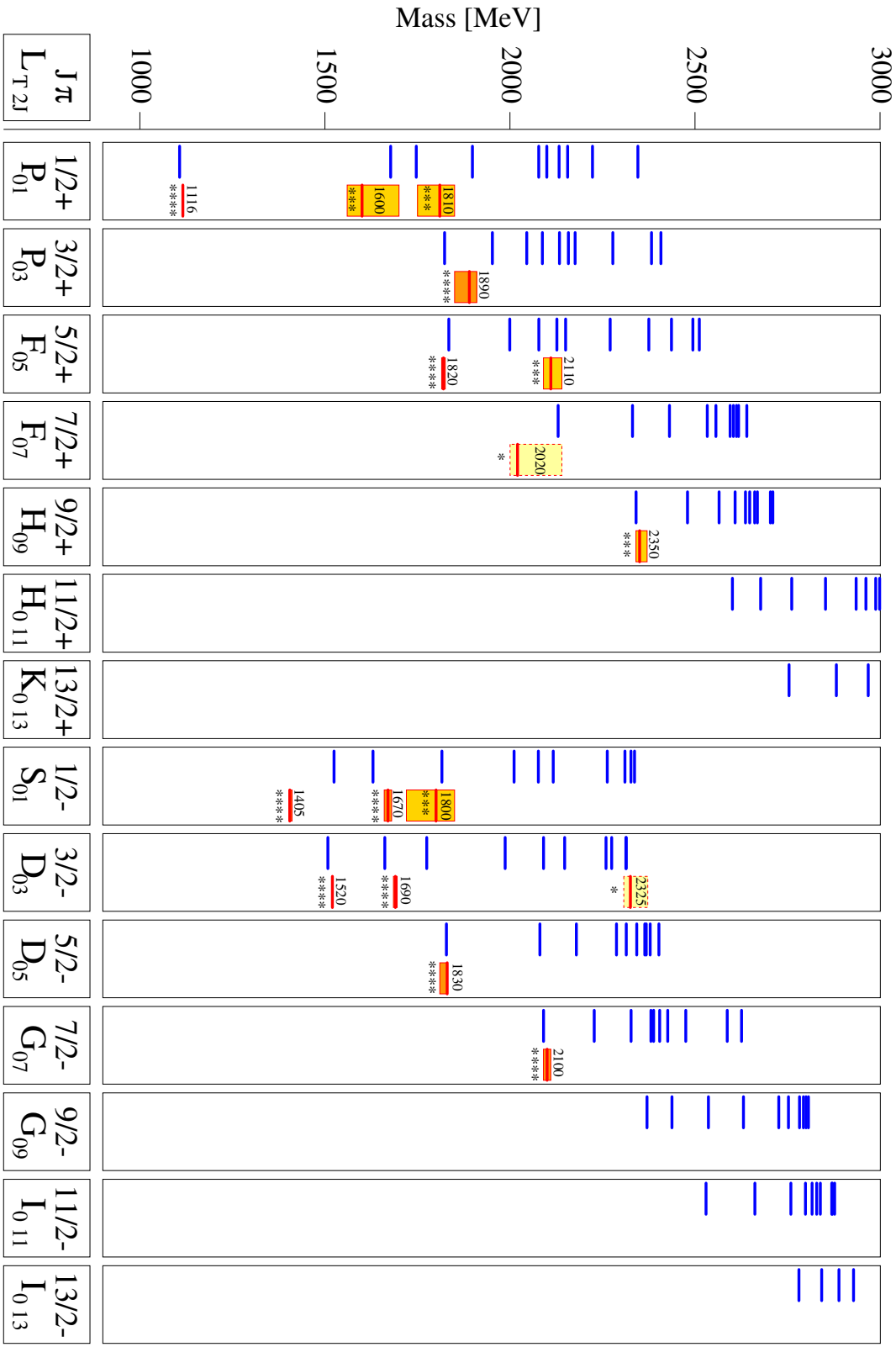

Figure 4.7 *The calculated Λ^* spectrum (isospin $T = 0$) for positive and negative parity states with spins up to $J = 13/2$ and masses up to 3000 MeV (left part of each column) is compared to the experimental spectrum taken from Ref. [137] (right part of each column, the status is given by the number of stars). The uncertainty on the experimental mass of each resonance is indicated by the shaded area around it. Figure is from Ref. [37].*

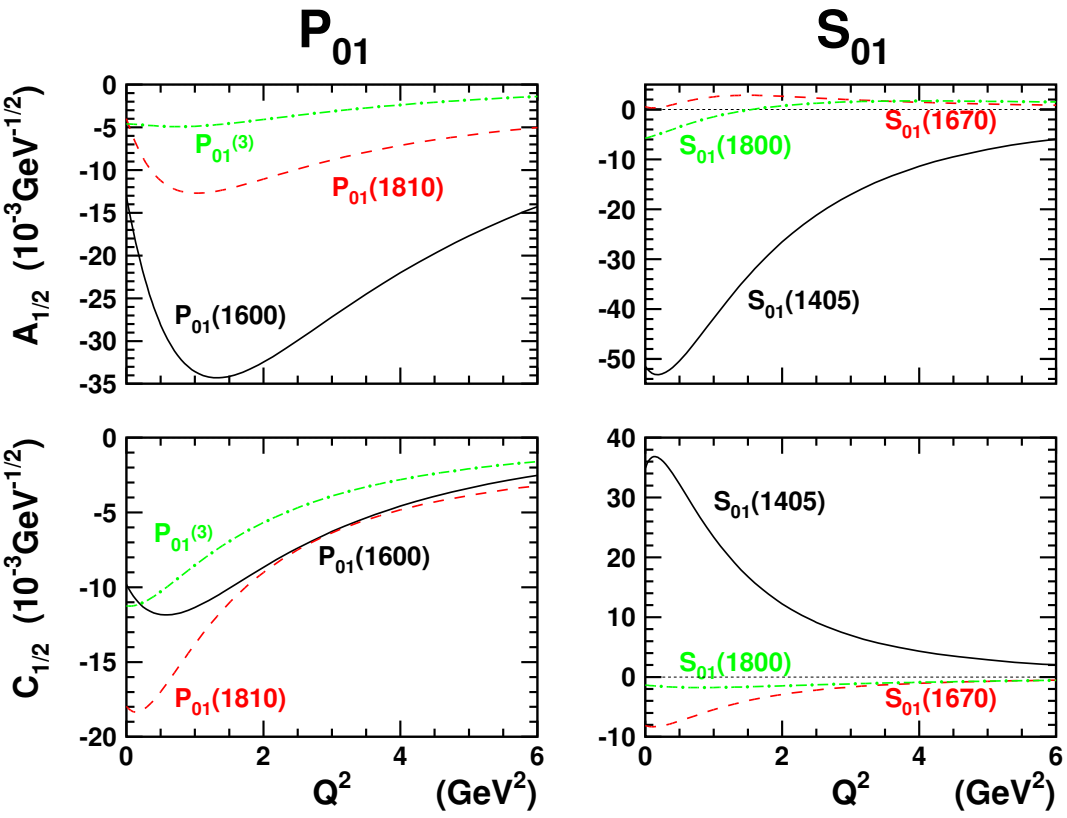

Figure 4.8 *The Q^2 dependence for the $\Lambda^* + \gamma^* \to \Lambda$ decays for spin $J = 1/2$ resonances : left (right) panels show the results for the positive (negative) parity Λ^* resonances.*

baryon octet.)

To illustrate the notation conventions, consider the "Λ" spectrum in Fig. 4.7. The ground state is denoted by $P_{01}^{(0)} \equiv P_{01}(1116)$. The first computed resonance, the $P_{01}^{(1)}$, can be identified with the experimentally observed $P_{01}(1600)$ resonance. For the $J^\pi = 3/2^-$ resonances, the two lowest computed states, the $D_{03}^{(1)}$ and the $D_{03}^{(2)}$, can be recognized as the measured $D_{03}(1520)$ and $D_{03}(1690)$ resonances respectively. The third computed resonance is as yet unobserved experimentally, and will thus be called the $D_{03}^{(3)}$. Note that we use the PDG notation for the strange baryons : $L_{I,2J}$ with the isospin I, spin J, and $L = S, P, D, \ldots$ the orbital angular momentum of the partial wave in which the resonance could be seen in $\bar{K}\Lambda$ scattering.

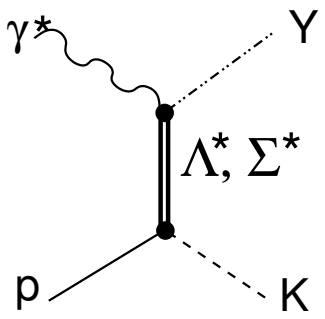

Figure 4.9 *The u-channel diagram for exchanged hyperon resonances in the tree-level isobar model for kaon production of Chap. 3. Note that the photon couples to the intermediate hyperon resonance, resulting in the outgoing (ground-state) hyperon.*

4.2.1 Λ-Resonances

$\Lambda^* + \gamma^{(*)} \to \Lambda$ **transitions**

Our results for spin $J = 1/2$, isospin $I = 0$ resonances are summarized in Fig. 4.8. Already for the lowest-lying Y^* resonances, one observes interesting features in the computed HA's. In the left panel of Fig. 4.8, the HA's of the three lowest $J^\pi = \frac{1}{2}^+$ Λ resonances are displayed. The first excited state with the same quantum numbers as the ground-state Λ is commonly referred to as the analogue of the *Roper resonance*. In the Λ spectrum, this state is observed experimentally with $m \approx 1600$ MeV. For the computed state which can be identified with the $P_{01}(1600)$ resonance, the $A_{1/2}$ amplitude reaches its maximum at $Q^2 \approx 1.5\,\text{GeV}^2$. Accordingly, the Roper-like resonance in the Λ spectrum may not show up in photoproduction experiments, but only in electroproduction reactions at intermediate Q^2 values. Indeed, if the photon has spacelike momentum-squared $q^2 = -Q^2$, it couples to the intermediate Y^* resonance with a strength proportional to its HA at that specific Q^2 (Fig. 4.9). Signals of the $P_{01}(1600)$ resonance in electromagnetically induced kaon production are predicted to become particularly important at $Q^2 \approx 1.5\,\text{GeV}^2$. Another interesting feature is that the $P_{01}(1810)$ has a relatively large $C_{1/2}$. The $C_{1/2}$ contributes to the longitudinal part of the kaon electroproduction strength (*cfr.* Eqs. (3.51b), (3.51d), and (3.56b)). Optimum conditions to detect signals of the $P_{01}(1810)$ are thus created when looking at the longitudinal part of the $p(e, e'K^+)\Lambda$ cross sections at small Q^2.

The most striking observation for the S_{01} resonances (right panels of Fig. 4.8),

is the dominance of the lowest excitation $S_{01}(1405)$. We denote this state with the experimental mass of the first excitation with quantum numbers ($J = 1/2$, $S = -1$, $T = 0$) and negative parity, but from Table 4.4 and Fig. 4.7, it is clear that its mass is not well reproduced. There is also a large overestimation of the EM decay width of this state by a factor about 50. At photo-amplitude level, this reduces to a factor of 7, which is enormous considering the quality of our calculations for the magnetic moments of the ground-state hyperons. We conclude that the $S_{01}(1405)$ is not well described in our CQ model. Possible explanations of this discrepancy is the inadequacy of the effective interactions used, strong rescattering effects with *e.g.* the $\bar{K}N$ channel, different degrees of freedom (a three-quark structure is possibly inadequate), *etc*. The resonance position of the $S_{01}(1405)$ is a very interesting topic. Recent studies within a coupled-channel chiral $SU(3)$ model generate this state dynamically [139–143]. For the higher-lying S_{01} resonances, our calculations predict very small electromagnetic couplings.

The HA's for the lowest-lying spin $J = 3/2$ hyperons are shown in Fig. 4.10. In the left panels, we consider P_{03} hyperons with positive parity. For the $A_{1/2}$, the $P_{03}(1890)$ reaches its maximum at $Q^2 \simeq 1.0$ GeV^2, after which it slowly falls to zero. The $P_{03}^{(2)}$ with a calculated mass of 1970 MeV (*cfr.* Table 4.4), has a reasonably large $A_{1/2}$, but falls off rather quickly compared to the first resonance. The other HA's, the $A_{3/2}$ and the $C_{1/2}$ are rather small for the P_{03} states. Only the $P_{03}^{(3)}$ with an expected mass of 2068 MeV gives a modest signal in $A_{3/2}$.

The results for the D_{03} helicity amplitudes are summarized in the right panels of Fig. 4.10. Again, one notices a peak in the Q^2 dependence of the first resonance at $Q^2 \simeq 1.0$ GeV^2 for the $A_{1/2}$, and at $Q^2 \simeq 0.2$ GeV^2 for the $C_{1/2}$. Both HA's fall off slowly for large Q^2-values. It appears that this behaviour is quite specific for the results presented in this section. The first resonance $L_{I,2J}^{(1)}$ reaches a maximum in $A_{1/2}$ and $C_{1/2}$ at moderate values of Q^2. For $J \geq 3/2$, on the other hand, the $A_{3/2}$'s reach their maximum at $Q^2 = 0$ GeV^2, and show a gradual falloff with growing Q^2. Furthermore, the maximum coupling is reached at smaller values of Q^2 for negative-parity resonances than for positive-parity resonances.

The other D_{03} resonances have smaller HA's. In fact, they are moderate. The $D_{03}(1520)$ has only a small *total* decay width of 15.6 ± 1.0 MeV, yet it will couple quite strongly to virtual photons with $Q^2 \approx 0.5$ GeV^2. So in a partial wave

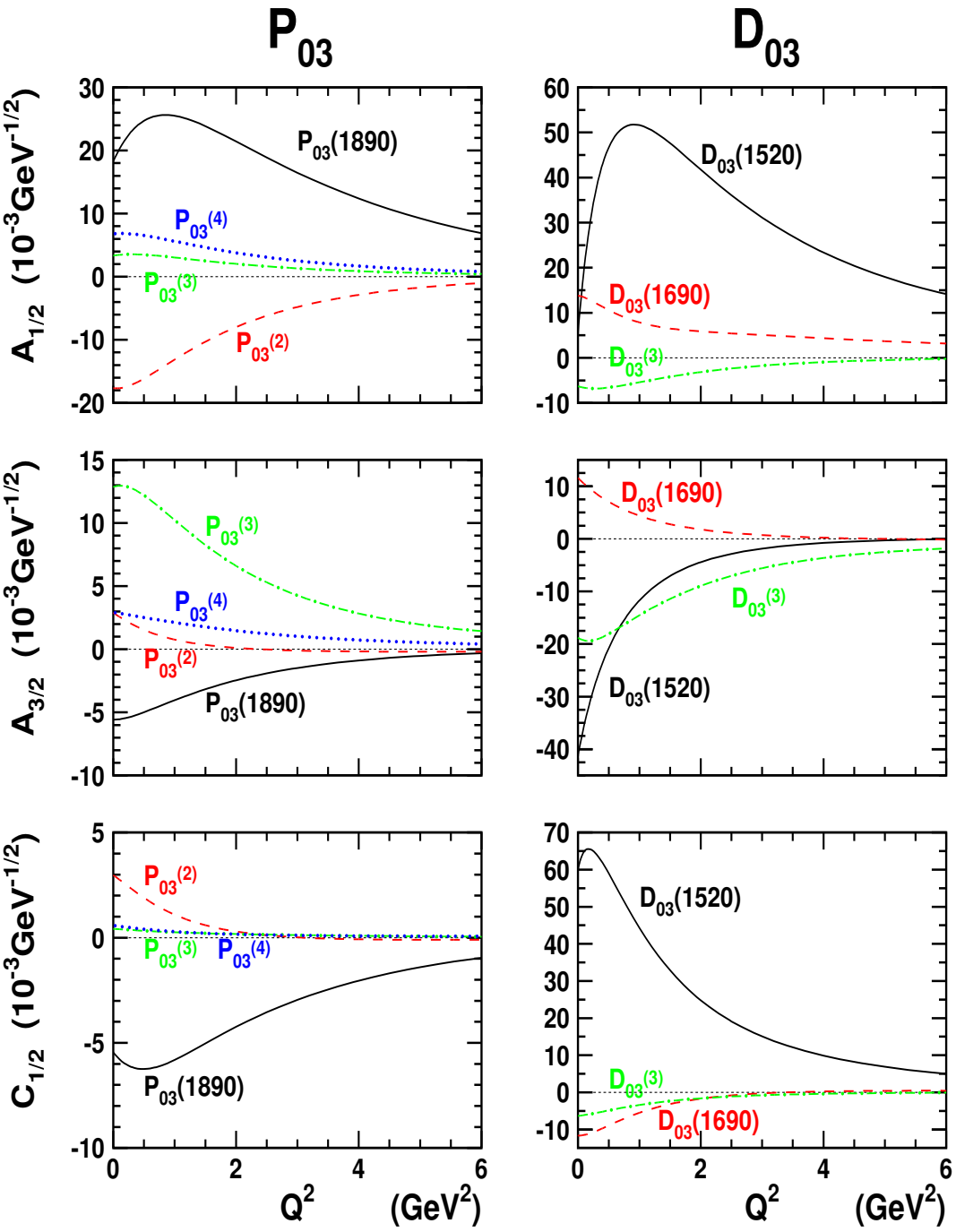

Figure 4.10 *The Q^2 dependence for the $\Lambda^* + \gamma^* \to \Lambda$ decays for spin $J = 3/2$ resonances : left (right) panels show the results for the positive (negative) parity Λ^* resonances.*

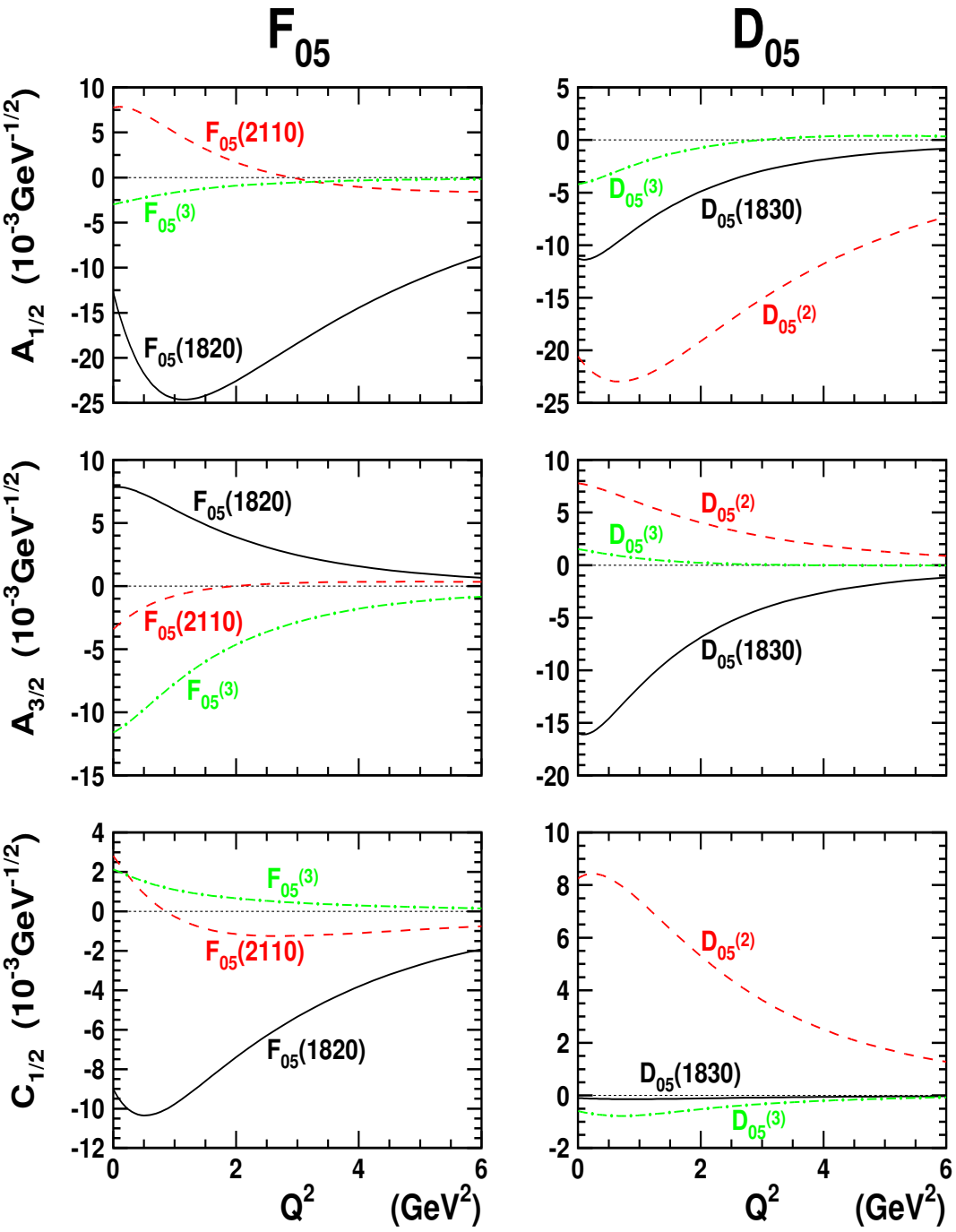

Figure 4.11 *The Q^2 dependence for the $\Lambda^* + \gamma^* \to \Lambda$ decays for spin $J = 5/2$ resonances : left (right) panels show the results for the positive (negative) parity Λ^* resonances.*

Table 4.4 Calculated masses, photo-amplitudes and EM decay widths for the $\Lambda^* + \gamma \to \Lambda(1116)$ transition. The last column presents the scarce experimental data for the EM decay widths of the Λ-resonances. Masses and decay widths are given in units of MeV, photo-amplitudes are given in units of 10^{-3} GeV$^{-1/2}$.

Resonance	M_{calc}	$\lvert A_{1/2}\rvert$	$\lvert A_{3/2}\rvert$	Γ_{calc}	Γ_{exp}
$P_{01}(1600)$	1752	13.0	—	0.104	—
$P_{01}(1810)$	1805	3.97	—	0.0105	—
$P_{01}^{(3)}$	1928	4.59	—	0.0174	—
$S_{01}(1405)$	1550	51.5	—	0.912	0.027 ± 0.008
$S_{01}(1670)$	1664	0.574	—	0.159×10^{-3}	—
$S_{01}(1800)$	1879	5.76	—	0.0252	—
$P_{03}(1890)$	1834	18.3	5.58	0.129	—
$P_{03}^{(2)}$	1970	17.7	2.90	0.142	—
$P_{03}^{(3)}$	2068	3.33	12.9	0.0893	—
$P_{03}^{(4)}$	2116	6.81	2.92	0.0293	—
$D_{03}(1520)$	1511	5.50	41.2	0.258	$0.125^{+0.042}_{-0.038}$
$D_{03}(1690)$	1678	13.8	11.6	0.0815	—
$D_{03}^{(3)}$	1805	6.31	18.8	0.130	—
$F_{05}(1820)$	1837	12.8	7.82	0.0531	—
$F_{05}(2110)$	2012	7.74	3.41	0.0223	—
$F_{05}^{(3)}$	2104	2.98	11.6	0.0503	—
$D_{05}(1830)$	1843	11.3	16.0	0.0916	—
$D_{05}^{(2)}$	2114	20.6	7.78	0.172	—
$D_{05}^{(3)}$	2219	4.22	1.53	0.00805	—

analysis of kaon electroproduction data, the first resonance is likely to overwhelm the effect of others with identical quantum numbers. In Table 4.4, one notices that for the $D_{03}(1520)$, the EM decay width is known up to a factor of roughly two. The computed value is about 50% larger than the upper limit of the experimental width. However, the EM decay width could be influenced by strong mixing effects with the $\bar{K}N$-channel (threshold around 1433 MeV), which are not included in the model.

In the isobar model discussed in Chap. 3 and Appendix B, resonances up to $J \leq 3/2$ are included. Therefore, it is instructive to see whether there is evidence from

CQ calculations to justify this approximation. The HA's for the $J = 5/2$ hyperon resonances are shown in Fig. 4.11. In the left panels, the HA's of the three lowest-lying states with quantum numbers $J^\pi = \frac{5}{2}^+$ are displayed. Again, one observes an pronounced maximum in the $A_{1/2}$ and $C_{1/2}$ for the $F_{05}(1820)$. The state denoted by $F_{05}(2110)$ is actually the second resonance with $J^\pi = 5/2^+$. If we consider the masses in Table 4.4, however, it is easily seen that its computed mass is too small. As a matter of fact, from Fig. 4.7, it is clear that the third, fourth and fifth resonance have a (computed) mass approaching the experimentally determined value of 2110 MeV. In Ref. [138], it is argued that the second resonance is actually a *missing* hyperon resonance and that the experimentally determined state around 2110 MeV should be associated with one of the higher-lying F_{05} resonances of a CQ-model calculation. The smallness of the helicity amplitudes displayed in Fig. 4.11 suggests that in photo- and electroinduced Λ-production processes, it is unlikely that the $F_{05}^{(2)}$ and $F_{05}^{(3)}$ Λ^* resonances will result in strong signals.

The right panels of Fig. 4.11 contain the predictions for the three lowest-lying D_{05} resonances. The first resonance can be associated with the $D_{05}(1830)$ state from Ref. [1]. Like for the S_{01} and D_{03} resonances, the $A_{1/2}$ and $C_{1/2}$ reach their maximum at low, but finite Q^2 values. In contrast to the $J = 1/2$ and $J = 3/2$ Λ^* resonances, the second D_{05} resonance has larger HA's than the first resonance. The PDG [1] tables do not mention evidence for this $D_{05}^{(2)}$ state.

On the basis of their computed HA's, the $F_{05}(1820)$, the $D_{05}(1830)$ and the $D_{05}^{(2)}$ resonances may contribute to the $p(\gamma^{(*)}, K)\Lambda$ reaction dynamics. One should therefore take care when excluding all $J = 5/2$ Λ^* resonances from an isobar description of the $p(\gamma^{(*)}, K)\Lambda$ process.

The results for the photo-amplitudes are summarized in Table 4.4. This table is useful for any isobar model involving real photons which couple to a Λ^* resonance. Experimental numbers for the EM decay of Λ^*'s are rare. Essentially, only the decay widths for the two lowest-lying Λ resonances are known. Of these two, the $S_{01}(1405)$ is often suggested to have a structure different from a $3q$ state, which falls beyond the scope of CQ-model calculations [140, 143]. Our calculations seem to confirm this conjecture. The properties of the $D_{03}(1520)$ are, however, reasonably well reproduced. Table 4.4 also shows that the sole resonances for which PDG gives an EM decay width, emerge in our calculations with the highest $\Lambda^* \to \Lambda$

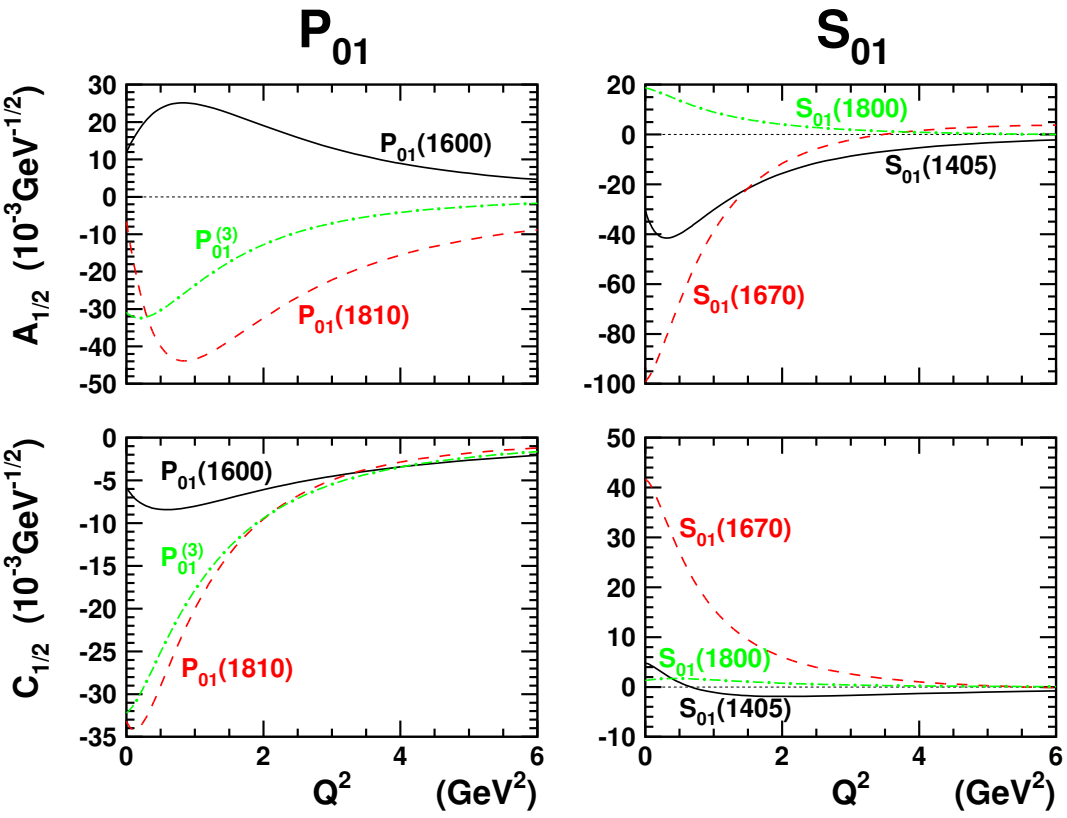

Figure 4.12 *The Q^2 dependence for the $\Lambda^* + \gamma^* \to \Sigma$ decays for spin $J = 1/2$ resonances : left (right) panels show the results for the positive (negative) parity Λ^* resonances.*

widths. More experimental information on the EM properties of the higher-lying Λ resonances would enable us to draw further conclusions about the quality of our calculations. An analysis of $p(\gamma^*, K)Y$ data based on input parameters from our CQ model would be a more indirect but stringent test of our model assumptions. At this point, we want to stress again that we have not introduced any new parameters in the current operator, which makes our results parameter-free predictions. In principle there is no obvious reason why the current operator of Eq. (2.30), which was fairly successful for the ground-state baryon octet, should do equally well in predicting the properties of the resonances, for which the internal dynamics are usually more complicated.

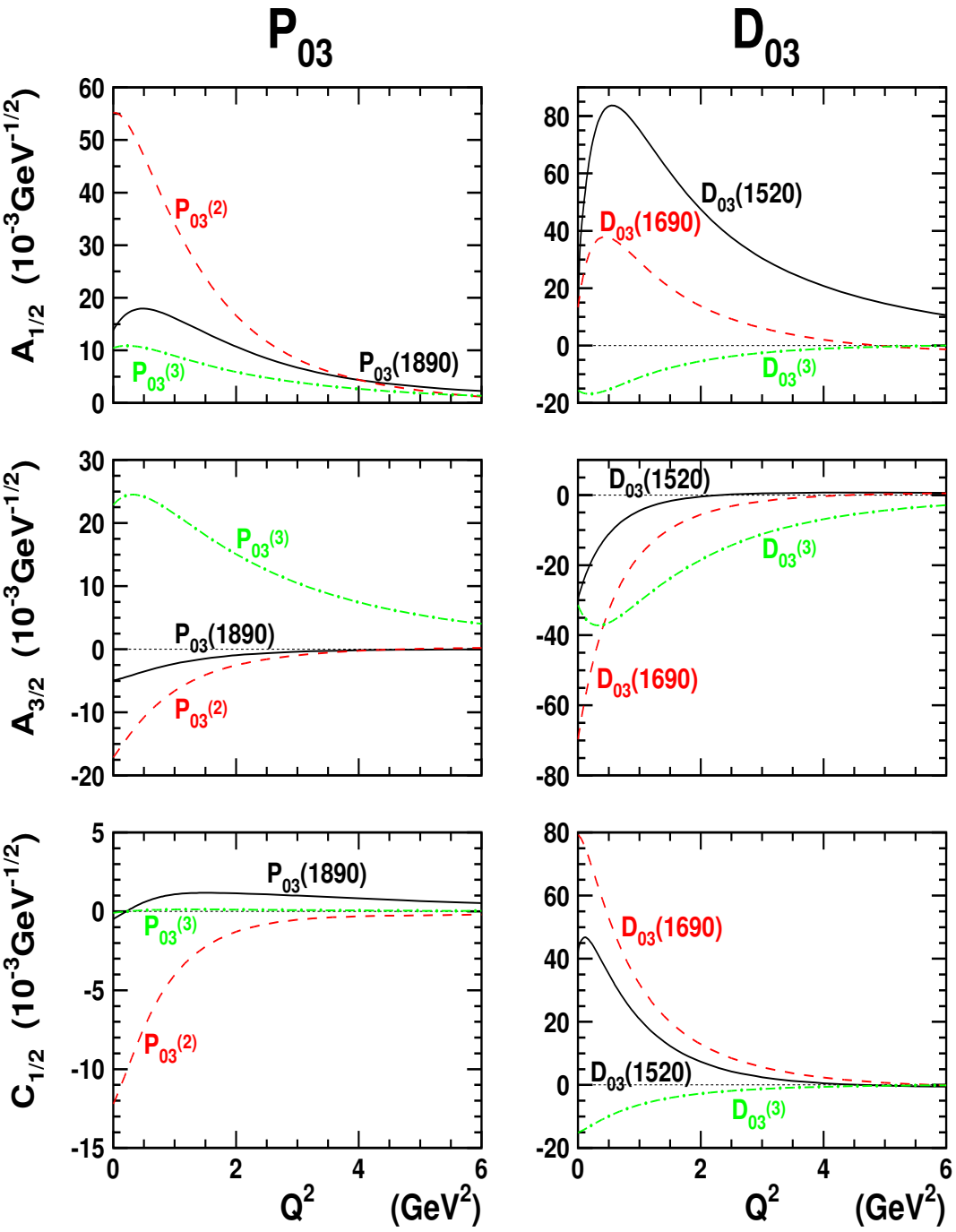

Figure 4.13 *The Q^2 dependence for the $\Lambda^* + \gamma^* \to \Sigma$ decays for spin $J = 3/2$ resonances : left (right) panels show the results for the positive (negative) parity Λ^* resonances.*

Table 4.5 Calculated masses, photo-amplitudes and EM decay widths for the $\Lambda^* + \gamma \to \Sigma^0(1193)$ transition are given below. Masses and decay widths are expressed in units of MeV, photo-amplitudes are given in units of 10^{-3} GeV$^{-1/2}$. Remark that some masses differ from the values given in Table 4.4, because they were computed in a larger basis.

Resonance	M_{calc}	$\lvert A_{1/2}\rvert$	$\lvert A_{3/2}\rvert$	Γ_{calc}	Γ_{exp}
$P_{01}(1600)$	1713	12.0	—	0.0679	—
$P_{01}(1810)$	1771	6.62	—	0.0240	—
$P_{01}^{(3)}$	1928	30.9	—	0.727	—
$S_{01}(1405)$	1538	30.3	—	0.233	0.010 ± 0.004/ 0.023 ± 0.007
$S_{01}(1670)$	1649	99.2	—	3.827	—
$S_{01}(1800)$	1855	18.7	—	0.231	—
$P_{03}(1890)$	1834	13.8	4.94	0.068	—
$P_{03}^{(2)}$	1970	55.2	17.1	1.367	—
$P_{03}^{(3)}$	2068	10.5	22.9	0.303	—
$D_{03}(1520)$	1506	23.3	30.0	0.157	$0.304^{+0.076}_{-0.070}$
$D_{03}(1690)$	1668	13.3	70.0	1.049	—
$D_{03}^{(3)}$	1790	15.6	31.4	0.353	—

$\Lambda^* + \gamma^{(*)} \to \Sigma$ transitions

Investigations of the $\gamma^{(*)} + p \to K^+ + \Sigma^0$ reaction in Ref.[4] have indicated that a proper modeling of the background terms requires the introduction of hyperon resonances with isospin $T = 0$ *and* $T = 1$, *i.e.* Λ as well as Σ resonances. The electromagnetic decay of Λ resonances to the Σ^0 ground state is allowed since the EM interaction can change the isospin, as long as the third component $T_z = Q - (B + S)/2$ is conserved (the charge Q, baryon number B and strangeness quantum number S are separately conserved in the EM interaction). It is clear that processes where a Σ^{0*} decays electromagnetically to the Λ ground state are also allowed. The results for these processes will be shown in Sect. 4.2.2.

In Figs. 4.12 and 4.13, we display the HA's for the spin $J = 1/2$ and $J = 3/2$ resonances respectively. Again, one observes that some HA's reach a maximum at moderate values for the momentum-transfer squared ($Q^2 < 1.5$ GeV^2). This maximum is particularly pronounced for the $A_{1/2}$ of the $P_{01}(1810)$ and $D_{03}(1520)$

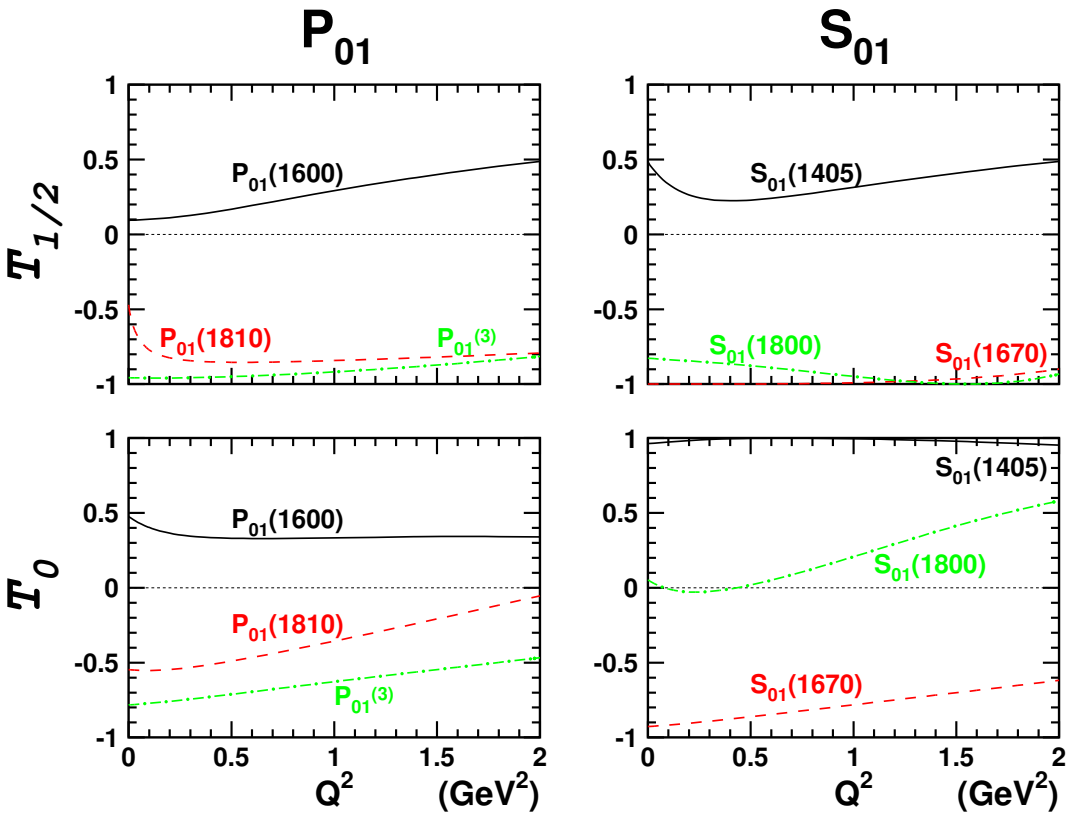

Figure 4.14 *The asymmetries as defined in Eqs. (4.4) for the EM decays to different isospin channels for the three lowest-lying ($J = 1/2$, $S = -1$, $T = 0$) Λ^* resonances with positive parity (left panels) and negative parity (right panels).*

resonances. For these states, the HA at its maximum is more than two times larger than the value at $Q^2 = 0$.

In Table 4.5, the results for the electromagnetic $\Lambda^*(J = 1/2, 3/2) \to \Sigma^0(1192)$ decay are summarized for $Q^2 = 0$. The EM decay width for $S_{01}(1405) \to \Sigma^0(1193)$ is clearly overestimated. This is similar to the $S_{01}(1405) \to \Lambda$ result of Table 4.4, and can be attributed to the special structure of this resonance. The predicted decay width of the $D_{03}(1520)$ is about a factor of 2 smaller than the experimentally determined value. This is in contrast with the $D_{03}(1520) \to \Lambda$ transition of Table 4.4, where the width is overestimated by about a factor of 2. The discrepancy between computed and measured values might be attributed to the $D_{03}(1520) \to \bar{K}N \to \gamma Y$ two-step process, which may interfere destructively with the direct

$D_{03}(1520) \to \gamma Y$ process if $Y = \Lambda$ and constructively if $Y = \Sigma^0$.

The computed EM decay width of 3.827 MeV for the $S_{01}(1670)$ is exceptionally large. It represents about 10% of the reported total decay width $\Gamma^{tot}_{exp} = 25 - 50$ MeV [1]. The *Crystal Ball Collaboration* at Brookhaven has investigated $\bar{K}^- p$ scattering up to $W \sim 1680$ MeV [144], and report a cross section for the $\bar{K}^- p \to \gamma\Sigma^0$ reaction of $\sigma_{tot} = 134\mu b$ at a kaon lab-momentum of $p_K^{lab} = 750$ MeV ($W = 1677$ MeV). This is roughly four times as large as the cross section for the $\bar{K}^- p \to \gamma\Lambda$ reaction ($\sigma_{tot} = 31\mu b$). This observation is clearly in line with the much larger EM decay width for the $S_{01}(1670) \to \Sigma^0$ transition, compared to the one for the $S_{01}(1670) \to \Lambda$ process.

The $\bar{K}^- p \to \eta\Lambda$ cross section at an invariant mass around 1670 MeV was analysed in Ref. [145], using six coupled channels ($\bar{K}N$, $\eta\Lambda$, $\pi\Sigma$, $\pi\Sigma^*(1385)$, $\pi\pi\Lambda$, and $\pi\pi\Sigma$). A partial decay width of 3.6 ± 1.4 MeV for the $S_{01}(1670) \to \eta\Lambda$ process was reported. This is comparable to the computed EM decay width in Table 4.5. Therefore, including the $\gamma\Sigma$ channel in a coupled-channel analysis of $\bar{K}^- p$ scattering at $p_K \approx 750$ MeV seems appropriate.

For the $\Lambda^* \to \Sigma^0$ transitions, the second and the third resonances have larger HA's than the first resonance. Furthermore, in general the helicity amplitudes at small Q^2 are quite large. The difference between $\Lambda^* \to \Lambda$ and $\Lambda^* \to \Sigma^0$ EM decays can be made more explicit through introducing the following asymmetries :

$$\mathcal{T}_{1/2} = \frac{|A^{\Lambda}_{1/2}|^2 - |A^{\Sigma}_{1/2}|^2}{|A^{\Lambda}_{1/2}|^2 + |A^{\Sigma}_{1/2}|^2} , \tag{4.4a}$$

$$\mathcal{T}_{3/2} = \frac{|A^{\Lambda}_{3/2}|^2 - |A^{\Sigma}_{3/2}|^2}{|A^{\Lambda}_{3/2}|^2 + |A^{\Sigma}_{3/2}|^2} , \tag{4.4b}$$

$$\mathcal{T}_{0} = \frac{|C^{\Lambda}_{1/2}|^2 - |C^{\Sigma}_{1/2}|^2}{|C^{\Lambda}_{1/2}|^2 + |C^{\Sigma}_{1/2}|^2} . \tag{4.4c}$$

Here, the superscript Λ (Σ^0) stands for the decay of the resonance to the Λ (Σ^0) ground state. It is clear that a positive (negative) value indicates that the resonance will preferentially decay to the Λ (Σ^0) ground state. As can be inferred from Figs. 4.14 and 4.15, the first resonance generally has positive isospin asymmetries, while the higher-lying resonances mostly have negative isospin asymmetry at low momentum-transfer squared ($Q^2 < 2.0$ GeV^2).

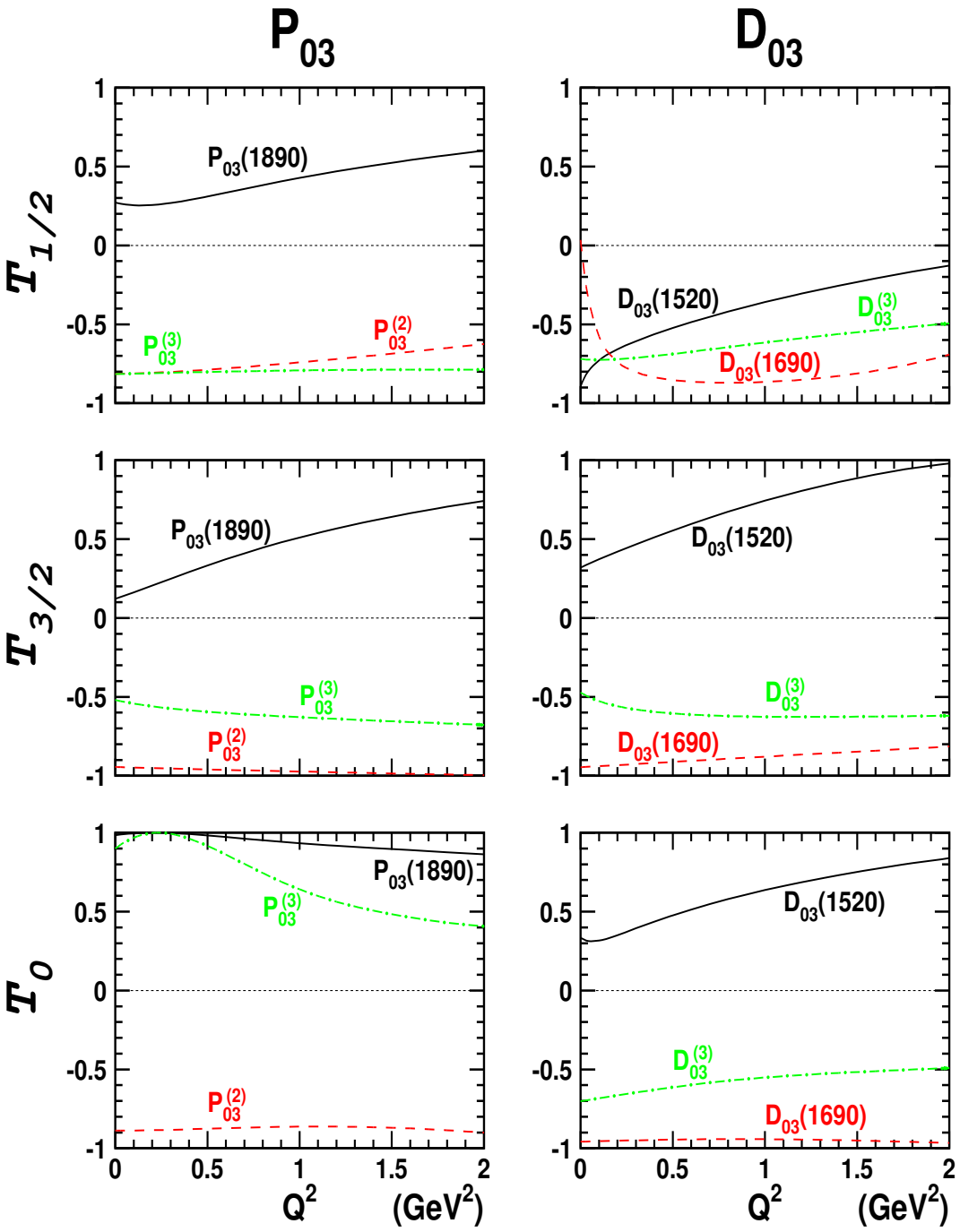

Figure 4.15 *The asymmetries as defined in Eqs. (4.4) for the EM decays to different isospin channels for the three lowest-lying ($J = 3/2$, $S = -1$, $T = 0$) Λ^* resonances with positive parity (left panels) and negative parity (right panels).*

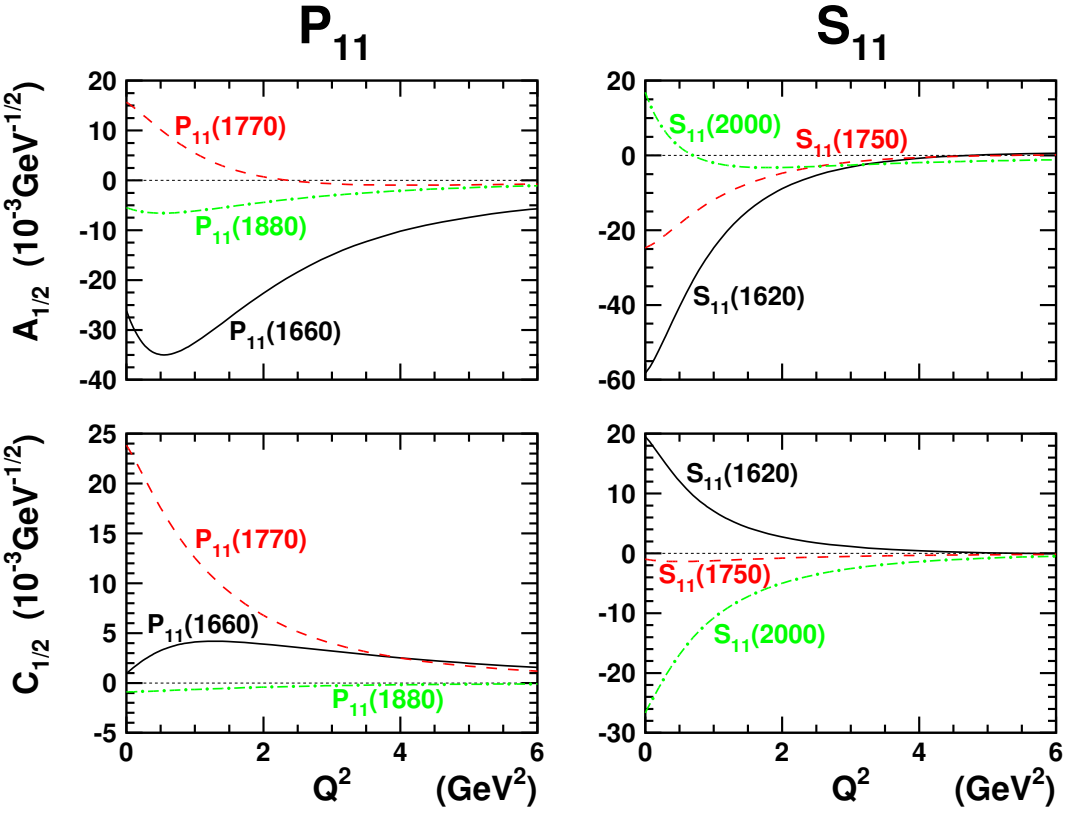

Figure 4.16 *The Q^2 dependence for the $\Sigma^{*0} + \gamma^* \to \Lambda$ decays for spin $J = 1/2$ resonances : left (right) panels show the results for the positive (negative) parity Σ^* resonances.*

4.2.2 Σ-Resonances

$\Sigma^{*0} + \gamma^{(*)} \to \Lambda$ transitions

In this section, we will discuss the EM helicity amplitudes of the $\Sigma^{*0}(J = 1/2) \to \Lambda$ process. The experimental situation for the Σ spectrum is even worse than for the Λ. Except for the octet $\Sigma(1193)$ and the decuplet $\Sigma^*(1385)$, only four 4-*star* and four 3-*star* resonances are reported in Ref. [1]. Of these, the spin and parity is unknown for the $\Sigma(2250)$. Furthermore, to our knowledge there are no data with regard to the EM properties of these resonances.

The predictions from the Bethe-Salpeter model for the photo-amplitudes and EM decay widths are presented in Table 4.6 for the $J = 1/2$ Σ^* resonances. The three lowest Σ^*'s from our calculations are referred to as $P_{11}(1660)$, $P_{11}(1770)$ and

Table 4.6 Calculated masses, photo-amplitudes and EM decay widths for the $\Sigma^{*0} + \gamma \rightarrow \Lambda(1116)$ transition are given below for the lowest-lying $J = 1/2$ resonances. Masses and decay widths are given in units of MeV, photo-amplitudes are given in units of 10^{-3} GeV$^{-1/2}$.

Resonance	M_{calc}	$\lvert A_{1/2}\rvert$	Γ_{calc}
$P_{11}(1660)$	1801	26.1	0.451
$P_{11}(1770)$	1967	15.7	0.216
$P_{11}(1880)$	2049	5.47	0.0294
$S_{11}(1620)$	1640	58.2	1.551
$S_{11}(1750)$	1800	24.7	0.403
$S_{11}(2000)$	1813	16.9	0.193

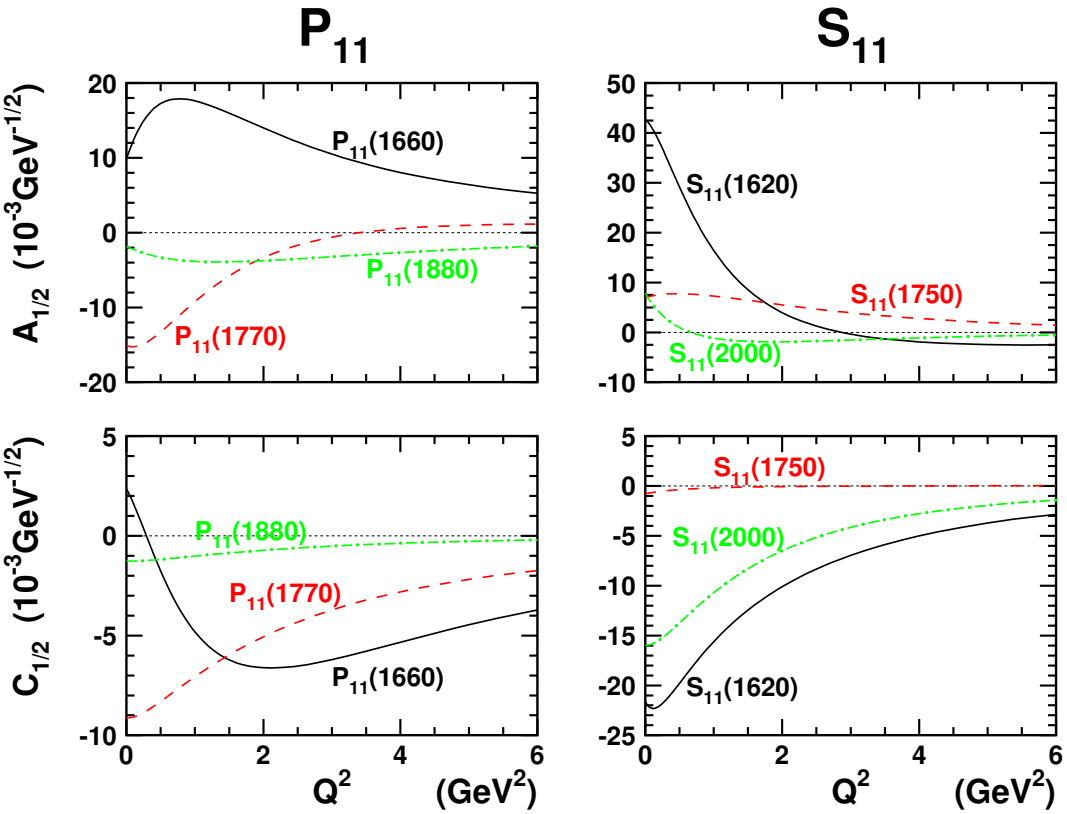

Figure 4.17 *The Q^2 dependence for the $\Sigma^{*0} + \gamma^* \rightarrow \Sigma^0$ decays for spin $J = 1/2$ resonances : left (right) panels show the results for the positive (negative) parity Σ^* resonances.*

Table 4.7 Calculated masses, photo-amplitudes and EM decay widths for the $\Sigma^* + \gamma \rightarrow \Sigma(1193)$ transition are given below. The charge of the Σ^* isospin-triplet member is indicated by the superscript $(^{0,+,-})$ in its name. Masses and decay widths are given in units of MeV, photo-amplitudes are given in units of 10^{-3} GeV$^{-1/2}$.

Resonance	M_{calc}	$\lvert A_{1/2}\rvert$	Γ_{calc}
$P_{11}^0(1660)$	1801	9.91	0.0578
$P_{11}^0(1770)$	1967	15.1	0.186
$P_{11}^0(1880)$	2049	1.83	0.00311
$S_{11}^0(1620)$	1640	42.7	0.688
$S_{11}^0(1750)$	1800	6.96	0.0284
$S_{11}^0(2000)$	1813	7.86	0.0373
$P_{11}^+(1660)$	1801	35.3	0.733
$P_{11}^+(1770)$	1967	54.8	2.446
$P_{11}^+(1880)$	2049	4.86	0.0219
$S_{11}^+(1620)$	1640	125.6	5.955
$S_{11}^+(1750)$	1800	4.80	0.0135
$S_{11}^+(2000)$	1813	10.3	0.0641
$P_{11}^-(1660)$	1801	15.5	0.141
$P_{11}^-(1770)$	1967	24.6	0.493
$P_{11}^-(1880)$	2049	1.20	0.00136
$S_{11}^-(1620)$	1640	40.3	0.613
$S_{11}^-(1750)$	1800	9.12	0.0488
$S_{11}^-(2000)$	1813	5.41	0.0177

$P_{11}(1880)$. However, the existence of the $P_{11}(1770)$ is based on one analysis, and is questionable [1]. Therefore, it is argued in Ref. [138], that the $P_{11}(1770)$ should be disregarded, and that the $P_{11}(1880)$ is actually the second-lowest resonance. Even then, the predicted masses are about 100 MeV too high. For the negative-parity Σ^* resonances, the situation for the $J = 1/2$ resonances is more clear. The identification of the two lowest-lying computed states with the experimentally observed ones is straightforward by comparing the measured and the predicted masses. The $S_{11}(2000)$ can be identified with the third computed state, since the value of 2000 MeV for its experimental mass is a very rough estimate [1]. The computed EM decay widths in Table 4.6 decrease with increasing mass for the P_{11} as well as for the S_{11} resonances.

For the P_{11} resonances, the results for the HA's are displayed in the left panels of Fig. 4.16. The $P_{11}(1660)$, which is the Roper-like resonance of the Σ spectrum, has the largest $A_{1/2}$, reaching a maximum at $Q^2 \approx 0.5$ GeV^2. The second resonance has the largest $C_{1/2}$ for small to moderate Q^2-values. The HA's for the P_{11} $\Sigma^* \to \Lambda$ decays are comparable to those for the P_{01} $\Lambda^* \to \Lambda$ decays. Therefore, the Σ^*'s can be expected to contribute significantly to the $p(\gamma^{(*)}, K)\Lambda$ and the $\bar{K}^- p \to \gamma\Lambda$ cross sections. This observation is even more applicable to the $J^\pi = 1/2^-$ resonances, for which the HA's are depicted in the right panels of Fig. 4.16. One observes a large $A_{1/2}$ for the $S_{11}(1620)$, which is a 2-*star* resonance in Ref. [1]. This is also clear from the large EM decay width of this resonance, reported in Table 4.6. However, the data for the $\bar{K}^- p \to \gamma\Lambda$ process [146], do not show a significant enhancement at $W \approx 1620$ MeV ($p_K \approx 629$ MeV). This could be explained by a small coupling of the $S_{11}(1620)$ resonance to the $\bar{K}N$ channel.

$\Sigma^* + \gamma^{(*)} \to \Sigma$ transitions

The $\Sigma^* + \gamma^{(*)} \to \Sigma(1193)$ process differs from the ones of previous sections in that it comes in three versions, one for each member of the Σ^* isospin triplet. Their EM properties are not independent, however, because of the presumed isospin symmetry of the interactions in the Bonn model (u- and d-quark have the same mass and the effective interactions do not depend on the third component of the isospin quantum number T_z of the quark). Knowledge of the helicity amplitudes for the Σ^{*+} and the Σ^{*-} allows one to obtain those for the Σ^{*0}, simply by taking the average. In the following, results for all three isospin-triplet members will be presented. The charge of the particle will be denoted in the superscript.

In Fig. 4.17, the HA's for the $\Sigma^{*0} \to \Sigma^0$ decays are displayed for the lowest-lying spin $J = 1/2$ resonances. Obviously, the HA's for the P_{11}^0 resonances are relatively small. This is reflected in the rather small values for the computed EM decay widths of the P_{11}^0 resonances given in Table 4.7. A larger EM response is seen for the negative-parity states, where the $S_{11}^0(1620)$ has HA's of similar magnitude as the ones for the decay to the $\Lambda(1116)$ (Fig. 4.16). The other S_{11}^0 resonances have rather small HA's.

The results for the positively charged members of the Σ^*-triplets, which are presented in Fig. 4.18, are quite surprising. In contrast with their neutral counterparts,

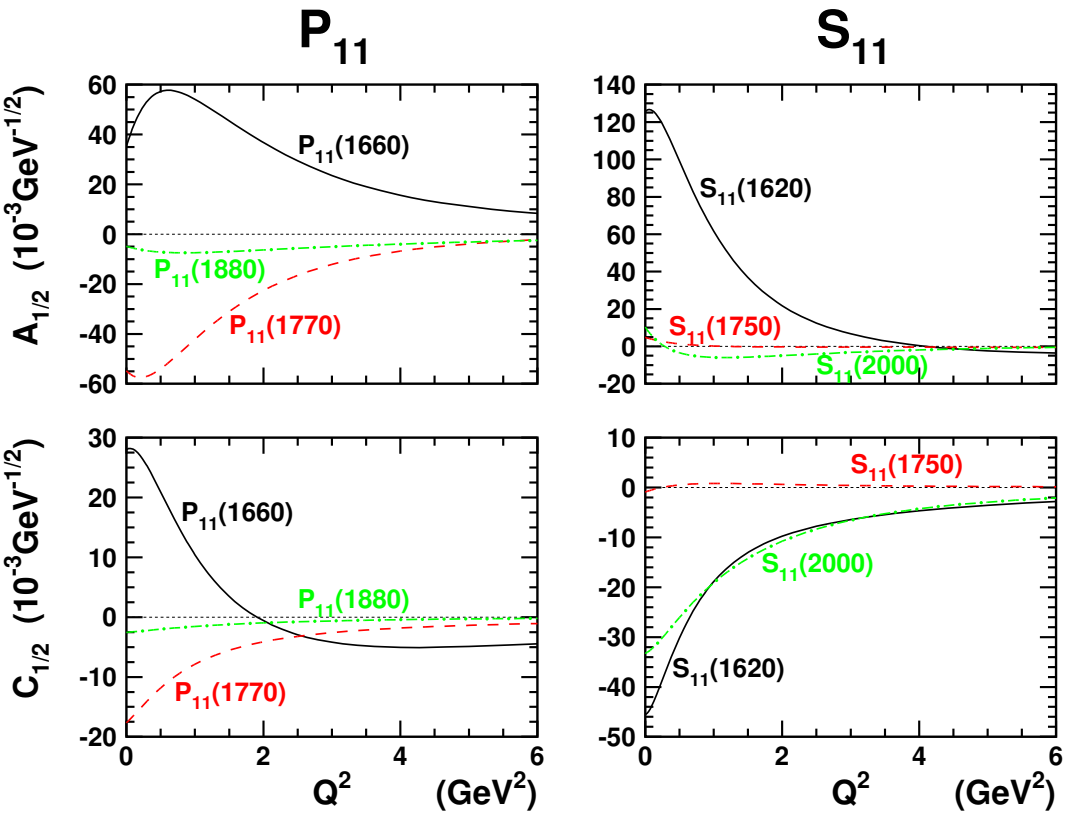

Figure 4.18 *The Q^2 dependence for the $\Sigma^{*+}+\gamma^* \to \Sigma^+$ decays for spin $J = 1/2$ resonances : left (right) panels show the results for the positive (negative) parity Σ^* resonances.*

the first and second P_{11}^+ resonances have large helicity amplitudes. This can also be deduced from the predictions for the EM decay widths in Table 4.7. These findings have serious implications when modeling the background contributions in $p(\gamma^{(*)}, K)Y$ processes. When Y is a neutral hyperon (Λ or Σ^0), the exchanged particle in the u-channel (Fig. 4.9) would necessarily be neutral. The P_{11}^0 resonances are likely to have a negligible effect because of their small EM couplings. When $Y = \Sigma^+$, the intermediate hyperon would be positively charged, and the P_{11}^+ resonances could constitute a sizeable term in the background description.

For the S_{11}^+ resonances, a striking feature is the large EM decay width of the first resonance in Table 4.7. Again, this indicates the large coupling of the $S_{11}^+(1620)$ to the γY decay channels. Furthermore, the EM decay width $\Gamma_{calc}^{EM} = 5.955$ MeV seems to be a significant fraction of the poorly known total decay width ($\Gamma_{exp}^{tot} =$

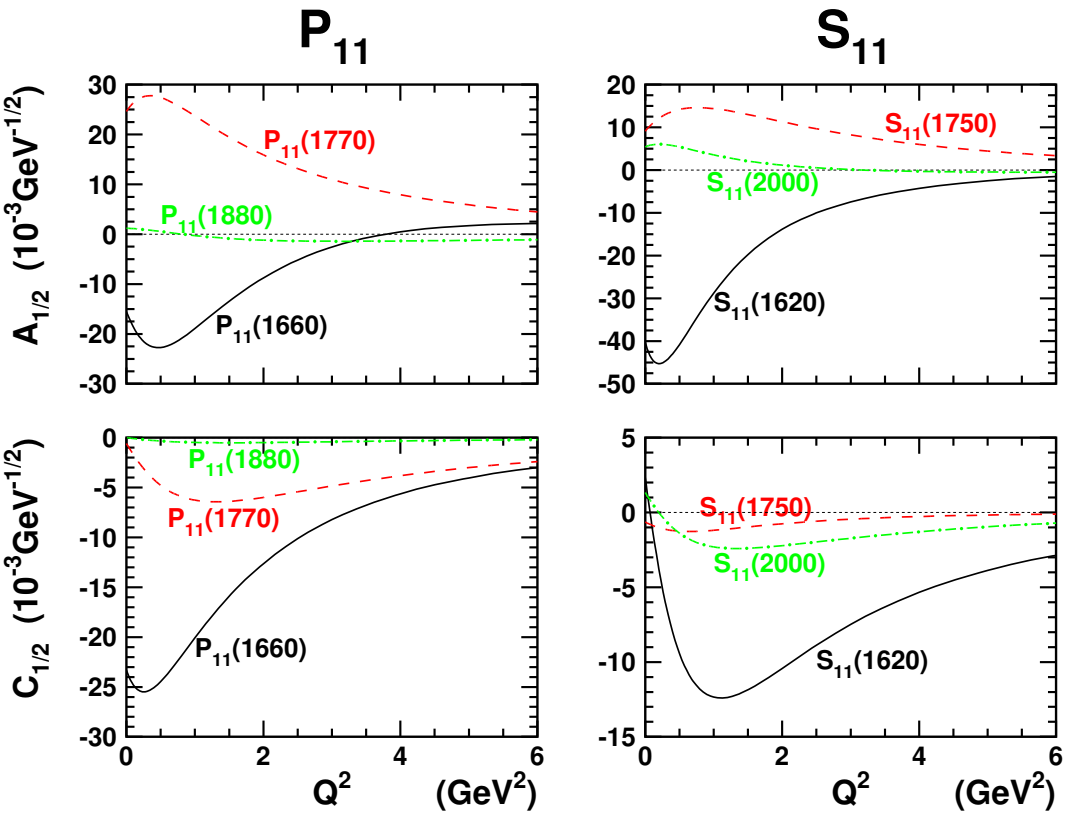

Figure 4.19 *The Q^2 dependence for the $\Sigma^{*-}+\gamma^* \to \Sigma^-$ decays for spin $J = 1/2$ resonances : left (right) panels show the results for the positive (negative) parity Λ^* resonances.*

$10 - 106$ MeV [1]). Since the latter was extracted from meson-baryon scattering experiments, the experimental status of this resonance could be improved considerably by investigating radiative processes. The computed HA's of the other S_{11}^+ resonances again turn out to be relatively small.

The calculated HA's for the P_{11}^- and S_{11}^- Σ^* resonances are displayed in Fig. 4.19. Moderate HA's and EM decay widths (Table 4.7) are observed for the positive-parity resonances. For the negative-parity resonances, one notices the large $A_{1/2}$ for the $S_{11}^-(1620)$ resonance.

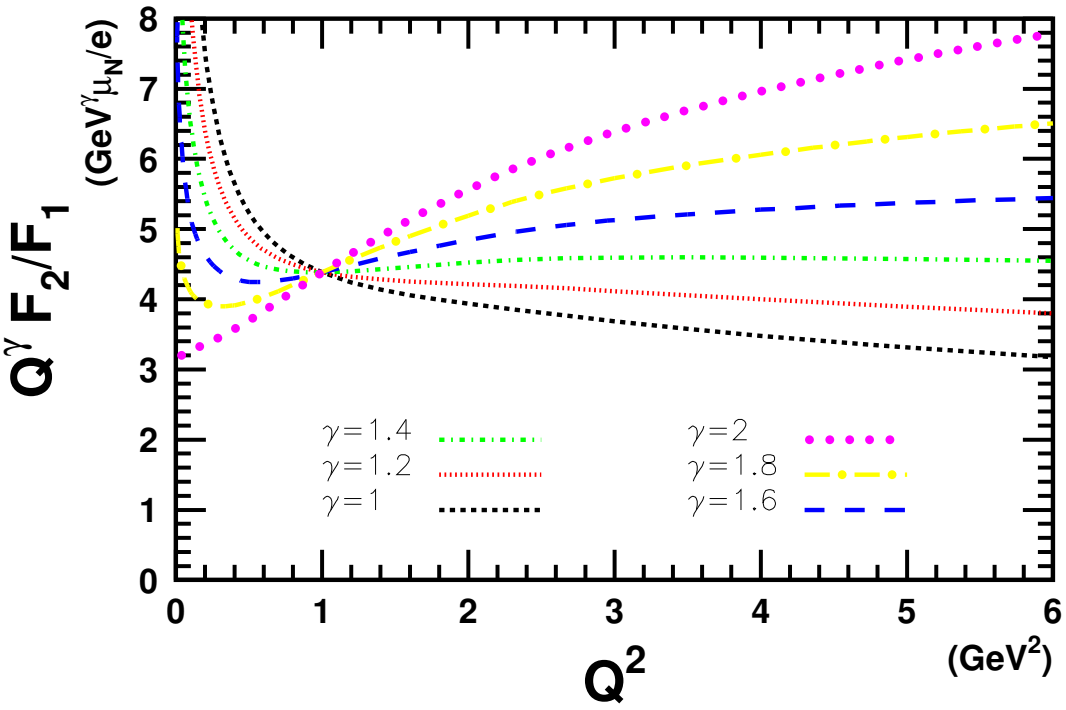

Figure 4.20 *The ratio of the Pauli and Dirac factors of the Λ hyperon, multiplied with a power of the transferred momentum Q^γ, for $\gamma = 1.0, 1.2, 1.4, 1.6, 1.8$ and 2.0. At sufficiently large Q^2, the ratio reaches a constant value for $1.4 \leq \gamma \leq 1.6$.*

4.3 Form Factors at High Q^2

4.3.1 Elastic Form Factors

The behaviour of form factors and helicity amplitudes at large Q^2 is an interesting topic. Perturbative QCD predicts that the ratio of F_2^p/F_1^p should go as $1/Q^2$ at large values of Q^2 [147]. However, the data seem to favour the ratio of $F_2^p/F_1^p \sim 1/Q$ for $2 \leq Q^2 \leq 6$ GeV^2 [62, 63]. In Fig. 4.20, the $Q^\gamma F_2^\Lambda/F_1^\Lambda$ ratio is displayed for different values γ of the exponent of $Q = \sqrt{Q^2}$. The ratio $Q^\gamma F_2/F_1$ becomes constant in the range $2.0 \leq Q^2 \leq 6.0$ GeV^2, for $\gamma \approx 1.4$. The prediction of perturbative QCD (constant ratio for $\gamma = 2$) is derived from the general requirement that massless particles conserve helicity, and that at high Q^2, the quarks are (asymptotically) free and can be considered massless due to the large boost. In the Q^2 regime under investigation, the constituent quarks are bound and cannot be considered massless. This

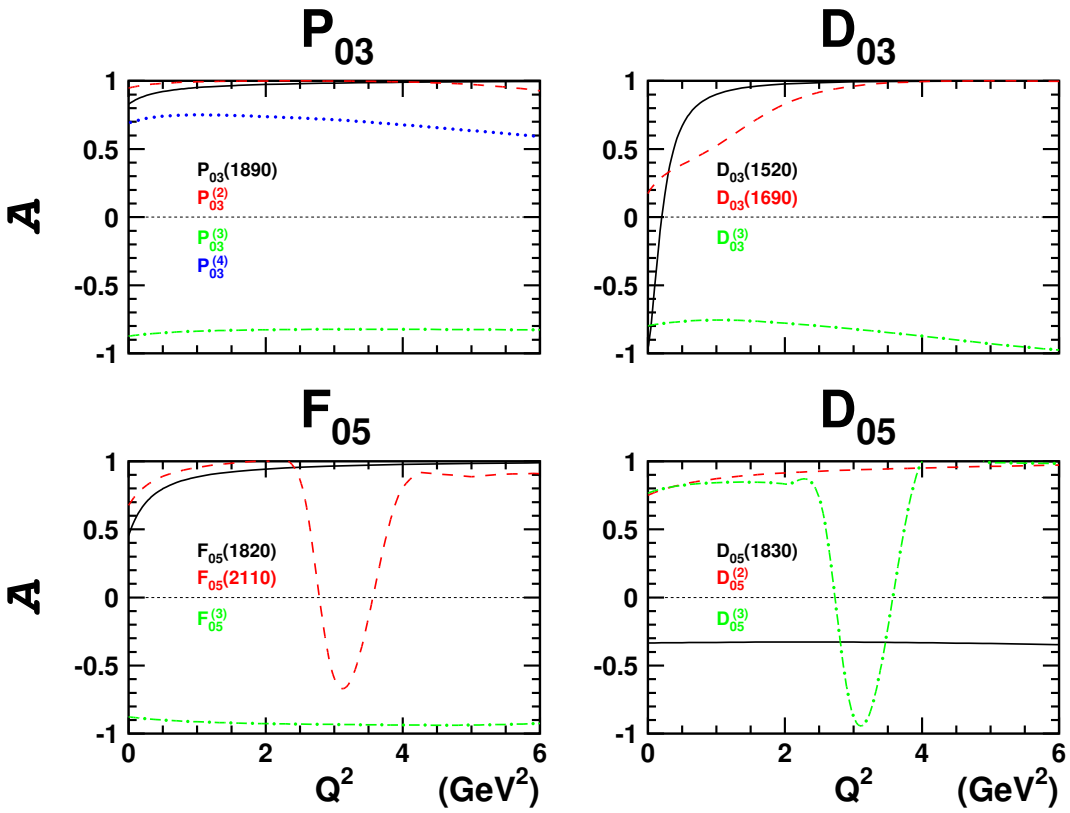

Figure 4.21 *The helicity asymmetry as defined in Eq. (4.5) for the lowest-lying spin $J = 3/2$ and $J = 5/2$ Λ-resonances decaying to the Λ ground state.*

holds in particular for the strange constituent quark ($m_s = 670$ MeV). Therefore, a deviation from the prediction from perturbative QCD could have been expected.

4.3.2 Helicity Asymmetries

For hyperon resonances with $J \geq 3/2$, the behaviour for the helicity asymmetries can be predicted. These asymmetries are defined analogous to the isospin asymmetries of Eq. (4.4) :

$$\mathcal{A} = \frac{|A_{1/2}|^2 - |A_{3/2}|^2}{|A_{1/2}|^2 + |A_{3/2}|^2} \,. \tag{4.5}$$

The helicity asymmetries of the lowest-lying $J = 3/2$ and $J = 5/2$ Λ^* resonances for the decay to the Λ ground state are shown in Fig. 4.21 and the asymmetries for

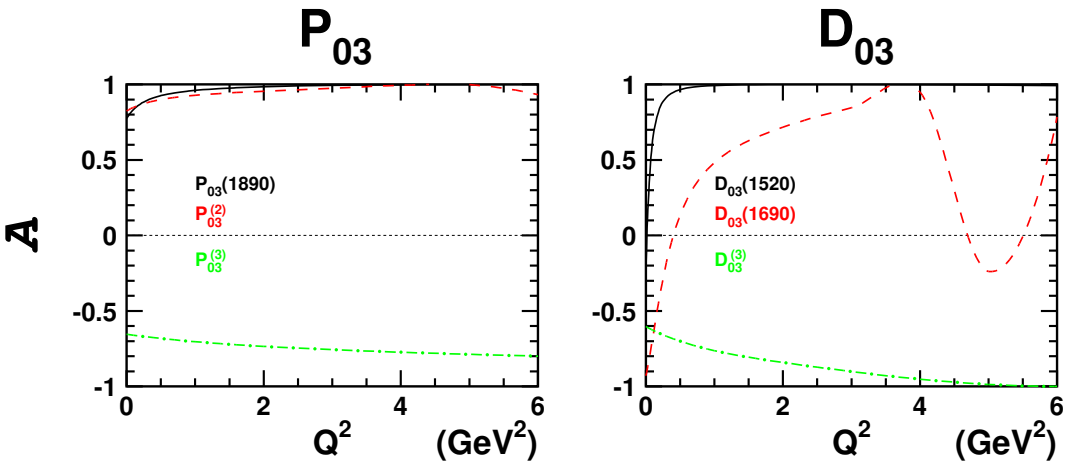

Figure 4.22 *The helicity asymmetry as defined in Eq. (4.5) for the lowest-lying spin $J = 3/2$ resonances decaying to the Σ^0 ground state.*

the $J = 3/2$ Λ^* resonance for the decay to the Σ^0 ground state are displayed in Fig. 4.22. In most cases the helicity asymmetries go to ± 1 for high Q^2.

To find out for which Y^*'s the asymmetries go to $+1$, and for which Y^*'s they go to -1, one should project the corresponding BS amplitude to the $SU(6)$ spin-flavour basis states [148]. This was done in Ref. [37]. It turns out that the BS amplitudes of the resonances for which the helicity asymmetry goes to $+1$, have the largest contribution from $SU(6)$ spin-flavour states for which the angular-momentum addition of the three CQ spins $S = S_1 \oplus S_2 \oplus S_3 = 1/2$. On the other hand, the BS amplitudes of the resonances for which the helicity asymmetry goes to -1, have the largest contribution from $SU(6)$ states for which $S = 3/2$. (Remark that the spin J of a baryon resonance in CQ models is the angular-momentum addition of the spins of the three CQ's and the orbital angular momentum L.)

This observation can be explained qualitatively by considering the EM decay of *e.g.* a D_{03} resonance to a ground-state hyperon Y in the resonance rest frame (see Fig. 4.23). For high Q^2, the photon preferentially couples to the separate CQ's, which means that the major contribution to the $A_{1/2}$ comes from the process in Fig. 4.23(a). There, one of the CQ's with negative spin projection emits a photon of positive helicity, and flips its spin. This process is allowed for all D_{03} resonances. When the BS amplitude has its main contributions from $SU(6)$ states for which

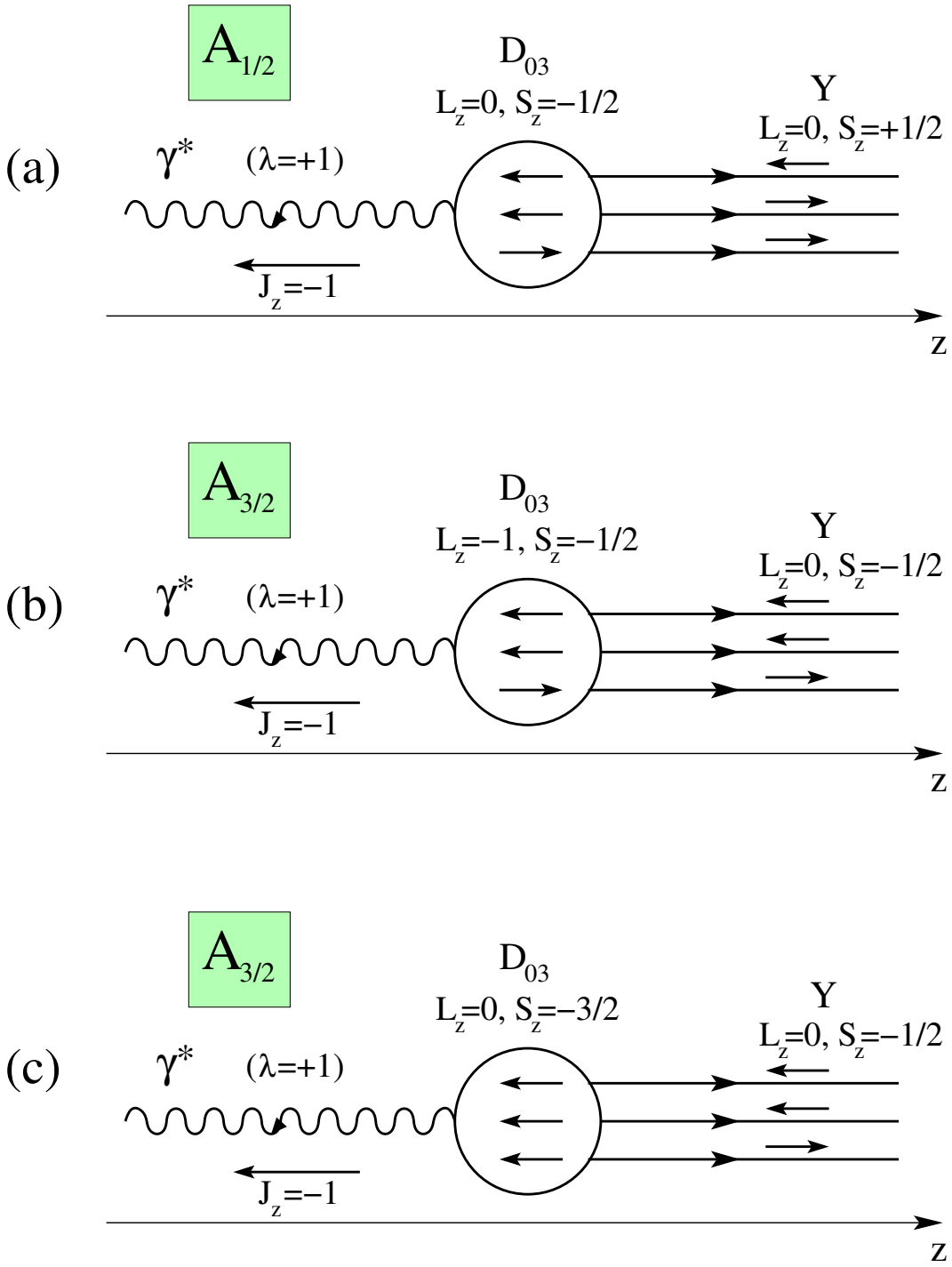

Figure 4.23 *A D_{03} resonance in its rest frame decays electromagnetically to a ground-state hyperon Y. The three depicted processes refer to different contributions to the helicity amplitudes $A_{1/2}$ (process (a)) and $A_{3/2}$ (processes (b) and (c)).*

$S = 1/2$, the major contribution to the $A_{3/2}$ comes from the process in Fig. 4.23(b). There, one could argue that the photon is emitted by the resonance as a whole, because the spin projections of the three CQ's remain unaltered and the projection of the orbital angular momentum (L_z) changes by 1. As mentioned before, at high Q^2, the photon preferentially couples to the separate CQ's than to the resonance as a whole. As a consequence, the process in Fig. 4.23(b) becomes much smaller than the one in Fig. 4.23(a). If now the BS amplitude of the resonance has its main contributions from $SU(6)$ states for which $S = 3/2$, the major contribution to the $A_{3/2}$ at high Q^2 comes from the process in Fig. 4.23(c). Here, the photon is emitted by a single CQ, which accordingly flips its spin. This process is similar to the one in Fig. 4.23(a), and thus of the same magnitude. However, in the process of Fig. 4.23(c), three CQ's can emit the photon, while in the one of Fig. 4.23(a), only two CQ's can do that. Therefore, the $A_{3/2}$ will be larger than the $A_{1/2}$ in this case, and negative helicity amplitudes can be expected.

It should be noted that in the above discussion, many things have been assumed explicitly or implicitly. Therefore, the relation between a negative helicity asymmetry and a large contribution from symmetric-spin states (with $S = 3/2$) in the BS amplitude of the resonance should be taken as a rule of thumb and not as a proven fact.

4.4 Numerical Accuracies

In this section, the numerical accuracy of the calculations reported in this chapter is discussed. In particular, we concentrate on the size of the basis for the vertex functions and the number of integration points.

The dependence of the computed results on the basis size is illustrated in Fig. 4.24, where the form factors of the Λ are shown for various basis sizes. The basis is a combination of $SU(6)$ spin-flavour states and spatial harmonic oscillator functions for each relative momentum. The spatial basis functions contain a spherical harmonic and a radial function Ψ_{NL}, where N is the radial and L the orbital quantum number. The highest value of N (N_{max}) determines the dimension of the basis. In Fig. 4.24, the results are shown for $N_{max} = 2$, 4, 6, 8, 10, and 12. It is quite clear that the curves converge as N_{max} increases. For the magnetic form factor, which is relatively large for the Λ, convergence is already reached at $N_{max} \approx 4$. For the

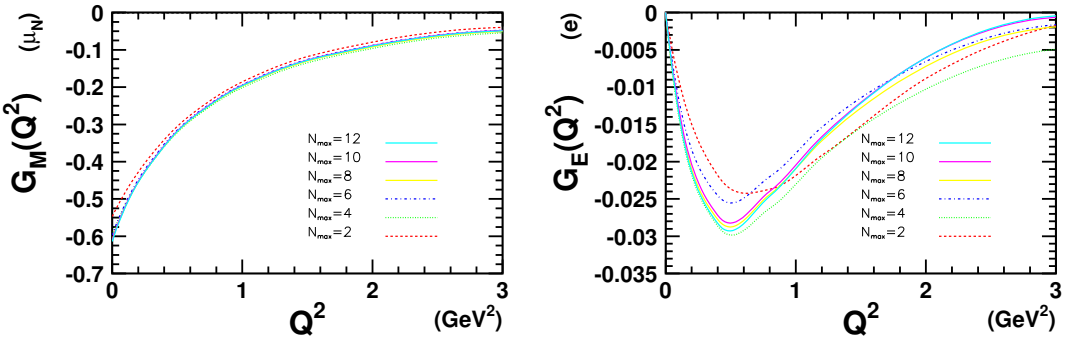

Figure 4.24 *The results for the magnetic (left) and electric (right) form factors of the Λ depend on the size of the basis in which the calculations are performed. N_{max} is the number of harmonic-oscillator shells taken into account.*

electric form factor, which is quite small in magnitude, a larger basis is required. However, the curves converge, and a basis including all states up to $N_{max} = 8$ produces accurate results.

The sensitivity of the integral of Eq. (2.46) to the number of integration points (NIP) is illustrated in Fig. 4.25. There, we present the results for the HA's of the $P_{01}(1810)$ Λ^* resonance decaying to the Λ and Σ^0 ground states, calculated with different NIP's. The eight-dimensional integral of Eq. (2.46) can be analytically reduced to a six-dimensional integral [39, 149] by means of complex-contour integration. Thereby, the energy components of the relative four-momenta p^0_ξ and p^0_η are integrated out. In the remaining integral over $\mathbf{p}_\xi$ and $\mathbf{p}_\eta$, the azimuthal dependence can be reduced to $(\phi_\xi - \phi_\eta)$, leaving one with five-dimensional integrals. After all this, there remains a five-dimensional surface consisting of two radial coordinates, two polar angles and one azimuthal angle. We have used Gauss integration methods with r, t and a integration points for the radial, polar and azimuthal integrations respectively. For Fig. 4.25, we used $(r, t, a) = (10, 10, 15)$, $(7, 7, 12)$, $(5, 5, 10)$, and $(3, 3, 5)$. These are denoted with their total NIP in Fig. 4.25. Also here, the numerical computations are apparently converging, and are esteemed accurate for $NIP = 28812$, corresponding to $(r, t, a) = (7, 7, 12)$.

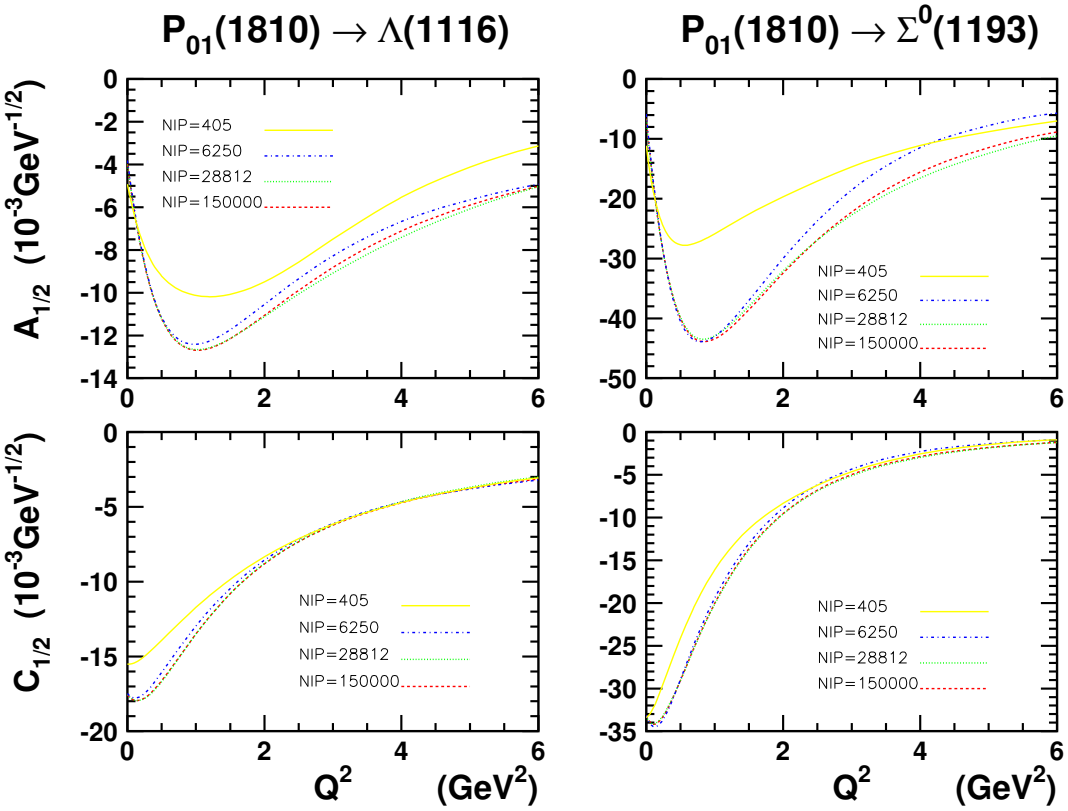

Figure 4.25 *The numerical results for helicity amplitudes of the $P_{01}(1810)$ decaying to the Λ ground state (left) and to the Σ^0 ground state (right) depend on the number of integration points (NIP) for the integral of Eq. (2.46).*

Chapter 5

Conclusions

The $p(e,e'K)Y$ reaction is a typical reaction to study a number of phenomena in medium-energy physics. It involves the electromagnetic interaction between the initial electron and proton. The strong interaction manifests itself through the creation of two hadrons, a kaon and a hyperon. At threshold, the three-momentum of the proton and virtual photon in their c.o.m. frame is around 530 MeV ($W_{th} = 1609$ MeV for $p(e,e'K^+)\Lambda$). This is already a large fraction of the proton mass and relativistic effects are bound to occur. For energy transfers from threshold to about 3.0 GeV, the invariant mass typically lies in the energy domain of the baryon resonances. Furthermore, the outgoing kaon and hyperon are *strange* particles, which can be most easily explained in the quark picture, where the reaction involves the creation of a strange quark/antiquark pair. The appearance of strange quarks, which are heavier than the nonstrange quarks, explicitly breaks the flavour symmetry. A description of the $p(e,e'K)Y$ process will have to incorporate most of these phenomena, but should remain tractable at the same time.

In the course of this thesis, we have presented the Bonn constituent quark model. This model is based on the Bethe-Salpeter (BS) approach for describing a system of interacting relativistic particles. In order to describe baryons, this approach is applied to a system of three interacting constituent quarks (CQ's). The quantity describing the bound states of the system is the BS amplitude. For instantaneous effective interactions, with a genuine three-particle irreducible interaction, this amplitude can be easily obtained from the Salpeter amplitude. The Salpeter amplitudes are the solutions to the Salpeter equation, which is an eigenvalue prob-

lem. The eigenvalues represent the masses of the three-CQ bound states.

Current matrix elements between two baryon states can be computed for the current operator corresponding with the coupling of a photon to a point-like quark. From these current matrix elements, one can easily derive the form factors of the baryon. For electromagnetic transitions, it is customary to compute the helicity amplitudes instead of the transition form factors. These are the strengths with which a baryon resonance decays electromagnetically to the ground state through the emission of a photon with certain helicity. The Bonn CQ model can describe electromagnetic and hadronic decays of baryons and baryon resonances, thereby correctly treating the relativistic boost effects.

A tree-level isobar model description of the $p(e, e'K)Y$ reaction requires the introduction of electromagnetic (EM) form factors of baryons and baryon resonances. In the u-channel of such a model, the virtual photon couples to the intermediate hyperon (resonance) with a strength given by the EM form factors of the $Y^{(*)}$. The description of the EM vertex depends on the spin and parity of the exchanged hyperon. We have presented the prescriptions for including all on-shell EM form factors of spin $J = 1/2$ $Y^{(*)}$'s in a gauge invariant manner. We have also given a review of the off-shell ambiguities introduced at the EM vertex. Unfortunately, off-shell form factors cannot be measured.

The Bonn CQ model has been applied to the computation of electromagnetic properties of strange baryons. The computed form factors of the ground-state hyperon have been presented as a function of Q^2, the squared photon momentum. The comparison with experimental data can be done in the real-photon point for the magnetic form factors. The latter reduces to the magnetic moment of the hyperon, which is measured with good accuracy. Our results are in excellent agreement with these experimental numbers. Also the magnetic and electric radii are presented. The electric radius of the Σ^- has been measured and our result compares favourably with it. It must be noted that the seven parameters entering the Bonn model were fitted to the masses of best known states in the baryon spectrum and were kept fixed during the calculation of the electromagnetic properties. Therefore, our results for the form factors, radii and magnetic moments, can be considered as genuine predictions.

With the exception of the Σ^-, the magnetic form factors of the ground-state hy-

perons can be modelled by dipoles with cutoff masses ranging from 0.79 GeV for the Σ^+ to 1.14 GeV for the Λ. This is different from the proton magnetic form factor which is commonly represented by a dipole with cutoff mass 0.84 GeV. Furthermore, the electric form factors of the neutral hyperons differ substantially with the one for the neutron. In fact, the signs of the Λ and Σ^0 electric form factor are negative, while the neutron electric form factor is positive. This can be attributed to the heavier strange CQ residing near the hyperon's center-of-mass. Therefore, the use of nucleon electromagnetic form factors to model the hyperon form factors is a highly questionable procedure.

The Bonn CQ model has also been employed to determine the electromagnetic transition current matrix elements between Λ^* and Σ^* resonances and the ground-state hyperons. We have presented our results in the form of helicity amplitudes for the lowest-lying hyperon resonances. Since the electromagnetic interaction only conserves the third component of the isospin and not the isospin quantum number, we have calculated the electromagnetic decays $\Lambda^* \to \Lambda(1116)$, $\Lambda^* \to \Sigma(1193)$, $\Sigma^* \to \Lambda(1116)$, and $\Sigma^* \to \Sigma(1193)$.

The presented results show some interesting features. The first excited state of a certain spin and parity (and sometimes also higher excited states) seems to couple considerably stronger to a photon with intermediate virtuality Q^2 than to a real photon. Therefore, these resonances can be better studied with kaon electroproduction than with kaon photoproduction reactions.

Further, the lowest-lying Λ^* with certain quantum numbers seems to decay preferably to the $\Lambda(1116)$, while the second and third excited states preferentially decay to the $\Sigma^0(1193)$ ground state. In background model B as discussed in Sect. 3.2.3, hyperon resonances in the u-channel of the $p(e,e'K)Y$ process interfere destructively with the Born terms, reducing the background strength. Therefore, taking into account the lowest resonance of a certain spin and parity will be more efficient when $Y = \Lambda$, while including higher-lying resonances will have more effect when $Y = \Sigma$.

In addition, the lowest-lying Y^* is the least off-shell in $p(e,e'K)Y$ reactions. Since an amplitude in the isobar model of Chap. 3 is proportional to the propagator of the exchanged particle, which on its turn is reversely proportional to the degree of off-shellness, the lightest hyperon resonance will induce larger effects.

Thus, if the lowest-lying resonance preferentially decays to the $\Lambda(1116)$, one could suggest that including hyperon resonances to reduce the background strength is more efficient for the $p(e,e'K^+)\Lambda$ than for the $p(e,e'K)\Sigma$ process. Further research will have to show whether this is the case.

In the isobar model of Chap. 3, resonances with spins $J \leq 3/2$ are taken into account. According to the computed helicity amplitudes, the $F_{05}(1820)$ and $D_{05}(1830)$ Λ resonances have a reasonable EM coupling to the $\Lambda(1116)$. A second resonance with $J^\pi = 5/2^-$, the $D_{05}^{(2)}$ with computed mass around 2100 MeV, remains unobserved experimentally, but seems to have larger helicity amplitudes than the first D_{05} resonance. On the basis of these observations, the question of whether $J = 5/2$ Λ resonances contribute considerably to the $p(\gamma^{(*)},K)\Lambda$ process, remains open.

The electromagnetic decay of a Σ^* resonance to the Σ ground state comes in three versions, one for each member of the Σ^* isospin triplet. The results show that the charged states of some Σ^* resonances (*e.g.* the $P_{11}(1660)$ and the $S_{11}(1620)$) have (much) larger helicity amplitudes than the neutral state. Therefore, these resonances will influence the $p(e,e'K^0)\Sigma^+$ process (much) more than the $p(e,e'K^+)\Sigma^0$ process.

Our investigations also lend support for the special structure of the $S_{01}(1405)$ resonance, which has been discussed elaborately in the literature [127, 140, 141, 150]. The predicted EM decay width is much larger than what is experimentally measured, both for decay to the $\Lambda(1116)$ as for decay to the $\Sigma(1193)$ ground state. In this respect, we would like to note that the lowest-lying Σ^* with negative parity, the $S_{11}(1620)$, also has large EM decay widths to the $\Lambda(1116)$ and $\Sigma(1193)$. In contrast to the $S_{01}(1405)$, the mass of the $S_{11}(1620)$ is well predicted by the Bonn CQ model.

We have reported rather large decay widths for the $S_{01}(1670) \rightarrow \Sigma(1193) + \gamma$ process. A high EM coupling of this resonance to the Σ ground state could have been expected from the observation that the cross section for the $\bar{K}^- p \rightarrow \gamma\Sigma$ process is roughly a factor of four larger than the one for the $\bar{K}^- p \rightarrow \gamma\Lambda$ reaction around a kaon momentum of 750 MeV/c (invariant mass around 1678 MeV) [144].

Finally, the behaviour of the electromagnetic form factors and helicity amplitudes was checked for high Q^2. For the Λ, the ratio F_2^Λ/F_1^Λ turns out to be proportional to $Q^{-\gamma}$ with $\gamma \approx 1.4$ in the range $2.0 \leq Q^2 \leq 6.0$ GeV^2. This value of γ differs from the perturbative QCD prediction of 2. The behaviour of the helicity asymme-

tries for $J \geq 3/2$ resonances is in agreement with the general statement that at high Q^2, the photon couples to the constituent quark, and not to the baryon (resonance) as a whole.

Appendix A

Interaction Potentials and Kernels

In this Appendix, a brief description of the quark-quark interactions used in the kernel of the Bethe-Salpeter equation (2.13) is given. As shown in Sect. 2.2, the Bethe-Salpeter equation can be reduced to a Salpeter equation if the interactions are instantaneous. In the model, two types of interactions appear. The three-particle-irreducible confinement potential was introduced in Eq. (2.18), en will be discussed in Sect. A.1. The two-particle-irreducible residual interaction of Eqs. (2.19) and (2.20) is the subject of Sect. A.2.

A.1 Confinement Potential

In the Bonn model, the confinement interaction is a string-like potential. This is very common in constituent-quark models, both relativistic and nonrelativistic, and refers to a flux-tube breaking picture of the hadronization process. In contrast with the usual string-potential, the confinement potential rises linearly with the interquark distances. This results in Regge trajectories for both mesons and baryons in the Bonn model.

The confinement potential is the only three-particle-irreducible interaction that enters the model. It is given by :

$$V^{(3)}\left(x_1,x_2,x_3;x_1',x_2',x_3'\right) = V^{(3)}_{\text{conf}}\left(\mathbf{x}_1,\mathbf{x}_2,\mathbf{x}_3\right)\ \delta^{(1)}\left(x_1^0-x_2^0\right)\ \delta^{(1)}\left(x_2^0-x_3^0\right) \\ \delta^{(4)}\left(x_1-x_1'\right)\ \delta^{(4)}\left(x_2-x_2'\right)\ \delta^{(4)}\left(x_3-x_3'\right)\ . \quad \text{(A.1)}$$

Here, the one-dimensional δ-functions of the time-components make sure that the

Table A.1 The parameters for the Bonn model are shown below. The seven parameters are the constituent-quark masses, the confinement offset and slope, the 't Hooft interaction range, and the 't Hooft nonstrange-nonstrange and nonstrange-strange interaction strength.

Parameter	Symbol	Value	Unit
nonstrange CQ mass	m_n	330	MeV
strange CQ mass	m_s	670	MeV
confinement offset	a	-744	MeV
confinement slope	b	470	MeV fm^{-1}
't Hooft nn strength	g_{nn}	136	MeV fm^3
't Hooft ns strength	g_{ns}	94	MeV fm^3
't Hooft range	Λ	0.40	fm

interaction is instantaneous. The actual confinement potential $V^{(3)}_{\text{conf}}(\mathbf{x}_1, \mathbf{x}_2, \mathbf{x}_3)$ is a function of the relative quark coordinates, but also comprises *Dirac* structures which act on the quark spinors. It can be written down as [38] :

$$V^{(3)}_{\text{conf}} \;=\; a\,\mathcal{W}_{\text{off}} \;+\; b\,r_{3q}(\mathbf{x}_1, \mathbf{x}_2, \mathbf{x}_3)\,\mathcal{W}_{\text{str}}\;, \tag{A.2}$$

where a and b are the confinement parameters, r_{3q} is a measure for the interquark distance, and $\mathcal{W}_{\text{off}}$ and $\mathcal{W}_{\text{str}}$ are the Dirac structures operating on the constituent-quark spinors. The parameters a and b are the sole parameters associated with the confinement potential. These parameters and the $m_u \equiv m_d \equiv m_n$ nonstrange constituent-quark mass are determined by optimizing the model results for the Δ spectrum to the experimentally best-known resonance masses. The exact numbers for a, b and the nonstrange mass m_n are presented in Table A.1.

The interquark distance measure r_{3q} for three constituent quarks can be defined in different ways. We use the sum of the three distances between the quarks, which is commonly referred to as a Δ-configuration :

$$r_{3q}\,(\mathbf{x}_1, \mathbf{x}_2, \mathbf{x}_3) \;=\; \sum_{i<j} |\mathbf{x}_i - \mathbf{x}_j|\;. \tag{A.3}$$

This is not the only possibility to define the interquark distance. In literature, one finds alternative definitions, such as the Y- and H-configuration as depicted in

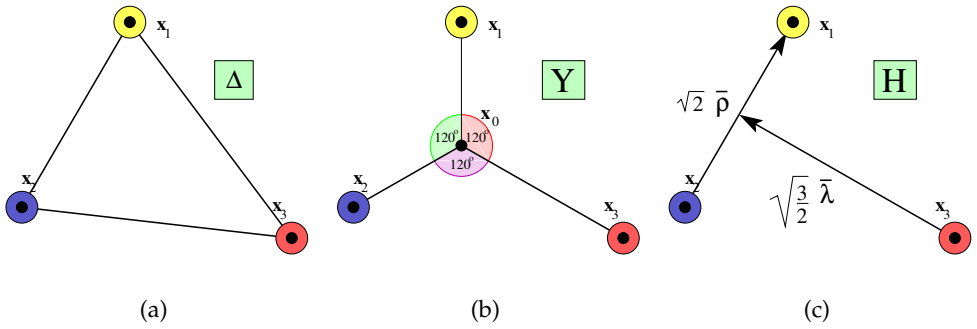

Figure A.1 *The Δ-, the Y- and the H-configuration for the interquark distance r_{3q} are shown in (a), (b) and (c) respectively. In (a) and (b), the length of the connecting lines is the interquark distance. In (c), r_{3q} is given by Eq. (A.5).*

Fig. A.1. The former uses the minimal length of string to connect three points :

$$r_{3q}\left(\mathbf{x}_1,\mathbf{x}_2,\mathbf{x}_3\right) \;=\; \min_{\mathbf{x}_0} \sum_{i<j} \left|\mathbf{x}_i-\mathbf{x}_0\right| , \tag{A.4}$$

and the latter takes the hyperradius as a measure of the interquark distance :

$$r_{3q}\left(\mathbf{x}_1,\mathbf{x}_2,\mathbf{x}_3\right) \;=\; \sqrt{|\rho|^2+|\lambda|^2} , \tag{A.5}$$

where $\rho = \frac{1}{\sqrt{2}}(\mathbf{x}_1-\mathbf{x}_2)$ and $\lambda = \frac{1}{\sqrt{6}}(\mathbf{x}_1+\mathbf{x}_2-2\mathbf{x}_3)$. However, it turns out that the slope parameter b of the confinement potential can always be scaled in a way that the results of the model are of the same quality for the three types of interquark-distance configuration. However, lattice results seem to favour a configuration in between the Δ- and the Y-configuration [151, 152]. The Δ-configuration is preferred, since it is numerically easier to handle in CQ-model calculations. The effect of the particular choice for the interquark distance on the electromagnetic form factors should be investigated further.

The Dirac structures $\mathcal{W}_{\text{off}}$ and $\mathcal{W}_{\text{str}}$ have a large impact on the computed baryon spectrum. The specific choice for these structures is constrained by the observation that there are hardly any spin-orbit interaction effects present in the baryon spectrum (note *e.g.* the small mass difference between the $S_{11}(1535)$ and $D_{13}(1520)$ nucleon resonances). Furthermore, $\mathcal{W}_{\text{off}}$ and $\mathcal{W}_{\text{str}}$ can differ. From several possibil-

ities, the best choice seems to be [37] :

$$\mathcal{W}_{\text{off}} = \frac{3}{4}\left[\,\mathbb{1}\otimes\mathbb{1}\otimes\mathbb{1} + \gamma^0\otimes\gamma^0\otimes\mathbb{1} + \text{cycl. perm.}\,\right], \tag{A.6a}$$

$$\mathcal{W}_{\text{str}} = \frac{1}{2}\left[\,-\mathbb{1}\otimes\mathbb{1}\otimes\mathbb{1} + \gamma^0\otimes\gamma^0\otimes\mathbb{1} + \text{cycl. perm.}\,\right]. \tag{A.6b}$$

With this specific choice for the Dirac structures, the $V^{(3)}_{\text{conf}}$ of Eq. (2.18) reduces to a spin-independent linear confinement potential in the nonrelativistic limit [37].

A.2 't Hooft Instanton Induced Interaction

In the Bonn model, the hyperfine splittings in the baryon spectrum are induced by a two-particle irreducible interaction based on the effects of instantons on the propagation of light quarks. Instantons are *classical*, non-perturbative solutions of the QCD Yang-Mills equations in Euclidean spacetime. They are localized in space and imaginary time and describe tunneling events. Instantons (anti-instantons) absorb right-handed (left-handed) light-flavoured quarks, and emit left-handed (right-handed) ones. As such they mediate a force between light quarks. Furthermore, instantons change the axial charge of the QCD vacuum in the presence of an external fermion source. Therefore, they provide an explanation for the non-conservation of axial charge. The crucial properties of instantons were discovered by 't Hooft [17]. Therefore, the resulting interaction between light quarks is sometimes referred to as the 't Hooft interaction.

The two-body part of the 't Hooft instanton-induced interaction, $V^{(2)}_{\text{III}}$, induces a flavour-, spin- and colour-dependent force between two light quarks. Moreover, it only acts upon pairs of constituent quarks which have an antisymmetric wave function in flavour-, spin- and colour-space *separately*. Its expression is given by :

$$V^{(2)}_{\text{III}}\left(x_1,x_2;x_1',x_2'\right) = V^{(2)}_{\text{'t Hooft}}\left(\mathbf{x}_1-\mathbf{x}_2\right)\delta^{(1)}(x_1^0-x_2^0)\delta^{(4)}(x_1-x_1')\delta^{(4)}(x_2-x_2'). \tag{2.19}$$

The 't Hooft two-body potential, $V^{(2)}_{\text{'t Hooft}}$, is a function of the distance between the two constituent quarks $(\mathbf{x}_1-\mathbf{x}_2)$, and comprises the appropriate Dirac structure and projectors on antisymmetric wave functions in dirac- ($\mathcal{D}$), flavour- ($\mathcal{F}$) and colourspace ($\mathcal{C}$) :

$$V^{(2)}_{\text{'t Hooft}}\left(\mathbf{x}_1-\mathbf{x}_2\right) = -4\,v_{reg}\left(\mathbf{x}_1-\mathbf{x}_2\right)\left(\mathbb{1}\otimes\mathbb{1}+\gamma^5\otimes\gamma^5\right) \times \mathcal{P}^{\mathcal{D}}_{S_{12}=0}\otimes\left(g_{nn}\mathcal{P}^{\mathcal{F}}_{\mathcal{A}}(nn)+g_{ns}\mathcal{P}^{\mathcal{F}}_{\mathcal{A}}(ns)\right)\otimes\mathcal{P}^{\mathcal{C}}_{\bar{3}}. \tag{2.20}$$

Here, $v_{reg}\left(\mathbf{x}_1 - \mathbf{x}_2\right)$ is a regulating function, describing the three-dimensional extension of the interaction :

$$v_{reg}\left(\mathbf{x}\right) \;=\; \frac{1}{\Lambda^3 \pi^{\frac{3}{2}}}\, e^{-\frac{|\mathbf{x}|^2}{\Lambda^2}} \;. \tag{A.7}$$

The range of the interaction, Λ, is a free parameter in the Bonn model. It is extracted to a fit of the model results to the best-know masses of the nucleon spectrum, and its value is given in Table A.1. The magnitude of Λ corresponds roughly to the average size of the instanton [38]. The two interaction strengths g_{nn} and g_{ns}, belonging to the antisymmetric nonstrange-nonstrange and the strange-nonstrange flavour projectors respectively, are also fitting parameters. The nonstrange-nonstrange coupling g_{nn} is fitted to the nucleon spectrum, and reproduces the hyperfine splitting between the nucleon and $\Delta(1232)$ resonance. In contrast to the nucleon, the $\Delta(1232)$ has a symmetric-spin wave function. Therefore, the $V_{\rm III}^{(2)}$ of Eq. (2.19) affects only the nucleon, lowering its mass compared to the Δ resonance. The strange-nonstrange coupling (g_{ns}) and the strange constituent-quark mass (m_s) parameters are determined in order to reproduce the masses of the experimentally best-known hyperons. As a matter of fact, the g_{ns} coupling is responsible for the $\Sigma^*_{(dec.)} - \Sigma_{(oct.)}$ and $\Xi^*_{(dec.)} - \Xi_{(oct.)}$ mass splittings. Values of g_{nn}, g_{ns} and m_s are listed in Table A.1.

Appendix B

Interaction Lagrangians and Amplitudes for the Isobar Model

The amplitude $\mathcal{M}_{\lambda_i}$ entering Eq. (3.47), and the amplitudes $\mathcal{M}_{\lambda}^{\lambda_i,\lambda_f}$ in Eq. (3.53) are constructed within the framework of relativistic field theory. We will adopt the approach of Ref. [6], and start from a set of effective interaction Lagrangians to derive the tree-level amplitudes for the different diagrams of Fig. 3.2. The difference with Ref. [6] is that the electromagnetic interaction vertices of spin $J = 1/2$ baryon resonances is extended with a longitudinal coupling.

In the following sections, both the Lagrangians and the amplitudes for the different diagrams of Fig. 3.2 will be briefly presented. The different channels are denoted with a letter. These letters stand for an exchanged particle with specific identity, spin and parity.

B.1 Born Terms

The Born terms are depicted in the upper row of Fig. 3.2. In the s- and t-channel, the exchanged particle is a proton and kaon respectively. In the u-channel, the intermediate particle can be a Λ and a Σ hyperon. When the final hyperon is a Λ, the diagram with an intermediate Σ^0 is called the extended Born term, and vice versa. We will denote the extended Born term as the a-channel.

The Born terms have a common hadronic vertex. For this vertex, one can choose between a psuedoscalar and pseodovector coupling, or a combination of the two.

The work presented in Refs. [2–6] uses a purely pseudoscalar coupling, since the pseudovector option leads to Born strengths which are unrealistally large. Thus, the Lagrangian describing the hadronic vertex for the Born terms is given by :

$$\mathcal{L}_{KYp} \;=\; -i\, g_{KYp}\, K^{\dagger}\, \overline{Y}\, \gamma_5\, N + h.c.\;. \tag{B.1}$$

The Lagrangian describing the hadronic vertex for the extended Born term (a-channel) is of the same form, but Y is exchanged for Y'.

B.1.1 s-channel

The electromagnetic interaction Lagrangian for the proton in $p(\gamma^*, K)Y$ processes is given by :

$$\mathcal{L}_{\gamma pp} \;=\; -e\, \overline{N}\, \Gamma_\mu\, N\, A^\mu\;. \tag{B.2}$$

Using the hadronic vertex Lagrangian of Eq. (B.1), the amplitude for the Born s-channel reads :

$$\mathcal{M}_s \;=\; e\, g_{KYp} \overline{u}_Y \gamma_5 \frac{\not{p} + \not{q} + M_p}{s - M_p^2} \Gamma^\mu_{pp} u_p \epsilon_\mu\;, \tag{B.3}$$

where the EM vertex for the proton Γ^μ_{pp} is :

$$\Gamma^\mu_{pp} \;=\; \gamma^\mu\, F_1^p(Q^2) \;+\; \frac{i\sigma^{\mu\nu} q_\nu}{2M_p}\, F_2^p(Q^2)\;. \tag{B.4}$$

The complex conjugated amplitude becomes :

$$\mathcal{M}_s^* \;=\; -e\, g_{KYp}\, \overline{u}_p\, \gamma^0\, \Gamma^{\mu\,\dagger}_{pp}\, \gamma^0\, \frac{\not{p} + \not{q} + M_p}{s - M_p^2} \gamma_5 u_Y \epsilon_\mu\;, \tag{B.5}$$

where the EM structure $\gamma^0 \Gamma^{\mu\,\dagger}_{pp} \gamma^0$ is easily obtained :

$$\gamma^0\, \Gamma^{\mu\,\dagger}_{pp}\, \gamma^0 \;=\; \gamma^\mu\, F_1^p(Q^2) \;-\; \frac{i\sigma^{\mu\nu} q_\nu}{2M_p}\, F_2^p(Q^2)\;. \tag{B.6}$$

B.1.2 t-channel

The EM Lagrangian for the kaon-exchange contribution is :

$$\mathcal{L}_{\gamma KK} \;=\; -i\, e\, \left(K^\dagger \partial_\mu K \;-\; K \partial_\mu K^\dagger\right)\, A^\mu\;. \tag{B.7}$$

This results in the amplitude :

$$\mathcal{M}_t \;=\; e\, g_{KYp} \overline{u}_Y\, \Gamma^{\mu}_K\, \frac{1}{t - M_K^2}\, \gamma_5\, u_p\, \epsilon_\mu \;. \tag{B.8}$$

The EM vertex for the kaon is :

$$\Gamma^{\mu}_K \;=\; \left(2p^{\mu}_K - q_\mu\right)\; F^K(Q^2)\;, \tag{B.9}$$

where $F^K(Q^2)$ is the EM form factor of the kaon.

The complex conjugated amplitude becomes

$$\mathcal{M}^*_t \;=\; -e\, g_{KYp} \overline{u}_p \gamma_5\, \Gamma^{\mu}_K\, \frac{1}{t - M_K^2} u_Y \epsilon_\mu \;. \tag{B.10}$$

B.1.3 u-channel

For the u-channel Born term, the EM vertex Lagrangian reads

$$\mathcal{L}_{\gamma YY} \;=\; -e\, \overline{Y} \Gamma_\mu\, Y\, A^\mu \;. \tag{B.11}$$

This results in the amplitude for the Born term with an exchanged hyperon :

$$\mathcal{M}_u \;=\; e\, g_{KYp}\, \overline{u}_Y\, \Gamma^{\mu}_{YY}\, \frac{\not{p}_Y - \not{q} + M_Y}{u - M_Y^2}\, \gamma_5\, u_p\, \epsilon_\mu \;, \tag{B.12}$$

where the EM vertex Γ^{μ}_{YY} has the same form as the one from Eq. (B.4), but with the form factors of the hyperon instead of the proton :

$$\Gamma^{\mu}_{YY} \;=\; \gamma^\mu\, F_1^Y(Q^2) \;+\; \frac{i\sigma^{\mu\nu} q_\nu}{2M_p}\, F_2^Y(Q^2) \;. \tag{B.13}$$

The complex conjugated amplitude is then

$$\mathcal{M}^*_u \;=\; -e\, g_{KYp}\, \overline{u}_p\, \gamma_5\, \frac{\not{p}_Y - \not{q} + M_Y}{u - M_Y^2}\, \gamma^0\, {\Gamma^{\mu}_{YY}}^\dagger\, \gamma^0\, u_Y\, \epsilon_\mu \;, \tag{B.14}$$

with the EM structure given by :

$$\gamma^0\, {\Gamma^{\mu}_{YY}}^\dagger\, \gamma^0 \;=\; \gamma^\mu\, F_1^Y(Q^2) \;-\; \frac{i\sigma^{\mu\nu} q_\nu}{2M_p}\, F_2^Y(Q^2) \;. \tag{B.15}$$

B.1.4 a-channel

The EM Lagrangian and amplitude for the extended Born term are very similar to those for the Born u-channel term. The EM interaction vertex is :

$$\mathcal{L}_{\gamma YY'} \;=\; -e\,\overline{Y'}\Gamma_\mu\,Y\,A^\mu \;+\; h.c.\,. \tag{B.16}$$

The amplitude is obtained from Eq. (B.12) by changing Y for Y' in the coupling constants and form factors.

$$\mathcal{M}_a \;=\; e\,g_{KY'p}\,\overline{u}_Y\,\Gamma^\mu_{YY'}\,\frac{\not{p}_Y - \not{q} + M_{Y'}}{u - M^2_{Y'}}\,\gamma_5\,u_p\,\epsilon_\mu\;, \tag{B.17}$$

where this time, the EM vertex is given by :

$$\Gamma^\mu_{YY'} \;=\; \left(\gamma^\mu \;-\; \frac{m_Y - m_{Y'}}{q^2}\,q^\mu\right) F_1^{YY'}(Q^2) \;+\; \frac{i\sigma^{\mu\nu}q_\nu}{2M_p}\,\kappa_{YY'}\,F_2^Y(Q^2)\,. \tag{B.18}$$

The complex conjugated amplitude for the extended Born term is :

$$\mathcal{M}^*_a \;=\; -e\,g_{KY'p}\,\overline{u}_p\,\gamma_5\,\frac{\not{p}_Y - \not{q} + M_{Y'}}{u - M^2_{Y'}}\,\gamma^0\,{\Gamma^\mu_{YY'}}^\dagger\,\gamma^0\,u_Y\,\epsilon_\mu\;, \tag{B.19}$$

with the EM structure

$$\gamma^0\,{\Gamma^\mu_{YY'}}^\dagger\,\gamma^0 \;=\; \left(\gamma^\mu \;-\; \frac{m_Y - m_{Y'}}{q^2}\,q^\mu\right) F_1^{YY'}(Q^2) \;-\; \frac{i\sigma^{\mu\nu}q_\nu}{2M_p}\,\kappa_{YY'}\,F_2^{YY'}(Q^2)\,. \tag{B.20}$$

B.2 Nonstrange Resonances

In the isobar model presented in Chap. 3, $J = 1/2$ and $J = 3/2$ nucleon and Δ resonances are taken into account. For the spin $J = 1/2$ resonances, new Lagrangians which involve coupling to the longitudinal channels in kaon electroproduction are presented. For the terms corresponding to the exchange of spin $J = 3/2$ resonances, we refer the reader to Ref. [6] for the Lagrangians and amplitudes.

B.2.1 d-channel

The EM vertex Lagrangian for the coupling of a positive-parity spin $J = 1/2$ nonstrange resonance (d-channel) to the proton ground state is :

$$\mathcal{L}_{\gamma pp'} \;=\; -e\,\overline{N'}\,\Gamma_\mu\,N\,A^\mu \;+\; h.c.\,. \tag{B.21}$$

For the Lagrangian describing the hadronic vertex $p' \to K + Y$, the pseudoscalar option is used :

$$\mathcal{L}_{KYp'} \;=\; -i\, g_{KYp'}\, \left(K^{\dagger}\, \overline{Y}\, \gamma_5\, N' \;+\; \overline{N}'\, \gamma_5\, Y\, K \right) . \tag{B.22}$$

The d-channel amplitude is thus :

$$\mathcal{M}_d \;=\; e\, g_{KYp'}\, \overline{u}_Y\, \gamma_5\, \frac{\not{p} + \not{q} + m_{p'}}{s - m_{p'}^2 + i m_{p'} \Gamma_{p'}^{tot}}\, \Gamma^{\mu}_{pp'}\, u_p\, \epsilon_{\mu} \, . \tag{B.23}$$

Here, $\Gamma_{p'}^{tot}$ is the total decay width of the resonance, and $\Gamma^{\mu}_{pp'}$ is the EM vertex, given by :

$$\Gamma^{\mu}_{pp'} \;=\; \left(\gamma^{\mu} \;-\; \frac{m_{p'} - M_p}{q^2}\, q^{\mu} \right)\, F_1^{pp'}(Q^2) \;+\; \frac{i \sigma^{\mu\nu} q_{\nu}}{2 M_p}\, \kappa_{pp'}\, F_2^{pp'}(Q^2) \, , \tag{B.24}$$

where $m_{p'}$ and $\kappa_{pp'}$ are the resonance mass and anomalous magnetic transition moment. $F_1^{pp'}(Q^2)$ and $F_2^{pp'}(Q^2)$ are the on-shell electromagnetic transition form factors.

The complex conjugated amplitude is then

$$\mathcal{M}_d^{*} \;=\; -e\, g_{KYp'}\, \overline{u}_p\, \gamma^0\, \Gamma^{\mu\ \dagger}_{pp'}\, \gamma^0\, \frac{\not{p} + \not{q} + m_{p'}}{s - m_{p'}^2 - i m_{p'} \Gamma_{p'}^{tot}}\, \gamma_5\, u_Y\, \epsilon_m u \, . \tag{B.25}$$

The EM vertex structure is

$$\gamma^0\, \Gamma^{\mu\ \dagger}_{pp'}\, \gamma^0 \;=\; \left(\gamma^{\mu} \;-\; \frac{m_{p'} - M_p}{q^2}\, q^{\mu} \right)\, F_1^{pp'}(Q^2) \;-\; \frac{i \sigma^{\mu\nu} q_{\nu}}{2 M_p}\, \kappa_{pp'}\, F_2^{pp'}(Q^2) \, . \tag{B.26}$$

B.2.2 e-channel

For the contributions of negative-parity spin $J = 1/2$ nonstrange resonances, the Lagrangians and amplitudes are slightly different from the ones in Sect. B.2.1. The EM interaction Lagrangian still reads

$$\mathcal{L}_{\gamma pp'} \;=\; -e\, \overline{N}'\, \Gamma_{\mu}\, N\, A^{\mu} \;+\; h.c. \, , \tag{B.27}$$

but the Lagrangian for the hadronic vertex $p' \to K + Y$ changes into :

$$\mathcal{L}_{KYp'} \;=\; -i\, g_{KYp'}\, \left(K^{\dagger}\, \overline{Y}\, N' \;-\; \overline{N}'\, Y\, K \right) . \tag{B.28}$$

The resulting amplitude is

$$\mathcal{M}_e \;=\; e\, g_{KYp'}\, \overline{u}_Y\, \frac{\not{p} + \not{q} + m_{p'}}{s - m_{p'}^2 + i m_{p'} \Gamma_{p'}^{tot}}\, \Gamma^{\mu}_{pp'}\, u_p\, \epsilon_{\mu}\ . \tag{B.29}$$

Here, $\Gamma_{p'}^{tot}$ is again the total decay width of the resonance. $\Gamma^{\mu}_{pp'}$ is the EM vertex for a negative-parity spin $J = 1/2$ resonance :

$$\Gamma^{\mu}_{pp'} \;=\; \left[\left(\gamma^{\mu} \;-\; \frac{m_{p'} + M_p}{q^2}\, q^{\mu} \right) F_1^{pp'}(Q^2) \;+\; \frac{i \sigma^{\mu\nu} q_{\nu}}{2 M_p}\, \kappa_{pp'}\, F_2^{pp'}(Q^2) \right] \gamma_5\ . \tag{B.30}$$

The complex conjugated amplitude is

$$\mathcal{M}_e^{*} \;=\; e\, g_{KYp'}\, \overline{u}_p\, \gamma^0\, \Gamma^{\mu}_{pp'}{}^{\dagger}\, \gamma^0\, \frac{\not{p} + \not{q} + m_{p'}}{s - m_{p'}^2 - i m_{p'} \Gamma_{p'}^{tot}}\, u_Y\, \epsilon_m u\ , \tag{B.31}$$

where the EM vertex structure is

$$\gamma^0\, \Gamma^{\mu}_{pp'}{}^{\dagger}\, \gamma^0 \;=\; -\,\gamma_5 \left[\left(\gamma^{\mu} \;-\; \frac{m_{p'} + M_p}{q^2}\, q^{\mu} \right) F_1^{pp'}(Q^2) \;-\; \frac{i \sigma^{\mu\nu} q_{\nu}}{2 M_p}\, \kappa_{pp'}\, F_2^{pp'}(Q^2) \right]\ . \tag{B.32}$$

B.3 Hyperon Resonances

We present the Lagrangians for the diagrams of Fig. 3.2 where an intermediate hyperon resonance with spin $J = 1/2$ is involved. Remark that for $p(\gamma^*, K)Y$ processes, the propagators of the hyperon resonances should not involve a decay width as was the case for the nonstrange resonances. This is because in the isobar picture of strong interactions, only on-shell hadrons can decay. The restrictions on the kinematical region for the $p(\gamma^*, K)Y$ reaction prohibit hyperon and kaon resonances to be on their mass shell. In the case of radiative kaon capture processes, the s- and u-channel diagrams are interchanged. One should then include the hyperon-resonance decay widths, but leave out the nonstrange-resonance decay widths.

B.3.1 f-channel

The Lagrangians and amplitude for an intermediate hyperon resonance with $J^{\pi} = 1/2^{+}$ are the same as for the extended Born term, if the total decay widths can be left out as mentioned in the previous paragraph. In the following, the Lagrangians and amplitudes are presented explicitly for the sake of clarity.

The EM interaction Lagrangian is :

$$\mathcal{L}_{\gamma YY'} \;=\; -e\,\overline{Y'}\Gamma_\mu\,Y\,A^\mu \;+\; h.c.\,, \tag{B.33}$$

and the hadronic vertex is described by the Lagrangian :

$$\mathcal{L}_{KY'p} \;= -i\,g_{KY'p}\,\left(K^\dagger\,\overline{Y'}\,\gamma_5\,N \;+\; \bar{N}\,\gamma_5\,Y'\,K\right)\,. \tag{B.34}$$

The amplitude is easily obtained :

$$\mathcal{M}_f \;=\; e\,g_{KY'p}\,\bar{u}_Y\,\Gamma^\mu_{YY'}\,\frac{\not{p}_Y - \not{q} + M_{Y'}}{u - M^2_{Y'}}\,\gamma_5\,u_p\,\epsilon_\mu\,, \tag{B.35}$$

with the EM vertex given by :

$$\Gamma^\mu_{YY'} \;=\; \left(\gamma^\mu \;-\; \frac{m_Y - m_{Y'}}{q^2}\,q^\mu\right)\,F_1^{YY'}(Q^2) \;+\; \frac{i\sigma^{\mu\nu}q_\nu}{2M_p}\,\kappa_{YY'}\,F_2^Y(Q^2)\,. \tag{B.36}$$

The complex conjugated amplitude becomes :

$$\mathcal{M}^*_f \;=\; -e\,g_{KY'p}\,\bar{u}_p\,\gamma_5\,\frac{\not{p}_Y - \not{q} + M_{Y'}}{u - M^2_{Y'}}\,\gamma^0\,{\Gamma^\mu_{YY'}}^\dagger\,\gamma^0\,u_Y\,\epsilon_\mu\,, \tag{B.37}$$

with the EM structure

$$\gamma^0\,{\Gamma^\mu_{YY'}}^\dagger\,\gamma^0 \;=\; \left(\gamma^\mu \;-\; \frac{m_Y - m_{Y'}}{q^2}\,q^\mu\right)\,F_1^{YY'}(Q^2) \;-\; \frac{i\sigma^{\mu\nu}q_\nu}{2M_p}\,\kappa_{YY'}\,F_2^{YY'}(Q^2)\,. \tag{B.38}$$

B.3.2 g-channel

The exchange of a $J^\pi = 1/2^-$ hyperon resonance can be described with the same EM interaction Lagrangian as for positive-parity resonances

$$\mathcal{L}_{\gamma YY'} \;=\; -e\,\overline{Y'}\Gamma_\mu\,Y\,A^\mu \;+\; h.c.\,, \tag{B.39}$$

and with the following hadronic vertex Lagrangian :

$$\mathcal{L}_{KY'p} \;= -i\,g_{KY'p}\,\left(K^\dagger\,\overline{Y'}\,N \;-\; \bar{N}\,Y'\,K\right)\,. \tag{B.40}$$

The amplitude for this diagram is :

$$\mathcal{M}_g \;=\; e\,g_{KY'p}\,\bar{u}_Y\,\Gamma^\mu_{YY'}\,\frac{\not{p}_Y - \not{q} + M_{Y'}}{u - M^2_{Y'}}\,u_p\,\epsilon_\mu\,, \tag{B.41}$$

with the EM vertex given by :

$$\Gamma^{\mu}_{YY'} \;=\; \left[\left(\gamma^{\mu} \;-\; \frac{m_{Y'} + m_Y}{q^2}\, q^{\mu} \right) F_1^{YY'}(Q^2) \right. \\ \left. +\; \frac{i\sigma^{\mu\nu} q_{\nu}}{2M_p}\, \kappa_{YY'}\, F_2^{Y}(Q^2) \right] \gamma_5 \;. \quad \text{(B.42)}$$

The complex conjugated amplitude is then :

$$\mathcal{M}_g^{*} \;=\; e\, g_{KY'p}\, \overline{u}_p\, \frac{\not{p}_Y - \not{q} + M_{Y'}}{u - M_{Y'}^2}\, \gamma^0\, {\Gamma^{\mu}_{YY'}}^{\dagger}\, \gamma^0\, u_Y\, \epsilon_{\mu} \;, \quad \text{(B.43)}$$

where the EM structure is given by :

$$\gamma^0\, {\Gamma^{\mu}_{YY'}}^{\dagger}\, \gamma^0 \;=\; -\,\gamma_5 \left[\left(\gamma^{\mu} \;-\; \frac{m_{Y'} + m_Y}{q^2}\, q^{\mu} \right) F_1^{YY'}(Q^2) \right. \\ \left. -\; \frac{i\sigma^{\mu\nu} q_{\nu}}{2M_p}\, \kappa_{YY'}\, F_2^{YY'}(Q^2) \right] . \quad \text{(B.44)}$$

Bibliography

[1] S. Eidelman *et al.* Review of Particle Physics. *Physics Letters B*, 592:1+, 2004. URL http://pdg.lbl.gov.

[2] S. Janssen, J. Ryckebusch, W. Van Nespen, D. Debruyne, and T. Van Cauteren. The role of hyperon resonances in $p(\gamma, K^+)\Lambda$ processes. *European Physical Journal*, A11:105, 2001.

[3] S. Janssen, J. Ryckebusch, D. Debruyne, and T. Van Cauteren. Kaon photoproduction: background contributions, form factors and missing resonances. *Physical Review*, C65:015201, 2002.

[4] S. Janssen, J. Ryckebusch, D. Debruyne, and T. Van Cauteren. Σ photoproduction in the resonance region. *Physical Review*, C66:035202, 2002.

[5] S. Janssen, J. Ryckebusch, and T. Van Cauteren. Constraints on background contributions from $K^+\Lambda$ electroproduction. *Physical Review*, C67:R052201, 2003.

[6] S. Janssen. *Strangeness Production on the Nucleon*. PhD thesis, Ghent University, 2002.

[7] M. Q. Tran *et al.* Measurement of $\gamma p \to K^+\Lambda$ and $\gamma p \to K^+\Sigma^0$ at photon energies up to 2 GeV. *Physics Letters*, B445(1-2):20, 1998.

[8] S. Goers *et al.* Measurement of $\gamma p \to K^0\Sigma^+$ at photon energies up to 1.55GeV. *Physics Letters*, B464(3-4):331, 1999.

[9] T. Mart and C. Bennhold. Evidence for a missing nucleon resonance in kaon photoproduction. *Physical Review*, C61:012201(R), 1999.

[10] D. G. Ireland, S. Janssen, and J. Ryckebusch. A genetic algorithm analysis of N^* resonances in $p(\gamma, K^+)\Lambda$ reactions. *Nuclear Physics*, A740:147, 2004.

[11] J. W. C. McNabb *et al.* Hyperon photoproduction in the nucleon resonance region. *Physical Review*, C69:042201(R), 2004.

[12] D. S. C. et al. First measurement of transferred polarization in the exclusive $\vec{e}p \longrightarrow e' K^+ \vec{\Lambda}$ reaction. *Physical Review Letters*, 90(13):131804, 2003.

[13] R. M. Mohring *et al.* Separation of the longitudinal and transverse cross sections in the ${}^1H(e, eK+)\Lambda$ and ${}^1H(e, eK+)\Sigma^0$ reactions. *Physical Review*, C67: 055205, 2003.

[14] K.-H. Glander *et al.* Measurement of $\gamma p \rightarrow K^+\Lambda$ and $\gamma p \rightarrow K^+\Sigma^0$ at photon energies up to 2.6 GeV. *European Physical Journal*, A19:251, 2004.

[15] R. Lawall *et al.* Measurement of the reaction $\gamma p \rightarrow K^0\Sigma^+$ at photon energies up to 2.6 GeV. *European Physical Journal*, A:DOI 10.1140/epja/i2005–10002–x, 2005.

[16] R. G. T. Zegers *et al.* Beam polarization asymmetries for the $p(\gamma, K^+)\Lambda$ and $p(\gamma, K^+)\Sigma^0$ reactions at $E_\gamma = 1.5 - 2.4$ GeV. *Physical Review Letters*, 91(9): 092001, 2003.

[17] G. 't Hooft. Computation of the quantum effects due to a four-dimensional pseudoparticle. *Physical Review*, D14:3432–3450, 1976.

[18] M. Gell-Mann. Symmetries of baryons and mesons. *Physical Review*, 125:1067, 1962.

[19] M. Gell-Mann. A schematic model of baryons and mesons. *Physics Letters*, 8: 214, 1964.

[20] Y. Ne'eman. Derivation of strong interactions from a gauge invariance. *Nuclear Physics*, 26:222, 1961.

[21] G. Zweig. *CERN Reports*, 8182/TH:401, 1964.

[22] G. Zweig. *CERN Reports*, 8419/TH:412, 1964.

[23] S. Aoki *et al.* Quenched light hadron spectrum. *Physical Review Letters*, 84(2): 238, 2000.

[24] S. Sasaki, T. Blum, and S. Ohta. Lattice study of the nucleon excited states with domain wall fermions. *Physical Review*, D65:074503, 2002.

[25] F. Lee, D. Leinweber, L. Zhou, J. Zanotti, and S. Choe. N^* masses from an anisotropic lattice QCD action. *Nuclear Physics B (Proc. Suppl.)*, 106:248, 2002.

[26] F. X. Lee. Baryon resonances from lattice QCD. Talk at the Workshop: The Physics of Excited Nucleons, NSTAR 2004.

[27] L. Y. Glozman, W. Plessas, K. Varga, and R. F. Wagenbrunn. Unified description of light- and strange-baryon spectra. *Physical Review*, D58:094030, 1998.

[28] T. Nakano *et al.* Evidence for a narrow $S = +1$ baryon resonance in photoproduction from the neutron. *Physical Review Letters*, 91:012002, 2003.

[29] V. V. Barmin *et al.* Observation of a baryon resonance with positive strangeness in K^+ collisions with Xe nuclei. *Physics of Atomic Nuclei*, 66:1715, 2003.

[30] S. Stepanyan *et al.* Observation of an exotic $S = +1$ baryon in exclusive photoproduction from the deuteron. *Physical Review Letters*, 91:252001, 2003.

[31] J. Barth *et al.* Evidence for the positive-strangeness pentaquark Θ^+ in photoproduction with the SAPHIR detector at ELSA. *Physics Letters*, B572:127, 2003.

[32] A. L. Yaouanc, L. Oliver, O. Pène, and J.-C. Raynal. *Hadron Transitions in the Quark Model*. Gordon and Breach Science Publishers, 1988.

[33] M. Koll, R. Ricken, D. Merten, B. C. Metsch, and H.-R. Petry. A relativistic quark model for mesons with an instanton-induced interaction. *European Physical Journal*, A9:73, 2000.

[34] U. Löring, K. Kretzschmar, B. Metsch, and H.-R. Petry. Relativistic quark models of baryons with instantaneous forces. *European Physical Journal*, A10: 309, 2001.

[35] D. Merten, U. Löring, K. Kretzschmar, B. Metsch, and H.-R. Petry. Electroweak form factors of non-strange baryons. *European Physical Journal*, A14: 477, 2002.

[36] E. E. Salpeter and H. A. Bethe. A relativistic equation for bound-state problems. *Physical Review*, 84:1232, 1951.

[37] U. Löring. *A Covariant Quark Model of Baryons with Instanton-induced Forces*. PhD thesis, Rheinische Friedrich-Wilhelms-Universität Bonn, Germany, 2001.

[38] U. Löring, B. Metsch, and H.-R. Petry. The light baryon spectrum in a relativistic quark model with instanton-induced quark forces. the non-strange baryon spectrum and ground-states. *European Physical Journal*, A10:395, 2001.

[39] D. Merten. *Hadron Form Factors and Decays*. PhD thesis, Rheinische Friedrich-Wilhelms-Universität Bonn, Germany, 2002.

[40] J. J. Kelly. Nucleon charge and magnetization densities from sachs form factors. *Physical Review*, C66:065203, 2002.

[41] P. Mergell, U.-G. Meißner, and D. Drechsel. Dispersion-theoretical analysis of the nucleon electromagnetic form factors. *Nuclear Physics*, A596:367, 1996.

[42] M. Adamovich *et al.* First observation of $\Sigma^- - e^-$ elastic scattering in the hyperon beam experiment WA89 at CERN. *European Physical Journal*, C8:59, 1999.

[43] I. Eschrich *et al.* Measurement of the Σ^- charge radius by Σ^--electron elastic scattering. *Physics Letters*, B522(3-4):233, 2001.

[44] S. Capstick. Photo- and electroproduction of nonstrange baryon resonances in the relativized quark model. *Physical Review*, D47(7):2864, 1992.

[45] F. E. Close and Z. Li. Photo- and electroproduction of N^* in a quark model. *Physical Review*, D42(7):2194, 1990.

[46] J. D. Bjorken and J. D. Walecka. Electroproduction of nucleon resonances. *Annals of Physics*, 38:35, 1966.

[47] S. U. Chung. General formulation of covariant helicity-coupling amplitudes. *Physical Review*, D57(1):431, 1998.

[48] C. Becchi and G. Morpurgo. Connection between BBP and VPP vertices in the quark model. *Physical Review*, 149(4):1284, 1966.

[49] D. Faiman and A. W. Hendry. Harmonic-oscillator model for baryons. *Physical Review*, 173(5):1720, 1968.

[50] L. Micu. Decay rates of meson resonances in a quark model. *Nuclear Physics*, B10:521, 1969.

[51] J. Kogut and L. Susskind. Hamiltonian formulation of Wilson's lattice gauge theories. *Physical Review*, D11(2):395, 1975.

[52] R. Kokoski and N. Isgur. Meson decays by flux-tube breaking. *Physical Review*, D35(3):907, 1987.

[53] P. Stassart and F. Stancu. $N + \rho$ decay of baryons in a flux-tube-breaking mechanism. *Physical Review*, D42(5):1521, 1990.

[54] S. Capstick and W. Roberts. Quark models of baryon masses and decays. *Progress in Particle and Nuclear Physics*, 45(Suppl. 2):S241, 2000.

[55] A. Y. Korchin and O. Scholten. Comparing phenomenological recipes with a microscopic model for the electric amplitude in strangeness photoproduction. *Physical Review*, C68:045206, 2003.

[56] S. S. Hsiao, D. H. Lu, and S. N. Yang. Pseudovector versus pseudoscalar coupling in kaon photoproduction reexamined. *Physical Review*, C61:068201, 2000.

[57] H. Haberzettl. Gauge-invariant theory of pion photoproduction with dressed hadrons. *Physical Review*, C56(4):2041, 1997.

[58] W.-T. Chiang, F. Tabakin, T.-S. H. Lee, and B. Saghai. Coupled-channel study of $\gamma p \to K^+\Lambda$. *Physics Letters*, B517:101, 2001.

[59] S. Janssen, D. G. Ireland, and J. Ryckebusch. Extraction of N^* information from the limited $p(\gamma, K^+)\Lambda$ data set. *Physics Letters*, B562:51, 2003.

[60] S. Krewald, S. Schneider, and J. Speth. Two pion production in the Jülich model. In D. Drechsel and L. Tiator, editors, *NSTAR 2001, Proceedings of the Workshop on The Physics of Excited Nucleons*, page 93. World Scientific, 2001.

[61] L. Andivahis *et al.* Measurements of the electric and magnetic form factors of the proton from $Q^2 = 1.75$ to 8.83 (GeV/c)^2. *Physical Review*, D50(9):5491, 1994.

[62] M. K. Jones *et al.* G_{E_p}/G_{M_p} ratio by polarization transfer in $\vec{e}p \rightarrow e\vec{p}$. *Physical Review Letters*, 84(7):1398, 2000.

[63] O. Gayou *et al.* Measurement of G_{E_p}/G_{M_p} in $\vec{e}p \rightarrow e\vec{p}$ to $Q^2 = 5.6$ GeV^2. *Physical Review Letters*, 88:092301, 2002.

[64] P. A. M. Guichon and M. Vanderhaeghen. How to reconcile the Rosenbluth and the polarization transfer methods in the measurement of the proton form factors. *Physical Review Letters*, 91(14):142303, 2003.

[65] R. M. Davidson and R. Workman. Form factors and photoproduction amplitudes. *Physical Review*, C63:025210, 2001.

[66] M. E. Peskin and D. V. Schroeder. *An Introduction to Quantum Field Theory*. Perseus Books Publishing, 1995.

[67] G. Penner and U. Mosel. $\pi N \rightarrow \omega N$ in a coupled-channel approach. *Physical Review*, C65:055202, 2002.

[68] *Sections for Reactions of High Energy Particles*, volume 12A of *Landolt-Börnstein: Numerical Data and Functional Relationships in Science and Technology - New Series Group I Elementary Particles, Nuclei and Atoms*. Springer-Verlag Heidelberg, 1988.

[69] J. J. de Swart. The octet model and its Clebsch-Gordan coefficients. *Review of Modern Physics*, 35(4):916, 1963.

[70] J. F. Donoghue and B. R. Holstein. Evidence for $SU(3)$ breaking in Cabibbo-type fits of semileptonic hyperon decay. *Physical Review*, D25(7):2015, 1982.

[71] A. M. Bincer. Electromagnetic structure of the nucleon. *Physical Review*, 118 (3):855, 1960.

[72] G. Knöchlein, D. Drechsel, and L. Tiator. Photo- and electroproduction of eta mesons. *Zeitschrift für Physik*, A352:327, 1995.

[73] A. D'Angelo *et al.* Meson photoproduction at GRAAL. In D. Drechsel and L. Tiator, editors, *NSTAR 2001, Proceedings of the Workshop on The Physics of Excited Nucleons*, page 347. World Scientific, March 2001.

[74] H. Aihara *et al.* Investigation of the electromagnetic structure of *eta* and *eta'* mesons by two-photon interactions. *Physical Review Letters*, 64(2):172, 1990.

[75] H. J. Behrend *et al.* A measurement of the π^0, η and η' electromagnetic form factors. *Zeitschrift für Physik*, C49:401, 1991.

[76] M. Acciarri *et al.* Measurement of $\eta'(958)$ formation in two-photon collisions at LEP1. *Physics Letters*, B418:399, 1998.

[77] J. Gronberg *et al.* Measurements of the meson photon transition form factors of light pseudoscalar mesons at large momentum transfer. *Physical Review*, D57:33, 1998.

[78] C. N. Brown *et al.* Coincidence electroproduction of charged pions and the pion form-factor. *Physical Review*, D8:92, 1973.

[79] C. J. Bebek *et al.* Measurement of the pion form-factor up to $Q^2 = 4\text{GeV}^2$. *Physical Review*, D13:25, 1976.

[80] C. J. Bebek *et al.* Charged pion electroproduction from protons up to $Q^2 = 9.5\text{GeV}^2$. *Physical Review Letters*, 37:1525, 1976.

[81] C. J. Bebek *et al.* Electroproduction of single pions at low ϵ and a measurement of the pion form-factor up to $Q^2 = 10\text{GeV}^2$. *Physical Review*, D17:1693, 1978.

[82] S. R. Amendolia *et al.* A measurement of the space-like pion electromagnetic form-factor. *Nuclear Physics*, B277:168, 1986.

[83] E. B. Dally *et al.* Direct measurement of the negative kaon form-factor. *Physical Review Letters*, 45:232, 1980.

[84] S. R. Amendolia *et al.* A measurement of the kaon charge radius. *Physics Letters*, B178:435, 1986.

[85] R. I. Dzhelyadin *et al.* Study of the electromagnetic transition form-factor in $\omega \to \pi^0 \mu^+ \mu^-$ decay. *Physics Letters*, B102:296, 1981.

[86] C. Herberg *et al.* Determination of the neutron electric form factor in the $D(e, e'n)p$ reaction and the influence of nuclear binding. *European Physical Journal*, A5:131, 1999.

[87] M. Ostrick *et al.* Measurement of the neutron electric form factor $G_{(E,n)}$ in the quasifree $^2H(\vec{e}, e'\vec{n})p$ reaction. *Physical Review Letters*, 83:276, 1999.

[88] I. Passchier *et al.* The charge form factor of the neutron from the reaction $^2\vec{H}(\vec{e}, e'n)p$. *Physical Review Letters*, 82:4988, 1999.

[89] T. Eden *et al.* Electric form factor of the neutron from the $^2H(\vec{e}, e'\vec{n})^1H$ reaction at $Q^2 = 0.255$(GeV/c)^2. *Physical Review*, C50:R1749, 1994.

[90] R. Schiavilla and I. Sick. Neutron charge form factor at large q^2. *Physical Review*, C64:041002, 2001.

[91] H. Anklin *et al.* Precise measurements of the neutron magnetic form factor. *Physics Letters*, B428:248, 1998.

[92] G. Kubon *et al.* Precise neutron magnetic form factors. *Physics Letters*, B524: 26, 2002.

[93] A. D. Guerra *et al.* Measurements of threshold π^+ electroproduction at low momentum transfer. *Nuclear Physics*, B99:253, 1975.

[94] A. D. Guerra *et al.* Threshold π^+ electroproduction at high momentum transfer: a determination of the nucleon axial vector form factor. *Nuclear Physics*, B107:65, 1976.

[95] P. Brauel *et al.* π^+ electroproduction on hydrogen near threshold at four-momentum transfers of 0.2, 0.4 and 0.6GeV^2. *Physics Letters*, B45:389, 1973.

[96] E. Amaldi *et al.* On pion electroproduction at 5fm^2 near threshold. *Nuovo Cimento*, A65:377, 1970.

[97] E. Amaldi *et al.* Axial-vector form factor of the nucleon from a coincidence experiment on electroproduction at threshold. *Physics Letters*, B41:216, 1972.

[98] P. Joos *et al.* Determination of the nucleon axial vector form-factor from $\pi\Delta$ electroproduction near threshold. *Physics Letters*, B62:230, 1976.

[99] E. D. Bloom *et al.* Measurements of inelastic electron scattering cross sections near one-pion threshold. *Physical Review Letters*, 30:1186, 1973.

[100] W. Bartel *et al.* Electroproduction of pions near the $\Delta(1236)$ isobar and the form factor of $G_M^*(q^2)$ of the $(\gamma N\Delta)$-vertex. *Physics Letters*, B28:148, 1968.

[101] F. Foster and G. Hughes. Electroproduction of nucleon resonances. *Reports on Progress in Physics*, 46:1445, 1983.

[102] S. Stein *et al.* Electron scattering at 4° with energies of $4.5 - 20\text{GeV}$. *Physical Review*, D12:1884, 1975.

[103] V. V. Frolov *et al.* Electroproduction of the *Delta* (1232) resonance at high momentum transfer. *Physical Review Letters*, 82:45, 1999.

[104] V. Burkert (Ed.), F. Gross (Ed.), B. Mecking (Ed.), J. Mougey (Ed.), and R. R. Whitney (Ed.). Research program at CEBAF. 2. Proceedings, 2nd Summer Study Group, Newport News, USA, June 2 - August 29, 1986. Newport News, USA: CEBAF (1987) 728 p.

[105] C. Gerhardt. A resonance analysis of electroproduction data. *Zeitschrift für Physik*, C4:311, 1980.

[106] R. Thompson *et al.* The $ep \to e'p\eta$ reaction at and above the $S_{11}(1535)$ baryon resonance. *Physical Review Letters*, 86:1702, 2001.

[107] C. S. Armstrong *et al.* Electroproduction of the $S_{11}(1535)$ resonance at high momentum transfer. *Physical Review*, D60:052004, 1999.

[108] B. Krusche *et al.* New threshold photoproduction of *eta* mesons off the proton. *Physical Review Letters*, 74:3736, 1995.

[109] F. W. Brasse *et al.* Electroproduction of η mesons in the region of the resonances $S_{11}(1535)$ at momentum transfers of 2GeV^2 and 3GeV^2. *Zeitschrift für Physik*, C22:33, 1984.

[110] H. Breuker *et al.* Determination of $R = \sigma_L/\sigma_T$ from η-electroproduction at the $S_{11}(1535)$ resonance. *Physics Letters*, B74:409, 1978.

[111] F. W. Brasse *et al.* Separation of σ_L and σ_T in η electroproduction at the resonance $S_{11}(1535)$. *Nuclear Physics*, B139:37, 1978.

[112] J.-C. Adler *et al.* Electroproduction of η mesons in the region of the resonances $S_{11}(1535)$. *Nuclear Physics*, B91(3):386, 1975.

[113] U. Beck *et al.* Electroproduction of η-meson at the $S_{11}(1535)$ resonance. *Physics Letters*, B51:103, 1974.

[114] P. S. Kummer *et al.* Measurement of the electromagnetic-transition form factor for the $S_{11}(1535)$ resonance. *Physical Review Letters*, 30:873, 1973.

[115] H.-C. Kim, A. Blotz, M. V. Polyakov, and K. Goeke. Electromagnetic form factors of the $SU(3)$ octet baryons in the semibosonized $SU(3)$ Nambu–Jona-Lasinio model. *Physical Review*, D53(7):4013, 1996.

[116] A. Silva. Electromagnetic form factors in the CQSM. Private communication, 2004.

[117] B. Kubis, T. R. Hemmert, and U.-G. Meißner. Baryon form factors. *Physics Letters*, B456:240, 1999.

[118] B. Kubis and U.-G. Meißner. Baryon form factors in chiral perturbation theory. *European Physical Journal*, C18:747, 2001.

[119] J. W. Darewych, M. Horbatsch, and R. Koniuk. Photon decays of baryons with strangeness. *Physical Review*, D28(5):1125, 1983.

[120] E. Kaxiras, E. J. Moniz, and M. Soyeur. Hyperon radiative decay. *Physical Review*, D32(3):695, 1985.

[121] Y. Umino and F. Myhrer. Hyperon resonances in the chiral bag model. *Physical Review*, D39(11):3391, 1989.

[122] Y. Umino and F. Myhrer. Electromagnetic decays of excited hyperons. *Nuclear Physics*, A529:713, 1991.

[123] Y. Umino and F. Myhrer. Electromagnetic decays of excited hyperons (II). *Nuclear Physics*, A554:593, 1993.

[124] D. B. Leinweber, T. Draper, and R. M. Woloshyn. Baryon octet to decuplet electromagnetic transitions. *Physical Review*, D48(5):2230, 1993.

[125] M. N. Butler, M. J. Savage, and R. P. Springer. $E2/M1$ mixing ratio of $\Delta \to N\gamma$ and hyperon resonance radiative decay. *Physics Letters*, B304:353, 1993.

[126] C. L. Schat, C. Gobbi, and N. N. Scoccola. Hyperon radiative decays in the bound state soliton model. *Physics Letters*, B356:1, 1995.

[127] C. L. Schat, N. N. Scoccola, and C. Gobbi. $\Lambda(1405)$ in the bound state soliton model. *Nuclear Physics*, A585:627, 1995.

[128] A. Abada, H. Weigel, and H. Reinhardt. Radiative decays of hyperons in the Skyrme model: $E2/M1$ transitions. *Physics Letters*, B366:26, 1996.

[129] T. Haberichter, H. Reinhardt, N. N. Scoccola, and H. Weigel. Strangeness dependence in radiative hyperon decay amplitudes. *Nuclear Physics*, A615: 291, 1997.

[130] G. Wagner, A. J. Buchmann, and A. Faessler. Radiative decays of decuplet hyperons. *Physical Review*, C58:1745, 1998.

[131] G. Wagner, A. J. Buchmann, and A. Faessler. Electromagnetic properties of decuplet hyperons in a chiral quark model with exchange currents. *Journal of Physics*, G26:267, 2000.

[132] T. Van Cauteren, D. Merten, J. Ryckebusch, T. Corthals, S. Janssen, B. Metsch, and H.-R. Petry. Electric and magnetic form factors of strange baryons. *European Physical Journal*, A20(2):283, 2004.

[133] W. Plessas. Baryons as relativistic three-quark systems. In M. T. Pena, A. Stadtler, A. M. Eiro, and J. Adam, editors, *Nuclear Dynamics: From Quarks to Nuclei, Proceedings of the XXth CFIF Fall Workshop, Lisbon, Portugal*, volume 15

of *Few-Body Systems Supplement*. Springer-Verlag, Berlin, Heidelberg, XVIII, 2003.

[134] L. Y. Glozman, Z. Papp, W. Plessas, K. Varga, and R. F. Wagenbrunn. Effective $Q - Q$ interactions in constituent quark models. *Physical Review*, C57:3406, 1998.

[135] R. K. Bhaduri, L. E. Cohler, and Y. Nogami. A unified potential for mesons and baryons. *Nuovo Cimento*, A65(3):376, 1981.

[136] L. Theußl, R. F. Wagenbrunn, B. Desplanques, and W. Plessas. Hadronic decays of N and Δ resonances in a chiral quark model. *European Physical Journal*, A12:91, 2001.

[137] D. E. Groom *et al.* Review of particle physics. *The European Physical Journal*, C15:1+, 2000. URL http://pdg.lbl.gov.

[138] U. Löring, B. Metsch, and H.-R. Petry. The light baryon spectrum in a relativistic quark model with instanton-induced quark forces. the strange baryon spectrum. *European Physical Journal*, A10:447, 2001.

[139] D. Jido, E. Oset, and A. Ramos. Chiral dynamics of p-wave in $K^- p$ and coupled states. *Physical Review*, C66:055203, 2002.

[140] D. Jido, J. A. Oller, E. Oset, A. Ramos, and U. G. Meissner. Chiral dynamics of the two $\Lambda(1405)$ states. *Nuclear Physics*, A725:181, 2003.

[141] C. García-Recio, J. Nieves, E. Ruiz Arriola, and M. J. Vicente Vacas. $S = -1$ meson baryon unitarized coupled channel chiral perturbation theory and the $S(01)$ resonances $\Lambda(1405)$ and – $\Lambda(1670)$. *Physical Review*, D67:076009, 2003.

[142] C. García-Recio, M. F. M. Lutz, and J. Nieves. Quark mass dependence of s-wave baryon resonances. *Physics Letters*, B582:49, 2004.

[143] E. E. Kolomeitsev and M. F. M. Lutz. On baryon resonances and chiral symmetry. *Physics Letters*, B585:243, 2004.

[144] S. Prakhov. Progress on study of K^--proton reactions. Technical report, UCLA, 2001. URL http://bmkn8.physics.ucla.edu/Crystalball/Docs/documentation.html.

[145] D. M. Manley *et al.* Properties of the $\Lambda(1670)\frac{1}{2}^-$ resonance. *Physical Review Letters*, 88:012002, 2002.

[146] N. Phaisangittisakul. *First Measurement of the Radiative Process $K^-p \to \Lambda\gamma$ at Beam Momenta 520-750 MeV/c Using the Crystal Ball Detector*. PhD thesis, University of California, Los Angeles, 2001. URL http://bmkn8.physics.ucla.edu/Crystalball/Docs/Latex_ps/thesis_nakorn.ps.

[147] A. H. Mueller. Perturbative QCD at high energies. *Physics Reports*, 73:237, 1981.

[148] W. Greiner and B. Müller. *Quantum Mechanics - Symmetries*. Springer-Verlag New York, Berlin, Heidelberg, second edition, 1994.

[149] K. Kretzschmar. *Electroweak Form Factors in a Covariant Quark Model of Baryons*. PhD thesis, Rheinische Friedrich-Wilhelms-Universität Bonn, Germany, 2001.

[150] T. Hyodo, A. Hosaka, M. J. V. Vacas, and E. Oset. Study of $\Lambda(1405)$ in photoproduction of K^*. *Invited talk at the YITP workshop on "Multi-quark Hadrons; Four, Five and More?", Kyoto, Japan*, 2004.

[151] G. S. Bali. QCD forces and heavy quark bound states. *Physics Reports*, 343: 1–136, 2001.

[152] P. de Forcrand and O. Jahn. The baryon static potential from lattice QCD. In *Proceedings of the 10th International Conference on the Structure of Baryons (BARYONS 2004), Palaiseau, France*, 2005.

[153] B. Juliá-Díaz *et al.* Dynamical coupled-channel study of $K^+\Lambda$ photoproduction. 2005.

Nederlandstalige Samenvatting

Inleiding

Bij het opstellen van modellen om de vele fenomenen rondom ons te beschrijven, verklaren en voorspellen, rijzen telkens dezelfde twee vragen. Wat zijn de relevante vrijheidsgraden ? En hoe interageren die vrijheidsgraden met elkaar ?

De geschikte vrijheidsgraden in een fysisch model hangen sterk af van de tijds- en afstandsschaal waarop het bestudeerde fenomeen zich afspeelt. Bij hele grote afstanden en lange periodes, onderscheidt men sterren en planeten. Hier op aarde, spreekt men van geologische lagen, continentendrift, vulkanen en aardbevingen. Bij de kleinste afstands- en tijdsschalen, houden deeltjesfysici zich bezig met het gedrag van fermionen en bososen, geladen en neutrale objecten, leptonen en quarks.

De overvloed van interessante fenomenen in de natuur worden vooral veroorzaakt door de interacties tussen de verschillende vrijheidsgraden. Planetaire systemen zijn een gevolg van de gravitationele aantrekking tussen sterren en planeten. Warmteverschillen tussen de aardkern en -mantel veroorzaken convectiestromen die de continentale platen tegen en langs elkaar doen duwen. Door de wrijving tussen de platen ontstaan aardbevingen en vulkaanuitbarstingen. In het Standaard Model interageren materiedeeltjes met halftallige spin (fermionen) via uitwisseling van krachtenoverbrengende deeltjes met heeltallige spin (bosonen). Geladen deeltjes wisselen fotonen uit. Quarks interageren via gluon-uitwisseling, terwijl leptonen dat per definitie niet doen.

De processen die besproken worden in deze thesis spelen zich af op een afstandsschaal van ruwweg $0.05 \rightarrow 1.4$ fm. Om zo diep door te dringen in de materie,

moet de probe energieën kunnen bereiken van $0.14 \rightarrow 4$ GeV. Het onderzoek van fenomenen bij deze energieën is het domein van de intermediaire energie fysica. Soms wordt ook de term hadronenfysica gebruikt, om aan te duiden dat hadronen en hun interacties het belangrijkste onderzoeksonderwerp zijn.

Het proces dat centraal staat in dit werk is de elektroproductie van een kaon en een hyperon aan het proton, kortweg $p(e,e'K)Y$ genaamd. Deze reactie is neergeschreven in termen van elektronen en hadronen. Het proton bezit echter geen expliciete vreemdheid, terwijl kaon en hyperon dat wel hebben. Dit impliceert dat er tijdens deze reactie een vreemd quark/antiquark paar gecreëerd wordt. Om het proces volledig te beschrijven, heeft men dus ook quark vrijheidsgraden nodig.

In dit werk worden twee modellen voorgesteld. Het eerste is gebaseerd op constituentenquark vrijheidsgraden. In dit model wordt de octet-decuplet structuur van de lichtste baryonen en mesonen op een eenvoudige manier verklaard. Bovendien kunnen de constituentenquarks geïdentificeerd worden met valentiequarks die omgeven zijn door een wolk van gluonen en quark/antiquarkparen (zee-quarks). Valentiequarks, gluonen en zee-quarks zijn de vrijheidsgraden van Kwantum Chromodynamica (QCD), de fundamentele theorie voor sterke interacties.

Het tweede model is geformuleerd in termen van hadronische vrijheidsgraden, en wordt daarom een isobaar model genoemd. In dit model wordt de $p(e,e'K)Y$ reactie behandeld op 'tree'-niveau. Dit betekent dat alleen Feynmandiagrammen zonder lussen opgenomen worden in de beschrijving van de dynamica. In eerste instantie houdt dit model geen rekening met de onderliggende quarkstructuur van hadronen. Toch blijkt het, vooral bij hogere energieën, nodig om aan de verschillende interactievertices *vormfactoren* toe te kennen. Deze parametriseren de eindige afmetingen van de hadronen, en geven dus de inwendige structuur van hadronen weer. Daarom moeten ze af te leiden zijn uit de eigenschappen van de onderliggende quark-vrijheidsgraden. De vormfactoren van hadronen vormen dus het raakpunt tussen de twee verschillende modellen.

Elektromagnetische Vormfactoren

Het formalisme van de relativistische kwantumveldentheorie is ontwikkeld om de interacties van elementaire puntdeeltjes op een Lorentz-covariante manier te

behandelen. Wanneer de deeltjes eindige afmetingen hebben, worden de interactievertices echter sterk afhankelijk van de afstandsschaal waarop de interactie plaatsvindt, en dus van de viermomenta van de deeltjes. Deze afhankelijkheid wordt geparametriseerd door sterke of elektromagnetische vormfactoren, naargelang de interactie.

In het Bonn model, dat in Hoofdstuk 2 behandeld wordt, is een baryon of baryonresonantie een gebonden toestand van drie puntvormige constituentenquarks [34, 37]. De eindige extensie van het baryon is dan een gevolg van de afstanden tussen deze constituentenquarks. De gebonden toestand van het relativistisch veeldeeltjessysteem wordt beschreven door de Bethe-Salpeter amplitude. De koppeling van een foton met een baryon(-resonantie) wordt in laagste orde gegeven door de som van de fotonkoppelingen aan de drie puntvormige constituentenquarks.

Aangezien het foton een spin-1 boson is, wordt het fotonveld gegeven in de vorm van een viervector. Lorentz-invariantie zorgt er dan voor dat ook de baryonstroom waaraan het fotonveld koppelt een viervector is. De componenten van deze baryonstroom zijn de matrixelementen van de stroomoperator-componenten tussen ingaande en uitgaande baryontoestand. Aan de hand van Lorentz-symmetrie en het principe van ijkinvariantie, kan men aantonen dat maximaal drie onafhankelijke gereduceerde matrixelementen de foton-baryon koppeling karakteriseren. De elektromagnetische vormfactoren zijn niets anders dan lineaire combinaties van deze drie gereduceerde matrixelementen.

Het isobaar model voor $p(e,e'K)Y$ reacties dat besproken wordt in Hoofdstuk 3, is ontwikkeld *m.b.v.* het Lagrangiaans formalisme en Feynmandiagrammen [2–6]. In laagste orde bevat ieder diagram één hadronische en één elektromagnetische vertex, en een uitgewisseld hadron. Wanneer dit hadron in een grondtoestand verkeert (nucleon, kaon, Λ- of Σ-hyperon), noemt men de corresponderende amplitude een *Born*-term. De Born-termen zijn een deel van de *achtergrond* bij het $p(e,e'K)Y$ proces, gedefinieerd als de som van de termen waarbij het intermediair deeltje nooit *on-shell* kan zijn in het kinematisch regime van de $p(e,e'K)Y$ reactie. Naast de Born termen behoren hiertoe ook de termen die de uitwisseling van een kaonresonantie of een hyperonresonantie beschrijven. In principe kunnen ook nucleon- en Δ-resonanties deel uitmaken van de achtergrond, wanneer hun massa (een stuk) kleiner is dan de drempelenergie voor het $p(e,e'K)Y$ proces. In het

isobaar model van Refs. [2–6] worden zulke resonanties echter niet beschouwd, en hebben alle nucleon- en Δ-resonanties een massa net onder of boven de drempelwaarde. Het viermomentum van het uitgewisselde deeltje kan dan (bijna) on-shell zijn, waardoor de propagatoren van deze s-kanaal resonanties (bijna) een pool bereiken in het kinematisch regime van de $p(e,e'K)Y$ reactie. Resonantietermen kunnen dus aanleiding geven tot een brede structuur in de werkzame doorsnedes en polarisatie-observabelen, in tegenstelling tot de achtergrond, die een gladder energieverloop vertoont. Een correcte beschrijving van de achtergrond-contributies is echter essentieel om juiste informatie over de resonante bijdragen uit de data te kunnen distilleren.

In een isobaar model voor $p(e,e'K)Y$ reacties, moet een elektromagnetische vormfactor ingevoerd worden bij elke elektromagnetische vertex. Deze vormfactoren zijn echter niet voor alle deeltjes die aan het $p(e,e'K)Y$ proces deelnemen, gemeten. Dit betekent dat men een zekere graad van onzekerheid introduceert in het model. Om deze onzekerheid te beperken, kan men voor de niet-gemeten vormfactoren de voorspellingen gebruiken van het constituentenquark model van Bonn.

Het invoeren van de elektromagnetische vormfactoren in het isobaar model op een ijkinvariante manier is afhankelijk van het type deeltje dat met het foton koppelt. Een sterk onderscheid wordt gemaakt tussen de Born-termen en de rest. Voor de Born-termen geldt dat hun som ijkinvariant moet zijn, terwijl de termen waarbij het intermediaire deeltje een resonantie is, elk apart ijkinvariant worden verondersteld. Met deze benaderingen kan de invloed van een specifieke resonantie op het $p(e,e'K)Y$ proces veel gemakkelijker achterhaald worden.

De ijkinvariantie van de som van de Born-termen wordt verzekerd door gebruik te maken van de *Ward-Takahashi* (WT) identiteiten. Deze laatste leggen voorwaarden op aan de Born-amplitudes opdat de resulterende hadronstroom ijkinvariant zou zijn. De WT identiteiten zijn geldig voor zowel on-shell als off-shell deeltjes. Dit is belangrijk aangezien in een isobaar model op tree-niveau het intermediair deeltje in een achtergrondterm altijd off-shell is. In Sect. 3.3.2 wordt uitgebreid aandacht besteed aan de correcte implementatie van elektromagnetische vormfactoren bij elastische vertices.

Voor de resonante termen induceert de elektromagnetische interactie een tran-

sitie tussen een resonantie en de grondtoestand. In dit geval zijn de WT identiteiten niet meer van toepassing en moet men andere voorwaarden vooropstellen om ervoor te zorgen dat de uiteindelijke hadronstroom ijkinvariant is. In Sects. 3.3.3 en 3.3.4 worden deze voorwaarden voorgesteld en geïmplementeerd in de elektromagnetische vertex voor spin-$1/2$ resonanties.

Elektromagnetische Eigenschappen van Hyperonen

De experimentele informatie *m.b.t.* elektromagnetische vormfactoren en heliciteitsamplitudes van baryonen en baryonresonanties is vrij beperkt. Zelfs voor het best gekende baryon, het proton, is de huidige situatie niet ondubbelzinnig. Recent werd namelijk een discrepantie ontdekt in de verhouding G_E/G_M voor het proton wanneer twee verschillende technieken werden gebruikt : de Rosenbluth-separatie [61] en de polarisatie-transfer methode [62, 63]. Deze discrepantie zou verklaard kunnen worden door twee-foton uitwisselingsmechanismen [64], doch dit moet nog experimenteel bevestigd worden in verdere e^-p en e^+p-verstrooiingsexperimenten.

Bij het invoeren van vormfactoren in de elektromagnetische vertex, bechikt men dus niet over genoeg experimentele informatie omtrent de exacte Q^2-afhankelijkheid. Dit is vooral het geval voor de elektromagnetische koppeling aan vreemde baryonen, waarvoor zo goed als geen data beschikbaar zijn. Van de hyperonen in de grondtoestand zijn enkel de magnetische momenten, en van het Σ^- ook de elektrische ladingsstraal, gemeten. Van de hyperonresonanties zijn enkel de elektromagnetische vervalbreedtes van de laagstgelegen Y^*'s ($P_{13}(1385)$, $S_{01}(1405)$ en $D_{03}(1520)$) naar de Λ en Σ grondtoestand gekend, zij het met eerder grote fout. Om de schaarste aan experimentele informatie te compenseren, worden in deze thesis de resultaten gepresenteerd voor de elektromagnetische vormfactoren van hyperonen en heliciteitsamplitudes van hyperonresonanties, bekomen in het Bonnmodel.

In Sect. 4.1 worden de resultaten voor de elektrische en magnetische vormfactoren van de grondtoestandshyperonen besproken. Zoals gezegd kan men de resultaten enkel vergelijken met data in het reëel-foton punt ($Q^2 = 0$), waar de magnetische vormfactor de waarde voor het magnetisch moment weergeeft. De resultaten komen uitstekend overeen met de experimentele waarden. Ook de be-

rekende waarde voor de elektrische ladingsstraal van het Σ^- hyperon, evenredig met de afgeleide van de elektrische vormfactor in $Q^2 = 0$, komt overeen met de gemeten waarde. De zeven parameters die in het Bonn model voorkomen werden reeds vastgelegd in Refs. [37, 38] door ze aan het baryonenspectrum te fitten. Dit betekent dat de resultaten voor de vormfactoren als voorspellingen beschouwd kunnen worden.

De magnetische vormfactoren van alle octethyperonen met uitzondering van het Σ^-, kunnen beschreven worden met een dipool, waarvan de *cut-off* massa varieert tussen 0.79 GeV voor het Σ^+ en 1.14 GeV voor het Λ. Deze laatste waarde verschilt duidelijk van de gemeten waarde voor de cut-off massa 0.84 GeV van het nucleon. Ook de elektrische vormfactoren van de neutrale hyperonen verschillen duidelijk met die van het neutron. Deze zijn namelijk negatief voor het Λ- en het Σ^0-hyperon, terwijl de elektrische vormfactor van het neutron positief is. Dit kan toegeschreven worden aan de zwaardere s-constituentenquark, die zich dichtbij het massacentrum van het hyperon bevindt. De vaak gebruikte procedure om vormfactoren van hyperonen te parametriseren in termen van die van het nucleon, lijkt dus niet verantwoord.

In Sect. 4.2 worden de elektromagnetische eigenschappen van hyperonresonanties gegeven in de vorm van heliciteitsamplitudes. Deze beschrijven het elektromagnetisch verval van de Y^* naar de Λ- of Σ-grondtoestand en zijn recht evenredig met de stroommatrixelementen. We hebben de elektromagnetische processen $\Lambda^* \to \Lambda(1116)$, $\Lambda^* \to \Sigma(1193)$, $\Sigma^* \to \Lambda(1116)$ en $\Sigma^* \to \Sigma(1193)$ berekend voor de laagstgelegen hyperonresonanties.

De resultaten wijzen erop dat de lichtste resonantie met een bepaalde spin en pariteit duidelijk sterker koppelt aan een foton met intermediaire virtualiteit (waarvoor $0.1 \lesssim Q^2 \lesssim 2.0$ GeV^2) dan aan een reëel foton. Dit betekent dat deze resonanties een grotere rol kunnen spelen in de isobare beschrijving van $p(e,e'K)Y$ reacties dan in die van $p(\gamma,K)Y$ processen. Dit effect is ook in mindere mate zichtbaar in de resultaten voor de heliciteitsamplitudes van nucleon- en Δ-resonanties uit Ref. [35], waar het gesteund wordt door de experimentele data.

Verder blijkt de lichtste resonantie met bepaalde kwantumgetallen bij voorkeur naar de Λ-grondtoestand te vervallen, terwijl de tweede en derde resonantie preferentieel naar de Σ^0-grondtoestand vervallen. In sommige isobare modellen [2–

6, 153], interfereren hyperonresonanties in het u-kanaal van het $p(e,e'K)Y$ proces destructief met de Born-termen, hetgeen de achtergrondsterkte drukt. Het in rekening brengen van de lichtste resonantie met bepaalde spin en pariteit zal dus efficiënter zijn wanneer $Y = \Lambda$, terwijl de hogergelegen resonanties vooral effect hebben als $Y = \Sigma$. De laagstgelegen hyperonresonantie is bovendien het minst off-shell in de $p(e,e'K)Y$ reacties. Aangezien een amplitude in het isobaar model evenredig is met de propagator van het uitgewisselde deeltje, die op zijn beurt omgekeerd evenredig is met de mate waarin dit deeltje off-shell is, zal een lichte hyperonresonantie dus meer effect hebben. Wanneer de lichtste resonantie dan nog eens preferentieel naar de $\Lambda(1116)$ vervalt, suggereert dit dat het invoeren van hyperonresonanties om de achtergrond te drukken efficiënter zou kunnen zijn voor het $p(e,e'K^+)\Lambda$ proces dan voor het $p(e,e'K)Y$ proces. Verder onderzoek zal moeten uitwijzen of dit al dan niet het geval is.

Het isobaar model ontwikkeld in Gent [2–6] brengt baryonresonanties in rekening met $J \leq 3/2$. De berekende heliciteitsamplitudes van de $J = 5/2$ deeltjes $F_{05}(1820)$ en $D_{05}(1830)$ zijn echter niet verwaarloosbaar. Bovendien heeft de tweede resonantie met $J^\pi = 5/2^-$, de $D_{05}^{(2)}$ met een berekende massa van ongeveer 2100 MeV, grotere heliciteitsamplitudes dan de $D_{05}(1830)$-resonantie. Het al dan niet introduceren van $J = 5/2$ resonanties in het u-kanaal voor het $p(e,e'K^+)\Lambda$ proces kan dus op basis van deze resultaten niet beslist worden.

Het verval van Σ^*-resonanties naar de Σ-grondtoestand komt in drie ladingstoestanden voor. Uit de resultaten blijkt dat de geladen toestanden van sommige resonanties, zoals de $P_{11}(1660)$ en de $S_{11}(1620)$, (veel) grotere heliciteitsamplitudes hebben dan de ongeladen toestand. De invloed van deze resonanties op het $p(e,e'K^0)\Sigma^+$ proces zal bijgevolg (veel) groter zijn dan op het $p(e,e'K^+)\Sigma^0$ proces.

De berekende elektromagnetische vervalbreedtes voor het $S_{01}(1405) \rightarrow \Lambda(1116)$ en het $S_{01}(1405) \rightarrow \Sigma(1193)$ proces zijn beduidend groter dan de gemeten waarden. Bovendien wordt ook de massa van deze resonantie te groot voorspeld. Dit duidt op de speciale structuur van deze resonantie, hetgeen door ander onderzoek bevestigd wordt [127, 140, 141, 150]. Als echter de $S_{01}(1405)$-resonantie niet correspondeert met een toestand uit een constituentenquark-model, dan voorspelt het Bonn-model een extra toestand met $J^\pi = 1/2^-$ en massa rond 1550 MeV met sterke elektromagnetische koppelingen naar de Λ- en Σ-grondtoestand. Zo'n resonantie

is tot nu toe niet experimenteel waargenomen.

Voor de $S_{01}(1670)$-resonantie is de berekende elektromagnetische vervalbreedte naar het $\Lambda(1116)$ verwaarloosbaar, terwijl de breedte voor verval naar het $\Sigma^0(1193)$ groot is. Dit wordt kwalitatief gesteund door de $\bar{K}^- p$-verstrooiingsexperimenten gedaan door de *Crystal Ball Collaboration* in Brookhaven (VS). Rond een invariante massa van 1670 MeV is de werkzame doorsnede voor de $\bar{K}^- p \to \gamma\Sigma^0$ reactie namelijk ongeveer vier keer groter dan die voor het $\bar{K}^- p \to \gamma\Lambda$ proces.

Het gedrag van de verhouding $F_2^\Lambda / F_1^\Lambda$ wijkt af van wat door perturbatieve QCD voorspeld wordt. Volgens deze laatste is de verhouding van de Pauli- *t.o.v.* de Dirac-vormfactor recht evenredig met Q^{-2}. Volgens het resultaat uit Sect. 4.3.1 leunt deze verhouding echter dichter aan bij $Q^{-1.4}$ voor $2.0 \leq Q^2 \leq 6.0$ GeV^2. Het gedrag van de heliciteitsasymmetrieën lijkt te bevestigen dat bij hoge Q^2 het foton aan de constituentenquarks koppelt en niet aan de baryonresonantie als een geheel.

Conclusies en Vooruitzichten

In deze thesis werden twee modellen voor de beschrijving van $p(e,e'K)Y$ processen, werkend met resp. constituentenquark- en hadronvrijheidsgraden, op elkaar afgestemd. Het berekenen van de observabelen voor de $p(e,e'K)Y$ processen gebeurt in het raamwerk van een isobaar model. De dynamica van dit model vertoont echter enkele onzekerheden aan de elektromagnetische vertex. Deze onzekerheden zijn des te groter in het u-kanaal vanwege de schaarsheid aan experimentele informatie over de sterkte van de koppeling van een virtueel foton aan een hyperon. Om toch realistische elektromagnetische koppelingen in het isobaar model te kunnen invoeren, werden de elektromagnetische vormfactoren en heliciteitsamplitudes berekend in het constituentenquark-model van Bonn. Dit model is Lorentz-covariant, en beschrijft de Lorentz-boost die inherent is aan het proces op een correcte manier.

Een volgende stap bestaat eruit de berekende vormfactoren en heliciteitsamplitudes op ijkinvariante wijze te implementeren in het isobaar model. Dit uitgebreide model kan vervolgens aangewend worden om de experimentele resultaten voor de $p(e,e'K^+)\Lambda$ reactie te beschrijven, en die voor de $p(e,e'K)\Sigma$ reacties te voorspellen.